USING OPTICAL STIMULATION TO STUDY THE DEVELOPING THALAMOCORTICAL CIRCUIT IN MOUSE SOMATOSENSORY CORTEX.

by

André Marques-Smith

Merton College

A Dissertation submitted to the

University of Oxford

in partial fulfilment of requirements for the degree of

Doctor of Philosophy

Department of Physiology, Anatomy and Genetics

Le Gros Clark Building

Written under the direction of

Dr. Simon Butt, Ph.D.

and

Professor Zoltán Molnár, MD., D.Phil.

Abstract

USING OPTICAL STIMULATION TO STUDY THE DEVELOPING THALAMOCORTICAL CIRCUIT IN MOUSE SOMATOSENSORY CORTEX.

André Marques-Smith – Merton College

Submitted for DPhil, Hilary Term 2014.

Charting connectivity between neurons in the brain is one of the main goals of circuit neuroscience. Despite great advances in our understanding of cortical circuit organisation, comparatively little attention has been devoted to studying how the intricate cortical connectivity emerges. Current views are that early synaptic connectivity within the cortex and between thalamus and cortex is largely mediated via silent synapses. Early patterns of network activity synchronise firing in pre- and post-synaptic elements of circuits and promote correlated activity, enabling synaptic plasticity and maturation via unsilencing. However, little is known about which circuits may be in place to promote such patterns of activity. In my thesis I used optical stimulation and electrophysiology to clarify circuits involved in the maturation of the thalamocortical circuit in the mouse barrel cortex.

In Chapter 3, I attempted to use optogenetics to study the early organisation and plasticity of thalamocortical inputs by delivering ChR65 (channelrhodopsin 65) to the embryonic thalamus via *in utero* electroporation. Following a detailed characterisation of the response properties of ChR65-positive developing neurons to optical stimulation, I was able to demonstrate that expression levels strong enough to elicit laser-mediated spiking are only attainable post-P10, after the critical period for thalamocortical plasticity. I focused on characterising thalamic inputs onto excitatory neurons in L4, L5b and the subplate (SP), finding a focused barrel organisation in L4, broader horizontal organisation in L5b, and lack of thalamic inputs to subplate neurons (SPns) after P10.

SPns have been shown to have a key role in early network oscillations and thalamocortical plasticity. However, relatively little is known about the cortical circuits in which they are embedded early in development. In Chapter 4, I

characterised intrinsic electrophysiological and network development in the Lpar1-GFP population of SPns. These cells show highly mature intrinsic properties already at P6, and receive robust thalamic input from birth, which starts being retracted after P5. Using glutamate uncaging to map afferent excitatory inputs onto Lpar1-GFP SPns, I found that these cells start out receiving most of their cortical excitation from the SP. Between P2 and P3, this recurrent network loses prominence, and L6 becomes the major source of input. By P5, the organisation of cortical inputs onto Lpar1-GFP SPns appears stable.

In the Lpar1-GFP line, it is also possible to find fluorescently-labelled neurons in the cortical plate. These cells are mostly in L5 and L6, and have atypical, non-pyramidal morphologies. In Chapter 5 I studied these neurons, concluding that they are $Lhx6^{+}$ Martinotti cells, with axons extending to L1 and arborizing in L4. Lpar1-GFP Martinotti cells (Lpar1-GFP MCs) receive early, facilitating thalamic input, which is maintained into maturity. I mapped early cortical inputs onto these cells using glutamate uncaging and found that whereas early inputs arise from L4, by P10-P15 the totality of input comes from L5b/6. Conversely, I found, by mapping GABAergic inputs onto L4 spiny stellate neurons throughout development, that these cells initially derive most of their inhibition from L5b. L4 GABAergic inputs are upregulated throughout development, concomitant to a decrease and eventual elimination of L5b inhibition onto L4. I propose that Lpar1-GFP MCs and L4 excitatory neurons form a reciprocal connection. Using infraorbital nerve (ION) sectioning, I found that early GABAergic innervation is decreased in ION-sectioned animals compared to controls, suggesting GABAergic synapse formation is experience-dependent. However, the laminar organisation of GABAergic inputs was identical between the two groups. At P10-P15, laminar organisation differed, with ION-sectioned animals receiving more input from L5b and less from L4, compared to controls. Total GABAergic input was unaltered by this age, and I propose that it was compensated by an upregulation of input from infragranular layers.

The combined results of my experiments using optical and electrical stimulation approaches to study the early thalamocortical system revealed highly dynamic circuits involving thalamic relay neurons, Lpar1-GFP expressing subplate and L5b Martinotti

neurons, and L4 spiny stellate cells. In agreement with recent findings in the adult literature, my results support a view of emerging thalamocortical processing that is increasingly less centred in L4, pointing to the key influence of early transient circuits involving subplate neurons and infragranular Martinotti cells. These two pioneer cell types seem to integrate into cortical and thalamocortical circuits early in development and provide two di-synaptic pathways linking the thalamus to L4, one glutamatergic (via Lpar1-GFP SPns) and one GABAergic (via L5b Lpar1-GFP MCs). These transient pathways could collaborate to regulate early rhythmic patterns of activity in L4 that are fundamental for maturation of thalamocortical pathways.

Statement of Authorship

I can confirm that all work presented within this thesis is my own, with the following exceptions and important recognition of others:

- The DsRed2 plasmid used in electroporations in Chapter 3 was a kind gift from Dr. Fernando García-Moreno, from the Molnár Laboratory at the University of Oxford.
- The ChR65 plasmid used in electroporations in Chapter 3 was a kind gift from Professor Ed Boyden at MIT, USA.
- The Lhx6 antibody used in Chapter 5 was a kind gift from Professor Vassilis Pachnis, MRC National Institute for Medical Research, London, UK.
- Some recordings in Chapter 5 were performed by Anna-Kristin Kauffmann in the context of her MSc in Neuroscience Trinity Term project, for which I served as day-to-day supervisor. Anna is an extremely talented and diligent young scientist, and her collaboration was invaluable in attaining the results reported in Chapter 5.

Acknowledgements

This thesis is dedicated to the loving memory of my grandparents. Their lives and histories, and the memories of them that I carry with me, have had a greater impact on my own path than I was ever able to put into words during their lifetime. This document stands as my humble tribute to the guiding force they have been in my life. Rest in peace **Pawel**, **Marguerite**, **Tiló** and **António**.

I thank my mother **Paula** and my father **Michael**. Their love, counsel and support have held and carried me like wings throughout my entire life. I am lucky also to have a brother, **Patrick,** that serves double duty as my best friend. Christmas holidays with my family and **Zinha**, **Tiago**, **Sofia**, and **Ema** renewed every year the energy I needed to relentlessly pursue my experiments in Oxford.

After all the time I've spent in their labs, my supervisors feel like friends to me. I've been lucky to work under their guidance. **Zoltan** was always a great source of encouragement and support, especially during trying times. He gave me the confidence in myself that I needed to thrive and never lost faith. I would probably have given up and done something else with my life if it wasn't for Zoltan. Since most of my work is electrophysiology, I spent most of my time at **Simon**'s lab. In December 2011, I no longer had a rig to do experiments on, and it is not an understatement to say that Simon rescued my DPhil. Not only that, but through his creativity, intuition and brilliance, Simon has been the greatest force in shaping my approach to Science. I could fill pages to explain how proud, privileged and happy I have been working in the Butt lab for my PhD, but I shall condense all that by writing simply that I have come to see Simon as a great friend that I admire and look up to in a lot of ways. Thank you, **Boss** - that's why they pay you the big bucks. Though not officially my supervisor, I worked under her guidance for 2 months, and found **Tomomi Shimogori** to be one of the most talented and charismatic persons I have met in neuroscience. Wherever my career may take me, I shall never forget these three giants whose shoulders I stood on.

I would not have made it and come to Oxford to study Neuroscience were it not for the mentorship of **Professor Armando Machado**. Despite his eloquence and sheer brilliance, I think not even Professor Armando would have predicted I would end up as a developmental neurobiologist. The chief culprit for this decision was **Dr. Jeremy Taylor**, whose lectures on neural development during the MSc in Neuroscience inspired me to choose this as my field of research. **Abhishek Banerjee** further ignited my interest in developing circuit physiology and taught me how to patch-clamp in 2009. Through the years and across the Atlantic we've maintained a great friendship that allows us to discuss things even more important than subplate neurons. I learnt much from the members of the **Molnár lab** throughout my DPhil, and am grateful for their guidance on all things molecular and immunohistochemical. **Anna Hoerder-**

Suabedissen in particular was extremely helpful at many stages of my DPhil, and for that has my eternal gratitude. Though smaller in size, the **Butt lab** played no smaller part in my training. **Daniel Lyngholm** was always a most enlightened and wise partner for discussion, and kindly shared his expertise in many things with me. **Anna-Kristin Kaufmann** was the first student I ever supervised and I blame her for spoiling my future supervision experiences. Surely no MSc student can be as intelligent, hard-working, naturally talented and fun to be around as her. I am fortunate to be a few years ahead of her in my career, as Anna will be the first post-doc I ever hire. I miss the banter and humour of **Tom Lickiss**, former Chief Molecular Biology Officer of the Butt Lab and fellow appreciator of Rocky Balboa. I thank the **Cortex Club** for playing a great part in my training in neuroscience outside the lab. I am immensely proud to have served as President and Vice-President, and hope this club carries on through the years to be the kind of century-old learned society one only finds at Oxford. All the animal work in my thesis would have been nigh-impossible without the help of the BSB staff, especially **Denise Jelfs** and **James Ward**, and they too have my gratitude. **Subplate neurons** deserve a mention. So much mystery packed in a 50μm sheet of neurons. They are a dragon I suspect I'll continue to chase for a good while.

Life is not all about Science, and I do have friends outside the lab. **Andrei**, **Cassandra**, **Jingyi**, **Carlos**, **Filipa**, **Tiago**, **Miguel**, **Lisa**, **João Alpedrinha**, **João Lima**, **Daniella, Derek** and **Dave**, I could not have done this without you. Each of them in a different way has inspired, improved, encouraged and cheered me up me throughout the years. With each of these friends I share a special and different connection which I could fill this volume describing, and I look forwards to prolonging these friendships for many years to come, wherever the future may take us. In the past year **Derek Hollman** in particular has been a great and positive influence in my life, and besides my family, my thesis is dedicated also to this extraordinary friendship which will grow to span continents and decades. Stone tables need not be physical things.

Funding from the Wellcome Trust and FCT enabled me to do this DPhil, and I am grateful to these institutions for their generosity.

Last but certainly not least, life at Oxford since 2008 was a weird and wonderful mix of science, punting, kayaking, wine, whiskey and cheese tastings, high-table dinners, formal hall exchanges, bops, walks through Port Meadow, workouts at the gym, banterous thefts from rival colleges, pennying, pub crawls and concerts. What a privilege to have been part of all this, and to have had the perfect friends and colleagues to enjoy it with.

Table of Contents

Abstract **2**

Statement of Authorship **5**

Acknowledgements **6**

Table of Contents **8**

List of Figures **10**

List of Tables **13**

Abbreviations **14**

Chapter 1 - Introduction **17**

1.1. Network oscillations in the developing cortex **25**

1.2. The assembly of cortical circuits **31**

1.3. AMPA-silent synapses and cortical development **41**

1.4. Subplate neurons in cortical development **50**

1.5. The development of GABAergic circuits **64**

1.6. Thesis objectives **83**

Chapter 2 - Methods **86**

Chapter 3 – Using optogenetics to map developing thalamic inputs to somatosensory cortex **103**

3.1. Introduction **103**

3.2. Optical activation of ChR65-expressing neurons throughout development **109**

3.3. Using CRACM and sCRACM to study the thalamocortical synapse **121**

3.3.1. Determining stimulus parameters for CRACM **122**

3.3.2. Using CRACM to study thalamocortical inputs **126**

3.3.3. Combining CRACM with LSPS **131**

3.3.4. Subcellular CRACM **134**

3.4. Discussion **138**

Chapter 4 – The intrinsic maturation and development of excitatory synaptic inputs onto Lpar1-GFP subplate neurons **149**

4.1. Introduction **149**

4.2. Electrophysiological maturation and diversity of Lpar1-GFP SPns **152**

4.3. Thalamic Input **160**

4.4. Calibration of LSPS for glutamate uncaging **168**

4.5. Mapping excitatory cortical inputs onto Lpar1-GFP subplate neurons **177**

4.5.1. Laminar organisation of excitatory inputs onto Lpar1-GFP subplate neurons over the first postnatal week **179**

4.5.2. Maturation of single EPSCs onto Lpar1-GFP subplate neurons during the first postnatal week **188**

4.5.3. Horizontal organisation of excitatory inputs onto Lpar1-GFP subplate neurons during the first postnatal week **190**

4.6. Chapter summary and discussion **193**

Chapter 5 – Thalamocortical integration via a transient early developmental L5b-L4 circuit **207**

5.1. Introduction **207**

5.2. The intrinsic properties and electrophysiological maturation of Lpar1-GFP non-subplate neurons **207**

5.3. Morphological and immunohistochemical characterisation of Lpar1-GFP interneurons **212**

5.4. Characterisation of thalamic inputs onto Lpar1-GFP interneurons **216**

5.5. Mapping excitatory cortical inputs onto Lpar1-GFP interneurons **221**

5.5.1. Maturation of single EPSCs onto Lpar1-GFP interneurons **227**

5.5.2. Horizontal organisation of excitatory inputs onto Lpar1-GFP Martinotti cells **230**

5.6. The output of Lpar1-GFP Martinotti cells **234**

5.6.1. Mapping the development of GABAergic input onto L4 spiny stellate cells **234**

5.7. Experience-dependence of the development of GABAergic input onto L4 spiny stellate neurons **240**

5.8. Discussion **246**

Chapter 6 – Summary and final discussion **264**

6.1. Introduction **264**

6.2. Summary of findings **265**

6.3. Integration of my findings **269**

6.4. Future directions **278**

6.5. The importance of bridging developing circuit and network physiology **291**

References **294**

List of Figures

Chapter 1

Figure 1.1. Migrating cortical plate neurons split the preplate into marginal zone and subplate **19**

Figure 1.2. The canonical cortical circuit **22**

Figure 1.3. Plasticity at the thalamocortical synapse **34**

Figure 1.4. Possible mechanisms for thalamocortical synapse unsilencing **35**

Figure 1.5. Maturation of cortical lamination and thalamic axon ingrowth **37**

Figure 1.6. Model for labile AMPA signalling in the developing brain **45**

Figure 1.7. Diversity of subplate neurons **52**

Figure 1.8. Efferent projection targets of SPns **56**

Figure 1.9. Afferent input onto SPns **59**

Figure 1.10. The subplate as a fundamental network node in the developing cortex **63**

Figure 1.11. Embryonic origin and diversity of cortical GABAergic interneurons **66**

Figure 1.12. Development of cortical GABAergic microcircuits **76**

Figure 1.14. A hypothetical cortical hub neuron **82**

Chapter 2

Figure 2.1. Current input protocols used to calculate electrophysiological parameters **90**

Figure 2.2. pCAG-DsRed and CAG-ChR65-GFP expression vectors **98**

Chapter 3

Figure 3.1. *In utero* electroporation of the thalamus **110**

Figure 3.2. Targeted recording from thalamic relay and thalamorecipient neurons **112**

Figure 3.3. Characterisation of ChR65+ thalamic relay neurons to optical stimulation **116**

Figure 3.4. Characterisation of ChR65+ L2/3 pyramidal neurons to optical stimulation **120**

Figure 3.5. Determining stimulus parameters for CRACM **125**

Figure 3.6. Lack of thalamic inputs to subplate neurons post-P10 **128**

Figure 3.7. CRACM of thalamic inputs onto L4 spiny stellate cells and L5b

pyramidal neurons **130**
Figure 3.8. Combined CRACM and LSPS of thalamic inputs onto L4 spiny stellate and L5b pyramidal neurons **133**
Figure 3.9. $EPSC_{CRACM}$ amplitude in cells where sCRACM was successful versus unsuccessful cases **135**
Figure 3.10. CRACM versus sCRACM maps in L4 spiny stellate neurons **137**

Chapter 4

Figure 4.1. The Lpar1-GFP mouse line **154**
Figure 4.2. Key maturation points for electrophysiological properties of Lpar1-GFP SPns. **159**
Figure 4.3. Thalamic input onto Lpar1-GFP subplate neurons between P0 and P15 **163**
Figure 4.4. Short-term plasticity of thalamic inputs onto Lpar1-GFP SPns **167**
Figure 4.5. Direct activation profile for an example L5b pyramidal neuron at P8 **170**
Figure 4.6. Calibration of laser intensity to postnatal age. **170**
Figure 4.7. Mapping afferent cortical excitatory inputs onto Lpar1-GFP subplate neurons **175**
Figure 4.8. Pre-synaptic action potential and post-synaptic EPSC detection window **176**
Figure 4.9. Mapping excitatory inputs onto Lpar1-GFP SPns **178**
Figure 4.10. Normalised vertical profile for LSPS maps of excitatory input onto all Lpar1-GFP SPns recorded **184**
Figure 4.11. LSPS of afferent cortical excitatory input to Lpar1-GFP SPns **185**
Figure 4.12. Analysis of single SP and L6-evoked EPSCs onto Lpar1-GFP SPns **189**
Figure 4.13. Horizontal organisation of excitatory input onto Lpar1-GFP SPns **192**
Figure 4.14. An overview of Lpar1-GFP SPn maturation during the critical period for thalamocortical plasticity **194**

Chapter 5

Figure 5.1. Electrophysiological properties of Lpar1-GFP interneurons at P10-P15 **211**
Figure 5.2. Biocytin morphological reconstructions of Lpar1-GFP interneurons **213**
Figure 5.3. Immunohistochemical characterisation of Lpar1-GFP interneurons in the barrel cortex **215**
Figure 5.4. Thalamic input onto Lpar1-GFP MCs **220**
226

Figure 5.5. Cortical excitatory input onto Lpar1-GFP MCs **229**
Figure 5.6. Developmental analysis of single EPSCs onto Lpar1-GFP MCs
Figure 5.7. Columnar organisation of excitatory cortical inputs onto Lpar1- **233**
GFP MCs **239**
Figure 5.8. Development of GABAergic input onto L4 spiny stellate cells
Figure 5.9. Development of GABAergic input onto L4 spiny stellate cells of **245**
ION-sectioned and control animals

Chapter 6

Figure 6.1. Schematic diagrams for possible wiring of the thalamus-SP-L4 circuit that would permit amplification of thalamic inputs to L4 via activity relayed through the subplate **290**

List of tables

Chapter 4	
Table 4.1. Electrophysiological maturation of Lpar1-GFP subplate neurons	**158**
Table 4.2a. Post-hoc comparisons for Membrane Properties	**159**
Table 4.2b. Post-hoc comparisons for Action Potential Properties	**159**
Table 4.3. Proportion of synaptic input onto Lpar1-GFP SPns per layer	**180**
Table 4.4. Total synaptic input onto Lpar1-GFP SPns per layer	**183**
Table 4.5a. Normalised layer post-hoc comparisons P0-P1	**186**
Table 4.5b. Normalised layer post-hoc comparisons P2-P5	**186**
Table 4.5c. Normalised layer post-hoc comparisons P6-P8	**186**
Table 4.6a. Raw layer post-hoc comparisons P0-P1	**187**
Table 4.6b. Raw layer post-hoc comparisons P2-P5	**187**
Table 4.6c. Raw layer post-hoc comparisons P6-P8	**187**
Table 4.7. Horizontal organisation of excitatory input onto Lpar1-GFP SPns	**191**
Chapter 5	
Table 5.1. Electrophysiological maturation of Lpar1-GFP interneurons	**210**
Table 5.2a. Post-hoc comparisons for Membrane Properties	**210**
Table 5.2b. Post-hoc comparisons for Action Potential Properties	**210**
Table 5.3. Proportion of total excitatory synaptic input onto Lpar1-GFP interneurons	**223**
Table 5.4. Proportion of total excitatory synaptic input as a function of distance from soma	**223**
Table 5.5. Proportion of total GABAergic synaptic input onto L4 spiny stellate neurons	**236**
Table 5.6. Total GABAergic synaptic input onto L4 spiny stellate neurons	**238**
Table 5.7. Proportion of total GABAergic synaptic input onto L4 spiny stellate neurons in ION-section vs Control groups	**242**
Table 5.8. Total GABAergic synaptic input onto L4 spiny stellate neurons in ION-sectioned vs Control groups	**243**

Abbreviations

4-AP	4-aminopyridine
5HT3aR	5-hydroxytryptamine receptor 3A
aCSF	Artificial Cerebrospinal Fluid
AMPA	α-Amino-3-hydroxy-5-methyl-4-isoxazolepropionic acid
AMPAR	AMPA receptor
ANOVA	Analysis of variance
APV	((2R)-amino-5-phosphonovaleric acid
BF	Basal forebrain
BrdU	Bromodeoxyuridine
CA1	Cornum ammonis 1
CB	Calbindin
cENO	Cortical early network oscillations
cGDPs	Cortical giant depolarising potentials
CGE	Caudal ganglionic eminence
ChR	Channelrhodopsin
ChR2	Channelrhodopsin 2
ChR65	Channerhodopsin 65
CP	Cortical plate
CR	Calretinin
CRACM	Channelrhodopsin-assisted circuit mapping
CSD	Current source density
CV	Coefficient of variation
DAPI	4',6-Diamidin-2-phenylindol
DIC	Differential interference contrast
DNA	Deoxyribonucleic acid
E16	Embryonic day
EEG	Electroencephalogram
Egins	Early-generated interneurons
EPSC	Excitatory post-synaptic current
EPSP	Excitatory post-synaptic potential
FS	Fast-spiking
GABA	Gamma-Aminobutyric acid
GDP	Giant depolarising potential
GE	Ganglionic eminence
GFP	Green fluorescent protein
GluR1	AMPA receptor subunit 1
HC	High-connectivity
HDC	High divalent cation
Hz	Hertz
IC	Internal capsule
ION	Infraorbital nerve
IPSC	Inhibitory post-synaptic current
ISI	Inter-stimulus interval

IUE	In utero electroporation
IZ	Intermediate zone
IZ	Intermediate zone
KA	Kainate
KAR	Kainate receptor
KCC2	potassium chloride symporter 5
L1	Layer 1
L2/3	Layer 2/3
L4	Layer 4
L5	Layer 5
L6	Layer 6
LC	Low-connectivity
LGE	Lateral ganglionic eminence
Lgins	Late-generated interneurons
Lpar1	Lysophosphatidic acid receptor
LSPS	Laser-scanning photostimulation
LTP	Long-term potentiation
M1	Primary motor cortex
M2	Secondary motor cortex
MC	Martinotti cell
MGE	Medial ganglionic eminence
ms	Millisecond
MUA	Multi-unit activity
mV	Millivolt
MZ	Marginal zone
NE	Neuroepithelial
NFS	Non-fast spiking
NGS	Normal goat serum
NKCC1	Sodium potassium chloride transporter
NMDAR	N-methyl-D-aspartate
NMDAR	NMDA receptor
NR1-3	NMDA receptor subunit 1-3
NS	Non-significant
OCT	Optimal cutting temperature embedding medium
P0	Postnatal day zero
pA	Pico ampere
PBS	Phosphate-buffered saline
PBST	PBS-Triton
POA	Pre-optic area
Pom	Posterior medial nucleus of the thalamus
PP	Preplate
PPR	Paired-pulse ratio
PSC	Post-synaptic current
PV	Parvalbumin
R(in)	Input resistance

RGCs	Radial glial cells
RMP	Resting membrane potential
S1	Primary somatosensory cortex
sCRACm	Subcellular channelrhodopsin-assisted circuit mapping
SP	subplate
Spike HW	Spike Half-width
SPn	Subplate neuron
SST	Somatostatin
STDP	Spike timing-dependent plasticity
TC	Thalamocortical
Thal	Thalamus
TTX	Tetrodotoxin
UV	Ultraviolet
V1	Primary visual cortex
VB	Ventrobasal nucleus of the thalamus
Vhold	Holding potential
VIP	Vasointestinal peptide
VPM	Ventro-posterior medial nucleus of the thalamus
VZ	Ventricular zone
WT	Wild-type
μm	Micrometer

1. Introduction

"I could be bounded in a nutshell, and count myself a king of infinite space, were it not that I have bad dreams."

William Shakespeare, Hamlet, Act II, Scene II

Apart from the skull of Yorick it is perhaps a stretch to imagine William Shakespeare ever peered through a cranium and contemplated the mystery of what lies within. Nevertheless, crack open a walnut shell and as a neuroscientist you'll be hard-pressed not to discern similarities between the edible seed and our dear object of study. Delicate dark veins line a complex symmetric surface of grooves and sulci strangely reminiscent of the neocortex. This is considered the newest evolutionary addition to the human brain and it encases the circuitry thought to underlie complex human cognitive abilities (Rakic, 2009). Equipped with a remarkable neocortex, we count ourselves kings of infinite space; its fine circuitry and dense interconnectivity permit us to perceive the world in high detail, plan, anticipate, imagine, remember. We travel extensively in a vast mental landscape of uncertain boundaries. This near limitless mindscape can prove treacherous to navigate and like the Prince of Denmark we too may have "bad dreams". Cognitive psychology posits that maladaptive cognitive schemata predispose individuals to disorders such as depression, and negative biases in cognitive processing can maintain them in that state (Kovacs & Beck, 1978; Beck & Clark, 1988). Delving into the biology of psychiatric and neurodevelopmental conditions, it is thought that malformations in circuits involving excitatory and inhibitory cells can give rise to debilitating conditions such as schizophrenia, autism or Fragile X syndrome (Gaspard & Vanderhaeghen, 2010; Rubenstein, 2010; Rico &

Marín, 2011; Marín, 2012). This is because the neocortex is not an undifferentiated mass of cells, but shows a very organised and balanced architecture, the hallmarks of which are laminar and columnar organisation (Douglas & Martin, 2004).

A short overview of the development of pyramidal neurons

The neocortex can be divided into several, historically 6-7 layers, on the basis of cell density and morphology (Cajal, 1907) and distinct cortical regions can be identified anatomically and functionally (Brodmann, 1909; Economo & Koskinas, 1929). Lamination is an important feature of the cortex that is tightly linked to developmental events (Gao et al., 2013). Most glutamatergic excitatory neurons arise from progenitor cells that lie in the ventricular zone of the dorsal telencephalon. The central nervous system differentiates from the neural tube and during the earliest stages of development it is composed of neuroepithelial (NE) cells (Breunig et al., 2011) which generate the first wave of postmitotic neurons. These then migrate radially and form the transient primordial plexiform zone or preplate (Marin-Padilla, 1970; 1971; 1978; Del Río et al., 2000). Throughout development, NE cells transform into radial glial cells (RGCs), which are an important population of neuronal progenitors in the dorsal telencephalon (Malatesta et al., 2000; Miyataet al., 2001; Noctor et al., 2001; Fishell & Kriegstein, 2003; Malatesta et al., 2003; Anthony et al., 2004; Noctor et al., 2004). These cells populate the ventricular zone (VZ) and each has a process that touches the ventricular wall and another that reaches the outer edge of the developing cortex (Figure 1.1).

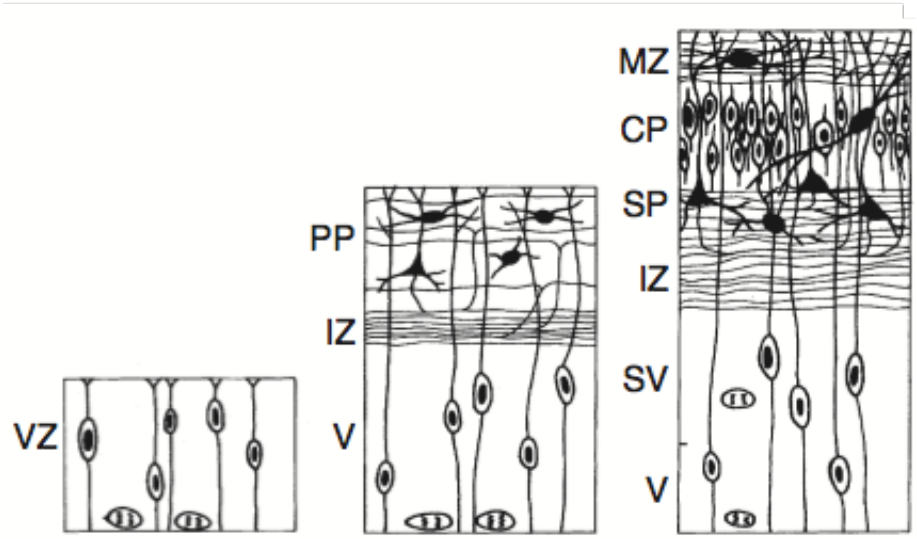


Figure 1.1. Migrating cortical plate neurons split the preplate into marginal zone and subplate. The three panels illustrate consecutive stages of embryonic development of the telencephalon. Early in development (left), progenitor cells in the ventricular zone (VZ) proliferate extensively. Postmitotic neurons then migrate radially past the fibrous intermediate zone (IZ) to the outer limits of the cerebral wall to form the preplate (centre). At later stages, newborn postmitotic neurons migrate along the processes of radial glial cells to form the cortical plate (CP), which splits the preplate into marginal zone (MZ) and subplate (SP). Modified after Parnavelas, 2000.

RGCs undergo extensive asymmetric division, maintaining the progenitor pool as well as generating post-mitotic neurons, which migrate along the scaffold provided by RGC processes. Migrating newborn neurons split the existing preplate into a superficial marginal zone (MZ) and the deep subplate (SP), forming the future cortex, the cortical plate (CP), in between them (Marin-Padilla, 1971; Luskin & Shatz, 1985; Osheroff & Hatten, 2009). Successive generations of newborn neurons migrate in an inside-out fashion forming layers 2-6 over earlier-born cells (Angevine & Sidman, 1961).

Order in cortical connectivity

The cortex is not only organised horizontally in layers, but also vertically, in columns. Vernon Mountcastle first introduced the concept of the "neocortical functional

column", following seminal observations that neurons sharing properties such as common peripheral receptors, receptive fields and spiking latencies to sensory stimuli were organised in a radial column spanning the entire cortical depth (Mountcastle, 1957; Powell & Mountcastle, 1959). These functional properties were similar for neurons located in the same column, but differed between adjacent columns (Mountcastle, 1997). The concept of a neocortical column gained great traction following the work of David Hubel and Torsten Wiesel in the cat visual cortex. In this system, neurons with similar orientation selectivity were organised in "orientation columns" detectable via single electrode penetrations, spanning cortical layers from the pial surface to the white matter (Hubel & Wiesel, 1962; 1963). The concept of neocortical column has greatly influenced research in circuit neuroscience and shaped the way we think about cortical information processing. However, cortical columns are defined based on functional properties of neurons, and a structural basis for such columns has proved elusive (Horton & Adams, 2005; da Costa & Martin, 2010). Recent research efforts have nonetheless provided evidence for lineage-dependent circuit assembly in the neocortex, bridging the gap between ontogenetic and functional columns (Yu et al., 2009; Li et al., 2012; Ohtsuki et al., 2012; Yu et al., 2012; Gao et al., 2013). Perhaps the best example of a functional neocortical column is located in the rodent primary somatosensory cortex. In L4 of this region, each whisker is represented by an aggregate of neurons organised in a barrel-shaped pattern (hence the designation of "barrel cortex"), with functionally-homogeneous thalamic afferents clustered at the centre (Woolsey & Van der Loos, 1970). Tactile whisker stimulation is processed somatotopically within the "barrel column", with deflection of a single particular whisker evoking neuronal activity in all layers of the corresponding column (Petersen, 2007). A barrel column could thus be defined by the

vertical span of the neocortex, laterally delimited by the width of the L4 barrel (Lefort et al., 2009).

Within a cortical column, neurons connect in precise fashion within and between layers. Based on electrophysiological and computational modelling studies in the cat visual cortex, Rodney Douglas and Kevan Martin came up with the influential notion of a "canonical cortical microcircuit", the idea that save for minor variations, a blueprint of local connectivity could be discerned and generalised across cortical sensory areas (Douglas et al., 1989; Douglas & Martin, 1991; 2004; 2007). After a wealth of circuit mapping studies elaborating the foundations of Douglas and Martin's work, we now have a good description of the local canonical excitatory pathways in the cortex (Figure 1.2) (Thomson, 2003; Douglas & Martin, 2004; Lübke & Feldmeyer, 2007; Thomson & Lamy, 2007; Lefort et al., 2009; Bastos et al., 2012; Hill & Greenfield, 2014).

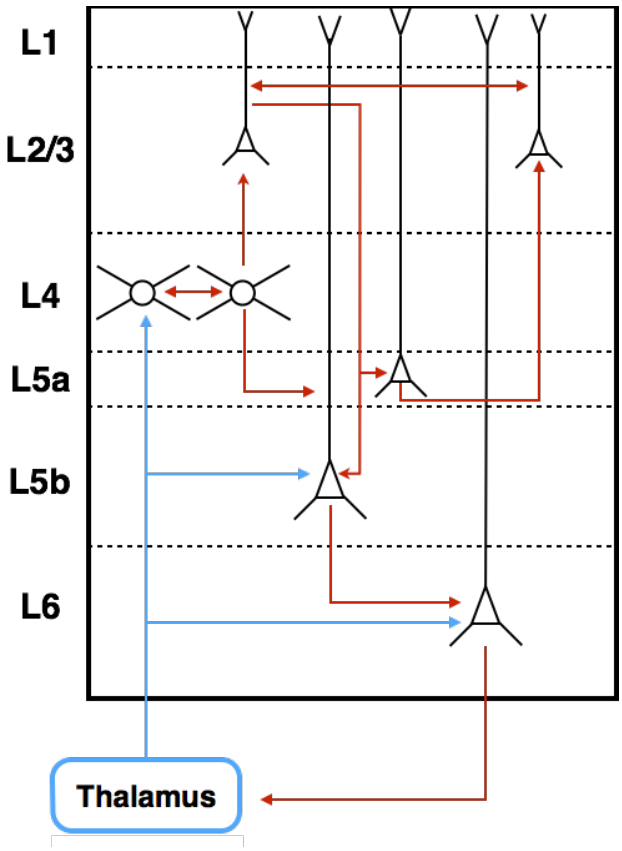


Figure 1.2. The canonical cortical circuit. Sensory information is relayed from the thalamus to L4 spiny stellate neurons, L5b and L6 pyramidal neurons. Neurons in L4 amplify thalamic input via a local recurrent excitatory network. Thalamic information is then distributed from L4 into L2/3 and L5a. Pyramidal cells in L2/3 form horizontal connections with excitatory neurons in their home layer, and relay sensory information into L5a and L5b. Pyramidal neurons in L5a provide excitation back into L2/3 while their L5b homologues project into L6, which sends feedback corticothalamic projections to primary sensory nuclei, closing the loop.

Thalamic relay neurons project mainly to L4, though they also target L5b and L6. Thalamic activation of L4 is amplified by a dense recurrent excitatory network. Activity in L4 is fed forward to L2/3 and L5a in columnar fashion, and within L2/3, pyramidal neurons form extensive horizontal connections with each other, as well as with pyramidal cells in L5. These neurons project to L6 and several subcortical targets, and L6 sends feedback excitation to primary thalamic sensory nuclei (Douglas & Martin, 2004; Lübke & Feldmeyer, 2007; Feldmeyer, 2012; Feldmeyer et al., 2012). Knowledge about the translaminar circuitry involving inhibitory interneurons has been progressing steadfast (Silberberg & Markram, 2007; Thomson & Lamy,

2007; Xu & Callaway, 2009; Kätzel et al., 2010) and it was recently discovered that despite greater cross-areal variation in motifs, this concept can also be applied to inhibitory connections to pyramidal neurons, and that these connections arise mostly from the home layer of each pyramidal neuron, though important translaminar connections exist (Kätzel et al., 2010). Excitatory and inhibitory connections to different interneurons in the same layer are highly cell-type specific and show marked diversity in laminar origin (Xu & Callaway, 2009), with inhibitory-inhibitory connections recently suggested to follow an elegant and reliable molecular logic (Pfeffer et al, 2013; Pi et al., 2013; Kepecs & Fishell, 2014; Pfeffer, 2014).

The developing neocortex: puzzle or house?

Despite great advances in our knowledge of the organization of columnar excitatory and inhibitory circuits (Lübke & Feldmeyer, 2007; Thomson & Lamy, 2007; Lefort et al., 2009; Kätzel et al., 2010; Feldmeyer, 2012), comparatively few studies have addressed how the canonical cortical circuit emerges (Dalva & Katz, 1994; Luhmann et al., 1999; Luhmann et al., 2000; Luhmann, et al., 2003; Ashby & Isaac, 2011; Anastasiades & Butt, 2012; Viswanathan, et al., 2012). It seems on this subject matter, amongst circuit neuroscientists a "back of the puzzle box" view abounds. A major objective of circuit neuroscience is to provide an accurate description of synaptic connectivity in the brain, but this endeavor seems to be proceeding under the tacit assumption that cortical circuits are assembled through piece-by-piece aggregation of their elements, much like a puzzle. Hence the analogy; looking at a puzzle box, one can observe the final result. Why bother mapping the intermediate steps of circuit construction? The problem with this view is that neural circuits develop under an environment that differs radically from the mature central nervous

system. For instance, GABA (gamma amino-butyric acid), the main inhibitory neurotransmitter in the adult brain, has been proposed to have a depolarizing action in the immature brain (Obata et al., 1978; Mueller et al., 1984; Ben-Ari et al., 1989; Blaesse, et al., 2009; Ben-Ari et al., 2012), and transient cell populations, circuits (Luhmann et al., 1999; 2003; Innocenti & Price, 2005; Kanold & Luhmann, 2010; Luhmann, et al., 2014) and activity patterns (Yang et al., 2009; Minlebaev, et al., 2011; Khazipov, et al., 2013; Yang et al., 2013b) play key roles in establishing cortical circuitry and function. Perhaps a more apt metaphor for neural circuit assembly is building a house. During construction there are transient support scaffolds and links between floors and rooms, besides workers and directing engineers that are absent from the final result.

To understand the formation of cortical circuits it is vital to examine the population/network and synaptic/circuit levels of analysis. Studying circuits enables us to understand the sequence of maturation of connectivity, whereas analysis of early network oscillations and signal flow informs scientists of the *in vivo* patterns of activity that promote the maturation of emerging circuits. The neonatal rodent has emerged as an excellent model for such experiments, as precise correspondence has been found between premature human EEG (electroencephalogram) and network activity in rodent neonates during the first postnatal week (Khazipov & Luhmann, 2006; Colonnese et al., 2010), and a variety of high-resolution recording and stimulation techniques are available to dissect emerging connectivity in rats and mice. In the following sections, I will review literature on early network activity patterns in the barrel cortex. I follow this up by examining the synaptic development of pathways of the excitatory cortical canonical circuit and exploring activity-dependent

emergence of AMPA (α-Amino-3-hydroxy-5-methyl-4-isoxazolepropionic acid) connectivity via NMDAR (N-methyl-di-aspartate receptor)-dependent mechanisms, delving into the concept of "silent synapse" and the fleeting, unstable nature of early AMPA connectivity. I then attempt to bridge the network and synaptic levels of cortical development, and propose the idea that early cortical networks contain privileged nodes that provide bedrocks of stability to fall back on. I conclude by exploring subplate neurons and certain GABAergic interneurons as candidates for such nodes. Curiously, consistent with the importance of SPns (subplate neurons) in the early organisation of cortical circuits, subplate-specific genes show significant associations with schizophrenia and autism (Hoerder-Suabedissen et al., 2013).

1.1. Network oscillations in the developing neocortex

Network activity patterns have been studied in the developing neocortex *in vivo* and *in vitro* using a variety of methods and preparations with widely differing spatial and temporal resolution (Ben-Ari, et al., 2004; Allène & Cossart, 2010; Kilb et al., 2011; Khazipov et al., 2013). Unsurprisingly, this has resulted in the identification of several different patterns of activity, some of which may represent manifestations of the same phenomenon observed under different technical conditions. Early activity patterns include spontaneous calcium transients observed in small cortical areas of around 100-200μm (Yuste et al., 1992; Kandler & Katz, 1998), spontaneous plateau assemblies (Crépel et al., 2007; Allène et al., 2008), cortical early network oscillations (cENOs) (Garaschuk et al., 2000; Corlew et al., 2004; Adelsberger et al., 2005; McCabe et al., 2006; Allène et al., 2008), cortical giant depolarising potentials (cGDPs) (Ben-Ari et al., 1989; Garaschuk et al., 1998; Crépel et al., 2007; Allène et al., 2008; Rheims et al., 2008) spindle bursts (Khazipov et al., 2004; Minlebaev, et al.,

2007, 2009; Sun & Luhmann, 2007; Yang et al., 2009; Golshani et al., 2009) early gamma oscillations (Yang et al., 2009; Minlebaev et al., 2011; Yang et al., 2013b;) and long oscillations (Yang et al., 2009).

These different activity patterns have been reported at different phases of development and show a diversity of mechanisms for their generation (Allène & Cossart, 2010). In spite of this bewildering variety, the two most discernible patterns of activity occurring *in vivo* in the neonatal rodent are spindle bursts and early gamma oscillations (Khazipov et al., 2004; Yang et al., 2009; Minlebaev et al., 2011; Yang et al., 2013b). Spindle bursts consist of rhythmic activity in the 5-25Hz frequency band that synchronise activity in a 200-400μm wide cortical column over a period of approximately 1 second (Sun & Luhmann, 2007; Yang et al., 2009; Yang et al., 2013b;). Gamma bursts are shorter (~200ms) periods of oscillatory activity in high frequencies (40-55Hz) that occur over approximately 200μm diameter cortical ensembles in the barrel field (Yang et al., 2009; Minlebaev et al., 2011; Yang et al., 2013b).

Spindle bursts

Khazipov and colleagues found that spindle bursts are triggered somatotopically via sensory feedback from neonatal muscle twitches, limb and body jerks (Khazipov et al., 2004). De-afferentiation or thalamic barreloid lesioning reduce the rate of occurrence of spindle bursts to approximately half, suggesting they can not only be triggered by sensory stimulation, but also occur spontaneously (Khazipov et al., 2004; Yang et al., 2009; Yang et al., 2013b;). In terms of neocortical circuitry, spindle bursts at P4-P7 are associated with major current sinks in the middle and deep layers,

as identified by current source density (CSD) analysis (Minlebaev et al., 2007; 2009), although experiments at P0-P2 clearly show participation of the subplate, with multiple unit activity in this layer preceding the spindle burst negative peak (Molnár et al., 2003; Yang et al., 2009). In support of this role, subplate stimulation can elicit spindle-like network activity in the cortical plate (Sun & Luhmann, 2007) and conversely, ablation of these cells decreased the incidence of spindle bursts by 80% (Tolner et al., 2012). At the synaptic level, whole-cell recordings from pyramidal cells at P1-P7 show that spindle bursts involve EPSCs (excitatory post-synaptic currents) coincident with the field potential response, followed by longer latency barrages of GABAergic PSCs (post-synaptic currents) that presumably effect delayed feedback inhibition (Minlebaev et al., 2007). This delayed, sensory-evoked GABAergic barrage is similar to events previously described in response to robust thalamic afferent stimulation in the neonatal slice (Agmon & O'Dowd, 1996). Pharmacological dissection has shown that the EPSC phase of the spindle burst consists of two components: a slow NMDAR-mediated delta wave with a superimposed AMPA/Kainate-based alpha-beta oscillation (Minlebaev et al., 2007; 2009). In contrast to the hippocampus, where early network activity (giant depolarising potentials, GDPs) is largely facilitated by depolarising GABA (Ben-Ari et al., 1989; Ben-Ari et al., 1997; Leinekugel, et al., 1997; Dzhala et al., 2005; Sipilä et al., 2006), in the neocortex $GABA_A$ receptor blockade prolongs the duration, increases the incidence, and augments the spatial extent to which spindle bursts propagate, suggesting that the function of GABA is to spatially and temporally restrict spindle burst propagation (Minlebaev et al., 2007; 2009).

Cholinergic network activity

In 2006, Dupont and colleagues studied used an *in vitro* whole-cortical preparation to study synchronised cortical network activity induced by bath application of carbachol, a cholinergic agonist (Dupont et al., 2006). The elicited network activity patterns showed similar frequency and duration to spindle bursts and synchronised a cortical column. At P0-P3, cholinergic network oscillations were independent of GABA and glutamate, but relied crucially on gap-junction coupling. After P5, cholinergic oscillations relied more on NMDA receptors and less on gap junctions. At the cellular level, ablation of subplate neurons at P0-P3 abolished cholinergic oscillations, and these were the only neurons consistently and sufficiently activated by carbachol to support oscillations at higher frequencies, indicating their critical involvement in this type of network activity (Dupont et al., 2006; Hanganu et al., 2009). At P0-P4, under calcium imaging, subplate and L6 neurons respond to cholinergic stimulation with a high degree of synchronous spiking activity, superior to that exhibited by L4 and cortical plate cells (Hanganu et al., 2009). In addition to burst firing, cholinergic stimulation induced in subplate neurons a long-lasting membrane depolarisation mediated by tonic GABA release (Hanganu et al., 2009). Work on the visual cortex *in vivo* established a link between cholinergic network oscillations and spindle bursts. Blockade of muscarinic receptors or lesioning of the cholinergic basal forebrain nucleus decreased the occurrence of spindle bursts in V1, whereas methods of cholinergic stimulation increased the incidence, amplitude and duration of these events (Hanganu et al., 2007). These results suggest that spindle bursts can occur spontaneously in an endogenous manner, in response to sensory stimulation, or driven by cholinergic neuromodulatory inputs. These three sources of drive presumably

activate the same endogenous cortical/thalamocortical oscillator, of which the subplate appears to be a major component.

Early gamma oscillations

Although the field has accrued an impressive amount of information on the cellular and circuit mechanisms of spindle bursts, early gamma oscillations have only recently gained prominence (Yang et al., 2009; Minlebaev et al., 2011; Yang et al., 2013b). Yang and colleagues characterised in the neonatal rodent a gamma rhythm, present from birth, with an average frequency of 38Hz and duration around 200ms, that within S1 could only be recorded in the barrel field and synchronised small cortical domains of around 200-400μm diameter (Yang et al., 2009). Principal whisker deflection evoked a gamma oscillation in the corresponding barrel column (Yang et al., 2009; Minlebaev et al., 2011; Yang et al., 2013b). At P0-P2, gamma power and current sinks were prominent in the SP, and multi-unit activity (MUA) in the SP preceded the negative peaks of each oscillatory cycle, showing the importance of the subplate in maintaining/transferring network activity (Yang et al., 2009; Yang et al., 2013b). Following this early timepoint, gamma activity is transferred onto L4, with multi-unit activity, gamma power and current sinks maximal in this layer by P2-P7 (Minlebaev et al., 2011). Throughout the P0-P7 period, MUA in the ventral posterior medial nucleus of the thalamus (VPM) was strongly coherent with cortical activity, reliably preceding cortical gamma (Minlebaev et al., 2011; Yang et al., 2013b). The thalamus plays a critical role in generating/relaying early gamma oscillations, as 1) electrolytic lesioning of thalamic barreloids abolished gamma bursts and gamma-containing spindle bursts, and 2) electrical stimulation of barreloids resulted in gamma oscillatory activity in the corresponding cortical barrels (Yang et al., 2013b).

Although afferent input to the thalamus cannot be excluded as a source of gamma, intra-thalamic blockade of inhibition resulted in abolishment of activity, suggesting the early gamma oscillator could be a circuit involving the VPM and the thalamic reticular nucleus (Minlebaev et al., 2011). Moreover, temporary de-afferentiation of corticothalamic afferents decreased the rate of occurrence of early gamma oscillations, suggesting early corticothalamic axons could have a critical role in the circuit (Yang et al., 2013b). Interestingly, SPns have been proposed to pioneer this pathway, and possibly innervate the thalamic reticular nucleus, though more experiments are required to functionally characterise this pathway and determine the precise order of functional engagement of thalamic nuclei by L5, L6 and SP axons (McConnell et al., 1994; Grant et al., 2012).

Gamma frequency EPSCs disappeared transiently from L4 at P8 but re-emerged around P12. It has been suggested that early (prior to P8) and mature (post-P12) gamma oscillations are mechanistically distinct, with early gamma oscillations obeying a thalamic oscillator that drives thalamic barreloid and cortical barrel synchrony, whereas post-P12 gamma synchronises activity across columns horizontally and results from feed-forward perisomatic inhibition (Bartos et al., 2007; Fries, 2009; Wang et al., 2010; Whittington et al., 2011). Consistent with this hypothesis, at P2-P5, blockade of GABAergic transmission did not modify gamma oscillations, but strongly reduced them after P6. After P6, IPSCs in L4 began showing gamma rhythmicity (Minlebaev et al., 2011). These observations fit well with the fact that L4 fast-spiking (FS) interneurons are only engaged by thalamic input at P6-P8, and form connections with L4 excitatory neurons at this same timepoint (Daw et al., 2007a).

What could be the function of early gamma oscillations? Thalamic MUA was strongly coherent with its cortical equivalent, and thalamic units reliably fired shortly before cortical ones (Minlebaev et al., 2011; Yang et al., 2013b). During gamma oscillations, thalamocortical binding was maintained for around eight cycles, replaying sensory inputs multiple times at the thalamocortical synapse, and pairing of artificially-generated gamma-rhythmic subthreshold thalamic inputs with granular action potentials resulted in LTP (long-term potentiation) of the thalamocortical EPSP (excitatory post-synaptic potential) in slices (Minlebaev et al., 2011). Synchronisation of thalamic and cortical activity by early gamma oscillations could promote temporal summation of thalamic inputs onto L4 cells within an appropriate time window and support developmental thalamocortical plasticity (Minlebaev et al., 2011; Yang et al., 2013b). Spindle burst oscillations could perform a similar role in the maturation of canonical cortical excitatory circuitry, promoting correlated, temporally organised activity between pre and post-synaptic elements of the circuit. Having reviewed how population/network activity may support the wiring of early thalamocortical and intracortical circuits, in the next section I will examine mechanisms of developmental plasticity of cortical circuits at the synaptic level.

1.2. The assembly of cortical excitatory circuits

The thalamocortical synapse

The first postnatal week is a critical juncture in the development of whisker representation in the rodent primary somatosensory cortex (Erzurumlu & Gaspar, 2012). During this period, thalamic axons invade the cortex and form layer-specific synapses with excitatory and inhibitory neurons including spiny stellate neurons in L4

around P2-3 (Agmon et al., 1993; López-Bendito & Molnár, 2003; Erzurumlu & Gaspar, 2012). Shortly thereafter, between P3 and P5, it is possible to observe the characteristic barrel pattern (Woolsey & Van der Loos, 1970) in L4 (Erzurumlu & Gaspar, 2012). Sensory experience strongly modulates body map formation during the first postnatal week, and as such this period can be referred to as the critical period for somatosensory map development (Erzurumlu & Gaspar, 2012). Indeed, manipulation of sensory receptors or afferent nerve pathways prior to P4 results in permanent disruption of this patterned organisation of cytoarchitecture (Van der Loos & Woolsey, 1973), as does pharmacological or genetic ablation of cortical NMDAR function (Iwasato et al., 2000; Datwani et al., 2002; Lee et al., 2005). Concurrent to structural plasticity, it has been shown that, during the critical period, thalamocortical synapses possess the ability to undergo NMDAR-dependent synaptic plasticity via long-term potentiation (Crair & Malenka, 1995; Isaac et al., 1997). *In vitro,* this ability is limited to the period comprised between P3 and P8 (Crair & Malenka, 1995) (Figure 1.3), and this finding has recently gathered strong support *in vivo*, with An and colleagues reporting that LTP can be induced by repetitive whisker stimulation between P0 and P8, and that this plasticity is layer-specific, depending on age (An et al., 2012). At P0-P1, potentiation of the CSD sink could be seen in the cortical plate and deep layers, though not the subplate. At P3-P5, strong LTP was observed in L4 and lower L2/3, but not any other layers (An et al., 2012), consistent with the emergence of thalamic-driven early gamma activity in this layer (Minlebaev et al., 2011; Yang et al., 2013b). These results suggest an "outside-in" maturation of thalamocortical inputs, consistent with the progress of innervation evidenced by thalamic axons in the cortex (Agmon et al., 1993; López-Bendito & Molnár, 2003). Interestingly, even though the subplate is the first layer to receive thalamic contact

(Friauf et al., 1990; Friauf & Shatz, 1991; Higashi et al., 2002; Molnár et al., 2003), LTP of thalamic inputs onto this layer was not examined in the original work of Crair (Crair & Malenka, 1995) and could not be found by others *in vivo* or *in vitro* (An et al., 2012). This was in spite of the fact that at least in a subset of recorded SPns, thalamic inputs activate GluN2B-containing NMDARs (Hanganu et al., 2002).

Subsequent efforts sought to identify the mechanisms behind potentiation of thalamic inputs onto L4. Isaacs and colleagues found evidence that a significant proportion (43% at P4-P5) of thalamocortical synapses in L4 are silent, that is, they express NMDARs in the absence of any detectable AMPAR contribution (Isaac et al., 1995; Isaac et al., 1997; Isaac, 2003). LTP induction by pairing afferent stimulation with post-synaptic depolarisation led to the appearance of AMPA-mediated responses ("unsilencing", Figure 1.3) (Isaac et al., 1997). Accordingly, the proportion of silent synapses showed a prominent decrease throughout development, such that by P8, the end point for thalamocortical critical period plasticity (Crair & Malenka, 1995; An et al., 2012;), no silent synapses could be detected (Isaac et al., 1997).

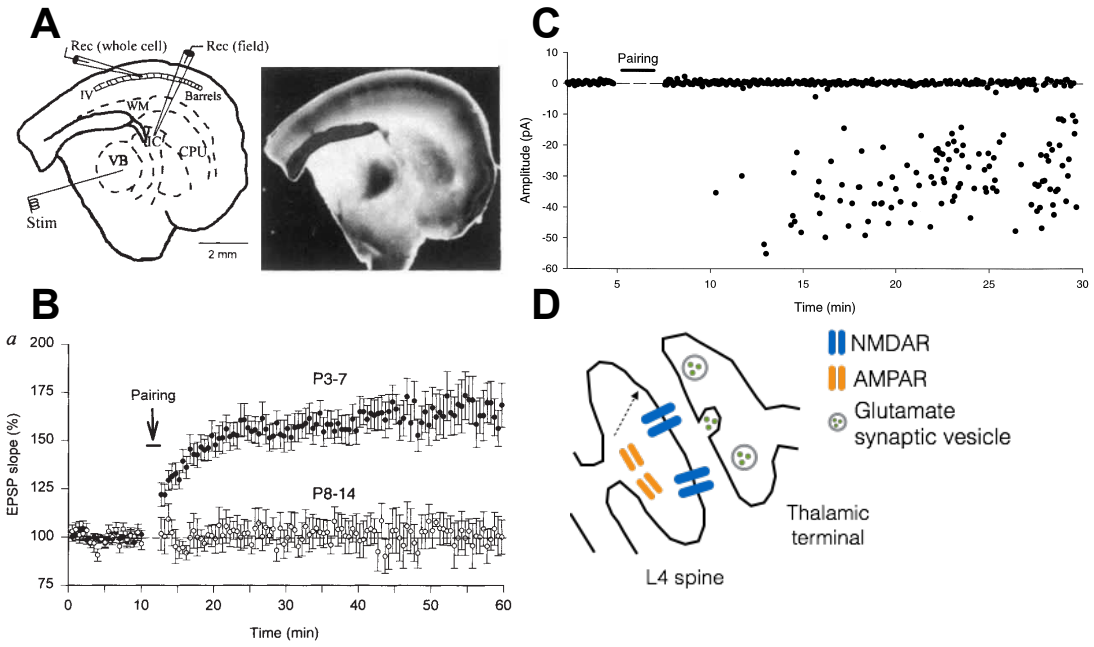


Figure 1.3. Plasticity at the thalamocortical synapse. A. Schematic of experimental setup. **B.** LTP at the thalamocortical synapse can be induced at P3-P7 but not after P8. **C.** Induction of LTP at a silent synapse. **D.** Schematic of a silent thalamocortical synapse. **A** and **B** taken from Crair & Malenka, 1995. **C** taken from Isaac et al., 1997.

This raises the question as to how silent, NMDAR-containing synapses could be sufficiently depolarized in order to enable LTP (Figure 1.4). One hypothesis stemmed from the observation that thalamic afferent stimulation evoked a dual AMPA-Kainate EPSC in L4 cells, but that these events were never observed at the same synapse. Moreover, Kainate receptor currents were greatly downregulated throughout development (Kidd & Isaac, 1999). This led to the suggestion that Kainate receptors could provide early depolarization for NMDA activation to occur, and would eventually be replaced by AMPA receptors (Kidd & Isaac, 1999; Bannister, 2005; Daw et al., 2007b). These studies do not however address the question of where putative Kainate inputs originate from, nor do they acknowledge the involvement of the subplate in the early thalamocortical circuit. Another possible source of depolarisation for unsilencing of the thalamocortical synapse is based on a circuit involving the subplate (Kanold, 2004; Kanold & Luhmann, 2010), consistent with its

important role in early gamma oscillations (Yang et al., 2009; Yang et al., 2013b). Subplate neurons receive early, robust thalamic input (Friauf & Shatz, 1991; Higashi et al., 2002; Molnár et al., 2003) and can relay this input to L4 before thalamic axons innervate it (Friauf & Shatz, 1991; Higashi et al., 2002; Molnár et al., 2003; Zhao et al., 2009). It is possible that early in development, thalamic input is amplified in the subplate via recurrent glutamatergic and gap junction connectivity (Hanganu et al., 2002; Dupont et al., 2006; Hirsch & Luhmann, 2008) and relayed to L4, aiding activation of this layer by weak thalamic inputs and resulting in heterosynaptic potentiation of the thalamocortical synapse (Kanold, 2004; Kanold & Luhmann, 2010).

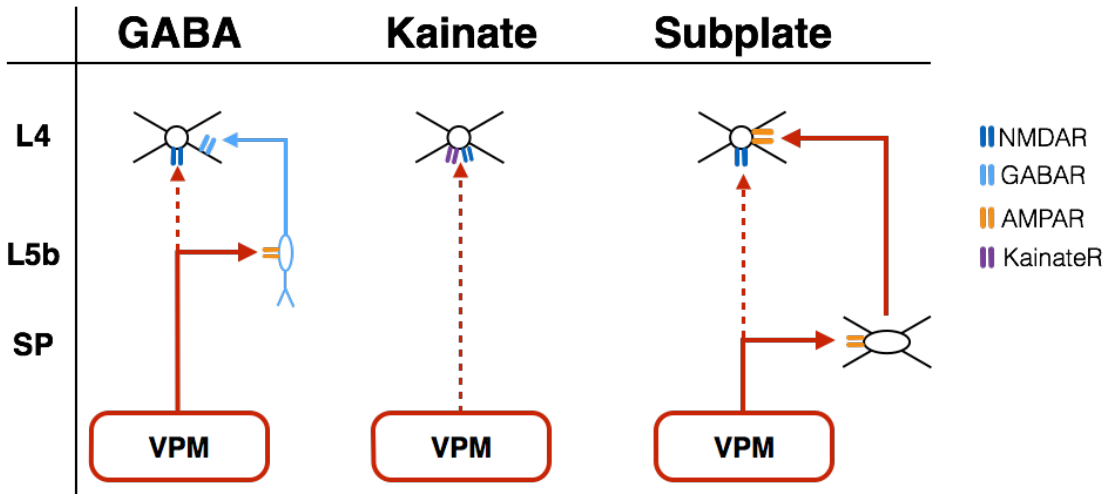


Figure 1.4. Possible mechanisms for thalamocortical synapse unsilencing. Left, Ventro-posterior medial (VPM) thalamic inputs may activate early thalamo-recipient deep-layer interneurons (blue cell). Synaptic GABA release from such cells onto L4 spiny stellate neurons could act to depolarize the cells to activate NMDA receptors at silent synapses engaged by immature thalamic inputs onto L4. Centre, spiny stellate neurons in L4 could be depolarized by early thalamic inputs onto Kainate receptors, which would result in activation of NMDA receptors and ensuing plasticity processes resulting in AMPA receptor insertion (Kidd & Isaac, 1999). Right, SPns receive robust thalamic input and project to L4 at a point when thalamic inputs to this layer are immature. Thalamic inputs onto SPns could activate these neurons strongly, and they would then depolarize L4 spiny stellate neurons sufficiently for L4 NMDA receptors to be coincidently activated by pre-synaptic thalamic glutamate release and post-synaptic L4 depolarisation, resulting in heterosynaptic induction of LTP (Kanold, 2004; Kanold & Luhmann, 2010).

Consistent with this hypothesis, thalamic stimulation resulted in short-latency responses in the subplate and long-latency responses in L4 (Friauf & Shatz, 1991; Higashi et al., 2002; Molnar et al., 2003) and selective subplate lesions prior to thalamic axon arrival at L4 result in immature thalamocortical synapses and absence of barrel organisation in the whisker somatosensory cortex (Kanold, 2003; Tolner et al., 2012). Moreover, this perspective fits with the developmental re-arrangement of thalamic-driven activation from the subplate to L4 suggested by previous reports (Friauf & Shatz, 1991; Higashi et al., 2002; Molnár et al., 2003; Yang et al., 2009; Yang et al., 2013b) (Figure 1.5). These data posit an important role for subplate neurons in the transfer of thalamocortical information to L4, suggesting this layer could act as a functional template for thalamic patterning of L4 (Grossberg & Seitz, 2003; Kanold, 2004; 2009; Kanold & Luhmann, 2010). One final source of depolarisation for L4 cells during thalamocortical maturation could be GABA (Ben-Ari et al., 1997; Hanse et al., 1997; Leinekugel et al., 1997; Wang & Kriegstein, 2008; Chancey et al., 2013). L4 spiny stellate cells are indeed on the receiving end of very powerful thalamic-driven local GABAergic input (Sun et al., 2006; Cruikshank et al., 2007; Daw et al., 2007a). However, GABAergic interneurons in L4 are only engaged by thalamic inputs late in the critical period (P6-P7), and as such appear unsuited for this task (Daw et al ., 2007a; Chittajallu & Isaac, 2010). This does not exclude that interneurons in other thalamorecipient layers, namely the earlier-maturing L5b/6, could not perform such a role, and this is a hitherto unexplored possibility.

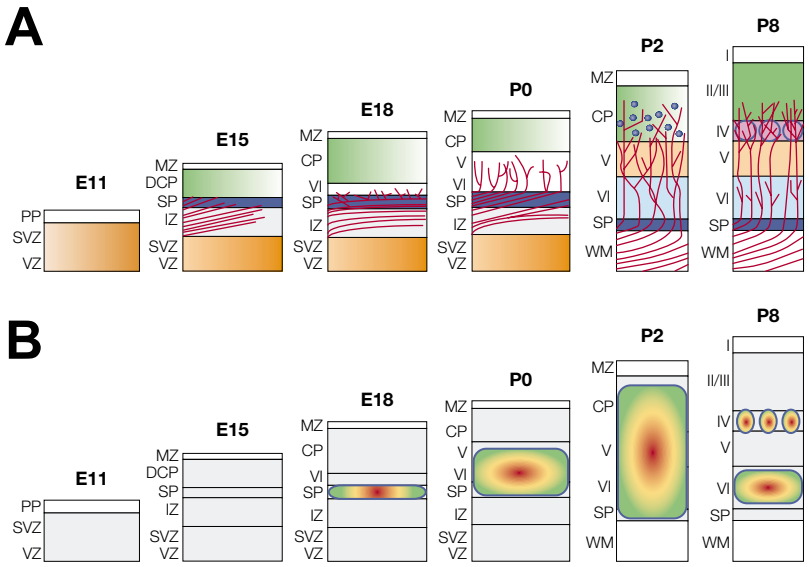


Figure 1.5. A. Maturation of cortical lamination and thalamic axon ingrowth. The first interactions and synaptic contacts between thalamic afferents and the cortex can be detected at the subplate (SP) around E15. At P0, thalamic axons have started innervating the deep cortical layers. At P2, the middle cortical plate (CP) is starting to differentiate into L4, and to be innervated by thalamic afferents. By P8, the mature barrel pattern can be observed in L4 and thalamic axon ingrowth is largely mature-like. **B. Maturation of cortical activation by thalamic afferent stimulation recorded optically using voltage-sensitive dyes.** Already at E18, stimulation of thalamic nuclei can elicit sustained depolarisation in the subplate. At P0, this depolarisation reaches the deep cortical layers, and at P2, spans most of the cortex. At P8, the mature pattern of activation can be observed, with thalamic stimulation depolarising L4 and L6. Taken from López-Bendito & Molnár, 2003.

The L4 recurrent excitatory network

Downstream to afferent thalamic input, L4 contains a powerful recurrent excitatory network that acts to amplify incoming thalamic inputs (Feldmeyer et al., 1999; Petersen & Sakmann, 2000; Lefort et al., 2009). Ashby and colleagues examined how this network is established in the barrel cortex (Ashby & Isaac, 2011). During the first postnatal week, the rate of connectivity between L4 spiny stellates is very low (approximately 4%). At P9, there is a 3-fold increase in probability of connection (to approximately 12%), concurrent to a sharp increase in spinogenesis and dendrite length. Trimming the whiskers prevents the developmental increase in connectivity. Interestingly, the development of EPSC amplitude, dendrite length and spine number

progresses normally after whisker deprivation, proving that these changes are genetically-driven or at least not altered by early sensory driven activation patterns. The one alteration induced by whisker trimming that explained the reduction in connectivity was an increased number of silent synapses concomitant to a reduction in AMPA-mediated currents. Conversely, no alteration was found in amplitude or connection probability for NMDA synapses (Ashby & Isaac, 2011). Ashby and colleagues' results suggest that NMDAR-mediated synaptic connections develop via experience-independent mechanisms and that sensory experience recruits AMPARs to these synapses to produce functional circuits.

Feed-forward excitation in the L4-L2/3 pathway

At mature stages, thalamic information processed in L4 spreads to L2/3 in a columnar fashion (Petersen, 2007; Lefort et al., 2009; Feldmeyer, 2012). Bender and colleagues studied the development of this feed-forward pathway by filling L4 spiny stellate neurons with biocytin and studying their axonal arborisations in L2/3 (Bender et al., 2004). At P6-P11, cells extended large numbers of branches into neighbouring columns across rows, and growth patterns appeared undirected. Topographic refinement occurred such that in mature animals (P14-P26), L4 axons were mainly restricted to the barrel-defined column in L2/3. Initial overarborisation was modest, and refinement occurred not by pruning of connections, but instead by selective addition/retention of axons within the home barrel column and growth of barrel columns relative to axon arbors (Bender et al., 2004). Using glutamate uncaging, Bureau and colleagues found that L2/3 pyramidal neurons already received barrel-constrained input from L4 at P8 (Bureau et al., 2004). Net input from L4 increased between P8 and P16, consistent with the critical period of plasticity for the L4-L2/3

synapse (Wen & Barth, 2011). Moreover, whisker deprivation significantly decreased input from L4 to L2/3 (Fox, 1992; Shepherd et al., 2003). Horizontal connections between L2/3 pyramidal cells also increased at P8-P16. This, similar to the findings of Bender and colleagues, argues against transient hyperconnectivity. In terms of axonal morphologies, L4 axonal density in L2/3 increased monotonically between P8 and P16. The horizontal, cross-whisker row spread of axons remained constant throughout development, suggesting that similar to functional synaptic input, L4 axons grow into L2/3 in a precise and directed fashion. These findings predict that L2/3 should show precise whisker receptive fields early on. Indeed, using *in vivo* whole-cell patch-clamp, sensory-evoked EPSCs could be detected at P8, and came under the form of barrages of events occurring throughout 100ms after stimulus onset. The whisker producing the largest response was the anatomically-defined principal whisker (PW), with EPSCs decreasing in amplitude and increasing in latency with distance from the PW (Bureau et al., 2004). These results refine and extend previous observations with sharp electrodes, where mature receptive field organisation in L2/3 was found to arise monotonically, in columnar fashion, between P12 and P16 (Stern et al., 2001).

The L2/3-L5 pathway

Following the canonical cortical circuit, activation of L2/3 pyramidal neurons propagates horizontally in L2/3 and vertically to L5 (Lübke & Feldmeyer, 2007; Petersen, 2007; Lefort et al., 2009). Anastasiades and Butt used glutamate uncaging to study the early development of the L2/3-L5 pathway (Anastasiades & Butt, 2012). Prior to P5, no consistent AMPAR-based synaptic connectivity could be detected for L5 pyramidal neurons. At P5-P8, the dominant input arose from L5, suggesting local recurrent networks are formed prior to interlaminar inputs, with L2/3 inputs emerging

subsequently. Total excitatory synaptic input to L5 pyramidal neurons underwent a gradual increase over the first 2 postnatal weeks, and after P12 most neurons showed a focused pattern of inputs. The authors also mapped afferent input activating NMDA receptors of L5 pyramidal cells at P8-P16. Interestingly, NMDA-driven input at P8 was highly skewed towards L2/3, whereas at P16 no bias in laminar input provenance could be observed. Moreover, whereas NMDAR-driven input accounted for a significant proportion of synaptic input points at P8 (27%), this number was greatly reduced by P16 (4%). Anastasiades and Butt then found that in early (<P12) but not late preparations (P13-P21), periods of increased network activity resulted in an enhancement of total synaptic input when remapped under quiescent conditions. Moreover, new synaptic inputs often originated distally from L2/3, consistent with the predominance of NMDAR-mediated synaptic inputs originating from this layer at early periods. Their results suggest that NMDAR-containing putative silent synapses form templates that predict the canonical circuit, and that periods of correlated activity can "unmask" these inputs (Anastasiades & Butt, 2012).

Experience and activity-dependent unsilencing of NMDAR-expressing synapses seems to be a ubiquitous mechanism for the maturation of synaptic connectivity in the neocortex and emergence of the canonical circuit (Crair & Malenka, 1995; Isaac et al., 1997; Shepherd et al., 2003; Clem et al., 2008; Ashby & Isaac, 2011; Wen & Barth, 2011; Anastasiades & Butt, 2012). It remains to be explored whether NMDARs are expressed precisely through predictive templates consistent with the future canonical circuit, which emerges by strengthening of these synapses, or whether they are expressed ubiquitously at post-synaptic cells, and the canonical circuit emerges by fine-scale pruning of erroneous silent connections (as opposed to

large-scale axonal remodelling) and strengthening of correct, canonical pathways. It has recently been shown that clonally-related pyramidal neurons preferentially develop early (P1-P2) electrical connections (Yu et al., 2012), and, later in development (P10-P15), are more likely chemically connected between themselves than with unrelated pyramidal cells (Yu et al., 2009). Thus, shared clonal origin could provide an additional mechanism for the wiring of the canonical cortical circuit. In this chapter I shall focus on the concept of the silent synapse, which will be elaborated in the next section.

1.3. AMPA-silent synapses and cortical development

NMDA receptors

Glutamate is the major excitatory neurotransmitter in the brain and, in most cortical synapses, acts predominantly on AMPA and NMDA receptors (Cull-Candy & Leszkiewicz, 2004). AMPA receptors are tetramers composed of several combinations of four different subunits (GluR1-GluR4) and they are involved in fast glutamatergic transmission. NMDA receptors are also tetramers, assembled in most cases from two NR1 and two NR2 subunits, although NR3 subunits (NR3A and NR3B) have also been described (Cull-Candy et al., 2001; Cull-Candy & Leszkiewicz, 2004; Cull-Candy, 2007). The NR2 subunits comprise a family (NR2A, NR2B, NR2C and NR2D), and expression of different NR2 subunits in a NMDA receptor confers distinct biophysical and pharmacological properties, including affinity for glutamate, modulation by glycine, sensitivity to Mg^{2+}, Ca^{2+} current magnitude and channel kinetics (Cull-Candy et al., 2001; Cull-Candy & Leszkiewicz, 2004; Cull-Candy, 2007). NMDARs are especially notable for three properties:

voltage-dependent block of the ion channel by Mg^{2+}, high calcium permeability, and slow rise and decay times conferred by specific NR2 subunit expression. The first property confers to the NMDAR the ability to act as a molecular coincidence detector. In order to conduct current, NMDARs require not only binding of glutamate, but also sufficient post-synaptic depolarisation for the Mg^{2+} blockade of their ion channel to be relieved. Therefore, NMDAR activity effectively signals temporally-correlated pre and post-synaptic activity. The second property, high Ca^{2+} permeability, contributes to a cascade of intracellular signalling events that can trigger plasticity processes such as LTP or LTD (long-term depression) (Lisman, 1989). The third property specifies the time window during which NMDARs can detect pre- and post-synaptic activity coincidence. Depending on the specific NR2 subunits expressed, deactivation times vary over a ~50-fold range, from NR2A (fastest, ~100-200ms) to NR2D (slowest, 4-5s), and therefore subunit expression can to a large degree influence the threshold of plasticity (Cull-Candy et al., 2001; Cull-Candy & Leszkiewicz, 2004; Cull-Candy, 2007). In fact, a ubiquitous developmentally-regulated NR2B to NR2A subunit switch has been reported in the developing neocortex, and has been suggested to contribute to closure of critical periods of plasticity although several other factors are likely to influence this process (Yashiro & Philpot, 2008). At the very least, the NR2B to NR2A subunit switch results in a reduction in duration of the coincidence-detection window for plasticity. More than an absolute closure of critical period plasticity, this implies an elevation in the temporal precision threshold of plasticity induction, requiring tighter temporal correlations in afferent activity and post-synaptic depolarisation that are characteristic of more mature circuits.

AMPA-silent synapses

The key properties highlighted above place NMDA receptors at the centre stage for activity-dependent modification of excitatory synaptic weights in the central nervous system. This capability is fundamental not only for dynamic and plastic encoding of information and memory (Morris, 2006), but also for the formation and maturation of excitatory synapses in the developing brain (Katz & Shatz, 1996; Cull-Candy et al., 2001; Daw, Scott, & Isaac, 2007b; Kerchner & Nicoll, 2008; Yashiro & Philpot, 2008). The concept of "silent synapse" has become a central tenet of developmental plasticity, and originated in the mid-1990s. Kullman observed that the coefficient of variation of the AMPA/Kainate receptor mediated EPSC ($CV_{A/K}$) is consistently larger than that of the NMDA component (CV_{NMDA}) and that LTP induction is associated with a reduction in $CV_{A/K}$, but no change in CV_{NMDA}. Based on these results and quantal analysis, Kullman proposed that whereas NMDARs are present at all active glutamatergic synapses, AMPA/Kainate receptors are present and functional only at a certain fraction of these (Kullmann, 1994). Convergent work from three groups arrived at the finding that it was possible to isolate synapses that yielded no detectable EPSC at resting membrane potential but revealed an NMDA-mediated component at depolarised potentials (Isaac et al., 1995; Liao et al., 1995; Durand & Konnerth, 1996). Following LTP induction using a pairing protocol, an AMPA component emerged, suggesting conversion from a "silent" to functional synapse (Isaac et al., 1995; Liao et al., 1995; Durand & Konnerth, 1996). Although initial reports were confined to the hippocampus, silent synapses with similar characteristics were subsequently reported at the thalamocortical synapse of the barrel field (Isaac et al., 1997) and at synapses between pyramidal neurons in visual cortex (Rumpel et al., 1998; Rumpel et al., 2004). Moreover, several reports showed that the prevalence of

silent synapses is consistently higher earlier in development, and that these synapses are present in very low numbers in the mature brain (Durand & Konnerth, 1996; Liao & Malinow, 1996; Isaac et al., 1997; Hsia et al., 1998).

AMPA-silent versus AMPA-labile synapses

Synapse unsilencing presents an appealing mechanism for circuit assembly. It is possible that glutamatergic synapses are formed without AMPA receptors and that, following correlated pre and post-synaptic activity and NMDAR activation through other mechanisms, AMPA receptors are inserted, such that synapse formation/strengthening is favoured between neurons that fire together. Evidence from immunohistochemical studies has been contradictory: some found evidence for lack of AMPA receptors at nascent synapses (Gomperts et al., 1998; Liao et al., 1999; Pickard et al., 2000; Liao et al., 2001), whereas others reported a constant AMPA/NMDA ratio throughout development (Lissin et al., 1998; Rao et al., 1998;Hohnke et al., 2000; Washbourne, Bennett, & McAllister, 2002; Voigt et al., 2005;). Differences in subunit-specific staining, antibodies used and detection criteria for expression likely influenced the results. Resolution of this issue came from functional assays. Within minutes to hours of initial synaptic contact, it has been shown that glutamatergic synapses are equipped with both AMPARs and NMDARs (Friedman et al, 2000; Okabe et al., 2001; Washbourne et al., 2002; Bresler et al., 2004; Zito et al., 2009). Moreover, studies examining spontaneous excitatory transmission under TTX (tetrodotoxin) found similar proportions of AMPAR-mediated and NMDAR-mediated miniature EPSCs, meaning detection of AMPA signalling at nascent synapses depends on whether spontaneous or evoked EPSCs are analysed, and that the mode of signalling at emerging glutamatergic synapses is dual

rather than silent (Groc et al., 2002; Myme et al., 2003; Xiao et al., 2004). These apparently contradictory findings can, however, be reconciled. It has been proposed that at newly-born glutamatergic synapses AMPA signalling is not stable, but can easily switch between two states, independently of NMDA and metabotropic glutamate receptors: a silent state and a labile state, where AMPA receptors are absent or present in the membrane, respectively. Correlated pre- and post-synaptic activity and NMDAR activation could then transfer a synapse from this switching behaviour to a stable, AMPA-mature state (Figure 1.6) (Groc et al., 2006; Hanse et al., 2009; Hanse et al., 2013).

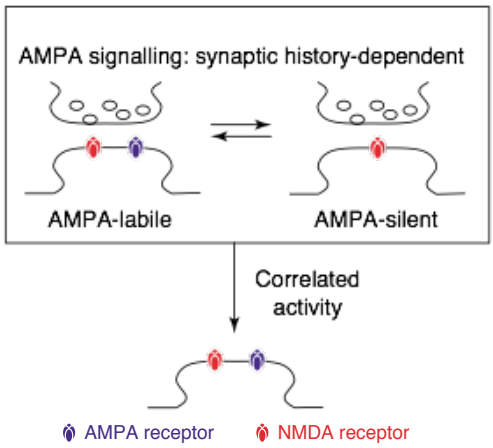


Figure 1.6. Model for labile AMPA signalling in the developing brain. Early glutamatergic synapses can switch, based on synaptic history, between AMPA-silent and AMPA-labile states. Correlated pre- and post-synaptic activity stabilises AMPA synapses and prevents AMPA silence. From Groc et al., 2006.

Several lines of evidence support this model in the developing brain. It has been found that while inactive synapses retain AMPA signalling capabilities, sporadic synaptic activity at low test frequencies can render a synapse AMPA silent, while NMDA signalling is unaffected (Xiao et al., 2004; Abrahamsson et al., 2005; 2007). After silencing, a synapse can regain AMPA signalling by prolonged inactivity (Abrahamsson et al., 2007) or NMDAR-dependent induction of LTP (Liao et al.,

1995; Isaac et al., 1995; Durand & Konnerth, 1996; Abrahamsson et al., 2008;). However, whereas LTP induction stabilises and protects a synapse from subsequent silencing (Abrahamsson et al., 2008), unsilencing induced by inactivity maintains the synapse in labile state, meaning it can revert to silence (Abrahamsson et al., 2007). This silent-to-labile switching behaviour of AMPA synapses decreases with development (Abrahamsson et al., 2005; 2007; 2008). In addition to the aforementioned studies from Eric Hanse's laboratory, there are inconsistencies between *in vivo* and *in vitro* data that could be explained by the labile AMPA synapse model. For instance, the developing thalamocortical synapse has recently been proven to support oscillatory activity in the gamma frequency range (Minlebaev et al., 2011; J. W. Yang et al., 2013b). In contrast, *in vitro* studies of neonatal thalamocortical transmission, including my own observations (see Chapter 4), have found it necessary to use very low stimulation frequencies (0.033 to 0.33Hz) to avoid fatiguing, and in many cases, abolishing transmission, at moderate frequencies (Crair & Malenka, 1995; Agmon et al., 1996; Gil & Amitai, 1996; Isaac et al., 1997; Gil et al., 1999; Zhao et al., 2009; Tolner et al., 2012). It may be that this "fatigue" effect at moderate test frequencies corresponds in fact to AMPA silencing (Xiao et al., 2004). Likewise, using glutamate uncaging, my own personal observations and previous reports in the lab (Anastasiades & Butt, 2012) show that AMPA-mediated synaptic responses are rare in pyramidal neurons before P5, even though previous *in vivo* work has shown that it plays a crucial role (albeit at unspecified, possibly thalamocortical synapses) in the propagation of early network oscillations (Minlebaev et al., 2007; 2009). Interpreting these observations in the light of the labile AMPA theory, it is well known that during early postnatal development, cortical neurons are exposed to periods of correlated activity (Khazipov et al., 2004; Dupont et al., 2006; Yang et al.,

2009) that are predicted by this theory to promote AMPA stabilisation (Groc et al., 2006; Hanse et al., 2009; 2013). Upon slicing the brain, such activity patterns are greatly compromised, leaving the cortex in an activity environment unfavourable to AMPA stabilisation that may in fact result in underestimation of AMPA contribution to early glutamatergic synaptic activity (Anastasiades & Butt, 2012). Functional lability constitutes an additional layer of plasticity in the neonatal brain which allows neurons to constantly survey their synaptic milieu and quickly and reversibly modulate connectivity, eventually retaining only those inputs which consistently produce post-synaptic responses (Groc et al., 2006; Hanse et al., 2009; 2013).

Early network activity, canonical circuit formation and labile AMPA synapses

Typically, synapse unsilencing is produced in the slice preparation by repeatedly pairing afferent stimulation with post-synaptic depolarisation. What activity patterns could produce appropriate correlations between afferent presynaptic activity and postsynaptic depolarisation *in vivo*? Endogenous network activity is a ubiquitous feature of maturing neural circuits, as exemplified by giant depolarising potentials in the hippocampus (Ben-Ari et al., 1989) and spindle bursts in the neocortex (Hanganu-Opatz, 2010; Kilb et al., 2011; Khazipov et al., 2013). In the neocortex, bursts of 10-20Hz frequency firing occur against a backdrop of network silence (Khazipov et al., 2004; Yang et al., 2009), synchronising cortical columns of 200-400μm (Sun & Luhmann, 2007; Yang et al., 2009). Spindle bursts rely on both AMPA and NMDA receptors (Minlebaev et al., 2007; 2009). An appealing model is that early network oscillations provide a means for correlated pre- and post-synaptic activity to conduct through the canonical cortical circuit, offering a test signal for incipient synaptic connections. During oscillatory events, NMDA receptors are activated and AMPA

synapses that are in phase with burst activation would maintain AMPA signalling, whereas those that are only sporadically, non-rhythmically active, or out-of-phase with the oscillation, would become AMPA-silent and eventually eliminated (Hanse et al., 2009; 2013; Anastasiades & Butt, 2012). Promoting pre- and post-synaptic correlated activity along with NMDA receptor activation should therefore increase AMPA signalling and decrease AMPA silence (Liao et al., 2001; Zhu & Malinow, 2002; Voigt et al., 2005). These results are also consistent with a model according to which glutamatergic synapses are born silent and acquire AMPA receptors following LTP driven by correlated pre- and post-synaptic activity. However, such models require an additional third component to drive post-synaptic depolarisation and thereby NMDA receptor activation. One interesting postulate is that if correlated activity and NMDA receptor activation were inhibited, the silent and labile synapse models would actually predict opposite results: i) if nascent synapses are absolutely AMPA-silent (silent synapse model), in the absence of correlated activity we would expect a very high prevalence of AMPA-silent synapses, since no un-silencing activity had been present; ii) if nascent synapses are AMPA-labile (labile synapse model), since they are not exposed to any silence-inducing sporadic activity, we would expect them to retain AMPA signalling. Following *in vivo* blockade of neuronal activity by TTX (Groc et al., 2003) or chronic blockade of NMDA receptors using intracerebral infusion of AP5 (Colonnese et al., 2003) no AMPA-silent synapses were found, in agreement with the labile AMPA synapse model.

One potential weakness of the labile AMPA model is that it may confer a lot of instability to a developing network. Even though lack of activity protects connectivity by preventing silencing or switching AMPA-silent synapses back to labile mode, the

early patterns of activity that are observed *in vivo* (Khazipov et al., 2004; Dupont et al., 2006; Yang et al., 2009; Minlebaev et al., 2011; Yang et al., 2013b) are complex and rely on timely, consistent glutamatergic signalling (Minlebaev et al., 2007; 2009). One way around this issue would be the existence of early, privileged nodes in the network, which would attain stable glutamatergic synapses very early in development, in an experience-independent fashion. These nodes would serve as the essential synaptic backbone required to keep oscillatory activity going and prevent its degeneration into sporadic activity. Subplate neurons are interesting candidates for such a function. They are known to receive functional and robust thalamic synapses embryonically/perinatally (Friauf & Shatz, 1991; Hanganu et al., 2002; Higashi et al., 2002; Molnár et al., 2003), which must be established in an experience-independent fashion. Interestingly, a recent report showing *in vivo* induction of LTP of thalamocortical inputs to deep layer, cortical plate and L4 neurons during the first postnatal week reported failure to induce this form of plasticity *in vivo* and *in vitro* in subplate neurons (An et al., 2012), suggestive of a rigid, hard-wired synapse. Additionally, previous reports have found subplate neurons to influently participate in network oscillations at early neonatal stages (Dupont et al., 2006; Yang et al., 2009). In the next section, I will review literature on the importance of subplate neurons in cortical circuit formation. I shall examine an alternative hypothesis on thalamocortical synapse maturation unexplored by Crair and Malenka (Crair & Malenka, 1995). A second interesting candidate which is thought to be fundamental in hippocampal circuit development (Ben-Ari et al., 1989) are GABAergic interneurons. Their involvement in early circuit formation will be explored following the subplate.

1.4. Subplate neurons in cortical development

The subplate is a cortical layer located below the cortical plate and above the white matter in placental mammals (Figure 1.7) (Kostovic & Molliver, 1974; Rakic, 1977; Rickmann et al., 1977; Kostovic & Rakic, 1980; Luskin & Shatz, 1985). The relative width of the embryonic cortical plate and subplate has been reported to be largest in monkeys and humans (Molnár et al., 2006), suggesting the subplate to not be an evolutionary relic, but rather a structure that evolved together with the cortical plate, hypothesised to be associated with the increased complexity in cortical organisation and inter-areal connectivity found in primates (Aboitiz, 1999; Aboitiz et al., 2005). Montiel and colleagues suggested that there are ancestral and newly derived cell populations in the subplate in their "dual subplate origin hypothesis" (Montiel et al., 2011). Subplate neurons show remarkable molecular diversity, and although several genetic markers have been identified for these cells, the overlap between them is only partial (Hoerder-Suabedissen et al., 2009; Osheroff & Hatten, 2009; Hoerder-Suabedissen & Molnár, 2012). SPns have been reported to constitute a transient population (Kostovic & Rakic, 1980; Luskin & Shatz, 1985; Al-Ghoul & Miller, 1989; Price et al, 1997), but in several species (namely rat and mouse) a subplate layer remains evident as layer 6b in adolescence and adulthood (Reep, 2000; Torres-Reveron & Friedlander, 2007; Marx & Feldmeyer, 2012). Some of the previously identified molecular markers for SPns label layer 6b in adulthood (Hoerder-Suabedissen et al., 2009). CTGF (connective tissue growth factor) is the marker with most widespread expression in the young postnatal subplate, and persists into adulthood, labelling non-GABAergic cells in L6b (Hoerder-Suabedissen et al., 2009; Hoerder-Suabedissen & Molnár, 2012). Another marker of interest is Lpar1 (lysophospatidic acid receptor 1), which was identified in an initial micro-array screen

for subplate-enriched genes at E18 and P8 and validated by immunohistochemistry (Hoerder, 2007). In the Lpar1-GFP line, GFP labels a cohort of glutamatergic subplate neurons preferentially born at E11.5, and, after P2, an additional smaller population of neurons mostly located in L5 and L6, a substantial amount of which can be labelled by GABA immunohistochemistry (Hoerder-Suabedissen & Molnár, 2012).

Intrinsic physiology and morphology of SPns

SPns display relatively mature intrinsic electrophysiological characteristics even at the very initial stages of postnatal development. At P0-P3 they are able to fire repetitive overshooting action potentials (Figure 1.7), which are rarely observed in pyramidal neurons during early development, achieving frequencies over 10Hz (Friauf et al., 1990; Luhmann et al., 2000; Hanganu, 2001; Liao & Lee, 2011). During the first postnatal week, SPns display low rheobase and high input resistance, suggesting a state of higher excitability (Hanganu, 2001; Liao & Lee, 2011). In terms of electrophysiological profile, only two types of subplate neuron have been described: single-spiking neurons, which regardless of amplitude of suprathreshold current injection amplitude, fire only a single action potential shortly after the onset of injection, and regular-spiking neurons, which will fire action potentials at a frequency proportional to the amplitude of current injected, up to a maximum firing frequency value (Figure 1.7) (Friauf et al., 1990; Hanganu, 2001; Liao & Lee, 2011). Single spiking neurons are either transient or in a state of immaturity before transitioning to regular spiking identity, as after P3 their number greatly declines, and after P9 they are extremely rare (Hanganu, 2001; Liao & Lee, 2011; Marx & Feldmeyer, 2012). Therefore, in physiological terms, SPns appear to be a homogeneous cell type.

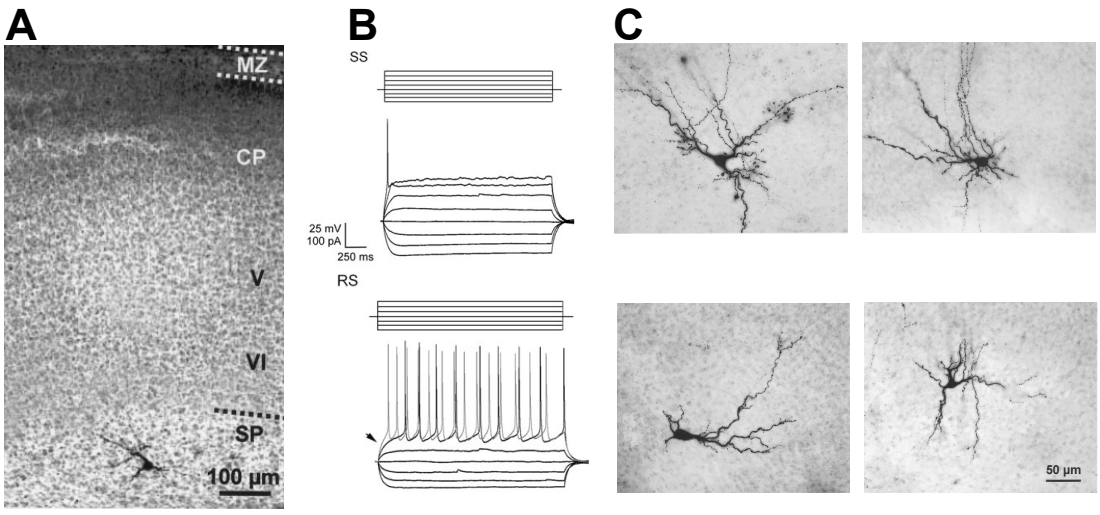


Figure 1.7. Diversity of subplate neurons. A. The subplate (SP) is located below cortical L6 and above the white matter (WM). **B.** Example of a single-spiking (top) and regular-spiking (bottom) subplate neuron. **C.** Example of subplate morphologies at P2. **A, C** taken from Hanganu et al., 2002; **B** taken from Liao & Lee, 2011.

Morphologically, SPns in rats and mice are well differentiated already during the first postnatal week, presenting well developed, complex dendritic trees (Figure 1.7) (Hanganu et al., 2002; Hoerder-Suabedissen & Molnár, 2011; Liao & Lee, 2011) and 5-6 morphological types have been consistently identified across studies: pyramidal, inverted pyramidal, horizontal (bi-tufted and mono-tufted), multipolar and tangential/oblique (Ferrer et al., 1986; Hanganu et al., 2002; Kanold & Luhmann, 2010; Hoerder-Suabedissen & Molnár, 2011). These morphological types find striking correspondence in mature layer 6b (Marx & Feldmeyer, 2012), a fact which, together with adult expression of early subplate markers such as CTGF, suggests that L6b could be the mature remnant of the subplate (Hoerder-Suabedissen et al., 2009). A few key studies have examined the morphology and projection targets of mature L6b neurons (Ferrer et al., 1986; Clancy & Cauller, 1999; Marx & Feldmeyer, 2012). Given the morphological and molecular marker expression similarities between early

SPns and L6b cells, in this section I consider these cell types together (using the term "subplate neurons") in an attempt to synthesize knowledge about their morphological characteristics.

A common feature of SPns regardless of age, morphology or molecular subtype is profuse axonal arborisation in the subplate and L6a (Ferrer et al., 1986; Friauf et al., 1990; Liao & Lee, 2011; Marx & Feldmeyer, 2012). Along with early and extensive gap-junction coupling in the subplate (Dupont et al., 2006), this suggests that SPns form a deep recurrent network, well-suited to amplify afferent input. Beyond establishing this dense local network, SPns project to several targets in the brain: all layers of the home and adjacent cortical columns (Ferrer et al., 1986; Finney et al., 1998; Friauf et al., 1990; Clancy & Cauller, 1999; Liao & Lee, 2011; Marx & Feldmeyer, 2012), the thalamus (McConnell et al., 1989; De Carlos & O'Leary, 1992; McConnell et al., 1994; Hoerder-Suabedissen & Molnár, 2011;), distant cortical regions (Tomioka et al., 2005; Higo, et al., 2007; Hoerder-Suabedissen & Molnár, 2011; Hooks et al., 2013) and across the corpus callosum (Hoerder-Suabedissen & Molnár, 2011). A small proportion of SPns, more commonly found at P2 than P7, project simultaneously to more than one of these targets (Hoerder-Suabedissen & Molnár, 2011).

In terms of the local columnar network, SPns have been found to project to virtually all layers of the overlying cortical layers, but their axons arborise most prominently in the subplate, L6, L4 and L1 (Friauf et al., 1990; Ferrer et al., 1986; Finney et al., 1998; Clancy & Cauller, 1999; Liao & Lee, 2011; Marx & Feldmeyer, 2012). Axonal arborisation in L4 and L1 has been a commonly reported feature of SPns early in

development (Friauf et al., 1990; Piñon, et al., 2009; Liao & Lee, 2011;), but it is contentious whether projections above L4 remain at later developmental stages. A study examining mature L6b neurons found that regardless of morphological class, L6b axons and dendrites were confined to cortical L4 and below (Marx & Feldmeyer, 2012). This is consistent with reports suggesting that SP neurites remodel between P2 and P7, starting out by reaching L1 until P2, but remaining confined to the L4/L5a border by P6-P8 (Piñon et al., 2009; Hoerder-Suabedissen & Molnár, 2011), with this remodelling depending on SPn projection target (Hoerder-Suabedissen & Molnár, 2011). Interestingly, neurites remodel also in the tangential dimension between P2 and P10, going from a disorganised appearance until P4 to focusing in the barrel hollow around P6, and subsequently the barrel septa at P8-P10 via a sensory activity-dependent process (Piñon et al., 2009). In spite of these data, other laboratories have reported SP-L1 projections after P7 (Clancy & Cauller, 1999; Liao & Lee, 2011). It is likely that methodological differences (tracer vs dye vs intracellular biocytin labelling) and subtype-specific projection patterns [one study examined the Golli-tau-eGFP cohort of SPn (Piñon et al., 2009) whereas the others studied unlabelled cells] underlie the different results obtained. Nonetheless, at least early in development SPns are likely to relay activity to all cortical layers. At later stages, they seem to mostly project within the subplate, L6b and L4. In a very thorough examination of axodendritic morphologies in mature L6b, Marx and colleagues show very clearly that morphological types of SPn differ in the columnar and laminar organisation of their neurites (Marx & Feldmeyer, 2012). Briefly, pyramidal, inverted pyramidal and tangential subplate neurons have dendrites confined to the home barrel column. Pyramidal dendrites extend to L5a, much like their axons which on occasion contact L4 of the home and adjacent barrel columns. Inverted pyramidal neuron dendrites are

confined to L6b and the L6a/b border. Their axons spread horizontally over great distances, running parallel to the pial surface, through the L6a/b border and the white matter. Dendrites of tangential neurons are confined to L6a, and axons arborise mostly in L6b, but also L6a and L4. The dendrites of horizontal and multipolar SPns do not respect the barrel boundary. Horizontal cell dendrites and axons extend into the adjacent barrel columns along the L6a/b border. For multipolar cells, dendrites "radiate" indiscriminately from the soma into adjacent barrel columns, extending well into the bottom of L5b. Axons span a few adjacent barrels, wider than horizontal cells, and arborise mostly in L5b-L6b, very often reaching L4. Interestingly, while L6b neurons showed considerable diversity in their firing properties, this did not correspond in any orderly pattern to the aforementioned morphological heterogeneity (Marx & Feldmeyer, 2012).

Shifting focus to long-range projections (Figure 1.8), researchers have so far been unable to reveal any correspondence between morphological subtype and projection target (Hoerder-Suabedissen & Molnár, 2011). Subplate neurons are known to project to the thalamus (McConnell et al., 1989; 1994; De Carlos & O'Leary, 1992; Hoerder-Suabedissen & Molnár, 2011) and in fact pioneer the corticothalamic projection (McConnell et al., 1989; De Carlos & O'Leary, 1992; Molnar & Blakemore, 1995; Molnar et al., 1998; Jacobs et al., 2007). It is unclear whether SPns, L6 or L5 pyramidal neurons are the first to actually make synaptic contact with thalamic nuclei, due to technical difficulties in selectively labelling the axons of each of these cell types (Grant et al., 2012). Due to the same reason, a subplate-thalamus synapse has yet to be functionally identified.

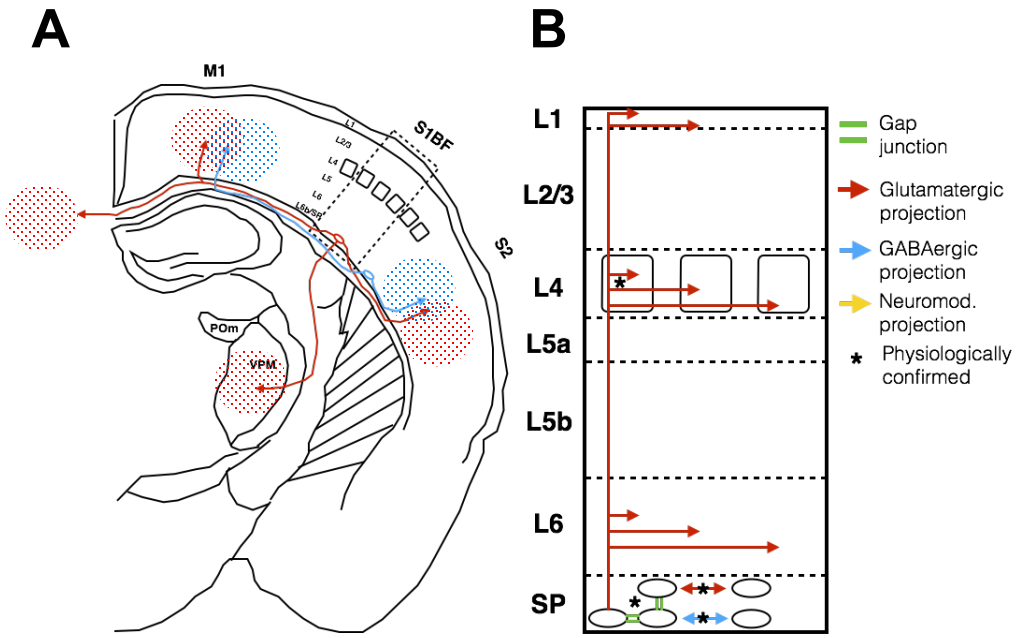


Figure 1.8. Efferent projection targets of SPns. A. Proposed long-range targets of S1BF subplate projections. Glutamatergic projections (red) have been shown to distant functionally related areas, across the corpus callosum, and into the thalamus. Long-range GABAergic projections have been observed into distant but functionally-related areas. **B.** Local circuit targets of subplate projections. SPns are extensively interconnected via gap junctions (green), glutamatergic (red) and GABAergic synapses. Their axons can project across all cortical layers, but mostly arborise in L6, L4 and L1. Glutamatergic projections have been physiologically confirmed from the SP to itself and L4. Intra-subplate gap-junction coupling and GABAergic synapses have also been confirmed by electrophysiological recordings.

In addition to the thalamus, SPns make long distance cortico-cortical connections (Tomioka et al., 2005; Higo et al., 2007; Hoerder-Suabedissen & Molnár, 2011; Hooks et al., 2013). Tracer injections into the adult mouse M1 resulted in abundant labelling of L6b neurons in S1 and S2 (Hooks et al., 2013). In a carbocyanine dye tracing study in the neonatal mouse, placement of crystals in S1 resulted in back-labelling of subplate neurons in motor regions and S2 (Hoerder-Suabedissen & Molnár, 2011). In two other studies, researchers examined long-range GABAergic projections in mature animals (Tomioka et al., 2005; Higo et al., 2007). Tracer injections routinely labelled distally-located GABAergic neurons which mostly clustered in L6 and the white matter, both in mouse (Tomioka et al., 2005) and cat (Higo et al., 2007), with a very

high proportion of these cells residing in L6b (Higo et al., 2007; Tomioka et al., 2005). Injections into mouse V1 retrogradely labelled neurons in orbitofrontal cortex, retrosplenial cortex, perirhinal cortex, M2, temporal cortex and occipital cortex. M1 injections labelled cells in the prefrontal, motor and somatosensory cortices. Finally, S1 injections identified pre-synaptic neurons in parietal cortex, M1 and M2 (Tomioka et al., 2005). Further supporting a role for SPns in long-range communication, DiI placements in the neonatal corpus callosum labelled subplate neurons in the cingulate, motor and somatosensory cortices (Hoerder-Suabedissen & Molnár, 2011). These results show that SP/L6b neurons may play a role in coordinating the activity of distant but functionally-related cortical areas.

Inputs onto subplate neurons

Subplate cells receive early synaptic inputs from the thalamus (Figure 1.9), which can be recorded from late embryonic stages onward (Friauf & Shatz, 1991; Higashi et al., 2002; Molnár et al., 2003). Thalamic inputs to SPns are strong even at the earliest neonatal stages, before thalamic afferents innervate L4, and often lead to action potential firing in the SP (Hanganu et al., 2002; Hirsch & Luhmann, 2008; Zhao et al., 2009; Liao & Lee, 2011). Due to the extensive recurrent connectivity observed in the SP, the predominant immediate relay will be local, onto nearby SPns (Hanganu et al., 2002; Hirsch & Luhmann, 2008). Subplate-subplate inputs evoked by electrical stimulation are facilitating and largely mediated by GluN2D receptors (Hirsch & Luhmann, 2008), which show the longest decay time of this class, enabling robust temporal summation of subplate activity (Cull-Candy et al., 2001). Convergent subplate and thalamic inputs interact positively, boosting glutamatergic signalling: when thalamic afferents were activated shortly before subplate afferents, robust (up to

3-fold) facilitation was observed (Hirsch & Luhmann, 2008). Thalamic input onto SPns has been proposed to be developmentally eliminated, as continued presence of the disynaptic thalamus-SP-L4 pathway could introduce noise and temporal imprecision in L4 (Kanold & Luhmann, 2010). The only experimental result so far supporting this idea was the finding that the release probability of thalamic synapses to SPns decreases throughout development (Liao & Lee, 2011). Nonetheless, it is an interesting idea that merits further exploration (see Chapter 4).

Beyond thalamic input, subplate neurons have been shown to integrate into the cortical excitatory network early in development, with spontaneous and evoked inputs (from the cortical plate, subplate and thalamus) evoked as early as P0 (Hanganu et al., 2002; Hirsch & Luhmann, 2008; Viswanathan et al., 2012). The axons of embryonic L2-5 neurons in macaque monkey branch in the subplate, suggesting excitatory neurons in all cortical layers potentially contact subplate neurons (Callaway, 1998). A recent study from the Kanold laboratory mapped local cortical inputs onto SPns using glutamate uncaging (Viswanathan et al., 2012). This data revealed that SPns form part of a deep-layer excitatory network involving L5b, L6 and the SP, and that the strongest excitatory inputs derive from L6 and SP, albeit a small subset of SPns was found which received input from L4 (Figure 1.9) (Viswanathan et al., 2012).

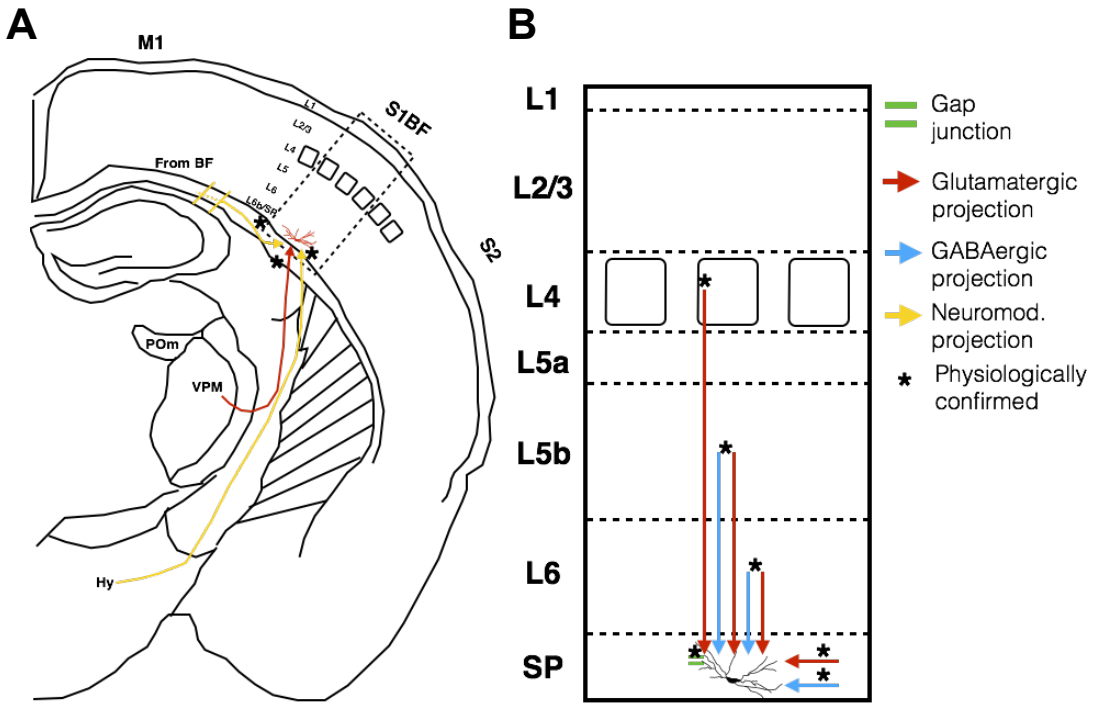


Figure 1.9. Afferent input onto SPns. SPns receive robust glutamatergic thalamic inputs. There is a powerful local recurrent network in the subplate, mediated by electrical synapses, GABA/Glycine and Glutamate. Intracortically, L4-L6 have been shown electrophysiologically to provide glutamatergic and GABAergic input to SPns. In addition, the subplate receives a rich repertoire of neuromodulatory inputs, especially cholinergic basal forebrain input and hypocretin/orexin inputs from the hypothalamus.

GABAergic PSCs have been reported from the earliest neonatal stages in SPns (Hanganu, 2001; Hanganu et al., 2002). GABA and Glycine have been shown to have a depolarising effect on SPns during the first postnatal week (Hanganu et al., 2002; 2009; Kilb et al., 2008), and tonic ambient activation by non-synaptically released GABA reportedly maintains SPns at a depolarised resting membrane potential that could enhance excitability in this layer (Hanganu et al., 2009). The study of Viswanathan and colleagues also mapped GABAergic inputs onto SPns (Viswanathan et al., 2012). GABAergic input was localised to the SP and L6 (Viswanathan et al., 2012), which is consistent with results obtained in our laboratory. In these experiments, we used a glutamate uncaging approach (see Chapter 4) to map global afferent GABAergic input onto Lpar1-GFP SPns. GABAergic inputs arose entirely

from the SP and L6 along a broad horizontal extent of 200-350μm away from the soma (unpublished observations, Daniel Lyngholm), consistent with a system of horizontally-projecting GABAergic subplate neurons, which could be important in synchronising early cortical activity (Voigt et al., 2001).

In addition to glutamatergic and GABAergic synaptic input, subplate neurons receive a diversity of neuromodulatory inputs (Figure 1.9) (Kanold & Luhmann, 2010), of which the best studied is the cholinergic afferent input from the basal forebrain. In the newborn rat, cholinergic fibres selectively innervate the subplate (Calarco & Robertson, 1995; Mechawar & Descarries, 2001), a feature which has been exploited to lesion subplate neurons selectively in this organism using immunotoxins (Kanold, 2003; Tolner et al., 2012). Cholinergic modulation has a strong excitatory effect on SPns, causing it to fire action potentials in repetitive 20Hz discharges (Hanganu & Luhmann, 2004; Hanganu et al., 2009). Amongst other peptidergic modulatory inputs (Kanold & Luhmann, 2010), SPns are the only cortical neurons that receive input from hypothalamic hypocretin-orexinergic neurons, an input that promotes widespread excitation in the subplate *in vitro* by closing a potassium conductance (Bayer et al., 2004).

The outputs of subplate neurons

The study of the subplate's functional outputs has been hampered by lack of a means to activate it selectively. The subplate's thin width and proximity to the white matter in mouse and rat precludes the use of electrical stimulation, as this would likely recruit L6 pyramidal cells and thalamocortical axons of passage. The lack of subplate-selective Cre-driver lines and diversity of partially overlapping molecular markers

exclude the use of optogenetic technology (Fenno et al., 2011; Yizhar et al., 2011) to selectively drive identified subplate neurons. Cre recombinase-independent viral-vector transfection would be an option, but the closeness to L6 implies that it would be impossible to target SP neurons without transfecting L6. The only circuit mapping option left is glutamate uncaging. This technique does not excite axons of passage, and laser beams can be calibrated to restrict optical activation to small areas of tissue (Anastasiades & Butt, 2012; Shepherd, 2012), preventing activation, respectively, of axons of passage and L6 pyramidal cells. Zhao and colleagues employed this methodology to identify a projection from the subplate to L4 in developing auditory cortex of the mouse (Zhao et al., 2009). This finding supported anatomical work, which documented subplate axonal arborisations in L4 (Friauf & Shatz, 1991; Finney et al., 1998; Liao & Lee, 2011; Piñon et al., 2009; Hoerder-Suabedissen & Molnár, 2012). However, the anatomical studies on subplate axonal projections reviewed above have shown that SPns project to potentially every cortical layer. Since the authors only recorded L4 cells in response to subplate optical stimulation in the putative primary auditory cortex, it is unknown whether SPns show a privileged synaptic relationship with L4, or whether they also provide excitation to other cortical layers, and how the strength of this excitation might compare to that in L4. Beyond L4, the only other identified functional synaptic contact of SPns is the subplate itself, with studies showing a strong local excitatory and GABAergic circuit in this layer (Hanganu et al., 2009; Viswanathan et al., 2012). Subplate axonal projections to the thalamus have been amply documented using anatomical tracers (McConnell et al., 1989; 1994; De Carlos & O'Leary, 1992), but so far it has been impossible to prove whether a functional synaptic contact is ever made between subplate neurons and thalamic relay cells in primary sensory nuclei. However, it has been reported that

cortical stimulation in neonatal rats results in activation of the thalamic reticular nucleus recorded by optical imaging, suggesting SPns could project to this structure (Grant et al., 2012). Anatomically-identified long-range cortical and cross-callosal projections are yet to be functionally characterised, due to the same technical difficulties.

The subplate – a privileged node in the early cortical network?

In line with others (Luhmann, 2009; Kanold & Luhmann, 2010), I would like to argue that subplate neurons are attractive candidates to provide a mature synaptic bedrock for early network activity (Figure 1.10). Subplate neurons receive early thalamic input which during the first few days of life is already sufficient and reliable enough to elicit action potentials (Friauf & Shatz, 1991; Hanganu et al., 2002; Higashi et al., 2002; Molnár et al., 2003; Zhao et al., 2009). The lack of ability to induce LTP at this synapse at a point when thalamic synapses with deep-layer and L4 neurons are highly plastic (An et al., 2012) hints that the thalamus-subplate synapse could be a fixed, hard-wired connection, or at least that plasticity rules fundamentally differ between this and other thalamocortical synapses. Rather, it would appear that SPns form an amplifying recurrent network (Dupont et al., 2006; Hirsch & Luhmann, 2008; Hanganu et al., 2009; Viswanathan et al., 2012) designed to relay thalamic inputs to the overlying cortical plate via widespread axonal projections (Friauf & Shatz, 1991; Zhao et al., 2009; Hoerder-Suabedissen & Molnár, 2011). This powerful recurrent network holds the potential for maintaining sustained, possibly rhythmic activity. Indeed, subplate neurons have been shown to clearly participate in early gamma, spindle burst and cholinergic oscillations (Dupont et al., 2006; Yang et al., 2009) and they likely form a critical part of an endogenous cortical oscillator (Dupont et al.,

2006; Sun & Luhmann, 2007; Tolner et al., 2012) sensible to sensory recruitment (Yang et al., 2013b) as well as cholinergic modulation (Dupont et al., 2006). Consistent with this assertion, subplate ablation largely prevents generation of spindle burst and cholinergic network oscillations (Dupont et al., 2006; Tolner et al., 2012), beyond more immediate deficits in thalamic afferent organisation (Kanold, 2003; Tolner et al., 2012), thalamus-L4 synapse maturity (Kanold, 2003; Tolner et al., 2012) and maturation of inhibition (Kanold & Shatz, 2006).

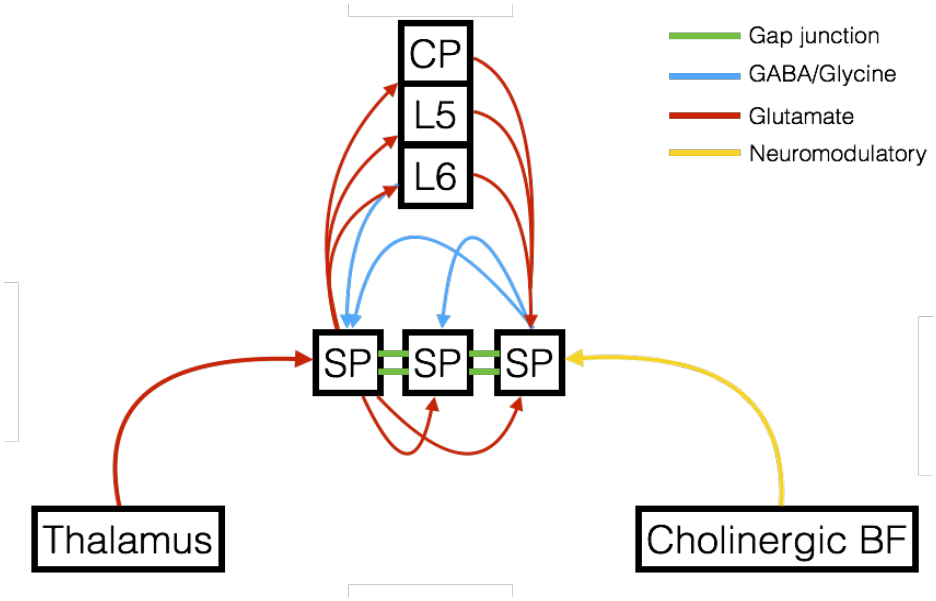


Figure 1.10. The subplate as a fundamental network node in the developing cortex. Subplate neurons are densely interconnected via gap junctions, glutamatergic and depolarising GABAergic projections. This recurrent network can act as an amplifier for thalamic and cholinergic afferents, sustaining activity and relaying it to the overlying cortical plate, which feeds back excitation to the subplate.

A simple prediction of the hypothesis that SPns are key nodes of the early cortical network is that thalamic and cortical glutamatergic inputs to SPns should show a high degree of maturity early in development, and as such this communication should be mediated via AMPA-stable signalling. Likely due to synaptic immaturity and AMPA receptor lability, we have found it difficult to use glutamate uncaging to map excitatory input onto pyramidal neurons before P5 (Anastasiades & Butt, 2012

unpublished observations). If SPns are part of a hard-wired cortical network, then I would expect them to show organised patterns of cortical input before pyramidal cells do.

1.5. The development of GABAergic circuits

So far I have focused on the development of feed-forward excitation in the canonical cortical circuit and the special characteristics of subplate neurons, which could make them cornerstones of early synchronised activity in the cortex. GABAergic interneurons represent 10-25% of the total number of cortical neurons (Meinecke & Peters, 1987) and perform a number of fundamental circuit computations in the mature system, including spatiotemporal control of excitatory activity via feed-forward and feedback inhibition, and synchronisation of pyramidal cell firing, enabling precise patterns of network activity (Isaacson & Scanziani, 2011; Hangya et al., 2014; Kepecs & Fishell, 2014). Given the fundamental role that interneurons play in supporting cortical oscillations in the mature brain (Cardin et al., 2009; Sohal et al., 2009), they too form attractive candidates for a synaptic backbone underlying early network activity. In the hippocampus, depolarising GABAergic signalling plays a key role in early network activity (Ben-Ari et al., 1989; Ben-Ari, et al., 2007). Rare GABAergic cells with widespread functional connectivity – hub neurons – have been shown to be able to influence activity patterns of very large numbers of cells and trigger, synchronise or terminate oscillatory events (Bonifazi et al., 2009). Although *in vivo* experiments in the cortex suggest that GABA does not contribute to early network activity beyond restricting spatially and temporally the spread of activity (Minlebaev et al., 2007; 2009), pharmacological dissection of transmitter contributions in a living animal presents a difficult challenge, and as such the

contribution of GABAergic interneurons to early network activity warrants further exploration. In this section, I will focus on how the maturation of GABAergic signalling and circuits could influence cortical early network activity and circuit assembly, drawing on examples from the hippocampal literature when pertinent.

1.5.1. Intrinsic and synaptic development of GABAergic interneurons

Embryonic generation

GABAergic interneurons arise from transient embryonic structures located in the ventral telencephalon, the ganglionic eminences (GEs) (Anderson et al., 1997; Wichterle et al., 1999; Wichterle et al., 2001; Anderson et al., 2002; Valcanis & Tan, 2003; Xu et al., 2004; Butt et al., 2005; Xu et al., 2008; Gelman & Marín, 2010). The GEs are often divided into three anatomical compartment, the lateral, medial and caudal GEs (LGE, MGE and CGE, Figure 1.11), with the MGE and CGE providing the source for most cortical interneurons (Nery et al., 2002; Butt et al., 2005; Fogarty et al., 2007; Xu et al., 2008). Progenitor cells in the MGE give rise to ~70% of cortical interneurons (Lavdas, et al., 1999; Fogarty et al., 2007; Xu et al., 2008) and CGE progenitors generate the remaining 30% (Nery et al., 2002; Butt et al., 2005; Miyoshi et al., 2007). The pre-optic area (POA) offers a small contribution, supplying the neocortex with an estimated 3% of its GABAergic population (Gelman et al., 2009). It has been suggested that in primates (including humans) a proportion of interneurons may originate dorsally, from the ventricular and sub-ventricular zones (Letinic et al., 2002; Jakovcevski et al., 2011; Xu et al., 2011; Zecevic et al., 2011), but this is still a contentious issue (Hansen et al., 2013; Ma et al., 2013; Molnár & Butt, 2013) and requires lineage analysis rather than methods that largely rely on

marker expression.

Diversity of GABAergic interneurons

GABAergic interneurons show a rich diversity in morphology, biochemical marker expression, electrophysiological properties and post-synaptic compartment innervation (Markram et al., 2004; Fishell & Rudy, 2011). For this reason, interneuron classification is a daunting task, with no single scheme encapsulating the rich variety espoused by this neuron family. A full description of the complexity of cortical interneuron diversity is beyond the scope of this chapter. Nonetheless, an appealing, parsimonious scheme emerged recently, which divides cortical interneurons into three groups, based on marker expression: parvalbumin (PV), somatostatin (SST) and 5HT3aR (Rudy et al., 2011) (Figure 1.11). I shall provide a brief overview of this scheme.

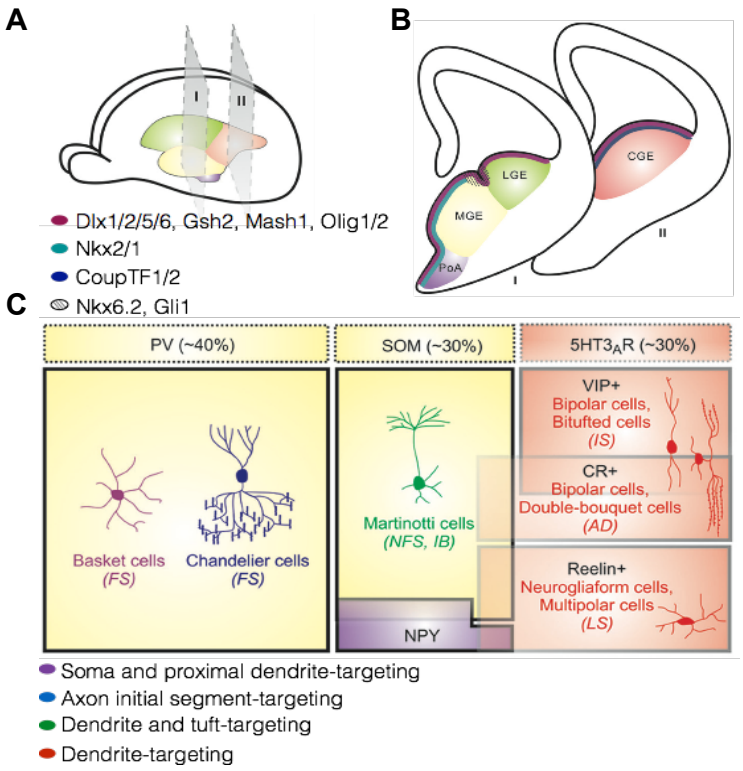


Figure 1.11. Embryonic origin and diversity of cortical GABAergic interneurons. A. Interneurons arise from progenitors in the MGE (yellow), LGE (green), CGE (red) and PoA

(purple). **B.** Expression of several transcription factors delineates spatially-restricted regions in the ganglionic eminences that produce different interneuron subtypes. **C.** According to Rudy and colleagues (Rudy et al., 2011), neocortical interneurons can be divided into PV+, SST+ and 5HT3AR-expressing groups. Figure 1.11C shows example morphological types and axonal targeting of interneurons in each of these groups. Figure adapted from (Sultan et al., 2013).

PV+ cells represent 40% of the cortical GABAergic interneuron population (Rudy et al., 2011) and are strongly associated with fast-spiking firing patterns (Kawaguchi et al., 1987; Cauli et al., 1997; Kawaguchi & Kubota, 1997; Gibson, et al., 1999; Ascoli et al., 2008). PV+ cells can be divided into basket cells and chandelier cells. The former innervate the soma and proximal dendrites of target neurons, whilst the latter target the axon initial segment of pyramidal neurons (Somogyi et al., 1998; Klausberger & Somogyi, 2008; Rudy et al., 2011). SST+ cells are a diverse population (Wang et al., 2004; Ma et al., 2006; Xu et al., 2006; McGarry et al., 2010; Xu et al., 2013), but are often associated with Martinotti cells, interneurons with an axon that ascends to L1 but also branches collaterals locally. Importantly, not all SST+ interneurons project to L1 and as such cannot be classically regarded as Martinotti cells (Ma et al., 2006; Xu et al., 2013). SST+ interneurons contact distal dendrites of their target neurons, which can be pyramidal cells (Silberberg & Markram, 2007) or other interneurons (Pfeffer et al., 2013). Martinotti cells can be found in layers 2-6, but are more abundant in L5 (Kawaguchi & Kubota, 1997; Wang et al., 2004), and another of their distinctive features is that they receive facilitating afferent excitatory inputs (Silberberg & Markram, 2007; Tan et al., 2008). Finally, Lee and colleagues discovered that 5HT3aR is a good marker for a heterogeneous population that does not express PV or SST, and accounts for 30% of the cortical interneuronal population (Lee, et al., 2010). 5HT3aR+ interneurons include vasoactive intestinal peptide (VIP)-positive cells and neurogliaform cells. VIP is

expressed by 40% of the 5HT3aR population, and VIP+ cells predominantly reside in L2/3. They are physiologically and morphologically diverse (Miyoshi et al., 2007), and have been proposed to inhibit other interneurons (Pfeffer et al., 2013; Pi et al., 2013; Kepecs & Fishell, 2014; Pfeffer, 2014). One other well-described 5HT3aR+ interneuron type is the neurogliaform cell (Lee et al., 2010). These neurons have highly characteristic morphologies, consisting of a small round soma with dendrites extending radially in all directions and wide, round axonal plexi composed of very fine branches (Kawaguchi & Kubota, 1997; Oláh et al., 2007). Two of the most interesting features of these interneurons are first, the fact that, contrary to other inhibitory cells, they form electrical synapses with other interneuron types (Price et al., 2005; Simon et al., 2005; Zsiros & Maccaferri, 2005). Second, neurogliaform cells elicit slow, long-lasting IPSPs on their target cells, mediated by $GABA_A$ and $GABA_B$ receptors (Oláh et al., 2007), and their axonal varicosities contain vesicles that are not associated with synaptic contacts, leading to the proposal that neurogliaform cells act on target neurons by volume transmission (Oláh et al., 2009).

The diversity of interneuron subtypes present in the brain is thought to arise from complex developmental genetic programs of specification and differentiation (Figure 1.11). It has been amply documented that interneuron subtype identity can be predicted from place and time of embryonic origin (Xu et al., 2004; Butt et al., 2005; Wonders & Anderson, 2006; Flames et al., 2007; Fogarty et al., 2007; Ghanem et al., 2007; Miyoshi et al., 2007; Gelman et al., 2009; Miyoshi et al., 2010). PV and SST interneurons are derived from the MGE (Xu et al., 2004; Butt et al., 2005; Fogarty et al., 2007; Miyoshi et al., 2007). Furthermore, within the MGE there is a spatial bias, such that the more ventral aspects give rise to PV cells, whereas the dorsal sections

originates SST interneurons (Flames et al., 2007; Fogarty et al., 2007; Wonders et al., 2008; Inan et al., 2012). It has been proposed that Nkx6.2 expression in the dorsal MGE specifies SST+ interneurons, whereas PV cells are derived from Nkx2.1 progenitors located more ventrally within the MGE (Flames et al., 2007). Despite difficulties in defining the CGE, 5HT3aR+ neurons are thought to be largely CGE-derived (Inta et al., 2008; Lee et al., 2010; Vucurovic et al., 2010).

Intrinsic property and synaptic development

In the mouse, the intrinsic properties of interneurons mature over the first 3-5 weeks of life (Le Magueresse & Monyer, 2013). Fast-spiking (FS) interneurons in the hippocampus (Doischer et al., 2008) and cortex show after P7 a pronounced decrease in input resistance, membrane time constant and action potential half-width, concurrent to increases in maximum firing frequency (Okaty et al., 2009; Goldberg et al., 2011; Lazarus & Huang, 2011;). Between P11 and P32, somatostatin (SST) positive interneurons in the mouse barrel cortex also undergo an increase their maximum firing frequency and rheobase, concurrent to a decrease in input resistance, membrane time constant and spike half-width (Kinnischtzke et al., 2012).

In terms of synaptic development, the first cortical GABAergic synapses can be identified structurally at E16, and are mostly found in the marginal zone and subplate, whereas glutamatergic synapses appear a day later (König et al., 1975). In hippocampal CA1, at P0 80% of pyramidal neurons received no GABAergic or glutamatergic PSCs. These neurons had no dendrites or only an anlage of apical dendrite (Tyzio et al., 1999). 10% of pyramidal cells received only GABAergic input and possessed short apical dendrites, whereas the remaining 10% received

GABAergic and glutamatergic input and possessed the most developed dendritic morphologies (Tyzio et al., 1999). In contrast, only 5% of CA1 interneurons at P0 were silent and possessed underdeveloped or no dendrites, whereas 17% of interneurons received only GABAergic inputs, displaying more complex dendritic morphologies. The majority of interneurons (78%) received both GABAergic and glutamatergic inputs, and showed extensively-developed morphologies (Hennou et al., 2002). These data suggest that 1) interneurons integrate into hippocampal circuits before pyramidal cells, 2) GABAergic synapses develop prior to glutamatergic ones, and 3) the earliest GABAergic synapses target dendrites (Ben-Ari et al., 2007; Le Magueresse & Monyer, 2013). The possibility that the earliest GABAergic synapses are dendrite-targeting is interesting, as this would suggest that SST+ interneurons pioneer GABAergic circuits (Somogyi et al., 1998; Markram et al., 2004; Fishell & Rudy, 2011; Kepecs & Fishell, 2014). Alternatively, soma and proximal dendrite-targeting PV+ cells could initially target apical dendrites and relocate their subcellular output target throughout development. In the mouse neocortex, GABAergic synaptic transmission also matures early and rapidly, as spontaneous IPSCs can be recorded in an increasing proportion of pyramidal cells throughout development, increasing from 14% of cells at E18-20 to 51% at P0-P2 and 73% at P3-P5 (Owens et al., 1999; Verhage, 2000). Synaptic inputs onto interneurons are also present early in development, as in the prefrontal cortex, spontaneous IPSCs and EPSCs were respectively recorded in 86% and 90% of FS interneurons (Yang et al., 2013a). These results suggest that the synaptic backbone is in place for interneurons to be an active part of early cortical circuits.

Early depolarising action of GABA

GABA is known to be the main inhibitory neurotransmitter of the adult brain. It acts mainly by binding to $GABA_A$ or $GABA_B$ receptors, causing Cl^- influx and consequent membrane hyperpolarisation (Wang & Kriegstein, 2009). This is due to a low intracellular concentration of chloride, put in place by the K^+-Cl^- cotransporter KCC2 (Rivera et al., 1999; Li et al., 2002; Wang et al., 2002). GABAergic synaptic inhibition implements many important computation processes in the brain, including synchronisation of the activity of pyramidal neurons, gain control and temporal and spatial sharpening of activity and receptive fields (Isaacson & Scanziani, 2011). However, there is ample evidence that early in development, GABAergic inputs have a depolarising action on pyramidal neurons (Obata et al., 1978; Mueller et al., 1984; Ben-Ari et al., 2012 for a comprehensive review), and that many developmental processes (including proliferation, migration, and synaptogenesis) are regulated by this depolarising action (Ben-Ari et al., 2007, 2012; Wang & Kriegstein, 2009; Kilb, 2012; Luhmann et al., 2014;). Depolarising GABA can generate sodium action potentials, activate voltage-gated calcium currents and remove the voltage-dependent Mg^{2+} block of NMDA receptors, leading to large calcium influx and signalling (Ben-Ari et al., 2012). Mechanistically, this early effect of GABA is explained by the transient predominant expression of the Na^+-K^+-$2Cl^-$ transporter NKCC1 over KCC2, whereby NKCC1 is expressed from mid-embryonic until the first postnatal week in rodents (Li et al., 2002; C. Wang et al., 2002; Blaesse et al., 2009;). This transporter imports Cl^- into cells, causing, upon $GABA_A$ receptor activation, efflux of chloride, resulting in depolarisation (Plotkin et al., 1997; Wang et al., 2002). Immature neurons receive GABAergic before glutamatergic inputs (Owens et al., 1999; Tyzio et al., 1999; Hennou et al., 2002). Because depolarising GABA can provide enough

membrane depolarisation to activate voltage-gated calcium channels, generate action potentials and relieve Mg2+ blockade of NMDARs, it has been suggested to be able to at least partially substitute for glutamate as an early excitatory neurotransmitter (Owens & Kriegstein, 2002; Wang & Kriegstein, 2009). These early properties of GABA imply that cortical GABAergic interneurons could be very important players in the formation of circuits and generation of network activity.

1.5.2. Development of cortical GABAergic microcircuits

Despite advances in understanding the principles of inhibitory cell afferent and efferent connectivity in the adult neocortex (Dantzker & Callaway, 2000; Yoshimura & Callaway, 2005; Kapfer et al., 2007; Silberberg & Markram, 2007; Xu & Callaway, 2009; Kätzel et al., 2010; Pfeffer et al., 2013; Pi et al., 2013), remarkably little attention has been devoted to the emergence and early engagement of GABAergic interneurons by thalamic and intracortical circuitry, and the few studies examining this question have focused on PV+ FS interneurons, using paired recordings (Daw et al., 2007a; Chittajallu & Isaac, 2010; Pangratz-Fuehrer & Hestrin, 2011; Yang et al., 2013a), as these cells can be found in reasonably high numbers in the neocortex.

Daw and colleagues studied the emergence of feed-forward inhibition in L4 of the barrel cortex (Daw et al., 2007a). Before P6, L4 spiny stellate neurons had a depolarised $GABA_A$ reversal potential of -55mV, suggesting early GABAergic inputs to these cells are depolarising. However, connection probability (under 10%) and unitary FS-spiny stellate IPSC amplitude (~6pA) were both low at P3-P5, suggesting the circuit is not yet assembled at this age and is indeed very weak. Thalamic stimulation-evoked feed-forward inhibition was weak and delayed at P3-P5, and was

shown to emerge at P8-P9 due to an abrupt strengthening of thalamic-FS synapses relative to thalamic-spiny stellate inputs, an event that occurred concomitant to increases in FS-spiny stellate connection probability and unitary amplitude. Indeed, whereas at P3-P5 thalamic-evoked EPSP amplitude at FS and spiny stellate cells was similar, by P8-P9 thalamic-FS EPSPs were nearly 3-fold larger than their spiny stellate counterparts. Concurrently, FS-spiny stellate synapses showed developmental strengthening, with connection probability (30%) and unitary IPSC amplitude (20pA) both increasing sharply at P8-P9 (Daw et al., 2007a). These experiments suggest that the thalamocortical feed-forward circuit of L4 is only assembled at the end of the first postnatal week. However, an earlier report showed that thalamic stimulation-evoked IPSCs could be recorded in L4-L6 excitatory neurons of the barrel cortex already at P3, suggesting that deep-layer interneurons could potentially receive early thalamic inputs and project to L4-L6 before L4 FS cells are recruited by the thalamocortical circuit and form synapses with L4 excitatory neurons (Agmon et al., 1996). The relatively late emergence of thalamic-FS connectivity has subsequently been shown to be experience-dependent (Chittajallu & Isaac, 2010). Whisker deprivation started at P5 resulted in a decrease in thalamic-FS relative to thalamic-spiny stellate EPSC peak amplitude, concurrent to increased thalamic-FS EPSC failure rate. Interestingly, there was a decrease in thalamic-mediated IPSC/EPSC amplitude ratio in the spiny stellate neurons of whisker-trimmed animals. This was likely due to activation of a reduced number of interneurons by thalamic input, as there was no change in thalamic-FS peak EPSC amplitude or FS-spiny stellate unitary IPSC amplitude (Chittajallu & Isaac, 2010). It is unclear however, whether thalamic-spiny stellate EPSC amplitude was altered in response to whisker trimming.

Two further studies used paired recordings to study the development of FS-FS and FS-Pyramidal microcircuits in L5/6 of mouse visual (Pangratz-Fuehrer & Hestrin, 2011) and L3/4 prefrontal (Yang et al., 2013a) cortices. Despite the different brain regions and cortical layers studied the findings were largely in accordance. In terms of FS-FS connectivity, GABAergic chemical connections were shown to emerge at P5 (20% probability) in visual cortex, with a sharp increase and subsequent stabilisation occurring at P9 (40%) (Pangratz-Fuehrer & Hestrin, 2011). In prefrontal cortex, chemical FS-FS connections emerged at P7-P8 (10%) and increased steadily in probability until P30 (70%) (Yang et al., 2013a). In both areas, GABA conductance showed a steady increase from the first postnatal week until P16 (Pangratz-Fuehrer & Hestrin, 2011; Yang et al., 2013a) Gap-junction coupling between FS cells emerged in both brain areas at P5-P6, showing a coupling rate of 10 and 26% for prefrontal and visual cortices respectively. Conductance and coupling probability increased until P15-P18, by which point connection probability reached approximately 50% (Pangratz-Fuehrer & Hestrin, 2011; Yang et al., 2013a). Gap-junction mediated connections were never observed between FS cells and pyramidal neurons (Pangratz-Fuehrer & Hestrin, 2011; Yang et al., 2013a). FS to pyramidal connections emerged at P5-P6 with 10-20% connection probability. The amplitude of GABAergic inputs to pyramidal neurons increased from this timepoint until P8-P11, after which it plateaued (Pangratz-Fuehrer & Hestrin, 2011; Yang et al., 2013a). Curiously, both studies found a peak in FS to pyramidal cell connection probability around P8-P11, followed by a transient decline and return to P8-P11 connection probability values after P15 (Pangratz-Fuehrer & Hestrin, 2011; Yang et al., 2013a). There was also a continuous developmental decrease in failure rate, indicating higher signalling reliability. These data are consistent with recordings of FS-spiny stellate neurons in

barrel cortex L4, which showed a trebling of connection probability and 4-fold increase in unitary IPSC amplitude between P3-P5 and P8-P9 (Daw, Ashby, & Isaac, 2007a). Yang and colleagues showed that pyramidal to FS connectivity can be detected by paired recordings as early as P3-P4 and that connection probability increases steadily throughout development from 10% at P3-P4 to 50% at P15-P16 (J. M. Yang et al., 2013a). Concurrent to increased connectivity, unitary IPSC amplitude increased more than 4-fold between P3-P10 and P15-P16 and failure rate decreased from ~40% to under 5%.

Together, results from the three studies reviewed suggest that bi-directional microcircuits involving pyramidal and FS interneurons can be detected as early as P3, but significant circuits and connectivity only emerge at the end of the first postnatal week, with connection probability and unitary amplitude increasing until P16 (Figure 1.12). Chemical and electrical communication between FS cells develops later, towards the end of the first postnatal week, and connection probability and conductance increase until the beginning of the third postnatal week. It seems therefore that GABAergic control of the pyramidal network emerges prior to disinhibitory control. Another conclusion that can be drawn from these experiments is that, at least for a particular subtype of interneuron, the FS cell, developmental programmes are set in motion such that integration into the cortical network occurs over very similar timescales regardless of region (visual, somatosensory, prefrontal cortex) and cortical layer (L3, L4, L5/6). Taking into account the differing developmental timelines of the three areas mentioned as well as results from whisker trimming experiments (Chittajallu & Isaac, 2010), circuit integration of FS cells

appears independent from sensory experience, indicative of cell-autonomous regulation and potentially genetic determination.

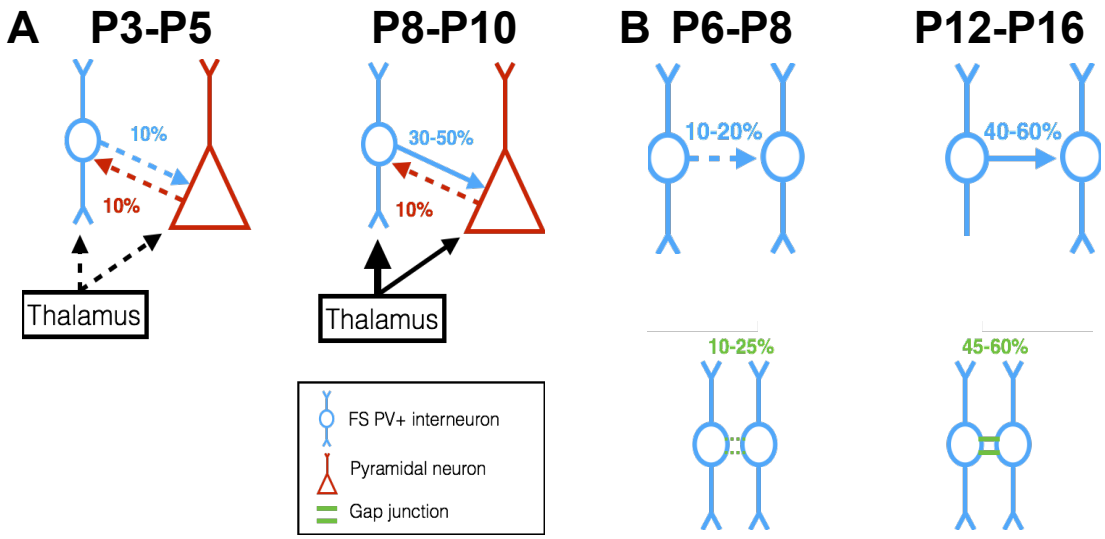


Figure 1.12. Development of cortical GABAergic microcircuits. A. Development of circuits between excitatory and inhibitory neurons. Left, top: reciprocal communication between pyramidal neurons (red) and FS/PV$^+$ interneurons (light blue) can be first detected at P3-P5 (connection probability in percent). Thalamic inputs (black) to both these cell types are weak and possess similar amplitudes at this age. Right, top: at P8-P10, connection probability from FS/PV+ cells to pyramidal neurons reaches the mature level. Thalamic inputs onto L4 FS/PV$^+$ cells are disproportionately strengthened throughout development, compared to inputs to excitatory neurons. **B.** Development of circuits between inhibitory neurons. Left, top: FS-FS GABAergic connections can be first detected at P6-P8. Right, top: FS-FS connection probability reaches mature levels between P12 and P16. Left, bottom: FS interneurons are gap junction-coupled, and this can first be detected at P6-P8. Right, bottom: By P12-P16, a high mature level of gap junction-coupling probability is reached.

Similar experiments are yet to be performed for other cortical interneuron subtypes, but appear of great importance, given the hypothesis that pioneer GABAergic synapses target apical dendrites (Tyzio et al., 1999; Hennou et al., 2002; Ben-Ari et al., 2007; Le Magueresse & Monyer, 2013) and that deep-layer interneurons possibly receive thalamic input and innervate L4 prior to FS neurons in that layer (Agmon et al., 1996). It is worth considering that in spite of their excellent resolution, paired recordings are a very low-throughput method of assaying connectivity. LSPS

approaches such as glutamate uncaging allow a form of multiplexing – single-input resolution is sacrificed at the reward of being able to test multiple connections in the same experiment. Moreover, paired recording is an unsuitable method for mapping cross-laminar communication, as connection probabilities drop very fast with increased distance.

1.5.3. Hub cells and early network activity

Early in postnatal hippocampal development, it is possible to record spontaneous, synapse-driven network oscillations termed giant depolarising potentials (GDPs) (Ben-Ari et al., 1989), which may be analogous to cortical spindle bursts. Work in the Cossart laboratory has established within developmental neuroscience the influential notion that rare, hyperconnected GABAergic "hub" neurons could play a key role in initiating, terminating and modulating such early network events (Bonifazi et al., 2009). Using two-photon calcium imaging in acute *in vitro* hippocampal slices, Bonifazi and colleagues built functional connectivity maps portraying the statistical relationship between the activity of imaged neurons (Bonifazi et al., 2009). This enabled targeted patching and network dynamic imaging of cells with a known degree of functional connectivity. In this study, the authors identified high connectivity (HC) and low connectivity (LC) neurons. HC cells displayed powerful cell/network interactions; phasic stimulation of these neurons could trigger GDP network synchrony, decrease GDP occurrence or modulate GDP frequency, leading the authors to term them "hub" cells. Further to functional connectivity, paired recordings revealed that GABAergic hub cells connected with 37% probability to "follower cells", neurons in which a calcium response could be triggered by stimulation of the hub cell. Comparatively, only 8% of follower cells were found to be connected with

HC pyramidal cells. Hub cells were able not only to influence high numbers of neurons, but also received spontaneous EPSPs four times as frequently as LC neurons, showing they likely sample inputs from a widespread pre-synaptic population (Bonifazi et al., 2009). Hub neurons have been proposed to obey the following features: 1) high output functional connectivity; 2) their stimulation affects network dynamics significantly; 3) they are GABAergic (although glutamatergic hub cells have also been reported, see Marissal et al., 2012) and their axons arborise widely, crossing subfield boundaries; and 4) they receive a higher number of EPSPs and have a lower spike threshold than other interneurons (Bonifazi et al., 2009; Picardo et al., 2011).

Subsequent work sought to clarify the identity of hub cells. Two main challenges precluded investigation of this issue. First, hub cells are a rare population. Second, many of the characteristics used to classify interneurons are not yet fully developed at the early timepoint at which hub cells were described (Bonifazi et al., 2009). To skirt around these issues it was necessary to permanently label hub cells, in order to enable their investigation in the adult. Picardo and colleagues hypothesised that hub neurons could be early generated interneurons (EGins). The reasons for this are that hub neurons were characterised by advanced morphophysiological features (Bonifazi et al., 2009), and that "preferential attachment" rules from graph theory (Barabasi & Albert, 1999) predict that in a developing network, new elements preferentially form connections with nodes that are already well connected (Picardo et al., 2011). This is an interesting principle that could also apply to SPns, as they are amongst the earliest-born neurons of the cortex (Allendoerfer & Shatz, 1994; Kanold & Luhmann, 2010). To fate map EGins, Picardo and colleagues tamoxifen-pulsed a Dlx1/2CreER^{TM} Cre

driver line at E7.5-E9.5, crossed to a Cre-dependent EGFP reporter line (Sousa et al., 2009). Short-term fate mapping and BrdU labelling suggested that EGins were likely to be born before E10.5 (Picardo et al., 2011). EGins had diverse morphologies, but were consistently found to target dendrites, not somata, and to reside in all hippocampal areas. A significant proportion of EGins could be labelled immunohistochemically by somatostatin (45%) and mGluR1alpha (72%). Over half of EGins expressed both markers. EGins very rarely stained for PV, VIP, CB or CR (Picardo et al., 2011). Contrary to late-generated interneurons (LGins), EGins displayed morphophysiological characteristics similar to hub cells, including a very extensive axonal arborisation, hyperpolarised spike threshold, depolarised resting membrane potential and higher spontaneous EPSP frequency (Bonifazi et al., 2009; Picardo et al., 2011). Importantly, calcium imaging experiments showed that EGins have high effective connectivity and influence network dynamics similarly to hub neurons (Bonifazi et al., 2009; Picardo et al., 2011). The study of Picardo and colleagues thus elaborated on the hub neuron concept by showing that cells with similar hub-like properties are generated early, express SST and form part of a dendritic-targeting class of interneuron (Picardo et al., 2011).

1.5.4. Are there hub cells in the neocortex?

At this point, neocortical equivalents of hub neurons have yet to be described. We should perhaps be cautious about directly translating the hippocampal hub neuron concept to primary sensory cortical areas. The neocortex and hippocampus show different architectural and connectivity features, with cortical circuits organising around thalamic input and columnar architecture (Douglas & Martin, 2004). Moreover, although early cortical networks express prominent network oscillations

like their hippocampal counterparts, there are important differences between the two systems, namely that *in vivo* recordings suggest that in the neocortex, GABAergic cells do not play a role in rhythm generation but rather serve to constrain spatiotemporally the spread of oscillatory activity (Minlebaev et al., 2007; 2009; 2011), whereas in hippocampal acute *in vitro* slices depolarising GABA has a crucial influence in the generation of GDPs (Ben-Ari et al., 2007; 1989). Nonetheless, despite having been proposed to influence network dynamics in several ways, hub neurons do not generate rhythms and are not necessarily pacemakers; they are defined chiefly by their high functional and effective connectivity, which allows them to act as crucial nodes in neuronal information flow and convey activity to very high numbers of neurons (Picardo et al., 2011). It should also be noted that *in vivo* recordings pose significant challenges to pharmacological dissection, as drug penetration into the tissue can be complicated, especially in the deep layers. Additionally, despite evidence for a depolarising action of GABA *in vitro* (Ben-Ari et al., 2012), studies have yet to replicate this effect *in vivo*. Taking these arguments into account, it is possible that *in vivo* studies are underestimating the role of GABA in early cortical network oscillations, and early GABAergic circuits, possibly involving hub cells, should not readily be discounted as important contributors towards developmental network activity. It should also be highlighted that *in vitro* studies could suffer from the converse problem: an underestimation of glutamatergic connectivity due to the silencing effect that slicing and lower activity levels have on nascent, labile glutamatergic synapses (Groc et al., 2006; Hanse et al., 2009; 2013).

Consistent with *in vivo* data (Minlebaev et al., 2007; 2009; Yang et al., 2009) and the spatial characteristics of early cortical network oscillations (Sun & Luhmann, 2007;

Yang et al., 2009), a neocortical GABAergic hub neuron could play an important role in constraining early network activity patterns to functionally-related neurons within the same cortical column (Figure 1.14). Since the thalamus is the chief external afferent of the neocortex (Douglas & Martin, 2004) and both gamma and spindle burst oscillations correlate highly with thalamic afference (Minlebaev et al., 2011; Yang et al., 2013b; Yang et al., 2009), we would expect a cortical hub neuron to receive early thalamic input, if such a cell is to have a significant impact on network activity. A second source of external drive that has been shown to generate network activity in the neocortex are basal forebrain cholinergic afferents (Dupont et al., 2006; Hanganu et al., 2007) and so cortical hub neurons could express cholinergic receptors, as has been shown for hippocampal EGins (Picardo et al., 2011). The axons of hippocampal hub cells span several fields (Bonifazi et al., 2009; Picardo et al., 2011). The two dominant patterns of cortical early network activity, early gamma oscillations and spindle bursts, have been shown to confine to local columnar domains across all layers (Sun & Luhmann, 2007; Yang et al., 2013b; Yang et al., 2009), and in order to sustain such activity patterns, the axons of a cortical hub neuron could cross laminar domains, influencing activity in multiple cortical layers. Hippocampal hub cells have been proposed to be early-born, dendrite-targeting interneurons (Bonifazi et al., 2009; Picardo et al., 2011). Putting together the pieces of this puzzle, an attractive candidate for a GABAergic cortical hub neuron could be a deep-layer Martinotti cell. Martinotti cells are early-born (Miyoshi et al., 2007) somatostatin-positive, dendrite targeting interneurons that can be found in layers 2-6 of the neocortex, but preferentially reside in layers 5 and 6 (Wang et al., 2004; Xu et al., 2006; Ma et al., 2006; Silberberg & Markram, 2007;). Their defining feature is an ascending axon that extends all the way to L1 and can arborise in L4 and L2, besides

branching collaterals in deep layers (Wahle, 1993; Wang et al., 2004; Ma et al., 2006; Xu et al., 2006), which provides these neurons with the capacity to influence activity in several cortical layers in a column. Martinotti cells have been shown to receive facilitating thalamic input in the mature barrel cortex (Tan et al., 2008). Moreover, cholinergic agonists have been shown to greatly excite somatostatin-positive neurons in L2/3 of the barrel cortex (Fanselow et al., 2008). Physiologically, Martinotti cells can be classified as low-threshold spiking interneurons (Kawaguchi & Kubota, 1997; Wang et al., 2004). Reported depolarised resting membrane potentials and spike thresholds for these cells (Wang et al., 2004) are similar to those reported for hippocampal hub neurons (Bonifazi et al., 2009; Picardo et al., 2011). In the absence of network activity data, is perhaps premature to put forward this population as a cortical hub neuron candidate, especially when the concept at this point in time appears somewhat fluid (Marissal et al., 2012; Picardo et al., 2011). Suffice to say for the moment that Martinotti cells show several characteristics that would position them well to be pioneers in modulating early intracortical and thalamocortical connectivity.

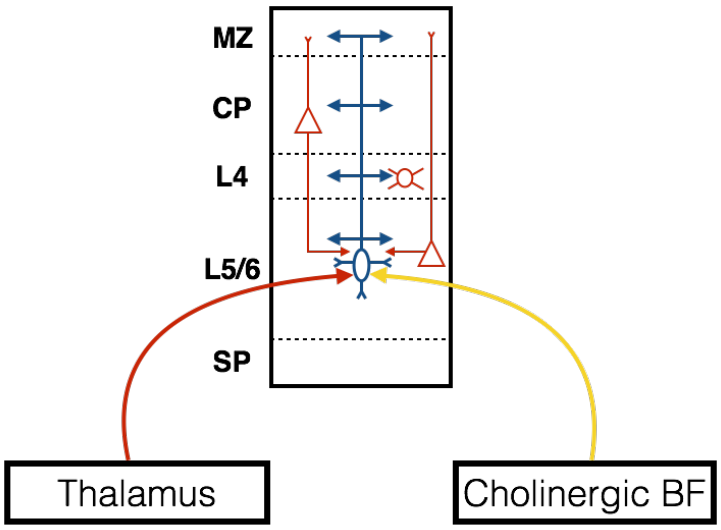


Figure 1.14. A hypothetical cortical hub neuron. In the neocortex, a hub neuron candidate could be predicted to receive thalamic and cholinergic input. Other characteristics would be a

high degree of cross-laminar functional output connectivity, endowing this cell will the ability to influence the activity of many post-synaptic neurons. On the pre-synaptic side, it would sample input from a high number of excitatory neurons, spread out across different layers.

1.6. Thesis objectives

"Is two years of pain and frustration all that it takes to make you give up on something?"

Professor Yang Dan, to me, over breakfast at the FENS-IBRO Causal Neuroscience Summer School. Bertinoro, Italy, June 2011.

In this chapter I reviewed the dominant early patterns of activity in the neocortex and a silent synapse-based framework for the emergence of the canonical pattern of excitatory cortical connectivity. I also assessed evidence on the possibility that subplate neurons and interneurons, particularly GABAergic hub cells, form early circuits fundamental for network activity. Despite a growing understanding of the patterns and characteristics of early network activity patterns in the cortex, we know surprisingly little about the primordial cortical circuits that may be in place to support such events. This knowledge would be informative not only from a basic scientific point of view, but also from a disease standpoint, as perturbations of early developmental events may result in the development, later in life, of psychiatric or neurological conditions (Ben-Ari & Spitzer, 2010; Marín, 2012).

In the experiments of my thesis, I sought to use optical stimulation techniques in the slice to clarify the organisation of early thalamocortical and peri-thalamocortical circuits that may provide fundamental conduits for early sensory information entering the cortex and to support early patterns of network activity. Optical stimulation

techniques have provided significant advances over electrical stimulation in dissecting circuitry. Glutamate uncaging allows stimulation of focused pre-synaptic domains without affecting axons of passage (Dalva & Katz, 1994; Anastasiades & Butt, 2012; Shepherd, 2012), permitting laminar identification of afferent inputs to a recorded cell. Channelrhodopsin-assisted circuit mapping can be used in a cell-type specific manner to selectively stimulate identified pathways (Boyden et al., 2005; Fenno et al., 2011; Zhang et al., 2007). Optogenetic stimulation offers a particular advantage in the study of thalamocortical circuits as it can enable selective stimulation of thalamic afferents, a difficult result to achieve with electrical stimulation due to the extensive reciprocal connectivity between the thalamus and cortex. Moreover, channelrhodopsin-assisted circuit mapping enables even the stimulation of afferents severed from their parent soma, bypassing the electrical stimulation requirement for full preservation of thalamocortical pathways in the slice (Petreanu et al., 2007). However, to date only one study has employed optogenetics to study developing neural circuits in the mouse, focusing on retinofugal pathways (Zhang et al., 2012). The objective of my first project (Chapter 3) was to apply optogenetics to the study of the developing thalamocortical pathway. I characterised the photoresponses of thalamic and cortical pyramidal neurons electroporated with channelrhodopsin, and then attempted to map and characterise identified thalamic inputs to L4 spiny stellate cells, L5b pyramidal neurons and subplate cells.

In this introduction, I have developed the hypothesis that subplate neurons could form key, privileged nodes of the developing cortical network. In Chapter 4 I test this hypothesis by using glutamate uncaging and electrical stimulation to characterise

early thalamic and cortical excitatory inputs to subplate neurons, focusing on the Lpar1-GFP$^+$ subtype.

In Chapter 5, I focused on a deep-layer interneuron population that is also labelled fluorescently in the Lpar1-GFP line (Hoerder-Suabedissen & Molnár, 2012). I characterised the intrinsic diversity of this cohort, then studied the maturation of its intrinsic properties and thalamic input characteristics. I followed by employing glutamate uncaging to characterise the integration of Lpar1-GFP interneurons into the cortical excitatory network during the first two postnatal weeks. Consequent to the results achieved, I recorded used glutamate uncaging to map the development of afferent inhibitory inputs (Xu & Callaway, 2009) into L4 spiny stellate neurons, as well as studying the role of afferent sensory activity in the establishment of such inputs.

2. Methods

2.1. Slice preparation

All animal experiments were approved by the local ethical review committee and conducted in accordance with Home Office personal and project (70/6767) licenses under the UK Animals (Scientific Procedures) 1986 Act. For optogenetic experiments, I used a CD1 wild-type (WT) line. To target subplate neurons and Martinotti cells, I recorded from the Lpar1-GFP line (Tg(Lpar1-EGFP)GX193Gsat, on an NIHS background) (Hoerder-Suabedissen & Molnár, 2012). Prior to slice preparation, mice were deeply anesthetized with isoflurane. Mice were removed from the anesthetic chamber and decapitated with surgical scissors. The brain was dissected in ice-cold, normal artificial CSF (aCSF), composed from (in mM): 125 NaCl, 2.5 KCl, 25 $NaHCO_3$, 1.25 NaH_2PO_4, 1 $MgCl_2$, 2 $CaCl_2$, 20 glucose. The aCSF had been previously infused with 95% O_2/5% CO_2 for at least 10 minutes. Thalamocortical slices (350-500 μm) containing the somatosensory regions of the neocortex (modified from (Agmon & Connors, 1991)) to newborn mice (Higashi et al., 2002; Molnár et al., 2003)) were cut in 1-3ºC ACSF using a vibratome equipped with a sapphire blade (Vibratome 3000 Plus; The Vibratome Company, St. Louis MO, USA) and transferred individually to a storage chamber (Harvard Apparatus, UK) containing normal ACSF maintained at room temperature, infused with 95% O_2/5% CO_2. Slices were allowed to recover for 45-60 minutes before recording (Anastasiades & Butt, 2012).

2.2. Whole-cell patch-clamp electrophysiology

Individual slices were transferred to the recording chamber and continuously perfused

with room temperature aCSF infused with 95% O_2/5% CO_2. A slice hold-down (Harvard Apparatus, UK) was used to stabilize brain slices. Intracellular recordings were obtained using borosilicate glass microelectrodes (Harvard Apparatus, UK) of 6-9MΩ resistance, pulled using a Narishige PC-10 electrode puller (Narishige, Japan). Microelectrodes were filled using a syringe with an intracellular solution of the following composition (in mM): 128 K-gluconate, 4 NaCl, 0.3 Li-GTP, 5 Mg-ATP, 0.0001 $CaCl_2$, 10 HEPES, and 1 glucose. pH was calibrated to 7.2-7.4 using KOH. In select recordings, either 0.2% Lucifer Yellow or 3 mg/ml biocytin (Sigma-Aldrich, UK) were included, to enable morphological reconstruction of recorded cells. Cells were visualized using an Axiocam MRM camera (Carl Zeiss Ltd., UK) attached to a Zeiss Axioscope FS-2 plus microscope (Carl Zeiss Ltd., UK), with a UPlanFL N 40x objective (Olympus Ltd., UK), IR-DIC filter block (Carl Zeiss Ltd., UK) and Axovision software (v4.6). Target neurons were selected from cells at >50μm depth below the surface of the slice. After attaining whole-cell patch-clamp configuration, neurons were further recorded from and included in experiments and analysis if they obeyed criteria for cell health which were briefly tested by baseline activity recording and current injection. These criteria were: 1) overshooting action potentials reaching at least +15 mV at peak; 2) action potential half-width appropriate for developmental stage and cell type recorded (interneurons: 1-4 ms prior to P8; 0.6-2 ms after P8; excitatory neurons: 2-5 ms prior to P8; 1.5-3 ms after P8); and 3) stable resting membrane potential exhibiting minor (< 5 mV) fluctuations (apart from periods of spontaneous synaptic activity). These parameters were checked throughout experiments to ensure cell health. Recordings where such parameters were not verified were discarded from further analysis. Depending on the experiment, recorded cells were DsRed2/ChR65-positive thalamic relay neurons in the ventrobasal nucleus

or L2/3 of S1; subplate neurons; L4 spiny stellate neurons; L5b pyramidal neurons; Lpar1-GFP positive subplate neurons and Lpar1-GFP positive L5 and L6 neurons. Pyramidal neurons were selected by their characteristic morphology, with prominent apical dendrite ascending towards the cortical surface. L4 spiny stellate cells were distinguished based on the small, round appearance of their soma. All cortical neurons were recorded from somatosensory cortex. The microelectrode was lowered onto selected neurons using a motorized micromanipulator (Luigs & Neumann, Germany), whilst applying constant positive pressure via a syringe connected to the pipette holder by silicone tubing and a stopcock (Harvard Apparatus, UK). As the microelectrode was lowered towards the cell, a 25mV test pulse at 20Hz frequency was applied in voltage clamp mode (Multiclamp 700B, Molecular Devices, USA, CA). The positive pressure was changed to negative pressure once a dip in the test pulse and a dimple on the target cell was observed, indicated the electrode was close to the cell. Negative pressure was then applied via a mouthpiece until a tight seal was achieved. This was indicated by a flat test pulse on the Axioclamp software, meaning that a gigaohm seal had been achieved. Once the seal was established, a short sharp pulse of negative pressure was applied at the mouthpiece, in order to rupture the membrane and enter whole-cell patch-clamp configuration.

2.3. Determining intrinsic properties of recorded neurons

After achieving whole-cell configuration, intracellular recordings were started in current clamp mode. To assess the intrinsic properties of a cell, 500ms square depolarizing or hyperpolarizing current pulses at 0.5Hz were programmed into Clampex software (Molecular Devices, CA, USA). In order to determine values for the different parameters of intrinsic physiology examined, different current protocols

were used (Figure 2.1). Pulse magnitude was chosen depending on the intrinsic excitability of the cell. Intrinsic properties were monitored occasionally throughout recordings, in order to check cell health and access. Cells showing significant deterioration in access or input resistance were discarded from further analysis. All cells were analysed offline using Clampfit (v10.1, Molecular Devices, CA, USA). Immediately after achieving whole-cell configuration, baseline activity of the cell was recorded in current clamp. Positive current was injected into the cell in order to achieve a general idea of its excitability and intrinsic maturity, and to determine the amplitude of current injection to be used in different protocols. This baseline recording also allowed monitoring of the health of a cell and patch quality. These were determined on the basis of a stable baseline, spike height reaching above +15mV and spike threshold more negative than approximately -30mV (Figure 2.1A). Patches with poor access or unhealthy cells typically displayed short spike heights and atypical spike thresholds. If a cell was determined to be healthy and showed good access, several current injection protocols were used. For each one, the current pulse was adjusted to produce: a threshold spike, hyperpolarizing responses to -100mV to determine voltage sag and presence of rebound spikes, hyperpolarizing responses of <10mV to determine input resistance and maximum firing frequency before spike failure. Based on these protocols, a number of additional parameters could be determined.

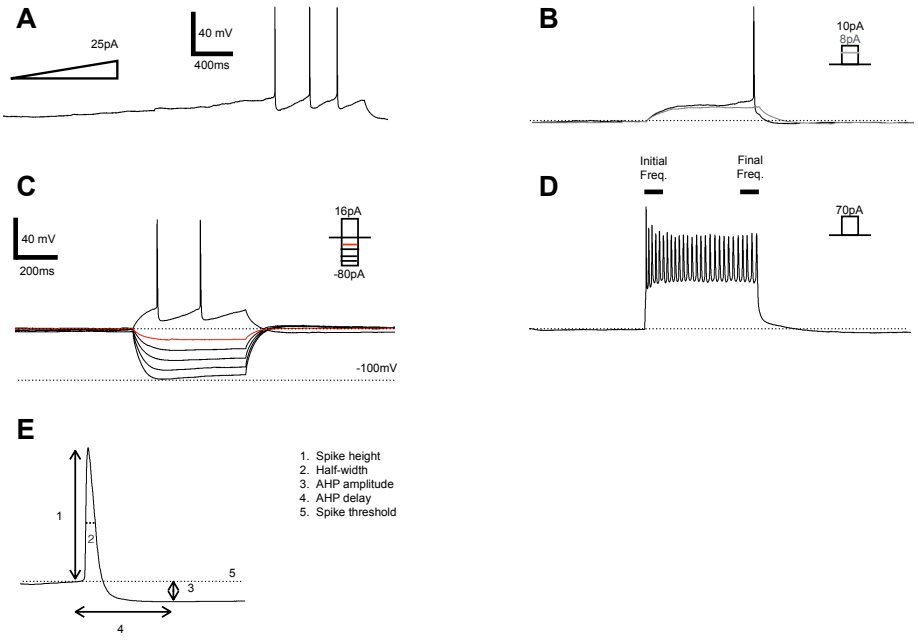


Figure 2.1. Current input protocols used to calculate electrophysiological parameters. **A-D** response of a cortical pyramidal neuron to current input protocols. **A.** Ramp to spike, to determine approximate threshold and rheobase of the cell. **B.** Small current steps to elicit a threshold spike. **C.** Response to hyperpolarizing current steps. Input resistance was calculated from the smallest hyperpolarizing step, which was 1/5 of the current needed to reach -100mV (red). **D.** Maximum firing frequency. Initial and final frequency were determined respectively for the first and last 100ms intervals in the spike train, in order to calculate accommodation. **E.** How each action potential property was calculated, from the threshold spike of the recorded cell. Current pulses in **B-D** were 500ms duration, and injected current is shown next to the trace in panels **A-D**.

2.4. Laser scanning photostimulation

Laser scanning photostimulation (LSPS) is a broad term used within neuroscience for a strategy where a laser beam is scanned over a defined region of brain tissue (*in vivo* or *in vitro*) in order to stimulate cells in different locations of that region by a variety of means. This includes direct activation of transgenic light-sensitive ion channels expressed by those cells (Boyden et al., 2005; Petreanu et al., 2007; Zhang et al., 2007) or photolysis of a caged compound, which will then diffuse and act on nearby cells (Zemelman et al., 2003; Anastasiades & Butt, 2012; Shepherd, 2012). This approach is mostly used for mapping synaptic inputs onto a given cell population. During stimulation of locations in the region of interest, experimenters monitor

putative synaptic responses onto a target cell, by recording its activity under voltage or current-clamp. In my experiments, LSPS was performed using an ultraviolet (UV) (DPSL-355/30), for glutamate uncaging, or 473nm wavelength laser (Vortran Stradus 473-80), for optogenetics experiments. In both cases, optical stimulation was directed to specific locations in a region of interest by using a UGA-40 targeting module (Rapp OptoElectronic GmbH). Depending on the experiment, either the UV or 473nm lasers were coupled to the microscope via a fiber-optic cable (62 μm core diameter for the UV laser; 50μm for the blue laser, both Thorlabs, Germany) and focused through a Zeiss Axioskop FS2-plus microscope and 10x UPLFLN objective (Olympus Ltd., UK). For both UV and 473nm stimulation experiments, beam diameter was approximately 50μm at the slice plane.

For glutamate uncaging experiments, after running a cell through the protocols for intrinsic properties, the perfusing medium was switched to a high divalent cation (HDC) aCSF solution, which was identical in composition to normal aCSF with the exception that it contained raised levels (4 mM) of $MgCl_2$ and $CaCl_2$, and in addition, 100 μM methyl 1-[5-(4- amino-4-carboxybutanoyl)]-7-nitroindoline-5-acetate hydrate-caged glutamate (Sigma-Aldrich, UK; Tocris, UK). This medium was continually infused with a 95% O_2/5% CO_2 gaseous mixture. The HDC aCSF and caged glutamate solution was washed into the recording chamber for a period of 4-6 minutes before beginning uncaging experiments. The solution was recirculated by collecting in clean glassware and adding it back to the initial solution. We programmed a laser-targeting grid manually in custom software provided by Rapp Optoelectronic (Hamburg, Germany). The software controlled galvanometric mirrors in the UGA-40 module, which directed the position of the laser beam across the slice.

The mapping grid was designed in a 9 by 17 spot pattern (width by height), with a spacing of 50μm between spots. Spot order was organized in a pseudorandom fashion to prevent sequential stimulation of adjacent sites. The laser was fired at 1 Hz, with no stimulation at adjacent sites occurring within 4 seconds. When mapping, the grid was aligned perpendicular to the surface of the slice, and the electrode tip position was aligned to a specific stimulation spot, which was noted at the time of recording. Before each experiment, a photomicrograph of the grid overlaid on the slice was taken. This allowed us to allocate the responses from each recording site to a particular marginal and tangential position in the cortex. Prior to mapping, we used the "click and fire mode" of the Rapp software to uncage glutamate at different spots over the cell in current clamp, in order to check the response of the recorded cell to glutamate uncaging. This allowed us to calibrate laser intensity to produce excitation restricted as much as possible to the vicinity of the recorded cell's soma. Thorough calibration experiments were also performed with putative pre-synaptic populations to the cells of interest. This will be discussed in detail in Chapter 4. Cells were then switched to voltage-clamp mode to record laser-evoked synaptic inputs. Voltage-clamp recordings were made with a high-pass filter set at 0.05Hz at a holding potential of -70mV. Several repeats of each map (typically 2-6) were performed for each cell. The recording trace was separated into 1 second recording bins, targeted from a Master-8 pulse isolator (A.M.P.I., Israel). Laser pulse duration was 100ms. UV laser power was calibrated to evoke ~2 action potentials when the laser was fired directly at the cell soma, but minimize suprathreshold responses elicited at distal sites (more detail in Chapter 4). Maximum power obtained at the specimen plane was 2 mW for the UV laser, but the actual power range used for mapping experiments was between 0.3mW and 1.2mW.

For optogenetic experiments, after obtaining intrinsic property recordings from cells, I briefly switched from IR-DIC to wide-field blue illumination to test the cell's channelrhodopsin-mediated response to light. This was done as a quick way to ensure we were recording, depending on the experiment, from a ChR65-positive neuron (which would spike or show a light-evoked potential) or from a cortical ChR65-negative neuron surrounded by ChR65-positive thalamic axons (which would show a light-triggered EPSP). For characterization of photo-responses of ChR65-positive neurons and single input experiments, a single spot was programmed into the custom Rapp Optoelectronic software, and aligned to the cell soma under the 10x UPLFLN objective (Olympus Ltd., UK). Laser stimulation was delivered at 0.2-1Hz and triggered by a Master-8 pulse isolator (A.M.P.I., Israel), similar to UV laser experiments. Laser pulse duration was 1-5ms and maximum laser power at the specimen plane was 3.5mW. The range of intensities used for experiments was from 70μW to 3.5mW. Since ChR65 expression varied between preparations, laser intensity had to be tailored to each slice. When recording from a cortical neuron for studying single thalamic inputs or mapping their distribution by LSPS, laser intensity was adjusted to produce a single monophasic, reliable EPSC. For single input experiments, stimuli were delivered every 5s. For LSPS experiments, the same 9 by 17 spot grid was used as previously described for glutamate uncaging. A photomicrograph of the grid overlaid on the slice was taken prior to recording, in order to allow correlation of evoked responses and stimulation spot position.

2.5. Mapping inhibitory inputs

For mapping global inhibition onto L4 spiny stellate neurons, a Cesium-based internal solution was used (Xu & Callaway, 2009), composed of the following, in mM: 100

gluconic acid, 0.2 EGTA, 5 MgCl, 40 HEPES, 2 Mg-ATP, 0.3 Li-GTP. CsOH was used to equilibrate pH to 7.2-7.4. This solution prevents neuronal spiking and thus allows users to voltage-clamp cells at depolarised membrane potentials, enabling recordings at the reversal potential for glutamate (Xu & Callaway, 2009). Under such conditions, outward currents represent GABA-mediated IPSCs. Reversal potentials for glutamate were worked out for each cell by uncaging glutamate at the cell soma and changing the membrane potential until only a minimal inward current could be evoked. This approach helped separate outward, putative GABAergic currents from inward glutamatergic ones. Reversal potential for glutamate using this solution was between +5 and +20mV. To ensure that under these recording conditions outward currents were GABAergic, I recorded maps of afferent synaptic input at the reversal potential for glutamate under standard aCSF and aCSF containing picrotoxin (50μm) (n = 3 cells). All putative synaptic responses recorded in standard aCSF at the reversal potential for glutamate were abolished under picrotoxin. Moreover, no synaptic responses were observed when recording at the reversal potential for glutamate during picrotoxin experiments.

2.6. Analysis of LSPS data

For both glutamate uncaging (excitatory and inhibitory input mapping) and optogenetic experiments, current traces were analyzed offline using Minianalysis 6.0 (Synaptosoft Inc.) and all EPSCs logged. In instances where multiple, summating EPSCs were observed within the event detection window, the minianalysis multipeak extrapolation function was used to ensure an accurate representation of total input. The number and amplitude of EPSCs that occurred within the response interval were subsequently extracted using a customized Matlab R2011 script (The MathWorks).

To generate the synaptic input map the sum amplitude of the time-locked EPSCs was calculated for each target spot per run, and then averaged across all sweeps. Input maps were further analysed by computing "laminar" and "columnar" profiles, as well as determining the layer of origin of mapped inputs. For laminar profiles, total input from each 50μm row was summed and the laminar distribution of total input in pA plotted. This allowed a depiction of the laminar organization of input into a cell, regardless of its horizontal origin. Laminar profiles could then be averaged across multiple cells by alignment along the pial surface, cell soma or a known fixed anatomical landmark, such as the L4-L5a border. Laminar profiles were calculated both in terms of total input (the total sum amount of synaptic input in pA per 50μm row) and normalized input, where the percentage of input arising from each 50μm row was calculated instead, relative to the total amount of input received by that cell. Columnar profiles were obtained by a similar process. Rather than summing input for 50μm rows, the calculation was performed for individual 50μm columns, resulting in a plot of the columnar integration width for each cell, i.e., how wide a cortical region it received input from. Similar to laminar profiles, columnar equivalents were calculated both in "raw" and normalized fashion. Finally, layer distribution of inputs was calculated by determining layer boundaries from DIC micrographs of the entire mapped region taken during recordings. These boundaries were applied to the input maps, and the total synaptic input arising from mapped spots at each layer was calculated. For each cell analysed, this was performed "raw" (total sum amount of synaptic input originating from each layer in pA) and normalized (proportion of input arising from each layer in percentage, relative to the total input received by that cell).

2.7. Electrical stimulation of thalamic afferents

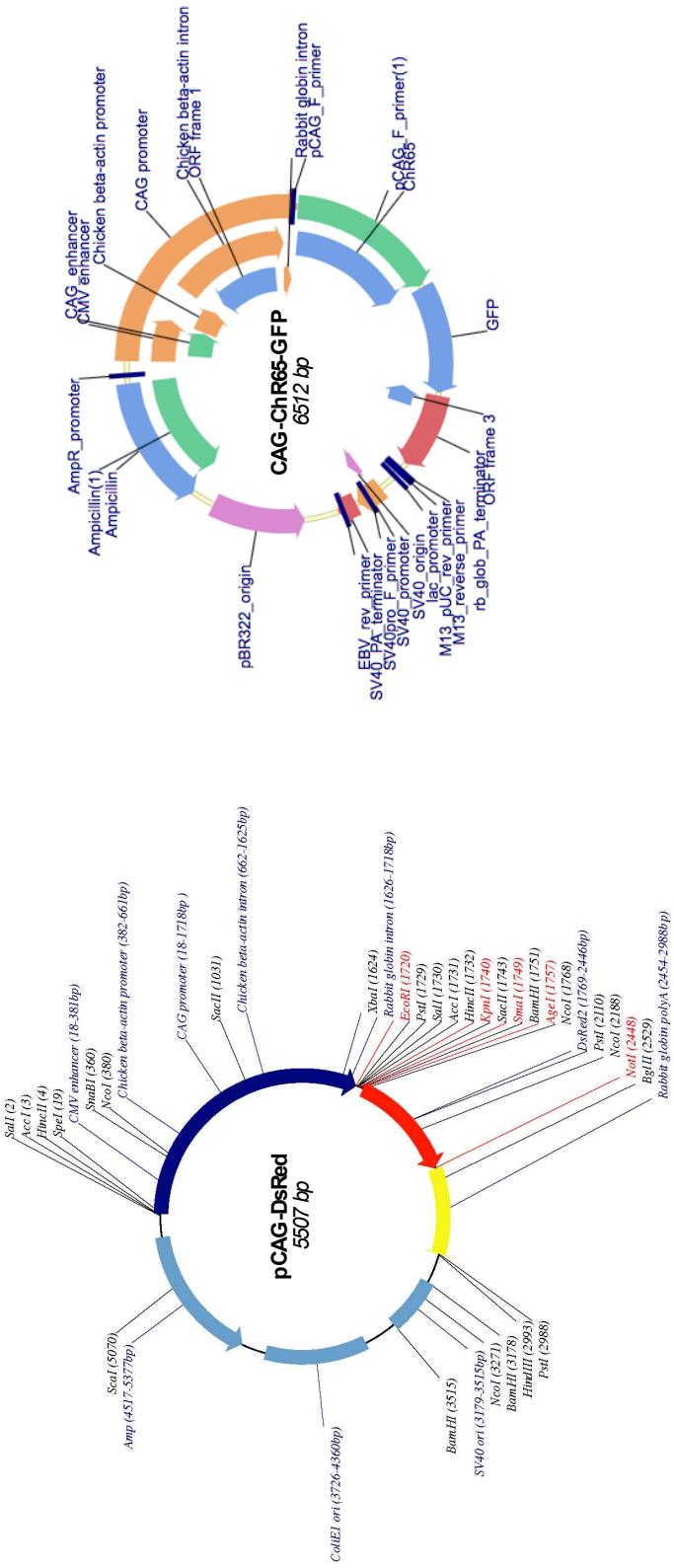
To probe for thalamic afferents innervating the recorded cells, a bipolar stimulating microelectrode (tip impedance 1 MΩ; 72-0375, Harvard Apparatus, UK) was placed in the ventrobasal nucleus (VB) of the thalamus or the internal capsule (IC) and connected to a current isolator (Constant Current Isolated Stimulator model DS3, Digitimer Ltd, UK). Stimulation strength was as necessary for evoking all-or-none, threshold responses according to a minimal stimulation protocol (Isaac et al., 1997; Raastad et al., 1992) between 15-1,000 μA pulses of 200 μs duration. Inter-stimulus interval was 30-60s.

2.8. Plasmid preparation

In my thesis, I used CAG-ChR65-GFP and DsRed-pCAGGS plasmids, both on pCAGGS expression vector. CAG-ChR65-GFP was obtained from the Boyden lab (Ed Boyden, MIT, USA). DsRed-pCAGGS was obtained locally, from the Molnár lab, from Dr. Fernando García-Moreno. DNA for CAG-ChR65-GFP was extracted from filter paper sent by Professor Boyden. Briefly, the filter paper portion containing DNA was placed in an Eppendorf tube with 50μl of nanowater and kept at room temperature for 2h. Competent bacteria were transformed by mixing with 10μl of DNA in an Eppendorf tube and heat shock for 30s at 42ºC followed by placement on ice for 5 minutes. 900μl of SOC medium (Invitrogen, UK) were added to the Eppendorf tube. This was then placed in a shaker incubator at 37ºC for 1h, at 250 rotations per minute (rpm). After incubation, the tube was centrifuged for 3 minutes at 5000rpm, ant the supernatant removed. The remaining pellet was dissolved in 100-200μl supernatant and spread on an agar plate. The agar plate was left to stand for 5 minutes at room temperature and then placed overnight in an incubator, at 37ºC. On

the next day, a single colony was picked and placed inside a 5mL culture tube with Luria-Bertani (LB medium). The culture tube was placed in a shaker-incubator (250rpm, 37ºC) for 8h. Following this period, 500μl of the culture were transferred to a sealed 250mL autoclaved Erlenmeyer flask, containing 50mL of LB medium and ampicillin (1:1000). This culture was then taken to the shaker incubator, where it was placed for 14-16h (250 rpm, 37ºC). The remaining culture was used to prepare glycerol stocks, by mixing with 70% glycerol in autoclaved nanowater. Glycerol stocks were kept at -80ºC. DNA from cultures was purified using Qiagen MaxiPrep kits and protocols (Qiagen, Hilden, Germany). After purification, typical DNA concentration yield was 1.0-1.5μg/μl. This was concentrated to 2-3μg/μl using 10kD ab93349 spin columns (Abcam, Cambridge, UK). Similar culturing and purification procedures were used for the DsRed-pCAGGS plasmids. DsRed and ChR65-expressing cDNA sequences are under control of the chicken β-actin/rabbit β-globin promoter and cytomegalovirus immediate-early (CMV-IE) enhancer element present in the pCAGGS backbone (Figure 2.2 A-C).

Figure 2.2. pCAG-DsRed and CAG-ChR65-GFP expression vectors.



2.9. *In utero* electroporation

I conducted initial *in utero* electroporation experiments at the laboratory of Dr. Tomomi Shimogori, in RIKEN (Tokyo, Japan), where I learnt this technique according to an approach developed by Dr. Shimogori (Fukuchi-Shimogori & Grove, 2001; Shimogori, 2006; Shimogori & Ogawa, 2008; Matsui et al., 2011). For initial experiments, timed-pregnant CD-1 mice were obtained from an in-house breeding facility at RIKEN BSI. Surgeries in Oxford were carried out on timed-pregnant C57Bl/6 mice bred at the BSB Level 2. Noon of the day when a vaginal plug was detected is termed E0.5. Laparotomies were performed at E11.5 and E15.5. Aanaesthesia was induced with sodium pentobarbital or 5% isoflurane and hair from the abdomen was shaved. An initial incision was made along the skin above the abdomen of the pregnant dam, and a second on the muscle wall, exposing the uterine horns. All horns were placed on top of 37˚C PBS (phosphate buffered saline)-moistened cotton gauze draped around the wound and embryos were visualized through the uterus with a fiber optic light source, whose tip was kept moist with PBS. For plasmid injection, either a mixture of a DsRed2-pCAGGS (concentration 0.5-1.0 μg/μl, volume 1-2μl) or CAG-ChR65-GFP (concentration 1.0-3.0 μg/μl, volume 1-2μl) plasmids was mixed with 2% fast blue (Sigma) and injected into the right or third cerebral ventricle of each embryo through a 30-70μm wide-tip glass capillary. For thalamic electroporations (E11.5), external tungsten and platinum electrodes were positioned outside the uterus, either side of the head of the embryo, at a 0 degree angle to the axial plane. The positive electrode was placed at the right side of the embryo's head, in order to target the right dorsal thalamus for transfection. Five square-wave current pulses (27 to 30V, 50 ms) were delivered, resulting in gene transfection of embryonic thalamic neurons. For cortical electroporations (E15.5),

external tungsten and platinum electrodes were positioned outside the uterus, with the positive electrode placed over the area of the right hemisphere to be transfected (in most cases putative S1). Five square-wave current pulses (46V, 50 ms) were delivered, resulting in gene transfection of cortical plate neurons (future L2/3 pyramidal neurons). Muscular and skin incisions were separately sutured and animals were kept warm until recovering from anaesthesia. For initial experiments testing targeted delivery of constructs, dams were allowed to recover and survive for 48h, after which they were sacrificed and embryos extracted and brains collected. Fluorescence expression in the brain was screened at low magnification under a fluorescent dissection microscope. Selected brains positive for DsRed2 were fixed overnight in 4% paraformaldehyde and cut into 40-60 μm sections for imaging under fluorescent microscopy. In all other cases, pregnancies were allowed to carry until natural delivery, for slice physiology experiments.

2.10. Immunohistochemistry

Frozen cryostat-cut OCT slices of P8 mice (14 μm) were thawed and washed in PBS (0.1 M). Non-specific binding sites were blocked with 10% normal goat serum (NGS) in 0.1% PBST (PBS-Triton) for two hours, followed by overnight incubation with a combination of the following primary antibodies: a) IgG2A mouse anti-GFP (1:400 in NGS-PBST, 4°C, Invitrogen), b) rabbit anti-Lhx6 (1:2000 in NGS-PBST, 4°C, kind gift from Vassilis Pachnis, National Institute for Medical Research, Medical Research Council, London) or c) rat anti-Somatostatin (1:400 in NGS-PBST, 4°C, Millipore MAB 354). The primary antibody was washed-off with PBS (0.1 M, 3x 5 mins), slices were incubated and shaken in 10% NGS in 0.1% PBST for half an hour and then incubated with the secondary antibody for two hours in the dark (goat-anti-

mouse conjugated to Alexa-488, 1:500 in NGS- PBST; donkey-anti-rabbit conjugated to Alexa-568, 1:500 in NGS- PBST; goat-anti-rat conjugated to Alexa-568, 1:500 in NGS- PBST, all at room temperature, Invitrogen). After washing off the secondary antibody with PBS, the slice was incubated in 4',6-Diamidin-2-phenylindol (DAPI, 1:500 in PBS) for half an hour and rinsed with PBS again. For fluorescence imaging, slices in PBS were then cover-slipped and imaged using a fluorescence microscope (Leica DMR fluorescence microscope with Leica DFC500 camera (Leica Microsystems, UK) or a confocal microscope (LSM 710, Carl Zeiss Microimaging, UK). For quantification, cortical slices were subdivided into 10 bins running parallel to the pial surface. Cells within each bin were then counted manually. Bins were subsequently assigned to the cortical layers by using the DAPI-image.

2.11. Morphological reconstruction of biocytin-filled neurons

Following recordings, slices with biocytin-filled neurons were fixed overnight in 4% paraformaldehyde and then washed in phosphate-buffered saline (PBS, 0.1 M). Subsequently, cell membranes were permeabilised using 1% Triton-X-100 in PBS (PBST, 30 minutes) and incubated for 12-24 hours with a streptavidin-Cy3 conjugate (1:500; Sigma, UK) in 0.5% PBST. After rinsing the slices several times in PBS (0.1 M), they were mounted in 70% glycerol, cover-slipped and sealed with nail polish for fluorescence confocal imaging (LSM710, Carl Zeiss Microimaging, UK). Confocal images of cells were then treated and analysed using the Simple Neurite Tracer plugin in Fiji (Longair et al., 2011; Schindelin et al., 2012).

2.12. Infraorbital nerve transection

Dr. Anna Hoerder-Suabedissen performed infraorbital nerve (ION) transection for a

subset of experiments at P0. Briefly, P0 Lpar1-GFP mice were anaesthetized by hypothermia. An incision was made on the left side of the snout, and the ION on the left side was cut with sterile micro-scissors. The wound was sutured with 3-0 silk thread and pups were warmed up and allowed to recover from anesthesia.

2.13. Statistical analysis

All statistical analysis was performed on GraphPad Prism (v6.0). The normality of the data was tested using Kolmogorov-Smirnov and Shapiro-Wilk tests. When these tests were in accordance and assumptions for parametric statistics were met, parametric tests were used. For comparing two populations, Student's t-tests were used. In cases where 3 or more groups were compared, a one-way ANOVA was used instead. Some experiments required two-way ANOVA for examining the effects of two independent variables and their interaction on a dependent variable. Whenever parametric assumptions were not met, non-parametric statistics were used, whenever a comparable test was available. Mann-Whitney tests were used to compare two groups. Wilcoxon signed-ranks tests were used to compare matched data between two timepoints or conditions and Friedman's tests were used for three timepoints/conditions. Finally, the Kruskal-Wallis test was used when comparing a dependent variable across 3 groups. All data are reported as mean ± standard error of the mean (SEM). For all tests, the threshold for significance was taken as $p = 0.05$, with data reported as falling within the 95% ($p < 0.05$), 99% ($p < 0.01$) or 99.9% ($p < 0.001$) significance levels.

Chapter 3 – Using optogenetics to map developing thalamic inputs to somatosensory cortex

3.1. Introduction

Over twenty years ago, the development of a slice preparation in which thalamocortical afferents are preserved afforded scientists a unique opportunity to study many properties of this fundamental synapse (Agmon & Connors, 1991). In this preparation it is possible to record monosynaptic EPSPs/EPSCs in cortical neurons, evoked by electrical stimulation of somatosensory thalamic afferents. Although subsequent similar preparations have been published in the auditory (Cruikshank et al., 2002) and visual cortex (MacLean et al., 2006), the barrel cortex remains the model system *par excellence* to study thalamocortical synaptic communication. Its advantages are that it processes sensory information in an ecologically-relevant modality to the rodent and exhibits a well-organised topographical pattern that can be traced from individual whiskers on an animal's snout all the way to its corresponding "barrel" in L4, an organised cluster of cells that respond chiefly to deflection of that exact whisker. This unequivocal correspondence between sensory periphery and thalamocortical domain enabled key experiments on the role of sensory activity in cortical development (Erzurumlu & Gaspar, 2012). Lesioning of specific rows of whiskers caused the corresponding barrels in L4 to shrink, and full de-afferentiation by ION transection resulted in a complete lack of barrels in the cortex. Crucially, it was found that such extensive topographic map plasticity could only be induced if the lesions were performed until postnatal day 4 (Van der Loos & Woolsey, 1973; Erzurumlu & Gaspar, 2012). This early work established that the concept of critical period, initially described in the visual cortex (Hubel & Wiesel, 1964), applied also to

other primary sensory cortices, highlighting the fact that sensory experience at critical junctures of development is key for correct circuit development in the cortex (Hensch, 2005). Sensory experience is relayed to the cortex via thalamic inputs, and concurrently to structural plasticity studies, a critical period for functional synaptic plasticity has also been defined for the thalamocortical synapse. In the barrel cortex, long-term potentiation can be induced by pairing low-frequency thalamic afferent stimulation with postsynaptic depolarization between P3 and P8 in the rat via an NMDAR-dependent mechanism (Crair & Malenka, 1995). Over this time window, the AMPA-NMDA ratio increases, and the decay time constant for NMDA EPSCs decreases significantly. Subsequent work investigated the hypothesis that silent synapses play a key role in expression of LTP at TC synapses (Isaac et al., 1997). The authors used minimal stimulation to active one or a few TC axons and found that under these conditions it was possible to elicit post-synaptic responses mediated via NMDA but not AMPA receptors. These synapses were termed silent, because at resting membrane potential the voltage-dependent Mg^{2+} block of NMDARs prevented any excitatory signaling, due to the lack of AMPARs (Feldman et al., 1999; Isaac, 2003; Hanse et al., 2013). Inducing LTP at such synapses led to "unsilencing", that is, the appearance of AMPAR-mediated responses (Isaac et al., 1997). It was shown also that the proportion of silent synapses decreased with development in a way that closely matched the critical period for TC plasticity (Isaac et al., 1997) described by Crair and Malenka (Crair & Malenka, 1995) *in vitro* and later by An and colleagues *in vivo* (An et al., 2012). These interesting results still left open, however, the question of how, in the absence of AMPA-mediated transmission, thalamic inputs depolarized L4 cells enough to relieve NMDARs of their voltage-dependent block and initiate signaling cascades that resulted in AMPAR insertion. One possible answer to this

question came after the observation that thalamic afferent stimulation evoked a dual-component EPSC in L4 cells, in the presence of the NMDAR blocker APV: one of them fast and AMPAR-mediated, the other slow and conducted via a Kainate receptor (KAR) (Kidd & Isaac, 1999). However, spontaneous and evoked mini-EPSC recordings never showed both components, suggesting that dual component EPSCs resulted from activation of two separate synapses and that AMPA and KA receptors did not co-localise at thalamocortical synapses (Kidd & Isaac, 1999; Bannister, 2005;). KARs display smaller peak amplitude than AMPARs, but, due to their slow decay time constant, total charge transfer is nearly five times higher than for AMPARs, suggesting they could provide enough drive to depolarize L4 cells beyond NMDAR-activation threshold (Daw et al., 2007b). Kidd and colleagues investigated the effect of LTP induction on ionotropic conductances in L4 and concluded that LTP induced an increase in the AMPAR component at the expense of the KAR component, whose contribution to transmission decreased throughout the course of the first postnatal week (Kidd & Isaac, 1999). Based on these results, it has been proposed that thalamocortical synaptic maturation involves LTP-induced conversion of synapses expressing KA and NMDA receptors to synapses containing AMPA and NMDA receptors (Daw et al., 2007b).

Though appealing, the body of work presented so far did not take into account the intimate association between the thalamus and the subplate (Allendoerfer & Shatz, 1994; Kanold & Luhmann, 2010). SPns receive functional thalamic inputs even before birth and their axons reach and innervate the overlying cortical plate, including L4, before thalamic axons do (Friauf et al., 1990; Friauf & Shatz, 1991; Higashi et al., 2002; Molnár et al., 2003). Additionally, there is evidence that SPns are important for

thalamocortical circuit maturation, as immunotoxic lesioning of the subplate prevents the formation of ocular dominance columns and results in the development of comparatively weak thalamic synapses with L4 (Kanold, 2003). Using the same technique, it has recently been reported that subplate lesioning largely abolishes barrel formation and the generation of early network oscillations (Tolner et al., 2012). Based on this body of work, an alternative model has been proposed, according to which thalamic information can reach L4 via two parallel routes: one mono-synaptic and the other di-synaptic, activating SPns which then project to L4. Weak activation of L4 via immature thalamocortical synapses would summate with di-synaptic thalamic inputs arriving via the subplate, which would induce action potentials in L4 correlated with pre-synaptic thalamic activity. This would lead to heterosynaptic LTP of the thalamic input to L4, presumably through STDP (spike timing-dependent plasticity) rules (Kanold, 2004; 2009; Kanold & Luhmann, 2010).

The two models are not mutually exclusive. One issue with the results presented in support of the first model is that the identity of the stimulated afferent inputs is not clear. This is an inherent limitation of using electrical stimulation, which can activate not only thalamic afferents as intended, but also other passing axons. This is problematic for the study of thalamic inputs to the cortex because L5, L6 and the subplate all project to thalamic nuclei (Grant et al., 2012). It is therefore possible, when stimulating the internal capsule or ventrobasal nucleus, to antidromically activate any of these neurons. This can lead to ambiguity when recording in L4 for instance, since neurons in this layer have been shown to receive inputs from the subplate (Friauf et al., 1990; Friauf & Shatz, 1991; Zhao et al., 2009). As noted by Kidd and colleagues (Kidd & Isaac, 1999), AMPA and Kainate receptors do not

coexist at the same thalamocortical synapses. It remains a possibility that distinct afferent inputs, one thalamic and one from the subplate, are separately activating these synapses, and such a hypothesis can only be ruled out by selectively stimulating identified afferents onto L4. Optical stimulation of thalamic afferents would represent a good option for such experiments. LSPS of caged glutamate would bypass the problem of antidromic activation, as uncaging glutamate at the cell body of VB neurons would not stimulate corticothalamic axons. The drawbacks of this particular approach are that it would still require the thalamocortical pathway from VB to S1 to remain largely intact and would preclude any pharmacological experimentation with glutamate channel blockers required for identification of AMPA, NMDA and KA pathways. Resorting to optogenetics would circumvent both of these issues. Channelrhodopsin-assisted circuit mapping (CRACM) has been used very effectively to map long-range projections, as it enables laser-evoked terminal release even from axons that have been severed from their somata (Petreanu et al., 2007; Petreanu et al., 2009; Cruikshank et al., 2010; Cruikshank et al., 2012). Since it relies on expression of a channelrhodopsin transgene, optical activation of afferents is entirely independent of glutamate, and therefore pharmacology experiments can be performed to isolate the contribution of different glutamate channel conductances. Despite its prolific use in the mature system, in the developing rodent channelrhodopsin has as of yet only been successfully used in the retina and spinal cord (Zhang et al., 2012; Hägglund et al., 2013). Possibly the reason for this is that individual channelrhodopsin channels have very small conductances and as such require long expression times, in order for enough copies of the channel to be expressed such that a cell can be reliably depolarized to spike threshold by an optical stimulus (Bamann et al., 2008; Schoenenberger et al., 2011). Typically, experimenters in the circuit mapping field

have allowed 10 days to 4 weeks between transfection of target structures with channelrhodopsin and slice experimentation (e.g. Petreanu et al., 2007; 2009; Cruikshank et al., 2010; Little & Carter, 2012), a prolonged time interval which precludes investigation of several important developmental phenomena.

Here, I attempted to use ChR65, a novel unpublished variant of channelrhodopsin with a reported faster expression time-course (E. Boyden, *personal communication*) in order to try to circumvent this problem. To improve our chances of achieving strong enough expression early in development, I delivered a high concentration solution of the plasmid (2-3 μg/μl) to the embryonic dorsal thalamus by performing *in utero* electroporation at E11.5. This would allow approximately 11 days between electroporation and the start of the thalamocortical critical period in the barrel cortex, which is just under the currently reported minimum expression times of 2-4 weeks. By adopting these measures, it was hoped that I could take advantage of channelrhodopsin to study the early postnatal development of thalamic inputs to the cortex. A further factor influencing the ability to generate action potentials using channelrhodopsin is the maturity of the transfected neurons. In mature rodents, for a particular cell population where channelrhodopsin has been expressed, intrinsic parameters have stabilized, whereas channelrhodopsin expression will continue increasing up to a plateau. In the developing neocortex, intrinsic properties change significantly over the first 2-3 postnatal weeks (Zhang et al., 2003; Maravall et al. 2004; Christophe et al., 2005; Oswald & Reyes, 2008), concurrently with channelrhodopsin expression. The interplay between these variables is therefore more complex, and the outcome, in terms of laser-evoked spiking, less predictable. It may be that the high input resistances and low rheobases evidenced by neonatal cells will

favor ChR65-elicited spiking. On the other hand, it could also be the case that ChR65 expression lags behind intrinsic maturation, precluding early experimentation. In the following section, I report experiments performed to address the use of optogenetics in early development.

3.2. Optical activation of ChR65-expressing neurons throughout development

I used *in utero* electroporation of the third ventricle at E11.5 in order to target CAG-ChR65-GFP transfection to primary sensory thalamic nuclei (Fukuchi-Shimogori & Grove, 2001; Shimogori, 2006; Shimogori & Ogawa, 2008; Matsui et al., 2011;) (Figure 3.1). The novel and unpublished ChR65 opsin construct was chosen because pilot experiments with the more commonly used ChR2 variant (Boyden et al., 2005; Zhang et al., 2007; Fenno et al., 2011) were unsuccessful, as I could only optically induce thalamic action potentials with reliability at P17, following E11.5 electroporation (experiments performed at the Tomomi Shimogori lab [Riken BSI, Tokyo]; data not shown). Moreover, ChR65 was reported to attain higher amplitude peak photocurrents and require shorter expression time (E. Boyden, *personal communication*). For ChR65 experiments, CAG-DsRed was co-electroporated at a 1:2 concentration level, as GFP levels were found to be too low for visualization in acute *in vitro* slices. Using this approach, I was able to obtain strong transfection of neurons in the somatosensory thalamus, mostly in the ventroposterior medial nucleus (VPM), but also the posterior medial nucleus (POm), which was evident as early as 48h after electroporation (Figure 3.1).

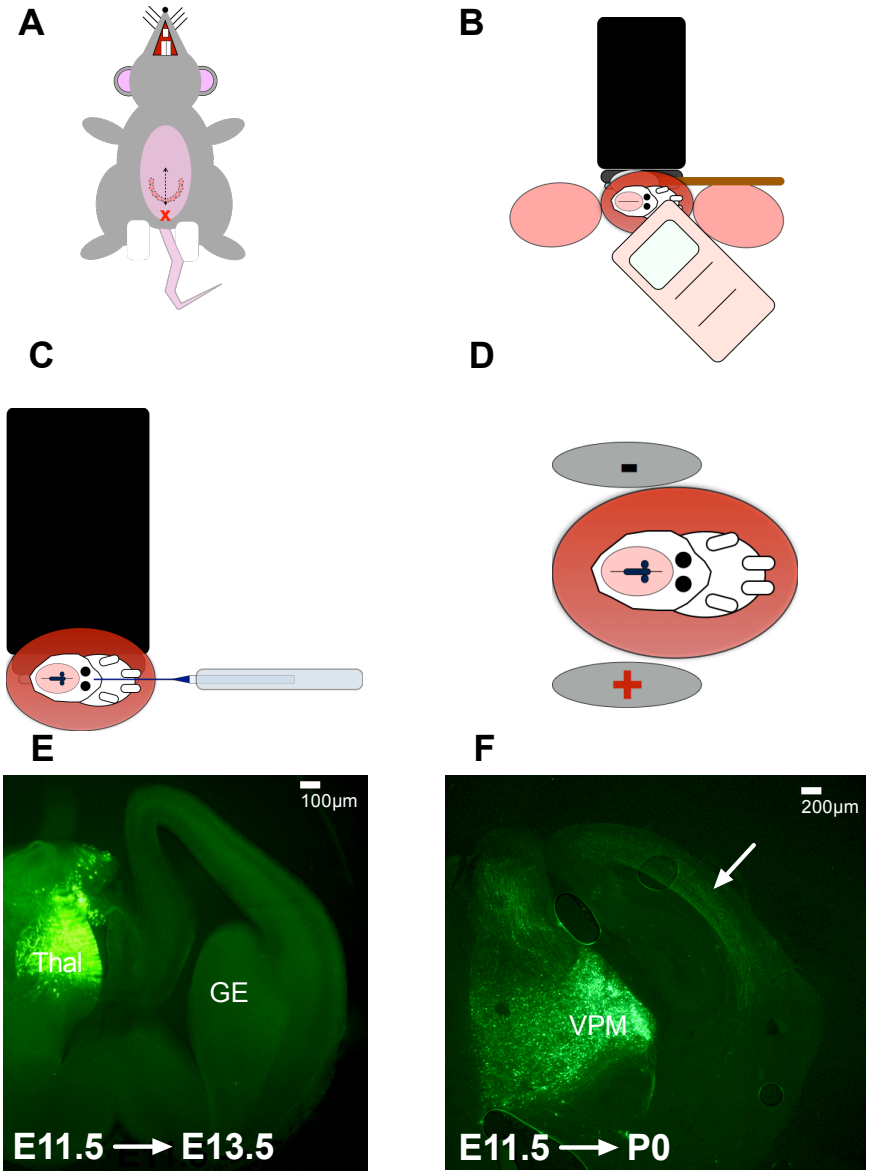


Figure 3.1. ***In utero*** **electroporation of the thalamus. A-D.** Schematic of surgical procedure. **A.** An incision is cut along the abdomen and muscle wall to reveal the uterine horns. **B.** Embryos are carefully positioned over a cold light source with the aid of a cotton bud, for trans-illumination. **C.** A plasmid solution mixed with a dye for easy visualization is injected into the third ventricle. **D.** Paddle electrodes are placed on either side of the embryo's head at a 0 degree angle. The positive electrode is placed at the right, to target transfection to thalamic nuclei on the right hemisphere. **E.** Example section of a thalamic electroporation performed at E11.5 with tissue harvesting at E13.5. **F.** Example section of a thalamic electroporation performed at E11.5 with tissue harvesting at P0. Note thalamic innervation of the deep cortical plate (arrow). Thal – thalamus; GE – ganglionic eminence. VPM – ventroposterior medial nucleus of the thalamus.

Transfection was usually stronger and more widespread in the VPM, but in most electroporations, expression was obtained also in the POm (Figure 3.2A). VPM and POm axons have different axonal arborisation patterns in the cortex, with VPM

terminals branching in L4 barrel hollows and the L5b/6 border, and POm terminals branching in L1 and L5a (Meyer et al., 2010a; Meyer et al., 2010b; Wimmer et al., 2010). I took fluorescent micrographs of thalamic terminals in the cortex and measured their fluorescence intensity profiles across the cortical depth for a sample of 7 slices taken from mice born following different surgeries (aged P12-P15). When I averaged the intensity profiles, a prominent fluorescence peak was found at L4, with minor peaks at L1, L5a, the L5b/6 border and the subcortical white matter tract, consistent with double POm and VPM labeling (Figure 3.2B-D). This lack of unequivocal identification of the pre-synaptic origin of input for mapping experiments means that conclusions are limited to general thalamic input rather than that arising from specific nuclei. As a prelude to investigating thalamic axon terminal stimulation, I first examined the response of transfected ChR65$^+$ thalamic relay neurons to 473nm laser stimulation. Co-electroporation with DsRed allowed me to visualize and target-patch fluorescent, ChR65$^+$ thalamic relay neurons (Figure. 3.2E, F). The rationale behind this was to establish the basic parameters for laser-evoked responses in ChR65$^+$ thalamic relay neurons.

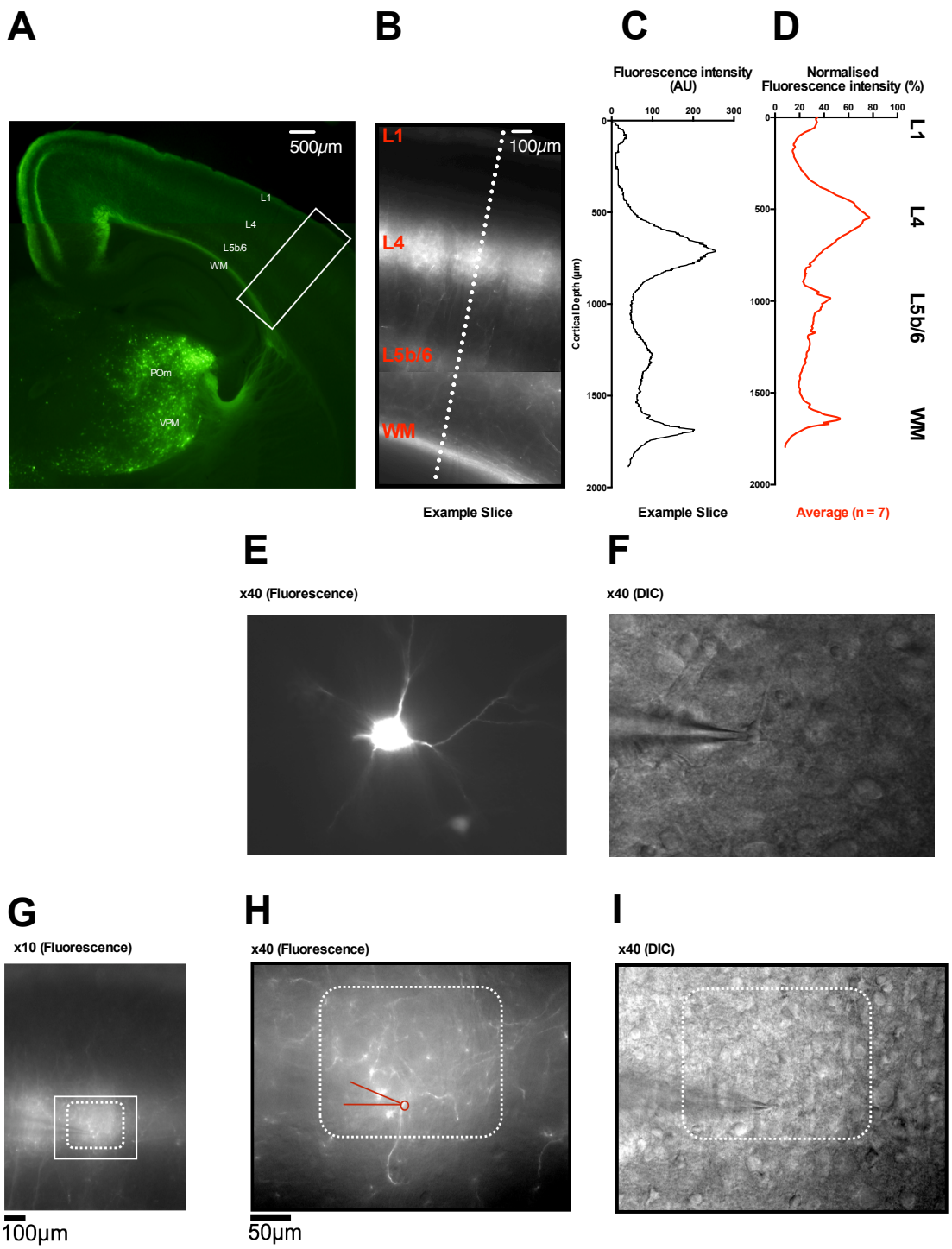


Figure 3.2. Targeted recording from thalamic relay and thalamorecipient neurons. A. Fixed thalamocortical slice (400μm) at P14, following thalamic electroporation with DsRed and ChR65-GFP at E11.5. Immunohistochemistry was performed for GFP in order to visualize ChR65 expression after fixation. **B.** Live thalamocortical slice image, following electroporation. **C.** Fluorescent intensity profile of slice in B was taken by measuring intensity levels along a radius of a barrel column (dotted line in B). **D.** Average fluorescence intensity profile for 7 slices originating from different electroporations. **E, F.** DsRed positive thalamic relay neuron under fluorescence and DIC, respectively. **G.** Recording a L4 spiny stellate cell in a DsRed/ChR65 labeled barrel. **H, I.** Same barrel as G, viewed under high power in fluorescence and DIC microscopy, respectively.

In total I recorded from 70 ChR65-positive thalamic neurons for direct response characterization experiments. Cells were arbitrarily divided into 3 age groups: P4-P9 (n = 38), P10-P12 (n = 13) and P13-P16 (n = 19). Channelrhodopsin has previously been shown to be sensitive to the frequency of stimulation (Cruikshank et al., 2010). As a first pass, I determined the ideal interval between laser pulses for ChR65 activation (Figure 3.3A). For these experiments, I used the maximum laser power (3.5mW at the slice interface). The 473nm laser pulse was targeted directly over the soma of the recorded cell and the frequency of pulses varied to ascertain the ideal interval for recovery of ChR65 function. Four cells (P10-P16) were recorded in these experiments, and for each cell, three different stimulation intervals were tested. Cells were recorded in voltage-clamp, under tetrodotoxin (TTX), and photocurrents were normalized, for each interval, to the current evoked by the first stimulus. For all intervals tested (1Hz, 0.5Hz and 0.2Hz) I observed a drop in photocurrent between the 1st and 3rd stimuli. This drop was more pronounced when using 1 or 2s intervals, and, for these intervals, continued until the 5th/6th stimulus, with photocurrents plateauing at around 50-60% of the amplitude evoked by the first stimulus. When I used 5s intervals, photocurrent amplitude stabilized by the 3rd stimulus at 79± 10% of the amplitude evoked by the first stimulus. Light has a clear sensitizing effect on ChR65 function, such that even 5s intervals do not allow full recovery. However, longer intervals would imply impractically prolonged recordings, and for all subsequent single-spot stimulation experiments I therefore used a 5s inter-stimulus interval.

I then set out to determine whether the stability in elicited direct photocurrent at 0.2Hz translated into an ability to reliably evoke action potentials in ChR65-

expressing thalamic neurons during the thalamocortical critical period for plasticity. Transfected thalamic neurons were recorded in current clamp at different timepoints with the 473nm laser targeted at the soma. Laser beam intensity was varied (70μW to 3.5mW), in order to establish the stimulus parameters required to reliably induce spikes. Pulse duration was kept constant at 1ms, and, for each cell, 10 stimuli were delivered in order to calculate spike probability. Figure 3.3B portrays probability of spiking as a function of postnatal age (days) and laser power (mW). Both variables had a powerful effect on spiking probability. Within each age, increasing laser power led to an increased probability of spiking. Likewise, spiking probability for any given laser power was higher at older ages. In fact, at P4-P9 spiking probability ranged from 0.13± 0.05 to 0.40± 0.08 (n = 38 cells). At P10-P12, values ranged from 0.35± 0.13 to 0.81± 0.10 (n = 13 cells), depending on laser power. It was only after P13 that action potentials could reliably be elicited using channelrhodopsin, with spiking probabilities ranging from 0.74± 0.10 to 0.95± 0.05 (n = 19 cells). An age-associated increase in probability of spiking could reflect an intrinsic property developmental effect or a ChR65 expression effect. To address this issue, I determined rheobase and input resistance of the recorded cells across development. Average rheobase varied from 28± 3pA at P4-P9 (n = 36) to 36± 8 at P13-P16 (n = 11). A Kruskal-Wallis test found no significant difference between age groups ($H(2) = 1.01$, $p = 0.602$). In contrast, the average input resistance did show a developmental change, going from 1078± 86MΩ at P4-P9 (n = 34 cells) to 493 ±72MΩ at P13-P16 (n = 10 cells) ($H(2) = 15.79$, $p < 0.001$). Plotting rheobase and channelrhodopsin-elicited spiking probability against age shows that both variables increase in value over development (Figure 3.3C). The maturation of intrinsic properties of thalamic neurons actually makes them less prone to spike, which suggests the age-associated increase in optically-evoked

spiking probability can be explained by developmentally accumulated ChR65 expression rather than intrinsic maturation.

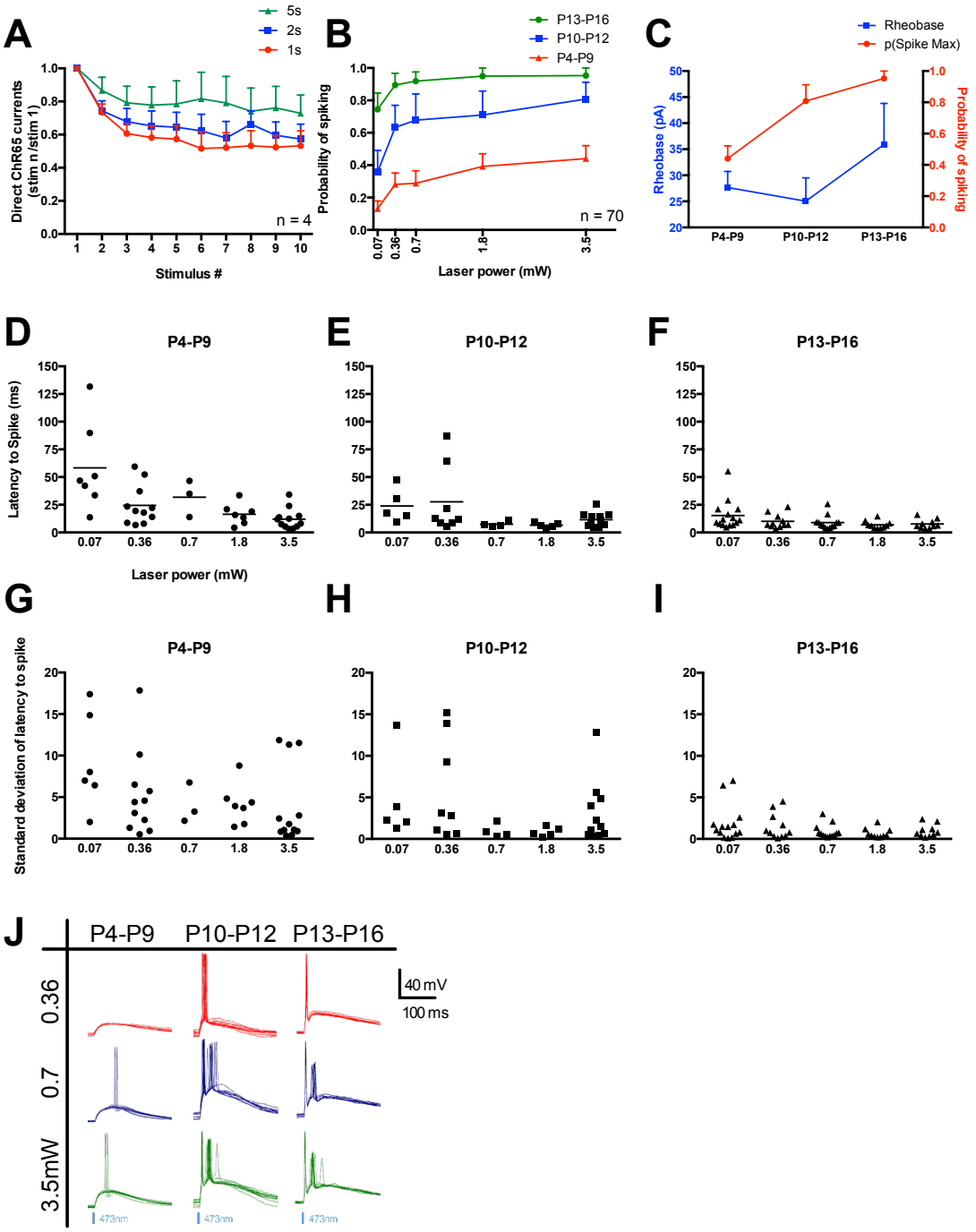


Figure 3.3. Characterisation of ChR65^{+} thalamic relay neuron responses to optical stimulation. **A.** Normalised photocurrent as a function of inter-stimulus interval (n = 4 cells). **B.** Probability of spiking as function of developmental stage and laser intensity (n = 70 cells). **C.** Relationship between rheobase and spiking probability as a function of age (P4-P9: n = 38 cells; P10-P12: n = 13 cells; P13-P16: n = 19 cells). **D-F.** Latency to spike as function of laser power at different developmental stages. Each symbol corresponds to the average value for 2-10 stimuli for a cell (P4-P9: n = 38 cells; P10-P12: n = 13 cells; P13-P16: n = 19 cells). It was not always possible to test the full range of stimulation powers for each cell. **G-I.** Standard deviation of latency to spike as function of laser power at different developmental stages. Cell numbers as in D-F. **J.** Example recording traces of laser-evoked potentials and spikes at increasing laser intensity and different developmental stages. Error bars are ±SEM.

It was apparent during recordings that increased age and laser power affected attributes beyond probability of spiking (Figure 3.3D-J). In particular, latency to spike onset seemed to decrease, and the temporal precision of spikes seemed to improve, denoting maturation in ChR65 functioning. This is evident in the example traces (Figure 3.3J), where spikes evoked at lower laser powers were characterized by a slow charging up phase, which was shorter at higher powers. The temporal precision of spikes was determined by calculating the standard deviation of latency to spike onset for a sequence of 10 stimuli for each cell. At P4-P9 there was substantial variability in responses, which decreased somewhat at higher laser powers. At P10-P12, responses seemed more consistent in their temporal characteristics, but it was only after P13 that the temporal reliability of channelrhodopsin truly emerged. Even at low laser powers, responses were remarkably consistent. Stimulation at high laser powers often elicited 2 spikes, and it was often the case that even the second spike showed considerably little variability in its onset (Fig. 3.3J bottom right).

Even a delivery approached geared to early development coupled with a fast-expressing channelrhodopsin was unable to result in expression sufficient to reliably drive action potentials in thalamic relay neurons before P10. To determine if this was a forebrain-wide phenomenon, I performed electroporation with the same constructs at E15.5, injecting this time into the lateral ventricle, in order to target L2/3 pyramidal neurons in S1. I recorded from a total of 18 ChR65^{+} L2/3 pyramidal cells. In order to further understand how photocurrents developed over the first postnatal week, I divided the first age group used for thalamic experiments (P4-P9) into three groups: P3-P4 (n = 3 cells), P5-P6 (n = 5 cells) and P7-P9 (n = 6 cells). I also recorded at P10-P12 (n = 4 cells). I determined laser-evoked spiking probability at each time point. In

each experiment, I followed this up by washing in tetrodotoxin (TTX) and determining photocurrent amplitude under voltage clamp. For each of these experiments, stimuli were repeated 10 times per cell. Spiking probability (Figure 3.4A) and peak photocurrent (Figure 3.4B) were plotted against age and laser power. At P3-P4, no spikes could be evoked regardless of laser power, and peak photocurrent was barely discernible above background, reaching 3± 1pA at maximum laser power. By P5-P6, there was a slight improvement in ChR65 performance, and photocurrent amplitude increased, ranging between 15± 2pA and 22± 3pA, however action potentials were only evoked 10-20% of the time. Figure 3.4C portrays the average amplitude of sub-threshold laser-evoked potentials at P3-P6. At P3-P4, this this ranged from 1.3± 0.4mV at the lowest laser power, to 2.4± 0.7mV for the highest. For cells recorded at P5-P6, depolarisations ranged from 7.4± 1.4mV to 11±2 mV. The transition between P5-P6 and P7-P9 appeared to be critical for ChR65 function. Spiking probability increased almost 4-fold at the highest laser power, and peak photocurrent amplitude practically doubled, ranging at this age from 31± 7pA at the lowest laser power to 49± 11pA at the highest. At P10-P12 it became possible to evoke spikes with >75% probability at all laser powers tested, similar to thalamic relay neuron data. There was a further increase in photocurrent amplitude, which ranged from 77± 24pA at the lowest laser power to 123± 22pA at the highest. I determined input resistance (MΩ) and rheobase (pA) for each L2/3 pyramidal neuron recorded. Input resistance was 2455± 248MΩ at P3-P4, 1900± 138MΩ at P5-P6, 1549±283 at P7-P8 and 870±105 at P10-P12. A Kruskal-Wallis test found a significant developmental decrease ($H(3) = 11.69$, $p < 0.001$). Rheobase was 10± 3pA at P3-P4, 9± 2pA at P5-P6, 17± 2pA at P7-P8 and 28± 5pA at P10-P12. A Kruskal-Wallis test found a significant developmental increase in rheobase (H (3) =

11.19, $p < 0.01$). In Figure 3.4D, I plotted rheobase and spiking probability against age group. As was the case for thalamic relay neurons, even though maturational changes in input resistance and rheobase made L2/3 pyramidal neurons less prone to spiking, laser-evoked firing probability and peak photocurrents increased steadily throughout development (Figure 3.4D, E). A two-way ANOVA comparing thalamic relay and L2/3 pyramidal neuron rheobase at P4-P9 and P10-P12 found no significant interaction ($F(1, 51) = 2.60$, $p = 0.113$), cell type ($F(1, 51) = 1.35$, $p = 0.25$) or age ($F(1, 51) = 1.28$, $p = 0.26$) effects. However, post-hoc comparisons revealed that rheobase was significantly lower for L2/3 pyramidal cells (13± 2pA) than thalamic relay neurons (28± 3pA) at P4-P9. At P10-P12, no significant differences were found between L2/3 (28± 4pA) and thalamic (25± 4pA) neurons. In Figure 3.4E I plotted rheobase against peak photocurrent. A two-way ANOVA revealed significant interaction ($F(3, 28) = 11.91$, $p < 0.001$), age ($F(3, 28) = 22.43$, $p < 0.001$) and measure (peak photocurrent vs rheobase) effects ($F(1, 28) = 26.71$). Post-hoc comparisons revealed that peak photocurrent significantly exceeded rheobase only at P7-P9 ($p < 0.05$) and P10-P12 ($p < 0.001$). The data presented for L2/3 pyramidal neurons corroborates that reported for thalamic relay cells and supports the idea that the function of ChR65 does not reach viable levels for spike generation until after the first 10 days of life, following *in utero* electroporation.

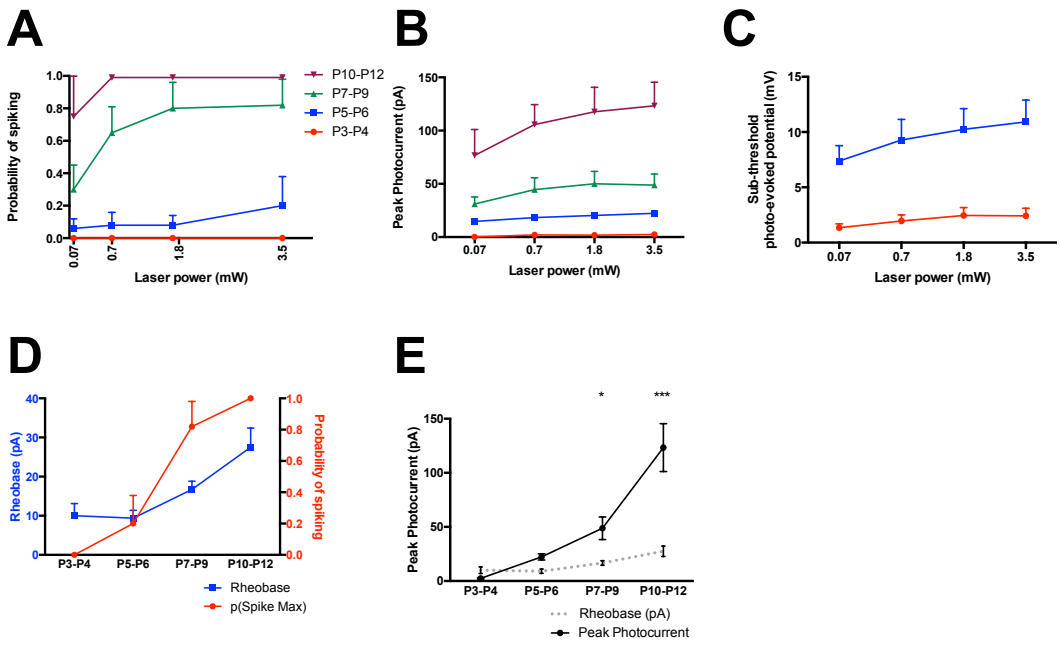


Figure 3.4. Characterisation of ChR65^{+} L2/3 pyramidal neuron responses to optical stimulation. A total 18 ChR65+ L2/3 pyramidal cells were recorded (P3-P4 n = 3; P5-P6 n = 5; P7-P9 n = 6; P10-P12 n = 4) **A.** Probability of spiking as function of laser power and developmental stage. **B.** Peak photocurrent amplitude under 1μm TTX as a function of laser power and developmental stage. **C.** Laser-evoked potentials at P3-P4 (red, n = 3 cells) and P5-P6 (blue, n = 5 cells) at different laser powers. **D.** Relationship between rheobase and spike probability as a function of developmental stage (P3-P4 n = 3; P5-P6 n = 5; P7-P9 n = 6; P10-P12 n = 4). **E.** Peak photocurrent amplitude under 1μm TTX as a function of age (P3-P4 n = 3; P5-P6 n = 5; P7-P9 n = 6; P10-P12 n = 4). Rheobase at each age plotted in dashed grey line. Error bars are ±SEM. *, $p < 0.05$; *** $p < 0.001$.

The sum of these data suggest that laser-evoked spike probability with ChR65 is very low during the first postnatal week, following *in utero* electroporation. Results for thalamic relay neurons and L2/3 pyramidal cells were similar in that spiking probability was very low during the first postnatal week. Furthermore, even though intrinsic developmental maturation of both cell types made them less prone to spike, laser-evoked spiking probability increased throughout development. An interesting difference was that L2/3 pyramidal cells achieved >75% spike probability at P7-P9 (Figure 3.4A), whereas thalamic relay neurons only overcame that threshold at P13-P16 (though spike probability at maximum laser power was 81% at P10-P12). This may be the consequence of differences in intrinsic properties, as L2/3 pyramidal cells

showed a significantly lower rheobase than thalamic relay neurons at P4-P9. Thus, standard channelrhodopsin approaches are not a viable experimental strategy during the first postnatal week. Moreover, given the extremely low photocurrent amplitude at P3-P4, either very little ChR65 expression occurs embryonically, or post-translational mechanisms interfere adversely with its function. Second, and lending further support to this first conclusion, even though thalamic electroporations were performed 4 days ahead of L2/3 ones (E11.5 vs E15.5), this did not confer any improvement in ChR65 function during thalamic recordings. If anything, thalamic ChR65 spiking reliability seemed delayed compared to L2/3, suggesting interactions between intrinsic property maturation and ChR65 function play an important, additional role to expression time course. In spite of its limitations for developmental use, ChR65 functioned with impressive reliability after P10. Therefore, I opted to change direction and use channelrhodopsin to characterize thalamic inputs to L4 spiny stellate cells, L5b pyramidal neurons and subplate (L6b) neurons after P10.

3.3. Using CRACM and sCRACM to study the thalamocortical synapse

Channelrhodopsin-assisted circuit mapping (CRACM) is the photo-activation of channelrhodopsin channels genetically encoded in select pre-synaptic neurons to activate identified afferent inputs to a particular cell population. Channelrhodopsin-expressing axon terminals can be stimulated using 473nm light sufficient to release neurotransmitter even if they are severed from their parent somata, making CRACM an ideal tool to map long-range projections that need not even be preserved in the brain slice (Petreanu et al., 2007; Cruikshank et al., 2010).

3.3.1. Determining stimulus parameters for CRACM

Experiments with ChR65$^+$ thalamic relay neurons informed me about experimental parameters to use in optogenetic experiments. However, CRACM involves the stimulation of ChR65$^+$ axon terminals, which are likely to respond differently from somata to stimulation. It was technically unfeasible for me to patch ChR65$^+$ axon terminals and therefore I recorded instead from putative post-synaptic L4 spiny stellate neurons whilst photo-stimulating thalamic axon terminals. Prior to performing input mapping experiments, I replicated previous thalamic relay neuron experiments to see whether principles derived from them held true for axon terminal stimulation. I recorded from 6 L4 spiny stellate cells between the age of P10 and P16, with the 473nm laser beam aimed at the soma, in order to stimulate ChR65$^+$ axon terminals closely apposed to it. Pulse duration was kept constant at 1ms and for each cell, and 10 stimuli were delivered. Figure 3.5A portrays sample CRACM-evoked TC-EPSCs in a L4 spiny stellate neuron at P15. Stimulation at higher laser intensities often resulted in summating EPSCs. In such cases, only the first event was analysed to prevent contamination by putative polysynaptic responses. During my thalamic relay neuron recordings, I determined that the vast majority of ChR65-evoked action potentials occurred within 25ms of laser stimulus onset. I therefore used the 25ms period after laser onset as my event detection window for laser-evoked EPSCs mediated by transmitter release from ChR65$^+$ thalamic axons. This value was used both for single-spot experiments (sections 3.3.1 and 3.3.2) and mapping experiments (sections 3.3.3 and 3.3.4). For the first experiment, for each cell, stimulus delivery frequency was varied (1Hz, 0.5Hz and 0.2Hz). For this experiment, laser stimulus intensity was calibrated to evoke a single, reliable monophasic EPSC. The same stimulus intensity was used for each interval. There was depression in EPSC

amplitude between the first and second stimulus, regardless of the interval used (Figure 3.5B). Amplitude depression between the first and second stimulus amounted to around 50%, but stabilised after the second stimulus such that no subsequent depression was evident. This was true for all intervals tested. Although varying the inter-stimulus interval (ISI) had no effect on EPSC amplitude, it did have consequences in terms of failure rate (Figure 3.5C). When laser stimuli were delivered at 1Hz, average failure rate was 23± 9%, decreasing to 8± 5% at 0.5Hz. At 0.2Hz, no failures were observed. For subsequent single-spot experiments I used a 0.2Hz stimulation rate, as this encouraged reliability.

Next I varied laser stimulus intensity and recorded laser-evoked thalamic EPSCS onto 10 L4 spiny stellate cells (age P10-P16) (Figure 3.5D, E). I used 360μW and 3.5mW stimulus intensity, with the purpose of evoking EPSCs that approximated the activation of a small number of inputs (360μW), and EPSCs corresponding to recruitment of several inputs (3.5mW). Increasing laser power resulted in a significant increase in EPSC amplitude (example traces Figure 3.5A), according to a Wilcoxon signed-ranks test ($p = 0.002$, $W = 55.0$). At 360μW laser power, average EPSC amplitude was 13± 2pA, whereas at 3.5mW a value of 20± 5pA was obtained (Figure 3.4D). Often at higher laser powers, delayed, summating EPSCs could be observed (Figure 3.5A, right). To prevent contamination by putative polysynaptic responses, only the earliest component of the EPSC was analysed. Increased laser power also resulted in a significant reduction in EPSC onset latency ($p = 0.004$, $W = -53.0$). At 360μW laser power, average EPSC onset latency was 6± 1ms, whereas at 3.5mW the value was 4± 1ms (Figure 3.5E). The data compare well with minimal stimulation experiments, where electrical stimulation is used at very low intensities to activate a

single or a few afferent fibers and study unitary afferent inputs (Raastad et al., 1992; Isaac et al., 1997). In these experiments, increments in stimulation intensity lead to a stepwise recruitment of additional afferent fibers, resulting in an increase in EPSC amplitude. To further explore how axon terminal stimulation power impacts post-synaptic responses, 3 more L4 spiny stellate neurons were recorded at an additional laser power of 70μW (Figure 3.5F-G). Stimulation at higher laser powers resulted in a continuous increase in EPSC amplitude (Figure 3.5A, E) (Friedman test, $p = 0.028$, F = 6.0). At 70μW, mean EPSC amplitude was 11± 2pA. Increasing laser power to 360μW resulted in a mean EPSC amplitude of 17± 1pA. At 3.5mW, average amplitude was 36± 12pA. There was a significant increase in amplitude between 70μW and 3.5mW stimulation power. Consistent with previous observations, increasing laser power resulted also in a decrease in average onset latency (Figure 3.3G Friedman test, $p < 0.028$, F =6.0). At 70μW, average latency was 9.0± 1.8ms. For 360μW stimulation power, latency was 4.2± 0.6ms, and at 3.5mW the value obtained was 2.3± 0.8ms. Again, a significant difference was found between 70μW and 3.5mW stimulation. Figure 3.5A displays sample voltage clamp recording traces (holding potential of -60mV) of Cell 2 (Figure 3.5F-G). It is tempting to propose that, similar to electrical minimal stimulation experiments (Raastad et al., 1992; Gil et al., 1999), increasing laser stimulation power could lead to a stepwise increase in recruitment of ChR65^{+} thalamic axon terminals and laser-evoked EPSC amplitude. Alternatively, channelrhodopsin is known to be calcium-permeable (Zhang & Oertner, 2007; Schoenenberger et al., 2011). Activation of increasingly larger numbers of channelrhodopsin channels may lead to larger calcium influx and mobilization of a higher number of synaptic vesicles for release.

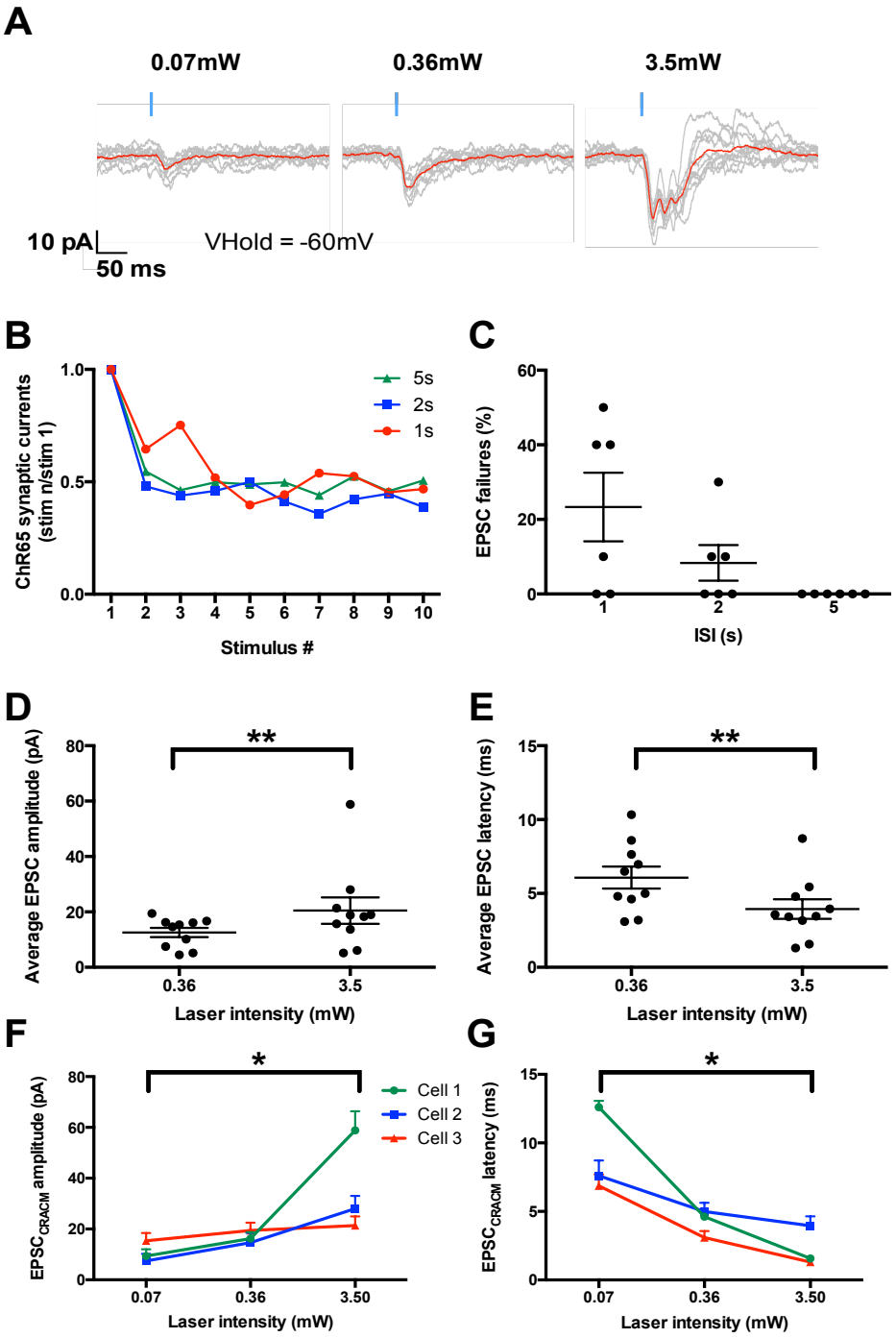


Figure 3.5. Determining stimulus parameters for CRACM. A. Example single (grey) and average (red) voltage-clamp traces of CRACM-evoked TC-EPSCs for a L4 cell at increasingly high stimulation powers. Blue rectangle indicates timing of photostimulation. **B.** Normalised amplitude of laser-evoked EPSCs as a function of inter-stimulus interval (n = 6 cells). **C.** Percentage of laser-evoked EPSC failures as a function of inter-stimulus interval (n = 6 cells). **D.** Average EPSC amplitude as a function of laser stimulus intensity (n = 10 cells). Each symbol corresponds to the average value for a single cell. **E.** Average EPSC latency as a function of laser stimulus intensity (n = 10 cells). Each symbol corresponds to the average value for a single cell. **F.** Stepwise increase in EPSC amplitude as a function of increases in stimulation power. Each symbol corresponds to the average value for a single cell. **G.** Decrease in EPSC latency as a function of increases in stimulation power. Each symbol corresponds to the average value for a single cell.

In conclusion, ChR65 expressed in thalamic axon terminals showed a pronounced (~50%) sensitization effect in EPSC amplitude recorded at L4 spiny stellate neurons. Contrary to somatic photo-activation of thalamic relay neurons, this effect was present across all stimulus intervals tested but peaked after the second stimulus. One advantage of prolonged inter-stimulus interval was a decrease in failure rate. Increasing laser power resulted in a stepwise increase in amplitude and a reduction in onset latency. The increase in amplitude could be explained by activation of more thalamocortical synapses, similar to what has been described in minimal stimulation experiments (Raastad et al., 1992; Isaac et al., 1997), or by the calcium-dependent recruitment of more vesicles from the same synaptic pool, driven by calcium entry through ChR65 channels or voltage-gated calcium channels activated by ChR65-mediated depolarisation. Although we could not test this directly, one hypothesis to explain the decrease in latency would be a reduced charging-up time in axon terminals for activation of voltage-dependent calcium channels, leading to a shorter lag to attain release threshold. When I photo-stimulated the soma of ChR65-positive thalamic relay neurons I observed a similar latency effect and when using lower laser powers, I observed a ramping depolarization until spike threshold, which was absent or much shorter at higher stimulus intensities (see section 3.3, Figure 3.3D-F; J). It is possible that this phenomenon is replicated at the axon terminal.

3.3.2. Using CRACM to study thalamocortical inputs

In this section I applied CRACM to compare thalamic input onto L4 spiny stellate cells, L5b pyramidal neurons and SPns, between P10 and P16. In these experiments, photostimulation was delivered to a single spot placed directly above the cell soma, and laser power was tuned to a point sufficient to elicit a single monophasic EPSC

with over 70% reliability, corresponding to previous reports that this equates to activation of a single or a small number of thalamic inputs (Raastad et al., 1992; Gil et al., 1999; Hanganu et al., 2002). Due to variable expression, this ranged from 140μW to 3.5mW, in different preparations. The objective was to contrast thalamic inputs onto L4 spiny stellate cells, L5b pyramidal neurons and subplate neurons, after P10. Using CRACM, all 32 L4 spiny stellate neurons recorded were found to receive direct thalamic input (n = 32/32). For L5b neurons, the value was 86% (n = 12/14). None of the SPns recorded received direct thalamic input (n = 0/9). Since SP cells present complex dendritic arbors (Luhmann et al., 1999; Marx & Feldmeyer, 2012), I confirmed the lack of thalamic connectivity by firing the laser in a 50μm grid pattern spanning a 450μm-wide column covering the entire depth of the cortex (Figure 3.6), as it could be possible that thalamic axons made synapses with more distal compartments of SP dendrites, which can reach L4-L6 (Marx & Feldmeyer, 2012). Maps were repeated 3 times for each cell and averaged. No reliable inputs were detected under these conditions either. In Figure 3.6A, I plotted the average map of thalamic afferent input for all 9 SPns recorded. Inputs were only observed spuriously, and for all 9 cells recorded, the only inputs observed never occurred in more than one map repetition, suggesting them to be spontaneously-occurring EPSCs that happened during the event detection window, rather than ChR65-evoked events. This is exemplified in Figure 3.6B and C. Figure 3.6B depicts an average map (3 repetitions) for a single subplate neuron. Only two input spots were observed. Figure 3.6C illustrates the recording traces of the corresponding inputs. Closer inspection concluded that these inputs were only observed in one of the map repetitions. This was the case for the few observed inputs in all 9 SPns whose thalamic inputs I mapped.

Given that CRACM can excite even axons that are completely severed from their parent soma, connectivity values reported here represent more accurate estimates of connectivity than could be achieved with electrical stimulation. For the remainder of this section, I shall focus on the attributes of thalamic inputs onto L4 spiny stellate and L5b pyramidal neurons. While no thalamic inputs onto SPns were detected post-P10, previous reports have shown robust early developmental connections (Friauf & Shatz, 1991; Hanganu et al., 2002; Higashi et al., 2002; Molnár et al., 2003; Hirsch & Luhmann, 2008). Due to the limitations of using ChR early in development, this was explored in further detail using electrical stimulation in Chapter 4.

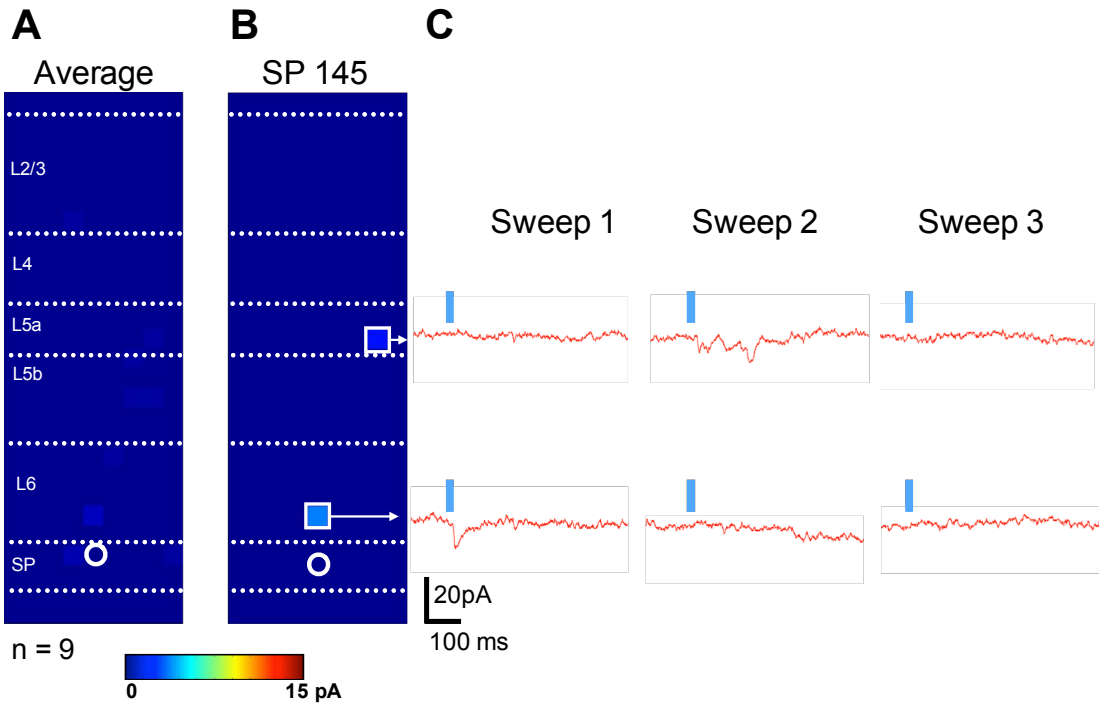


Figure 3.6. Lack of thalamic inputs to subplate neurons post-P10. The 473nm laser beam was scanned over a region covering the entire laminar extent of the cortex in order to create a map of putative thalamic input to SPns. **A.** Average map for all 9 cells recorded. **B.** Example average map (3 repetitions) for a single cell. Two responses were evoked, highlighted by white squares. **C.** However, each response was only evoked in one out of 3 map repetitions and likely corresponded to a mini EPSC occurring spontaneously during the event detection window.

I stimulated ChR65^{+} thalamic axon terminals in the vicinity of L4 and L5b excitatory neurons by aiming the laser beam at their somata. I analysed a total of 32 L4 spiny

stellate cells (n = 341 EPSCs) and 9 L5b pyramidal neurons (n = 87 EPSCs). Average $EPSC_{CRACM}$ latency was 5.2± 0.2ms for L4 spiny stellate neurons (Figure 3.7A), and 6.7± 0.5ms for L5b pyramidal cells. A Mann-Whitney test found no significant difference between L4 and L5b $EPSC_{CRACM}$ latency ($U(2) = 13046$, $p = 0.083$). Average $EPSC_{CRACM}$ amplitude was significantly higher for L4 spiny stellate neurons (16± 1pA) than L5b pyramidal cells (13± 1pA) (Figure 3.7B) ($U(2) = 12806$, $p < 0.05$). I plotted in figure 3.7C and 3.7D the relative frequency distributions for latency and amplitude of $EPSCs_{CRACM}$ of L4 and L5b neurons. Latency distributions for L4 and L5b $EPSC_{CRACM}$ peaked at the 4-6ms bin, and all events occurred within 20ms of laser stimulation (Figure 3.7C, E). To examine differences in the distributions, I calculated cumulative frequency distributions for L4 and L5b latencies (Figure 3.7E). L5b latency distribution appeared shifted towards higher values, compared to L4. This was corroborated by a two-sample Kolmogorov-Smirnov test, which determined the two distributions to be significantly different ($D(1) = 0.22$, $p < 0.01$). In terms of amplitude, for L4 spiny stellate neurons, the distribution was centered at the 10-15pA bin (Figure 3.7D). There seemed to be a second, albeit very small cluster of events at 55-80pA. The distribution for L5b events appeared narrower, and somewhat skewed towards lower values (Figure 3.7D, F). This was further examined with cumulative frequency plots, where accordingly, L4 neurons exhibited a shift towards higher amplitudes (Figure 3.7F). A two-sample Kolmogorov-Smirnov test determined the two distributions to be significantly different ($D(1) = 0.191$, $p < 0.05$).

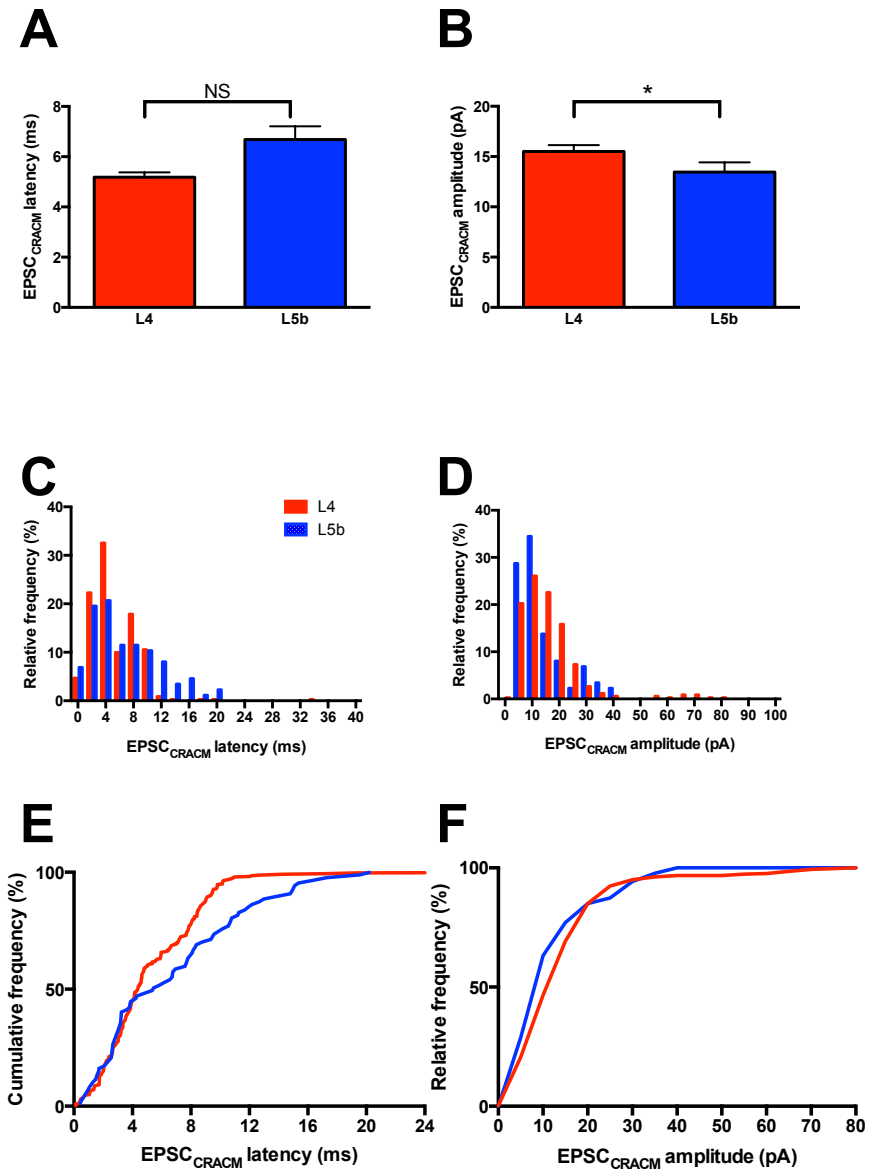


Figure 3.7. CRACM of thalamic inputs onto L4 spiny stellate cells (n = 32) and L5b pyramidal neurons (n = 12). A. Average $EPSC_{CRACM}$ latency for L4 spiny stellate and L5b pyramidal neurons. **B.** Average $EPSC_{CRACM}$ amplitude for L4 spiny stellate and L5b pyramidal neurons (n numbers as stated above). **C.** $EPSC_{CRACM}$ latency relative frequency distribution for L4 spiny stellate (n = 341 EPSCs, 32 cells) and L5b pyramidal neurons (n = 87 EPSCs, 9 cells). **D.** $EPSC_{CRACM}$ amplitude relative frequency distribution for L4 spiny stellate and L5b pyramidal neurons (n numbers as in D). **E.** Cumulative relative frequency distribution of $EPSC_{CRACM}$ latency for L4 and L5b neurons n numbers as in D). **F.** Cumulative relative frequency distribution of $EPSC_{CRACM}$ amplitude for L4 and L5b neurons n numbers as in D).

3.3.3. Combining CRACM with LSPS

I next combined CRACM with LSPS. Instead of single-spot stimulation of TC afferents apposed to the soma, I scanned the laser beam over a 50μm-spaced grid covering the entire laminar extent of the cortex over a 450μm-wide column, in order to study the distribution of thalamocortical inputs across the whole dendritic arbor. Based on patterns of dendritic and thalamic axonal bouton overlap, L5 pyramidal cells have been proposed to receive extensive thalamic input, which could theoretically arise both from VPM terminations in L5b/6 and L4, but also POm terminals at L1 and L5a. The same work has suggested that L4 spiny stellate cells are poised to receive only VPM input from terminals located in L4 (Bureau et al., 2006; Meyer et al., 2010a; Oberlaender et al., 2012). An important caveat of using CRACM is that spot illumination may cause spiking and action potential conduction in ChR^+ axons or local transmitter release from synaptic terminals, complicating inferences about the location of pre-synaptic axon terminals (Petreanu et al., 2007; Kätzel et al., 2010; Kätzel & Miesenböck, 2014). Nonetheless, this method allowed me to gain initial insight into the organization of thalamic innervation of spiny stellate and L5b pyramidal neurons.

I mapped afferent thalamic input onto a total of 22 L4 spiny stellate cells and 7 L5b pyramidal neurons. Figure 3.8A shows average maps for L4 and L5b excitatory cells. Since all maps were recorded at P10-P16, I aligned them by each cell's home barrel, drawing also the approximate layer boundaries and barrel location. I mapped only events occurring up to 20ms after stimulus onset, as this seemed to encapsulate all CRACM-evoked EPSCs, for both L4 and L5b cells (see previous section). CRACM-induced thalamic inputs onto L4 spiny stellate cells clustered within the barrel, with

weaker inputs detected upon stimulation of spots adjacent to the barrel in L4 and L5a. Substantial activation in L5a could also be seen, along with a cluster of weak events in L5b. No L1 input could be detected. For L5b pyramidal cells, most inputs were detected in response to stimulation at the L5b/6 border, close to the cell soma. Weak inputs could also be evoked from stimulation in L4, and could have resulted from backpropagation of action potentials generated in thalamic axons terminating in L4. Only weak activation was seen from L5a. Interestingly, no activation was detected when stimulating at L1, where POm axons are known to arborise. In figure 3.8B I plotted the average laminar profile for thalamic inputs onto L4 spiny stellate (left, blue) and L5b (right, red) pyramidal neurons. The normalized laminar distribution of thalamic inputs onto L4 and L5b is contrasted in Figure 3.8B (rightmost trace). L4 cells receive the vast majority of thalamic inputs from axons in L4, and L5b from axon clusters at the L5b/6 border. I plotted also the horizontal columnar distribution of thalamic inputs onto both cell types (Figure 3.8A, below each map). In addition to plotting horizontal profiles of total thalamic input, I also plotted the normalised horizontal profiles in Figure 3.8C. Thalamic inputs onto L4 spiny stellate cells are clearly stronger closer to the soma, as the proportion of thalamic input provided decreased the further from the soma I stimulated (Figure 3.8C, left, in blue). A one-way ANOVA contrasting proportion of thalamic input per 50μm column found a significant effect ($F(4, 105) = 7.768$, $p < 0.001$). Post-hoc comparisons determined that the 0 and 50μm columns both provided significantly more input than the 150 and 200μm columns. In terms of columnar organization, thalamic inputs onto L5b pyramidal cells appeared broader and not focused exclusively within the immediate barrel column, as found for L4 cells. A one-way ANOVA contrasting proportion of thalamic input per 50μm column was not significant ($F(4, 30) = 0.519$, $p = 0.723$).

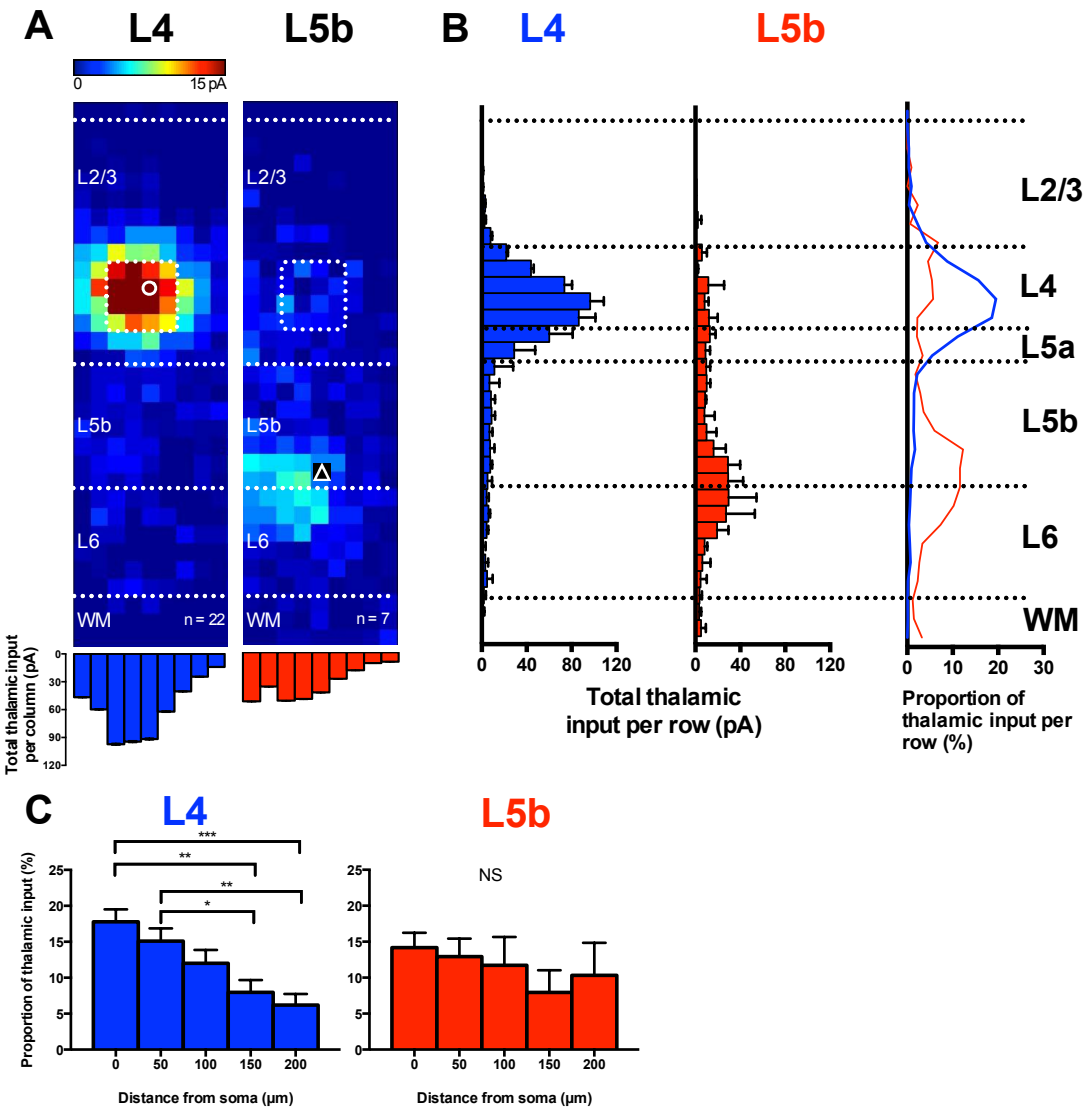


Figure 3.8. Combined CRACM and LSPS of thalamic inputs onto L4 spiny stellate (n = 22) and L5b pyramidal neurons (n = 7). A. Top, average input maps for L4 (left) and L5b (right) cells. Below, average horizontal profile of thalamic input distribution for L4 (n = 22 cells) and L5b (n = 7 cells) cells. **B.** Average vertical profile of thalamic input distribution onto L4 (blue) and L5b (red) neurons. Far right, overlay of the two distributions, normalized for each (n numbers as in A). **C.** Average horizontal distribution of thalamic inputs for L4 and L5b neurons (n numbers as in A).

3.3.4. Subcellular CRACM

My CRACM results in the previous section suggested all L4 spiny stellate neurons and a high proportion of L5b pyramidal cells receive direct thalamic input of similar amplitude and latency characteristics. For each cell type, there was a suggestion that weaker thalamic innervation might occur at the converse termination zone (L5b/6 border for L4 cells, and the barrel for L5b cells). Inputs originating from stimulation in L5a were observed for both cell types, which could indicate POm innervation. However, it is also possible that these responses reflected propagation of channelrhodopsin-evoked axonal spikes and terminal release at a different synapse, or a "smearing" effect from laser stimulation at layer borders. sCRACM (subcellular channelrhodopsin-assisted circuit mapping) was developed to address this type of issue (Petreanu et al., 2009). In this approach, TTX is added to the bath to prevent action potential generation and conduction. 4-aminopyridine (4-AP) is included to block axonal K+ channels critical for repolarization. This allows ChR-positive axon terminals to remain depolarized for long enough to trigger neurotransmitter release in response to photostimulation (Petreanu et al., 2009).

Following CRACM maps of thalamic inputs in 15 L4 cells (P13-P16), 1 μM TTX and 200-500 μM 4-AP were added to the bath. The effect of TTX was tested by periodically attempting to evoke action potentials by current injection. Once action potentials were abolished, 4-6 minutes after starting drug wash-in, sCRACM of thalamic inputs was attempted. For 3/15 cells, laser-evoked EPSCs could be evoked, and sCRACM maps were obtained. For the remaining 12 cells, responses were abolished and it proved impossible to recover responses by increasing laser power, stimulus duration or inter-stimulus interval. sCRACM was attempted for 7 L5b

pyramidal neurons, but 4-AP and TTX abolished photocurrents in all recorded L5b cells. Analysis of $EPSC_{CRACM}$ amplitude (prior to washing in drugs) suggests that L4 cells where sCRACM was successful received stronger thalamic inputs. Indeed, the frequency distribution of successfully versus unsuccessfully mapped cells by sCRACM shows that cells where sCRACM was successfully administered had a somewhat right-shifted distribution of EPSC amplitudes, towards higher values (Figure 3.9A). This can be seen more clearly in the cumulative frequency distribution (Figure 3.9B). A two-sample Kolmogorov-Smirnov test determined the two distributions to be significantly different ($D(1) = 0.259$, $p < 0.001$). Likewise, a Mann-Whitney test determined that average $EPSC_{CRACM}$ amplitude was significantly higher in cells were sCRACM was successful (15± 0.5pA), compared to those where it failed (10± 0.2pA) ($U = 437045$, $p < 0.001$) (Figure 3.9C).

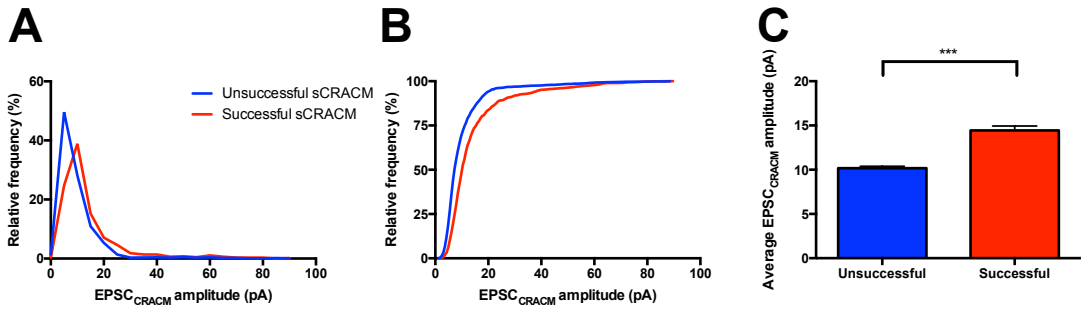


Figure 3.9. $EPSC_{CRACM}$ amplitude in cells where sCRACM was successful (n = 3 cells) versus unsuccessful cases (n = 12 cells). **A.** Relative frequency distribution of $EPSC_{CRACM}$ amplitude in cells where sCRACM was successful (red) and unsuccessful (blue). **B.** Cumulative relative frequency distribution of $EPSC_{CRACM}$ amplitude of $EPSC_{CRACM}$ amplitude in cells where sCRACM was successful (red) and unsuccessful (blue). **C.** Average $EPSC_{CRACM}$ amplitude in cells where sCRACM was successful (red, n = 3) and unsuccessful (blue, n = 12).

Figure 3.10A compares CRACM and sCRACM maps in the successful 3 cells (from animals aged P14, P15 an P16). Pixels highlighted with dashed white boxes surrounding responses represent those present only in the CRACM maps; red-

highlighted pixels represent responses present in sCRACM but not CRACM and are most likely spontaneous mini EPSCs that happen to occur during the event detection windows. In all 3 cells, in order to evoke $sCRACM_{EPSCs}$, I had to alter stimulus characteristics relative to CRACM maps, as previously reported (Petreanu et al., 2009). In all cases laser pulse duration, rather than laser power, was increased to 10-20ms, as opposed to 1ms for CRACM. It is possible that the longer stimulus duration activated putative weak thalamocortical synapses that went undetected using short CRACM stimuli. CRACM maps for all 3 cells show the strongest responses within the barrel. However, a lot of extra-barrel, L5a and L5b/6 activation can be seen. In sCRACM maps, most of these responses are abolished, and mapped inputs become more barrel-focused. Inputs from stimulation in L5a were drastically reduced during sCRACM, suggesting that they corresponded to smearing or action potential propagation, rather than POm innervation of L4 spiny stellate cells. In Figure 3.10B I plotted EPSC amplitude of each mapped spot in CRACM against its corresponding response under sCRACM. The red line depicts the y = x function and highlights the fact that many responses present under CRACM were abolished during sCRACM, and that EPSC amplitude generally decreased. Figure 3.10C portrays average maps for CRACM and sCRACm and their horizontal profiles, and 3.10D shows the vertical profiles for CRACM (blue) and sCRACM (red). Normalised horizontal profiles are plotted in figure 3.10E. Collectively, the data show that during sCRACM, inputs became more barrel-focused both on the laminar (Figure 3.10D) and columnar (Figure 3.10E) domains, and that L4 spiny stellate cells receive only VPM input, from terminals located within the barrel.

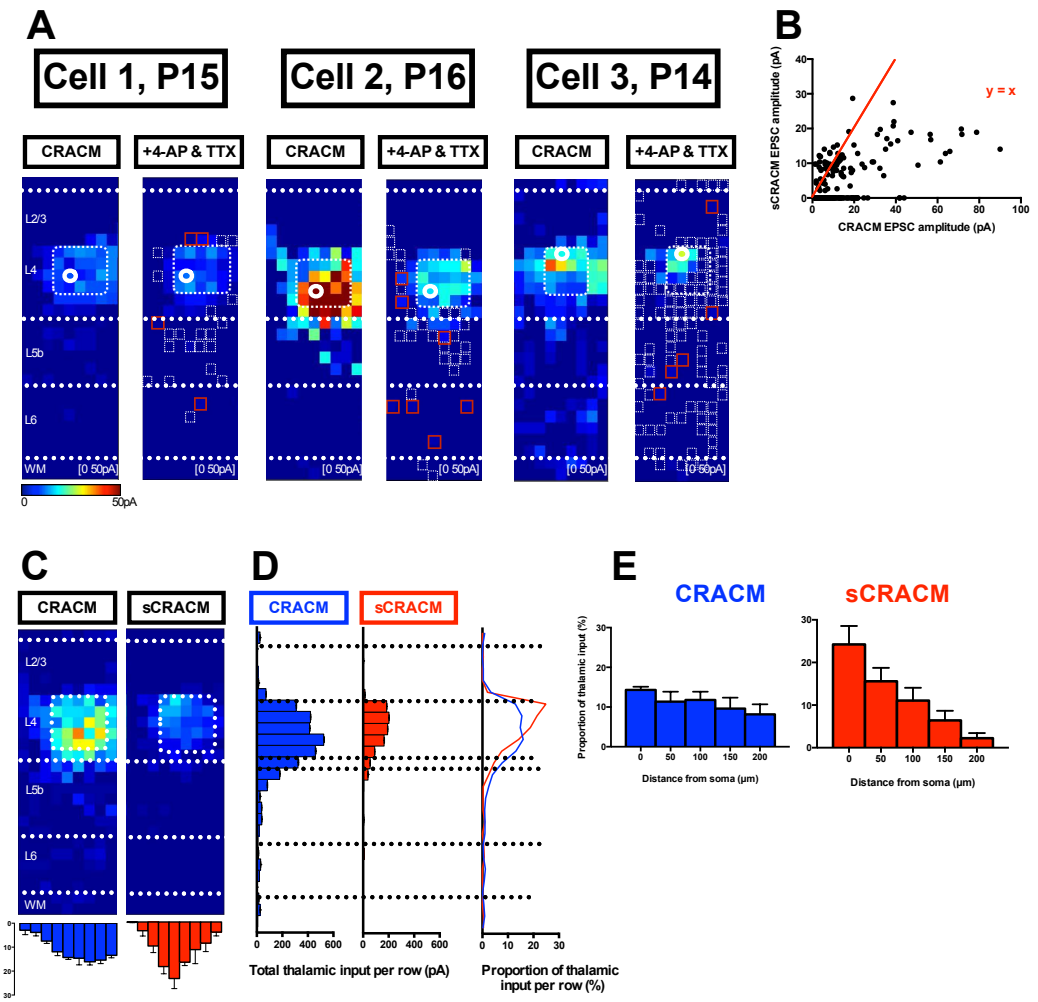


Figure 3.10. CRACM versus sCRACM maps in L4 spiny stellate neurons. A. CRACM (left of each panel) and sCRACM (right of each panel) maps for each L4 cell where sCRACM was successful. **B.** $EPSC_{CRACM}$ amplitude versus $EPSC_{sCRACM}$ amplitude in each stimulation spot where an input was recorded under CRACM. **C.** Average maps (top) and horizontal input profiles (bottom) for CRACM (n = 22 cells) and sCRACM (n = 3 cells) maps. **D.** Average vertical profile for thalamic inputs under CRACM (blue) and sCRACM (red). Far right, overlay of the two distributions, normalised. **E.** Average horizontal profile for thalamic inputs under CRACM (blue) and sCRACM (red).

3.4. Discussion

In this chapter, I used an early delivery approach to express channelrhodopsin in the VPM, in order to stimulate identified thalamocortical inputs to cortical neurons during the first postnatal week. Weak photocurrents and the inability to reliably drive thalamic spikes using ChR65 prior to P10 precluded such experiments. Nonetheless, it was possible to use ChR65 after P10 to activate thalamic afferents to cortical neurons in a specific manner and study some of their properties. I extended this work by using CRACM and, in a small subset of cells, sCRACM, to study the dendritic location of thalamic inputs to different cell types.

Using optogenetics in the developing rodent brain

The results presented in the current chapter showed that very little functional ChR65 expression occurs before P5. This was suggested by the fact that action potentials could only reliably be elicited by optical stimulation in thalamic and pyramidal neurons after P10, even when electroporation was performed as early as E11.5. Longer embryonic expression times did not appear to make a difference in the onset of reliable postnatal ChR65 function, as this was actually earlier for L2/3 pyramidal neurons transfected at E15.5 (P7-P9), compared to thalamic relay cells transfected at E11.5 (P10-P12). This could be explained by differences in the maturity of intrinsic properties of the two cell types. Even though the intrinsic properties of both thalamic and cortical pyramidal neurons transition from a state of high to lower intrinsic excitability throughout development, early ChR65-mediated photocurrents are barely above noise level, and unable to take advantage of the highly-excitable intrinsic profile of immature neurons. Nonetheless, spiking probability reached reliable values for both cell types by P10, indicating a fast ramp-up in functionality between P3 and

P10 that compensates well for the decreasing excitability of rapidly-maturing neurons.

One factor that could have adversely affected ChR65 expression in my experiments was the use of the same promoter for DsRed and ChR65 expression. Since native expression of the fused GFP protein was not strong enough, slice experimentation would always require co-electroporation of a genetic label. I opted to use the same promoter as this would enhance the probability of double-labeling and reduce the chance of recording from $DsRed^{+}/ChR65^{-}$ neurons, or post-synaptic cells in cortical areas labeled by fluorescent photo-insensitive axons. Nonetheless, it would be of interest to try a different promoter.

Optogenetics is a powerful approach that could enable several questions in circuit development to be answered by providing a means for activation of identified inputs. This would be useful not only in areas with a high degree of reciprocal connectivity, such as the thalamus and corticothalamic cells or callosally-projecting neurons, but also for the activation of single identified afferent inputs and the study of their characteristics during the initial stages of synapse maturation. Moreover, the optogenetics toolbox has provided in the adult a means for silencing of neuronal activity, through use of Halorhodopsin and Arch channels (Fenno et al., 2011; Yizhar et al., 2011; Packer et al., 2013). It would be a great advantage in the field of circuit development to be able to chronically silence identified cell types, rather than ablate them. For these reasons it is of great interest to adapt optogenetic tools for use in the developing rodent. My results suggest two broad avenues for such an enterprise. First, characterization of the gene expression interactions of channelrhodopsin expression and other factors that might be needed for its normal function. It is possible that such

factors are not present in the embryonic brain at sufficient level and that supplementation could resolve this problem. We attempted brain slice incubation with retinal, a factor known to be needed for the function of ChR2 (Boyden et al., 2005), but this did not affect laser-evoked spiking probability in any way. It could also be that ChR65 expression is repressed via an unknown pre- or post-translational mechanism in the rodent embryo. Further experimentation will be required for clarification. Second, since little embryonic ChR65 expression seems to occur, possibly a better strategy would be to perform transfection shortly after birth. Due to far greater ease of manipulation and robustness of neonates compared to embryos, this would also enable more precise targeting of expression and enhanced survival rates. Currently, a wide range of viruses can be used to express vectors in the rodent brain (Wickersham et al., 2010; Betley & Sternson, 2011), and some experimenters have reported expression times as low as 4-10 days (Kiritani et al., 2012). Whichever the strategy, use of optogenetics to achieve cell-type specific control of activity in the neonatal brain could greatly further our understanding of circuit maturation.

Cellular and sub-cellular specificity of thalamic inputs

Using single-spot stimulation of thalamic afferents I reported that all L4 cells recorded and a high proportion of L5b pyramidal neurons received thalamic input. This corroborates and extends previous reports of thalamocortical connectivity using glutamate uncaging (Bureau et al., 2006; Viaene et al., 2011b). Of note is the fact that no SPns were found to receive thalamic input after P10. This was not due to stimulation of thalamic axons overlapping the wrong dendritic compartment, as no inputs could be detected either by scanning the 473nm laser over cortical columnar regions including the putative dendritic arbor of SPns. SPns have been shown to

receive very strong early thalamic inputs in visual, somatosensory and auditory cortices (Friauf et al., 1990; Friauf & Shatz, 1991; Hanganu et al., 2002; Zhao et al., 2009). The use of CRACM is a refinement over electrical stimulation, as it obviates problems of antidromic activation of corticothalamic axons and connectivity integrity in the slice. It is entirely possible that thalamic inputs to the subplate serve an early developmental function (Kanold, 2004; Kanold & Luhmann, 2010) and are subsequently dismantled. Indeed, the subplate has been shown to provide a di-synaptic route for thalamic information into L4 (Zhao et al., 2009) that is thought to be important for functional maturation and plasticity of the thalamic-L4 synapse early in development (Kanold et al., 2003; Kanold, 2004; 2009; Kanold & Luhmann, 2010). It may be that in the mature system the presence of such a route would degrade the temporal precision of sensory-evoked signaling in L4, and that the thalamic input to SPns is dismantled after the end of the critical period for thalamocortical plasticity. The Kanold group has reported in the auditory cortex the emergence of an excitatory L4 feedback input to SPns after P10 (Viswanathan et al., 2012). One possibility is that the appearance of this synapse de-correlates spiking in the thalamus and SP. A mature thalamic input would evoke spiking in SPns and L4. The L4-SP projection could then elicit spikes in SPns that would be late and uncorrelated to thalamic activity, which would by STDP rules result in heterosynaptic depression of the thalamus-SP synapse (Caporale & Dan, 2008). A further possibility could be that thalamic inputs only impinge on particular types of SPn and that I happened to miss this type in my limited sample of cells.

Functional thalamic inputs to L4 have been extensively researched (Crair & Malenka, 1995; Gil et al., 1999; Gil & Amitai, 1996; Gabernet et al., 2005; Cruikshank et al.,

2007; Daw et al., 2007a), but curiously few studies have focused on characterising inputs to infragranular layers (Porter et al., 2001; Swadlow & Gusev, 2002; Beierlein & Connors, 2002; Tan et al., 2008; Viaene et al., 2011b; Wang et al., 2013; Rah et al., 2013). Here I used CRACM to activate a single or small number of thalamic afferents to L4 spiny stellate and L5b pyramidal neurons to contrast input characteristics, in an attempt to mimic minimal stimulation experiments (Gil et al., 1999). Interestingly, the values attained for the amplitude of putative single inputs to spiny stellate neurons approximate those previously reported (Feldman et al., 1998; Gil et al., 1999; Bannister, 2005). Moreover, in my characterization experiments, increasing laser stimulation power resulted in a stepwise increase in EPSC amplitude, which was likely driven by increased recruitment of thalamic afferents. Although additional and more thorough characterization experiments involving parallel minimal electrical and optical stimulation would be needed, my results suggest it is possible to use single-photon optogenetics in the slice to study putative single afferent inputs. Comparing TC–EPSCs in L4 spiny stellate and L5b pyramidal cells, I found that EPSCs observed in L4 cells were significantly higher in amplitude, and showed a narrower, faster distribution of onset latencies. This is in accordance with another optogenetic study, which reported somewhat higher thalamic EPSPs in regular-spiking L4 than regular spiking L5 cells (Cruikshank et al., 2010). Similarly, inputs to L6 pyramidal cells are reportedly weaker in amplitude than those to L4 star pyramid cells in mouse V1 (Wang et al., 2013). The difference in latency distribution parallels closely the results of a recent *in vivo* study, where the authors found that although L5 pyramidal neurons received thalamic inputs as early as L4 cells, their latency distribution was broader and extended into later periods (Constantinople & Bruno, 2013). Thalamic input evokes strong EPSPs and spiking in L4 (Ferster et al., 1996; Brecht & Sakmann,

2002; Wehr & Zador, 2003), which is redistributed to the cortical column (Feldmeyer et al., 2012). In spite of the small amplitude of unitary thalamic inputs to L4, the thalamus strongly drives this layer due to high bouton density and very strong convergence in L4, as each L4 neuron is the target of a high number of thalamocortical synapses (Bruno & Sakmann, 2006; Oberlaender et al., 2012). Although strong thalamic input convergence alone has been proposed to be able to account for reliable sensory-evoked responses in L4 (Bruno & Sakmann, 2006), relay of sensory information may be aided by a dense excitatory local recurrent network (Feldmeyer et al., 1999; Petersen & Sakmann, 2000; Lefort et al., 2009; Ashby & Isaac, 2011; da Costa & Martin, 2011). Higher unitary amplitude of thalamic inputs in L4 than other layers could serve as an additional mechanism to guarantee propagation of thalamic-driven excitatory flow in the neocortex. The difference in latency between L4 and L5b was interesting. It is possible that there are differences in the morphology (axon caliber) or organization of thalamic axon terminals at L4 and L5b/6 that favor fast axon terminal depolarization in L4. Such differences have indeed been reported for POm axons in L2/3 and L4 of S2 (Viaene et al., 2011a), but to my knowledge have not been communicated for VPM axons. An alternative possibility relates to the fact that L5b pyramidal neurons also receive thalamic inputs in their apical dendrites in L4 (Petreanu et al., 2009; Rah et al., 2013). When doing single-spot stimulation of thalamic afferents closely apposed to L5b somata, it is possible that on occasion I triggered an axonal spike, which propagated along the ascending thalamic branch to L4, resulting in terminal release of transmitter at a thalamus-L5b synapse located in L4, targeting the apical dendrite of the L5b cell. The cohort of late-occurring events I observed for L5b cells may correspond to such occurrences. One last account is that late events correspond to polysynaptic inputs. It is possible that stimulation of

terminals apposed to the recorded cell failed to evoke transmitter release at TC synapses to that cell, but evoked EPSPs strong enough to evoke spiking in a nearby L5b pyramidal cell that projected onto the recorded neuron. This interpretation is complicated by the fact that laser intensity was calibrated to evoke modest, monophasic EPSCs that would be unlikely to drive P10-P16 pyramidal cells to spike. Moreover, ChR inflates release probability during axonal stimulation due to calcium permeability (Schoenenberger et al., 2011). My CRACM characterization data is in agreement with this, as sufficient spacing of stimuli resulted in 0% failure rate (Figure 3.4B). Under these conditions, it is unlikely that axonal stimulation would fail to evoke transmitter release at a synapse onto the recorded neuron, and simultaneously evoke release powerful enough to drive an adjacent cell to spike.

A series of elegant computational anatomy papers studied the overlap between VPM and POm axon boutons and dendrites for several excitatory neuron types across different cortical layers, providing important hypotheses and constraints on thalamic innervation of different layers (Meyer et al., 2010a; Wimmer et al., 2010; Oberlaender et al., 2012;). According to these estimates, VPM and POm axons are well positioned to provide input to excitatory neurons in virtually every cortical layer. POm axon boutons show a high density in L1 and L5a, and as such could provide input to apical dendrites of L2 and L3 pyramidal neurons, as well as basal dendrites of L5a cells and apical dendrites of L5b pyramidal cells. VPM axons show a converse termination pattern, with high bouton densities at L4 and the L5b/6 border. Potentially, these boutons could contact L4 spiny stellate cells and pyramidal neurons in L3-L6. In most electroporations both VPM and POm nuclei were transfected, rendering it impossible to unambiguously identify thalamic input provenance to different cell types.

Nevertheless, taking advantage of the segregated termination zones of VPM and POm boutons, some inferences can be made from my results. Initial CRACM experiments suggested strong innervation of L4 spiny stellate neurons in L4 and L5a, which would be consistent with dual VPM and POm innervation. Another possibility would be stimulation of more distal zones of passing VPM axons afferent to L4, enabling sufficient depolarisation at a L5a stimulation site to spread into the axonal terminal actually located in L4. Subsequent sCRACM experiments reduced the laminar activation profile of thalamic inputs to spiny stellate neurons to L4, mostly within the barrel, suggesting that these cells receive only VPM, and not POm input, consistent with previous LSPS reports (Bureau et al., 2006; Viaene et al., 2011a). For L5b neurons, thalamic input originated mostly from the L5b/6 border, suggesting VPM origin, although weak inputs could also be detected from stimulation in L4. This is consistent with a previous report using sCRACM to map VPM inputs onto L5b pyramidal cells (Petreanu et al., 2009). The fact that axon illumination using CRACM can result in axonal spike generation and propagation or local terminal release limits the conclusions that can be drawn for L5b cells. I can't exclude that illumination in L5b or L4 could have stimulated passing POm axons, for instance. These limitations point to the importance of using sCRACM to unambiguously resolve dendritic location of identified inputs.

Parallel as opposed to sequential processing of thalamic information

The cross-laminar influence of thalamic input proposed by computational anatomy studies (Meyer et al., 2010a; Wimmer et al., 2010; Oberlaender et al., 2012) fits well with *in vivo* data showing short latency whisker-driven activation of neurons in L4, L5b and L6 (Armstrong-James et al., 1992; Manns et al., 2004; De Kock et al., 2007).

These data argue against the canonical view of sequential distribution of thalamic activity through the cortex via L4 (Douglas & Martin, 2004). According to this model, thalamic information would obey a L4→L2/3→L5 processing order. An opposing view that recently garnered strong experimental support is that thalamic information is processed in parallel in upper (L4) and lower (L5b/6) cortical strata (De Kock et al., 2007; Constantinople & Bruno, 2013). Evidence in favor of the latter hypothesis arose from early latency whisker-stimulation responses recorded by whole-cell patch-clamp in L5b and 6 as well as L4, and from the experimental observation that pharmacological inactivation of L4 does not affect whisker-related responses in L5b (Constantinople & Bruno, 2013). The dual strata hypothesis has interesting implications, in that L2/3 projection neurons tend to target other cortical areas, whereas L5b/6 cells target both cortical and subcortical structures, many of which are action-oriented (Constantinople & Bruno, 2013). My recordings showing direct early thalamic input onto L5b pyramidal cells (Figure 3.5) fit the *in vivo* data well, and raise the question of what other cell types in infragranular layers receive thalamic input, as well as whether thalamic information is processed differently in L4 and L5b. Porter and colleagues previously reported that a population of lower L5 interneurons received direct thalamic input and projected to layers 4 and 2/3 (Porter et al., 2001). Work in the Agmon lab showed that a set of somatostatin-positive interneurons in L5b, whose axons also arborised in L4, received modest, but direct and facilitating thalamic input. Fast-spiking parvalbumin-positive neurons in L5b were also found to be directly engaged by the thalamus, but the synapse was short-term depressing (Tan et al., 2008). During high-frequency stimulation FS cells get less and less recruited, whereas SST cells get increasingly activated and engaging of the cortical network. L5b thus seems to have the capacity to inhibit L4 in response to

high-frequency thalamic stimuli (Tan et al., 2008), but the post-synaptic partners of the cells previously described are unknown (Porter et al., 2001; Tan et al., 2008). Interestingly, polysynaptic GABAergic activity on L4-L6 was previously reported in response to robust thalamic activation in the neonatal rat (Agmon et al., 1996). The development timing at which these responses were recorded was prior to thalamic engagement of L4 interneurons (Daw et al., 2007a), suggesting GABAergic responses might have originated from deep-layer interneurons. An extensive body of work has characterized thalamic-driven feed-forward inhibition in L4, and the important role it plays in assuring time-locked signaling of afferent sensory information (Gabernet et al., 2005; Sun et al., 2006; Cruikshank et al., 2007; Hull et al., 2009; Bagnall et al., 2011), but cross-laminar thalamic-driven inhibition is still an unexplored research venue.

Could thalamic information be processed differently in the L4 and L5b/6 strata? The main sources of excitation onto L4 are the thalamus and the dense recurrent excitatory network present in that layer (Ashby & Isaac, 2011; Hooks et al., 2011), whereas L5b and L6 pyramidal cells receive excitatory inputs from other cortical layers, regions and the thalamus (Petreanu et al., 2009; Thomson, 2010; Hooks et al., 2011; Anastasiades & Butt, 2012; Feldmeyer, 2012). The L4 and L5b/6 thalamocortical strata could operate in different modes. The L4 thalamocortical circuitry, endowed by powerful thalamic convergence and feed-forward inhibition, as well as stronger TC-EPSCs than its infragranular counterpart, seems well tuned to signal in a very precise and time-locked way significant incoming sensory information. L5b/6 pyramidal cells receive a variety of columnar and cross-areal inputs, in addition to local excitation and thalamic input. The lower TC-EPSC amplitude and broader latency profile

suggest that thalamic information processing could act in this strata in a more integrative fashion that promotes summation of several inputs before a spike is relayed.

Clearly more experimentation is needed to determine why two thalamic processing streams could be needed in the cortex, and how their operating principles might differ. The field of thalamocortical processing is moving in an interesting direction, uncovering a complexity beyond the traditional L4-centric view. Early in development, subplate neurons form a core component of the thalamocortical circuit (Hanganu et al., 2002; Kanold & Luhmann, 2010), with my data suggesting that this connection could be dismantled after it fulfills its function. Compelling *in vivo* work has shown that thalamic information is processed in parallel (Constantinople & Bruno, 2013) and that deep-layer interneurons exist which could potentially modulate activity in L4 and supragranular layers (Agmon et al., 1996; Porter et al., 2001; Tan et al., 2008; Murayama et al., 2009). The field is ripe for experimentation, new ideas are emerging and clearly exciting times lie ahead.

Chapter 4 – The intrinsic maturation and development of excitatory synaptic inputs onto Lpar1-GFP subplate neurons

4.1. Introduction

The vast computational power of the mammalian brain is thought to arise from the precise organisation of inhibitory and excitatory synaptic connections between neurons organised in networks (Hestrin, 2009; Harris & Mrsic-Flogel, 2013;). Neuroscientists have long sought to chart connectivity between and within brain regions, in the hope of linking elementary neuronal circuit operations to behaviour and cognition. Previously, neuroscientists developed specialised brain slice preparations and used fine electrodes to stimulate afferent inputs to cells of interest and study the properties of these connections. While this approach yielded vast advances in our knowledge of brain circuit function (for instance, the thalamocortical slice (Agmon & Connors, 1991)), it offers no control over the pre-synaptic identity of the afferent input stimulated beyond strategic electrode placement and control of stimulation intensity (by varying the amount of current applied), and it required preservation of stimulated neural pathways. These limitations affect the resolution at which we can ask questions about a circuit and confine us to study either local circuits or specific long-range circuits for which slice preparations with good preservation of connectivity exist. Moreover, depending on the slice preparation, antidromic activation of neurons by stimulating electrodes can contaminate experimental results. In the past two decades, neuroscientists have developed a range of optical techniques to circumvent the issues associated with electrical stimulation, such as laser-scanning photostimulation (LSPS) via photo-uncaging of glutamate (hereby termed "glutamate uncaging") (Dalva & Katz, 1994) or cell-type specific stimulation of neurons

transfected with, or genetically engineered to express channelrhodopsin (ChR2 and other variants) (Boyden et al., 2005).

Optical stimulation can confine excitation to very small tissue volumes or even selective genetically-defined cell types, and, in the case of channelrhodopsin-assisted circuit mapping (CRACM), it can be used to study long-range connectivity even in cases where pre-synaptic axon terminals have been severed from their point of origin (Petreanu et al., 2007). These approaches have been used to great profit, but for all the progress in using them to understand the synaptic organisation of the mature brain, comparatively little attention has been devoted to mapping circuits in the developing brain. Previous studies have focused on subplate neurons of the auditory cortex (Zhao et al., 2009; Viswanathan et al., 2012;), feed-forward pathways in the mouse barrel cortex (Bureau et al., 2004), the eye-opening period in ferret visual cortex (Dalva & Katz, 1994) and the network maturation of somatosensory and motor L2/3 and L5 pyramidal neurons (Anastasiades & Butt, 2012).

The primary objective of my thesis was to harness the power of optical stimulation approaches in the brain slice to shed light on the organisation of early thalamocortical circuits in the mouse barrel cortex. One of the most important developmental populations in the cortex are subplate neurons (Kostovic & Molliver, 1974; Kostovic & Rakic, 1980). SPns define a largely transient ~50 μm cortical layer situated below L6 and above the cortical white matter, and they are amongst the earliest-generated neurons in the cerebral cortex (Allendoerfer & Shatz, 1994; Kanold & Luhmann, 2010). SPns are a diverse population across a number of criteria. Studies have reliably identified five to six morphological types: pyramidal, inverted, tangentially-oriented,

horizontal and multipolar (Hanganu et al., 2002; Hoerder-Suabedissen & Molnár, 2011; Marx & Feldmeyer, 2012) (Chapter 1, Figure 1.7). The picture is no less complex on the molecular side: the main subplate markers Cplx3, CTGF, Nurr1 and Lpar1-GFP all partially-overlap in labelling subplate neurons born between E10.5 and E13.5, showing no obvious correlation with morphology, but a conspicuous lack of co-labelling with GABA (Hoerder-Suabedissen et al., 2009; Hoerder-Suabedissen & Molnár, 2012). The functional development of subplate neurons is remarkably accelerated compared to pyramidal neurons, as judged by the subplate's intrinsic properties, in particular its ability to fire overshooting action potentials at frequencies above 10-20 Hz (Luhmann et al., 2000; Hanganu, 2001; Hirsch & Luhmann, 2008; Zhao et al., 2009; Viswanathan et al., 2012). In terms of synaptic development, subplate neurons receive prominent thalamic inputs before any other cortical layers in the mouse (Higashi et al., 2002; Molnár et al., 2003) and cat (Friauf et al., 1990; Friauf & Shatz, 1991). Other sources of early input (P0-P3) include glutamatergic inputs from the cortical plate and other subplate neurons (Hanganu et al., 2002; Hirsch & Luhmann, 2008). A study has also shown that bath application of GABA in the presence of glutamate channel blockers resulted in pronounced depolarisation and action potential firing of SPns (Hanganu et al., 2002). Despite all this information, remarkably little is known about how distinct populations of subplate neurons integrate into the cortical and thalamocortical circuitry and how they might differ in this respect (see Chapter 1). A previous report studied the CTGF-GFP population of SPns and divided them in a subpopulation that receives significant L4 input and one that does not (Viswanathan et al., 2012). It is possible that different molecular or morphological types of SPn participate in different neural circuits, and as such serve different functions. In this chapter, I combined targeted whole-cell patch-clamp

recordings of Lpar1-GFP positive subplate neurons with electrical stimulation of thalamic afferents and glutamate uncaging for activation of putative cortical pre-synaptic neurons. My aim was to characterise the electrophysiological properties, maturation and sources of glutamate input onto this molecularly-defined population of subplate neuron.

4.2. Electrophysiological maturation and diversity of Lpar1-GFP SPns

In the Lpar1-GFP mouse line, abundant GFP expression can be observed in the subplate, although a few labelled cells are also visible in L5 and L6 (Figure 4.1A; see Chapter 5). At P1, 33 ±9% of subplate neurons are labelled by GFP, with 29 ±13% remaining so by P8, as determined by NeuN and GFP co-localisation in this layer (Hoerder-Suabedissen & Molnár, 2012). A previous report determined that Lpar1-GFP$^+$ SPns belong to an early-born cohort of subplate cell, preferentially generated at E11.5 (Hoerder-Suabedissen & Molnár, 2012). This is especially pertinent given previous reports that early-born neuronal populations receive higher numbers of connections from subsequently born neurons and regulate early network activity (Bonifazi et al., 2009; Picardo et al., 2011; Marissal et al., 2012). The number of Lpar1-GFP SPns does not change between P1 and P8, and it has been suggested that this population is amongst the few SP populations that preferentially survive into adulthood (Hoerder-Suabedissen & Molnár, 2012). Although the Lpar1-GFP mouse is a BAC (bacterial artificial chromosome) transgenic, GFP expression data is in good agreement with *in situ* hybridisation data, with robust Lpar1 expression in the neocortex detectable in the subplate and a few neurons in layers 5 and 6, both in development and adulthood (http://www.gensat.org), suggesting GFP expression in this line is unlikely to be a fortuitous genetic artefact. However, to fully resolve this

issue and determine that GFP^+ cells are indeed expressing Lpar1, it is fundamental to perform immunohistochemistry for Lpar1 in the Lpar1-GFP mouse and quantify co-localisation with GFP. Unfortunately the lack of a reliable antibody for Lpar1 (A. Hoerder-Suabedissen, unpublished observations) has so far precluded this experiment. For this reason, in my thesis I refrain from making claims about the genetic and molecular significance of expression of this marker in the subplate and neurons in L5 and 6, but rather, I pragmatically used the Lpar1-GFP line to consistently and repeatedly target a specific neuronal population for patch-clamp recordings.

I performed whole-cell patch-clamp recordings from a total of 122 Lpar1-GFP positive subplate neurons in the somatosensory barrel cortex, between the ages of P0 and P15. Cells were divided into four groups corresponding to the period of deep layer thalamocortical invasion (P0-P1, n = 10), followed by the thalamocortical critical period for plasticity, divided into an early (P2-P5, n = 57) and late stage (P6-P8, n = 40) (Agmon & Connors, 1992; Agmon et al., 1993; Crair & Malenka, 1995), and a putatively mature, post-critical period group (P9-P15, n = 15). For each cell, a series of current injection protocols were administered (overview in Materials and Methods), in order to establish a number of intrinsic electrophysiological parameters that could be used to examine maturation of subplate neurons (Figure 4.1B, C).

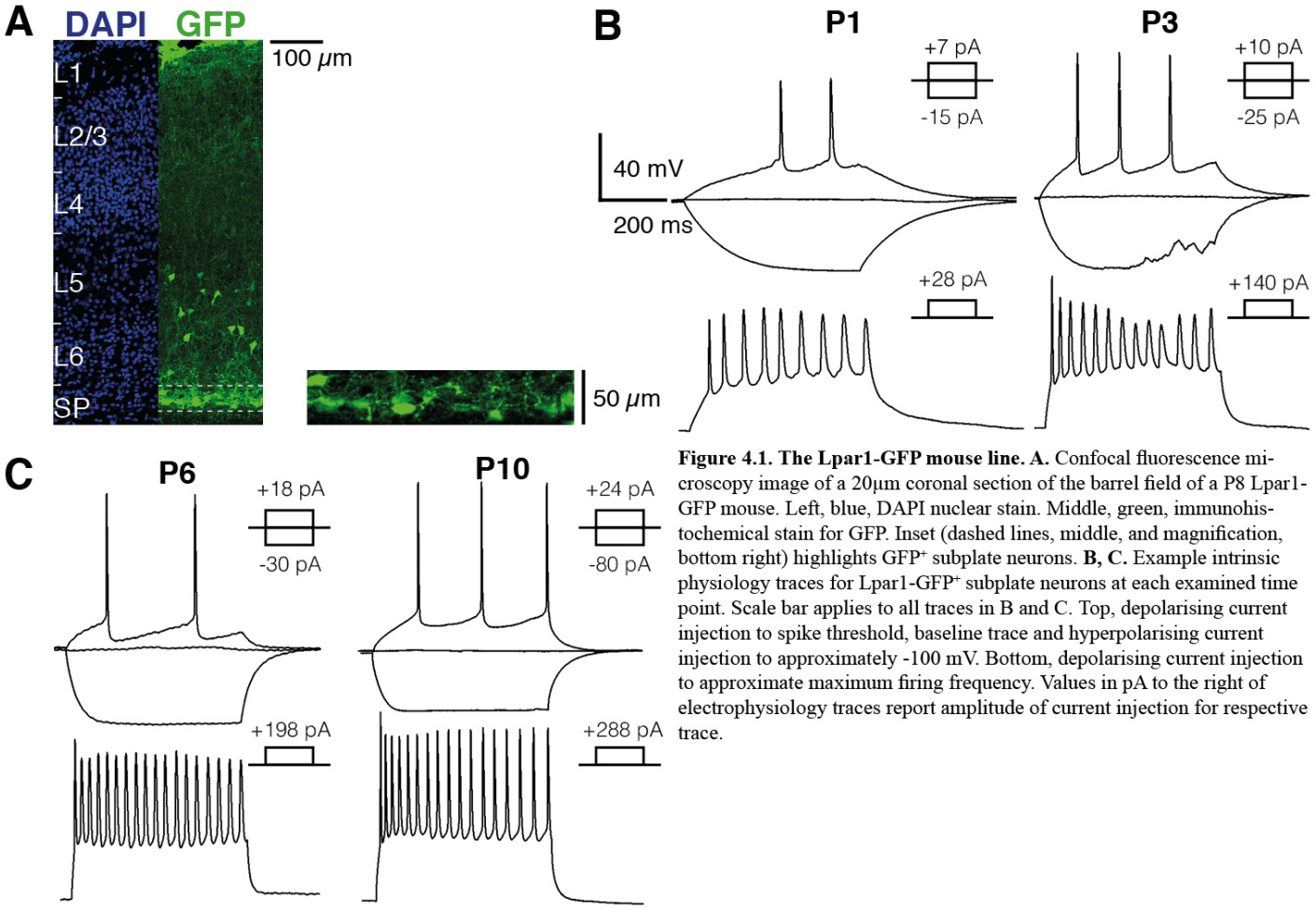


Figure 4.1. The Lpar1-GFP mouse line. A. Confocal fluorescence microscopy image of a 20µm coronal section of the barrel field of a P8 Lpar1-GFP mouse. Left, blue, DAPI nuclear stain. Middle, green, immunohistochemical stain for GFP. Inset (dashed lines, middle, and magnification, bottom right) highlights GFP$^+$ subplate neurons. **B, C.** Example intrinsic physiology traces for Lpar1-GFP$^+$ subplate neurons at each examined time point. Scale bar applies to all traces in B and C. Top, depolarising current injection to spike threshold, baseline trace and hyperpolarising current injection to approximately -100 mV. Bottom, depolarising current injection to approximate maximum firing frequency. Values in pA to the right of electrophysiology traces report amplitude of current injection for respective trace.

For all 122 Lpar1-GFP SPns recorded, I examined membrane and action potential properties. Most parameters examined matured significantly between P0-P1 and P9-P15 (see Table 4.1; Figure 4.1B, C), as determined by statistical analysis with one-way ANOVA or Kruskal-Wallis tests (see Methods section). Although SPns have previously been reported that generate only one action potential regardless of injected current amplitude ("single-spiking" SPns; Friauf et al., 1990; Hanganu et al., 2001; Liao & Lee, 2011) I never observed this type in my sample of 122 Lpar1-GFP SPns, but only "regular-spiking" SPns, whose firing frequency increased with higher amplitude current injection up to a saturation point (Figure 4.1B, C). Purely by examining raw recording traces, it was evident that despite showing advanced maturity of intrinsic physiological parameters relative to pyramidal neurons (Luhmann, 2000), the membrane and action potential properties of Lpar1-GFP SPns matured significantly over development. Despite already being able to reach maximum firing frequencies on the 20 Hz range at P0-P1 (Table 4.1; Figure 4.1B), this parameter practically doubled over development. Inspection of raw recording traces also revealed an increase in spike height, decrease in spike width and overall faster response to current injection, as expected from a maturing population (Figure 4.1B, C).

Statistically speaking, in terms of membrane properties, resting membrane potential became more hyperpolarised ($F(3, 114) = 3.20$, $p = 0.026$). Input resistance underwent a pronounced decrease ($H(3) = 60.77$, $p < 0.001$), concurrent to an increase in rheobase ($H(3) = 21.62$, $p < 0.001$)). The membrane time constant, tau, also decreased significantly over the course of development ($F(3, 100) = 29.65$, $p < 0.001$). When examining action potential properties, there was a significant

hyperpolarisation of the spike threshold ($F(3, 118) = 11.50$, $p < 0.001$) and an increase in maximum firing frequency ($H(3) = 36.67$, $p < 0.001$). Spike height increased throughout development ($H(3) = 37.88$, $p<0.001$) and spike half-width decreased ($H(3) = 46.99$, $p < 0.001$). No further statistically significant differences were observed throughout development for the remaining parameters tested. At all developmental stages tested Lpar1-GFP SPns showed spike adaptation between 30 and ~40%, and a single, slow spike hyperpolarisation.

Having established the electrophysiological characteristics of Lpar1-GFP SPns between P0 and P15, it was apparent from the data collected that parameters matured at distinct rates, and we hypothesised that there might be particular timepoints that are key in intrinsic maturation, with a view to determine when different electrophysiological properties became mature. To this end, I normalised for each developmental stage the average value of membrane and action potential properties to the value attained at the most mature timepoint examined (P9-P15), expressing this as a percentage. For parameters where values decreased throughout development (input resistance, tau and spike half-width), the reciprocal normalised percentage was calculated instead. Only data pertaining to properties that showed statistically significant changes over development was plotted (Figure 4.2). This method allowed direct visual comparison of developmental trends in different electrophysiological properties. To validate any observed trends statistically, I performed the following planned post-hoc statistical comparisons for each relevant variable (original, non-normalised): P0-P1 vs P2-P5, P2-P5 vs P6-P8 and P6-P8 vs P9-P15 (Tables 4.2A and 4.2B).

In terms of membrane properties (Figure 4.2A), the main transition point for maturation was from P2-P5 to P6-P8, with input resistance and tau appearing to mature further until P9-P15. These observations were validated statistically, with post-hoc tests revealing significant differences at P2-P5 vs P6-P8 in all Membrane Properties examined (decrease in resting membrane potential, input resistance and tau; increase in rheobase). Maturation in action potential properties appeared more gradual. Post-hoc tests revealed significant differences at P2-P5 vs P6-P8 for maximum firing frequency (increase) and spike half-width (decrease). Spike height increased significantly at the transition from P0-P1 to P2-P5, and from P2-P5 to P6-P8. Spike threshold decreased significantly from P2-P5 to P6-P8, and from this point to P9-P15.

It can be concluded from statistical analysis that Lpar1-GFP SPns acquire mature-like electrophysiological properties by the end of the first postnatal week. One caveat, however, is that since I did not record any neurons post-P15, I cannot claim that the observed properties would not show further maturation past this timepoint. Nevertheless, the evidence presented strongly suggests that the transition from P2-P5 to P6-P8 is critical in the intrinsic maturation of Lpar1-GFP SPns and that between P6-P8 and P9-P15 only spike threshold changed significantly (Table 4.1; Figure 4.2A, B; Table 4.2A, B).

Table 4.1

Electrophysiological maturation of Lpar1-GFP subplate neurons

Age		P0-P1 (n = 10)	P2-P5 (n = 57)	P6-P8 (n = 40)	P9-P15 (n = 15)
Membrane properties	*RMP (mV)	-64.6 ± 2.1	-64.4 ± 0.9	-68.3 ± 1.1	-67.8 ±1.3
	***R_{in} (MΩ)	2031.0 ±49.9	1847.0 ±98.4	851.2 ±64.8	516.3 ±29.5
	***Tau (ms)	90.0 ±13.6	98.5 ±5.2	49.9 ±3.3	33.2 ±2.5
	**Rheobase (pA)	12.5 ±2.2	15.3 ±1.6	30.3 ±4.1	26.8 ±3.6
Action potential properties	**Spike threshold (mV)	-33.7 ±1.5	-35.4 ±0.5	-37.9 ±0.7	-41.5 ±1.0
	***Spike height (mV)	48.2 ±3.4	62.5 ±1.2	69.2 ±2.2	76.9 ±2.6
	***Spike half-width (ms)	4.1 ±0.2	3.6 ±0.1	2.7 ±0.1	2.2 ±0.1
	Adaptation (%)	31.1 ±8.9	33.6 ±2.4	38.0 ±2.0	41.3 ±2.7
	AHP time (ms)	31.3 ±2.6	28.7 ±1.4	36.1 ±2.6	32.1 ±1.5
	AHP amp. (mV)	14.1 ±1.2	14.1 ±0.5	13.2 ±0.7	12.0 ±1.0
	***Max. Freq. (Hz)	24.0 ±4.3	28.4 ±1.0	42.0 ±2.3	42.7 ±4.0

Table 4.1. Electrophysiological maturation of Lpar1-GFP subplate neurons. Values reported in each cell are average ±SEM (standard error of the mean). Asterisks indicate one-way ANOVA or Kruskal-Wallis test significance *p* values: * $p < 0.05$; ** $p < 0.01$; *** $p < 0.001$.

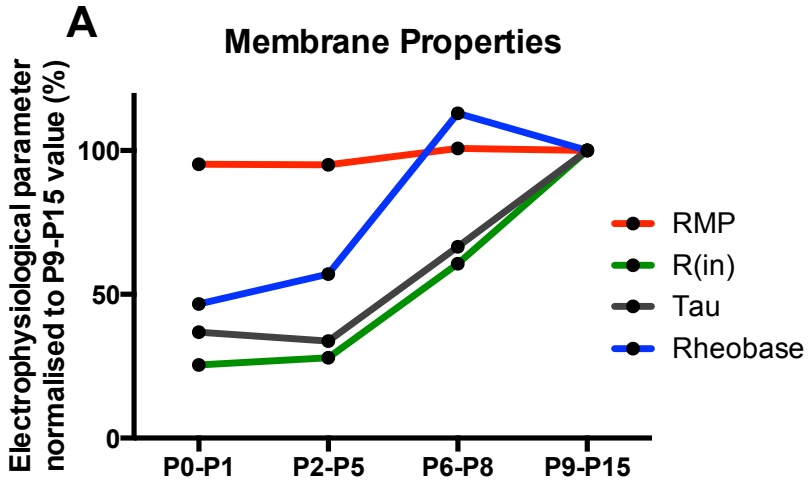


	Table 2a - Post-hoc comparisons for Membrane Properties			
	RMP	**R(in)**	**Tau**	**Rheobase**
P0-P1 vs P2-P5	n.s.	n.s.	n.s.	n.s.
P2-P5 vs P6-P8	*	***	***	**
P6-P8 vs P9-P15	n.s.	n.s.	n.s.	n.s.

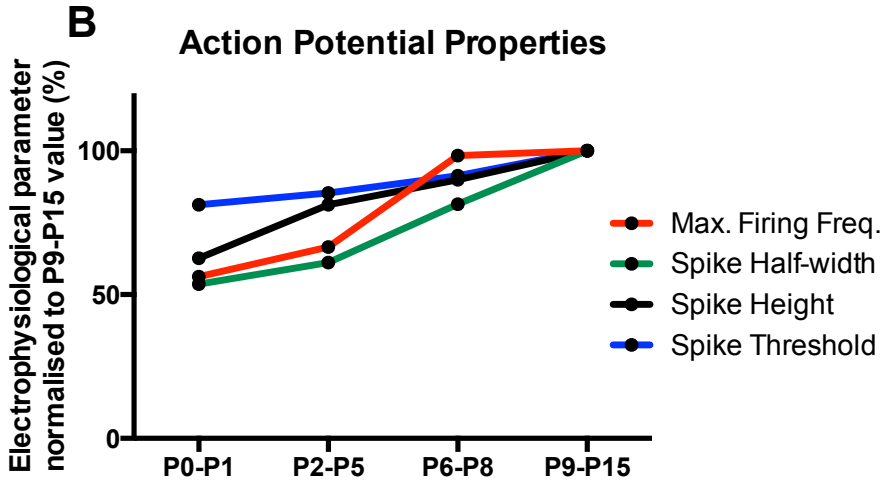


	Table 2b - Post-hoc comparisons for Action Potential Properties			
	Max. Firing	**Spike HW**	**Spike Height**	**Spike Thresh.**
P0-P1 vs P2-P5	n.s.	n.s.	*	n.s.
P2-P5 vs P6-P8	***	***	**	*
P6-P8 vs P9-P15	n.s.	n.s.	n.s.	*

Figure 4.2. Key maturation points for electrophysiological properties of Lpar1-GFP SPns. N numbers as in table 4.1. **A.** Membrane properties. **B.** Action potential properties. Values for each property and developmental stage were normalised in percentage or reciprocal percentage (for parameters whose values decreased throughout development) to the value attained at P9-P15. **Table 4.2a** below Figure 1a reports the result of post-hoc comparisons for Membrane Properties. **Table 4.2b** below Figure 4.2b reports the result of post-hoc comparisons for Action Potential Properties. n.s., non-significant; *, $p < 0.05$; **, $p < 0.01$; ***, $p < 0.001$.

One of the most important events occurring over the first postnatal week in the rodent barrel cortex is thalamic axon innervation and the ensuing critical period for thalamocortical plasticity (Agmon et al., 1993; Crair & Malenka, 1995; Inan & Crair, 2007; Erzurumlu & Gaspar, 2012). Subplate neurons have been previously shown to receive direct thalamic input from very early postnatal (and even embryonic) time points (e.g. Friauf & Shatz, 1991; Hanganu et al., 2002; Z. Molnár et al., 2003), and they have been hypothesised to play a key role in the developmental regulation of plasticity at thalamic inputs to L4 (Kanold, 2004; Kanold & Luhmann, 2010). In the next section I investigated whether the Lpar1-GFP subplate neuron cohort receives thalamic input.

4.3. Thalamic Input

Several studies have reported thalamic input to subplate neurons from very early ages in different model organisms and cortical areas (Friauf et al., 1990; Friauf & Shatz, 1991; Hanganu et al., 2002; Higashi et al., 2002; Molnár et al., 2003; Zhao et al., 2009), but no study has so far examined whether thalamic inputs onto these neurons are cell-type specific. Given the morphological and molecular diversity of these neurons (Hanganu et al., 2002; Hoerder-Suabedissen & Molnár, 2011; Marx & Feldmeyer, 2012), cell-type specific thalamo-cortical, cortico-cortical or cortico-thalamic circuits are an interesting possibility. To test this idea, I started by investigating whether Lpar1-GFP subplate neurons in the barrel field received input from the thalamic ventrobasal nucleus (VB), and how this input might change over the course of development. For these experiments, I placed a bipolar stimulating electrode in the VB nucleus of the thalamus and targeted GFP-positive subplate neurons for recordings. SPns pioneer the corticothalamic projection (McConnell et al.,

1994) and receive early synaptic inputs from the cortical plate (Hanganu et al., 2002), which likely originate from subcortically-projecting L5 and L6 pyramidal neurons. Therefore, it is possible, when attempting to orthodromically stimulate thalamic afferents, to simultaneously activate antidromically the axons of corticothalamic neurons, which could then project to recorded subplate neurons. As such, a thalamic stimulation-evoked EPSC was considered mono-synaptic only if it displayed a short onset latency (<10ms), unimodal latency distribution and negligible trial-to-trial variability in latency (Agmon et al., 1996; Gil & Amitai, 1996; Gil et al., 1999; Hanganu et al., 2002) (Figure 4.3A, 4.3B). A total of 69 Lpar1-GFP SPns (P0-P1: n =8; P2-P5 n = 25; P6-P8 n = 16; P9-P15 n = 20) were recorded for thalamic connectivity experiments. Recordings were performed at room temperature and latency values were within the range previously reported for slice preparations under similar temperature conditions and within the same postnatal window (Fig. 4.3B; (Agmon et al., 1996; Hanganu et al., 2002)), lending confidence to the claim that they represented genuine monosynaptic thalamic activation of the subplate. I attempted to activate single thalamic afferents by using an adapted minimal stimulation protocol (Isaac et al., 1997; Raastad et al., 1992). I began by finding the lowest stimulation intensity that would result in all-or-none synaptic events in 50-70% of trials (Figure 4.3C). These synaptic events are presumed to result from activation of a single pre-synaptic axon. Figure 4.3A illustrates an example of all-or-none thalamocortical EPSCs (TC-EPSCs) evoked in this fashion. For each cell, I recorded the response to 10 thalamic stimulation sweeps. Figure 4.3D displays the proportion of Lpar1-GFP subplate neurons that received monosynaptic thalamic input. This was at its highest early in development (P0-P1; 100%), decreasing to 70-75% at P2-P5 and P6-P8, before dropping to 30% at P9-P15. This decrease in thalamocortical connectivity

could not be explained by differential stimulation parameters or failure to engage pre-synaptic thalamic neurons, as no significant differences were found ($F(2, 38) = 1.137$, $p = 0.331$) for the stimulation amplitudes used between developmental periods (Figure 4.3C), and cells were only considered not to receive thalamic input if a L4 spiny stellate neuron in the same barrel column had previously been successfully shown to receive direct thalamic input. It is possible, however, due to smaller brain size at P0-P1 and P2-P5, that more connectivity is preserved in brain slices of the same thickness at these timepoints than at P9-P15, and that thalamocortical connectivity probabilities for this age group were underestimated due to greater axon severing. In the experiments performed for Chapter 3, thalamic inputs onto 9 unlabelled SPns were mapped using CRACM and no direct input could be detected, lending further support to a genuine drop in thalamic connectivity into the subplate, since this approach circumvents the problem of axon severance (Petreanu et al., 2007; 2009). It must still be cautioned, however, that since CRACM experiments were performed on wild-type electroporated animals, I could have been recording from a cohort of subplate neuron distinct to the Lpar1-GFP population.

Having established the strong prevalence of early thalamic connectivity onto Lpar1-GFP SPns, I then went on to characterise thalamic inputs onto this cell type (Figure 4.3E-J).

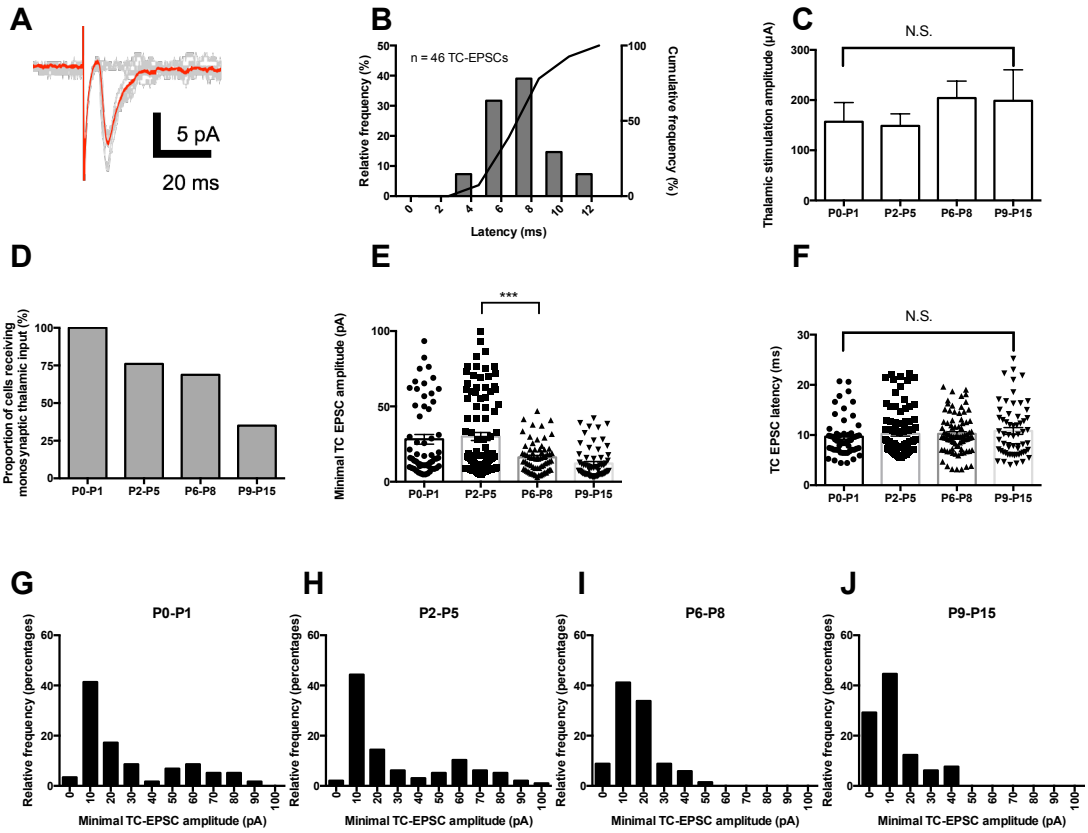


Figure 4.3. Thalamic input onto Lpar1-GFP subplate neurons between P0 and P15 (Total 69 cells; P0-P1 n = 8; P2-P5 n = 25; P6-P8 n = 16; P9-P15 n = 20). **A.** Example minimal TC-EPSCs from an Lpar1-GFP SPn at P5. Note the failures. **B.** Example latency distribution of monosynaptic TC-EPSCs in an Lpar1-GFP SPn. **C.** Average electrical stimulation amplitude used for thalamic afferents over development (Total 69 cells; P0-P1 n = 8; P2-P5 n = 25; P6-P8 n = 16; P9-P15 n = 20). **D.** Proportion of Lpar1-GFP SPns receiving monosynaptic thalamic input over development. **E.** Minimal TC-EPSC amplitude over development for Lpar1-GFP SPns. Each symbol corresponds to an individual EPSC recorded from a cell. Number of cells per age as reported in C. **F.** TC-EPSC latency over development for Lpar1-GFP SPns. Each symbol corresponds to an individual EPSC recorded from a cell. Number of cells per age as reported in C. **G-J.** Relative distribution of minimal TC-EPSC amplitudes for Lpar1-GFP SPns at P0-P1, P2-P5, P6-P8 and P9-P15. Number of cells per age as reported in C. *** $p < 0.001$; N.S, non-significant.

There was great variability in the amplitude of events recorded, with some minimal TC-EPSC amplitudes as low as 5pA and others as large as 100pA. At P0-P1, the average minimal TC-EPSC amplitude was 28± 3pA, with similar amplitudes of 30± 3pA obtained at P2-P5. At P6-P8 TC-EPSC amplitude was 16± 1pA and the value obtained for P9-P15 was 12± 1pA. One-way ANOVA detected a statistically significant change in minimal TC-EPSC amplitude changed over development ($F(3, 284) = 14.17$, $p < 0.001$). Planned post-hoc comparisons (P0-P1 vs P2-P5; P2-P5 vs P6-P8 and P6-P8 vs P9-P15) revealed a significant decrease in amplitude between P2-P5 and P6-P8.

It is apparent from Figure 4.3E that at P0-P1 and P2-P5 there was a cohort of large amplitude events (>50pA), which was not present at P6-P8 and P9-P15. In order to examine these events more closely, I plotted in Figure 4.3G-J the relative frequency distribution of TC-EPSC amplitude over development. At P0-P1 and P2-P5, a clear bi-modal distribution can be observed, with a main peak at the 10-20pA bin and a secondary peak centred at the 60-70pA bin. By P6-P8 the distribution had become unimodal, with an increase of events in the 0-10pA bin. This trend continued at P9-P15, with a complete disappearance of events over 50pA, an increase in weak events in the 0-10pA bin, and a decrease in events in the 20-30pA bin. The proportion of events in the 10-20pA bin remained constant throughout development (around 40%).

When examining latency, no significant developmental effect was observed ($F(3, 293) = 0.653$, $p = 0.582$), with values ranging from 9.7± 0.5ms at P0-P1 to 10.8± 0.7ms at P9-P15 (Figure 4.3F). Taken together, our data suggests that thalamic inputs onto Lpar1-GFP SPns are dynamically reconfigured throughout postnatal

development. Initially, the majority of Lpar1-GFP SPns receive direct thalamic input, but the proportion of thalamic-innervated neurons seems to decrease after the first postnatal week. Changes in minimal TC-EPSC amplitude pre-empt this drop in connectivity, with the disappearance of a cohort of large amplitude events and decrease in average minimal amplitude also occurring at the transition between P2-P5 and P6-P8.

Having determined the static characteristics of thalamic input onto Lpar1-GFP SPns, we next aimed to study a dynamic aspect of this synapse, its short-term plasticity characteristics. Short-term plasticity has been ascribed many functional roles, and its description for a synaptic input can provide insight into the circuit function of that input (Regehr, 2012). It has previously been shown that thalamic inputs onto regular spiking and fast spiking cells in L4 and L6 are strongly depressing (Beierlein & Connors, 2002; Cruikshank et al., 2010; Gil et al., 1997). One study examined the short-term properties of thalamocortical inputs onto unlabelled SPns in rat barrel cortex, finding that at P0-P7 paired-pulse ratio (PPR) was below 1 (short-term depression), whereas after P12 it was close to 1.5 (short-term facilitation) (Liao & Lee, 2011). For short-term plasticity experiments, I adjusted stimulation intensity in order to evoke a pair of EPSCs of reliable amplitude in ~70% of trials. This procedure ensured that the level of stimulation was close to that necessary to evoke a single fibre response, while avoiding high numbers of failures observed at lower stimulation amplitudes, which would preclude conclusive comparisons. I elected to use a 50ms inter-stimulus interval (ISI) between pulses (Figure 4.4A), as this frequency (20 Hz) is close to that of the spindle burst, the dominant pattern of activity in the neonatal cerebral cortex of the mouse and human (Khazipov & Luhmann, 2006). I recorded 11

Lpar1-GFP positive SPns across different ages for this experiment. Recordings from different ages were pooled together for analysis, as no developmental change was found in the direction of short-term plasticity (Figure 4.4A). 10 out of 11 SPns showed short-term depressing responses, with an average amplitude of 17± 3pA for the first stimulus and 11± 2pA for the second (Figure 4.4B). Short term depression was statistically significant for Lpar1-GFP SPns, as determined by paired-samples t-test ($t(10) = 2.63$, $p = 0.025$), and the average paired-pulse ratio was 0.7± 0.1. For comparison, I further recorded 11 L4 spiny stellate neurons. For this cell type, average TC-EPSC amplitude was 16± 3pA for the first stimulus, and 13± 2pA for the second (Figure 4.4C). A paired-samples t-test found no significant difference in TC-EPSC amplitude for the first and second responses ($t(10) = 1.8$, $p = 0.102$) and paired-pulse ratio for L4 spiny stellate neurons was 0.9± 0.1, suggesting no significant short-term dynamic for thalamic inputs onto this cell type.

The functional study of synaptic inputs onto SPns has not been limited to thalamocortical synapses. Previous studies have used electrical stimulation to show that SPns receive prominent inputs from the cortical plate and the subplate (Hanganu et al., 2002; Hirsch & Luhmann, 2008). One study used glutamate uncaging to map afferent inputs onto mixed subplate neuron populations (Viswanathan et al., 2012). In the next sections of this chapter I will discuss technical aspects of this technique and use it to map afferent excitatory cortical input onto Lpar1-GFP SPns.

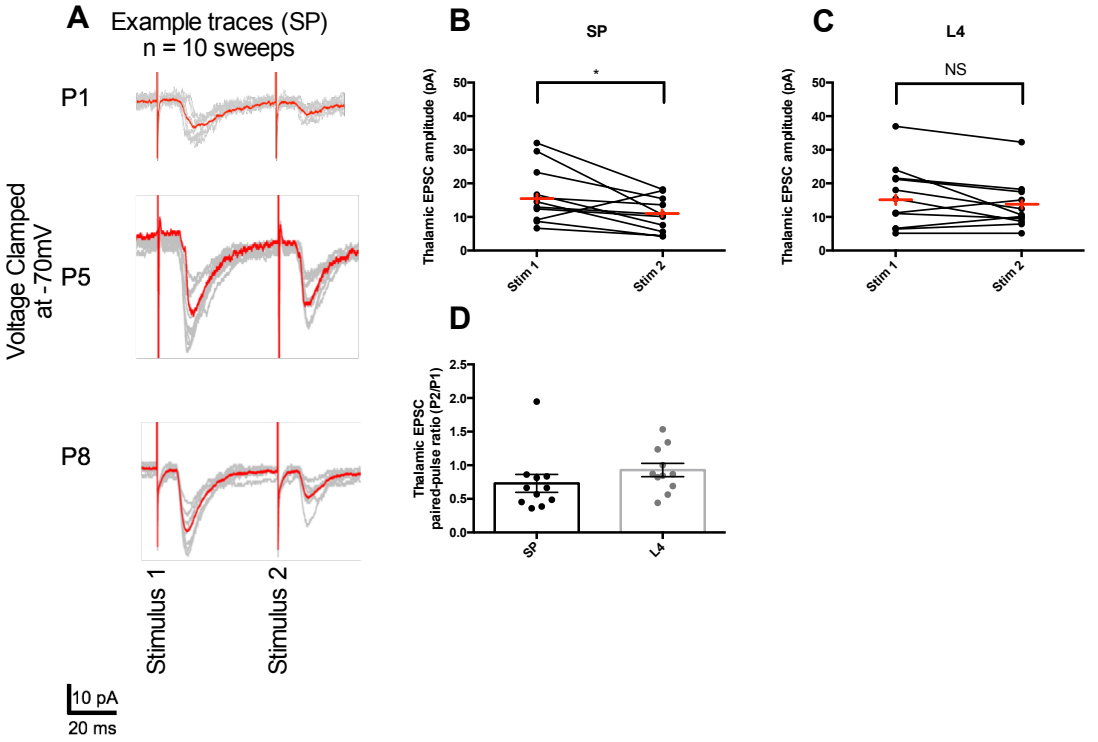


Figure 4.4. **Short-term plasticity of thalamic inputs onto Lpar1-GFP SPns. A.** Example paired-pulse traces of TC-EPSCs recorded in Lpar1-GFP SPns. Failures have been removed for clarity. Inter-stimulus interval was 50ms and a total of 11 Lpar1-GFP SPns were recorded. **B.** TC-EPSC amplitude recorded in Lpar1-GFP SPns for short-term plasticity experiments. Each point corresponds to a cell (n = 11 cells). For each cell, 10 sweeps were recorded and averaged. Red bars display mean and standard error of the mean. **C.** TC-EPSC amplitude recorded in L4 spiny stellate cells for short-term plasticity experiments. Each point corresponds to a cell (n = 10). For each cell, 10 sweeps were recorded and averaged. Red bars display mean and standard error of the mean. **D.** Average paired-pulse ratio for Lpar1-GFP SPns (n = 11) and L4 spiny stellate neurons (n = 10). * $p < 0.05$; N.S., non-significant.

4.4. Calibration of LSPS for glutamate uncaging

Glutamate uncaging is an effective technique for probing circuitry in the brain. Like any other technique in neurobiology it comes with limitations, and results derived from experiments are limited in their power by the rigour invested in controlling extraneous variables. There are several factors that should be addressed in order to take full advantage of the power of this technique. LSPS via glutamate uncaging is a well-established technique in the laboratory, and experiments in my thesis were conducted according to previously published protocols (Anastasiades & Butt, 2012). In this section I will discuss the main technical factors that can influence interpretability of LSPS experiments and describe how our laboratory protocols were adapted for mapping cortical inputs onto Lpar1-GFP SPns.

Pre-synaptic characterisation

When calibrating LSPS for glutamate uncaging, it is fundamental to adjust laser stimulation intensity such that pre-synaptic neurons are only activated from the vicinity of their soma and not other compartments, such as distal dendrites. My approach for calibrating LSPS conditions was to record putative pre-synaptic partners of subplate neurons in current-clamp and sequentially uncage glutamate over a grid of pseudo-random UV laser target spots in a 17x9 50µm-spaced virtual grid. I recorded a total of 30 L5 and L6 pyramidal neurons and varied laser intensity until I could elicit 2 or more action potentials at the fewest spots possible. Figure 4.5 displays an example of a L5b pyramidal neuron, where I recorded direct activation maps at 320-520µW laser power. For each power, 3 maps were performed and averaged (Figure 4A-C). Each pixel corresponds to an uncaging spot and is colour-coded according to the amplitude of the response, in mV, that was evoked in the recorded cell by

uncaging in that spot (see legend). Sample traces of responses closest to the soma are outlined (white dashed 3x3 box around cell soma) and displayed below each direct activation map (Figure 4.5A'-C'). At 320μW laser intensity no action potentials could be evoked (Figure 4.5A, 4.5A'). Increasing intensity to 400μW resulted in the generation of action potentials at the pixel corresponding to the soma and subthreshold depolarisations of ~15-20mV in the proximity of the soma and putative apical dendrite of the cell (Figure 4.5B, 4.5B'). When mapping at 520μW, action potentials were evoked not only from the soma, but also from one adjacent pixel and three pixels at the L4-L5 border, presumably overlying the apical dendrite (Figure 4.5C, 4.5C'). Additionally, a large depolarisation of around 12mV was evoked at L2/3, likely resulting from activation of apical dendrites. Thus, increasing laser intensity will result in an increase of spots from which action potentials can be evoked. These spots will be not only in close proximity of the cell soma, but often also along its dendrites. Ultimately, this will degrade mapping resolution, as the spatial range from which pre-synaptic spikes can be generated will increase, leading to uncertainty in the origin of synaptic inputs. This is especially problematic for spikes generated from the apical dendrite (Figure 4.5C, red boxes). Figure 4.6 depicts the average laser power used at each postnatal day, calibrated to generate 2-3 action potentials at the cell soma, whilst keeping the number of spots from which spikes are evoked as spatially restricted and perisomatic as possible. Laser intensities used between P0-P8 were similar, and statistically undistinguishable according to a Kruskal-Wallis test ($H(7) = 7.92$, $p = 0.34$). This is in agreement with published work from our lab on L2/3 and L5 pyramidal neurons, according to which laser intensity required to generate action potentials at the soma remained constant at P5-P8, but began increasing after P9 (Anastasiades & Butt, 2012).

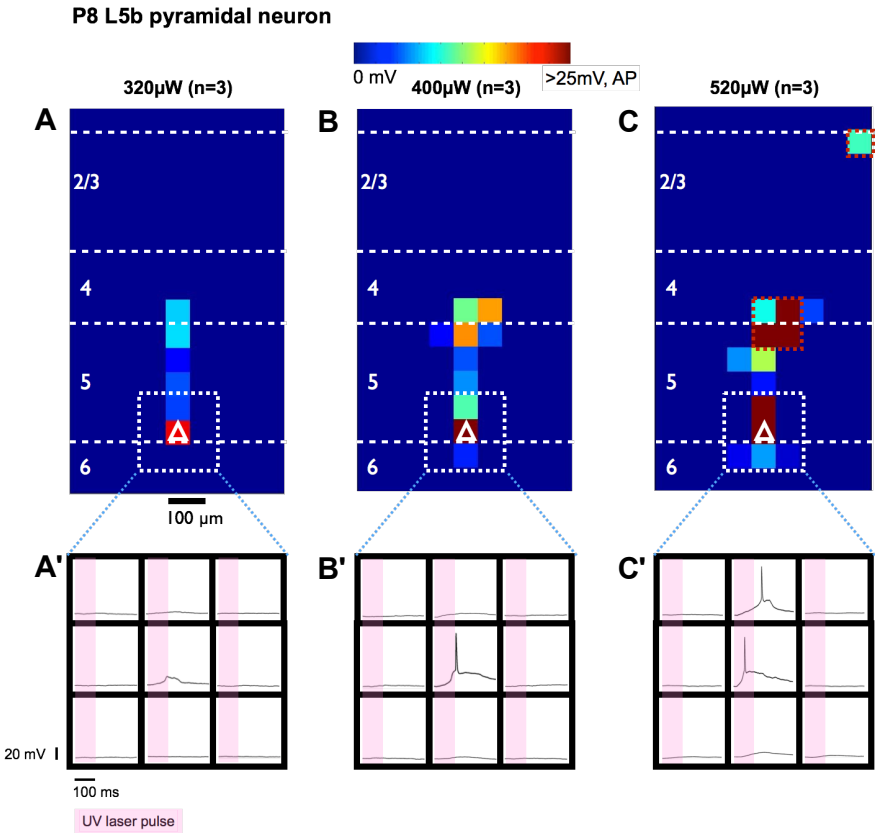


Figure 4.5. Direct activation profile for an example L5b pyramidal neuron at P8. Cell recorded in current clamp, held at approximately -65mV. Laser power was varied between 320 µW (**A**), 400 µW (**B**) and 520µW (**C**∫). For each power, 3 maps were recorded, then averaged. **A'-C'** highlight sample current-clamp recording traces from a 3x3 pixel (150x150µm) perisomatic region. Pink shaded area corresponds to the laser stimulation window.

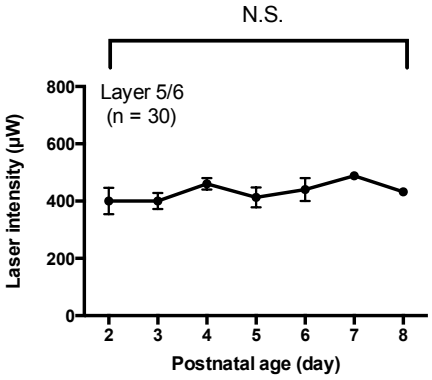


Figure 4.6. **Calibration of laser intensity to postnatal age.** 30 L5/6 pyramidal neurons were recorded and their direct activation maps obtained. Plotted for each age is the average laser intensity at which the cell fired 2-3 action potentials when glutamate was uncaged at the soma, whilst restricting activation from other cellular compartments.

Post-synaptic characterisation

Having established LSPS parameters for putative pre-synaptic neurons over the postnatal recording window, I shifted my focus to LSPS issues relating to the post-synaptic cell. There are two main technical challenges in this regard. First, Lpar1-GFP SPns are themselves sensitive to glutamate, and will therefore exhibit not only synaptic responses resulting from laser-evoked pre-synaptic action potentials, but also direct responses to glutamate uncaged near the soma or dendrites. Is it possible to tell the two apart with confidence? Second, while performing an LSPS map, both laser-evoked and spontaneous EPSCs will be recorded. How long should the mapping window be? A long window will imply more contamination with spontaneous events. A short window will mitigate spontaneous contamination, but likely exclude genuine, late-occurring evoked events. Our approach to address the direct versus synaptic response issue was to use a UV laser pulse of long duration (100 ms, see Figure 4.5A'-C' and Figure 4.6) and low intensity (100 to 800 μW at the slice plane). The benefits of this strategy are that it greatly facilitates distinction between direct and synaptic activation of the recorded cell and reduces the occurrence of distally-evoked spikes without compromising the ability to elicit action potentials at the soma (Anastasiades & Butt, 2012). Figure 4.7 illustrates the mapping process for an Lpar1-GFP SPn. Figure 4.7A displays the overlay of uncaging spots over the differential interference contrast image (DIC). For each cell, I performed 2-4 LSPS maps, which were then averaged onto a final glutamate input map. Each "pixel" in the map corresponds to an uncaging spot, and the amplitude of responses (in pA) evoked by uncaging at each spot is colour coded (Figure 4.7B). Figure 4.7C illustrates two repeats of example recording traces from different spots in the map. There are 3 possible outcomes when uncaging glutamate over a defined spot: spiking of a pre-

synaptic neuron leading to detection of a synaptic response at the recorded cell (Figure 4.7B, C spots and example traces 1 and 2); no synaptic response (4.7B, C spot and example trace 3) or a direct response (4.7B, C spot and example trace 4). The advantage of the low-intensity long duration strategy is that it exaggerates the difference in kinetic and amplitude profile between synaptic and direct responses to such an extent that telling them apart becomes trivial (compare Figure 4.7C traces 1 and 2 with trace 4; note the different scale). Typically, authors distinguish synaptic and direct responses based on latency and amplitude, with direct responses characterised by shorter latencies and larger amplitudes (Zhao et al., 2009; Jacob et al., 2012; Shepherd, 2012; Viswanathan et al., 2012). Often, however, there are stimulation sites where direct and synaptic responses cannot confidently be distinguished, and experimenters black out these areas, effectively losing information and resolution (Jacob et al., 2012; Viswanathan et al., 2012). Our low intensity long duration approach efficiently gets around this issue and enables us to resolve even inputs that are very close to the soma of the recorded cell (Anastasiades & Butt, 2012).

Leading to the issue of spontaneous versus synaptic event detection, the drawback of the low intensity long duration strategy is loss of temporal resolution. Effectively, owing to the long duration of the laser pulse, there is a long window over which pre-synaptic action potentials can be generated, resulting in considerable temporal variability in pre-synaptic spike onset (see Figure 4.5B', 4.5C' insets for examples). The pre-synaptic spike generation window determines the time range at which evoked EPSCs are expected in the post-synaptic cell. Therefore, in order to establish a

window for evoked EPSC detection, I set out to determine the timecourse of pre-synaptic laser-evoked action potential generation.

I recorded calibrated direct activation maps of L5/6 pyramidal neurons (n = 30). Owing to the difficulty in patching and holding P0-P1 pyramidal neurons throughout experiments, not enough data for this timepoint was obtained, and as such I shall report only data for the P2-P5 (n = 16 cells, 42 evoked bursts of action potentials) and P6-P8 periods (n = 14 cells, 54 evoked bursts of action potentials). For each cell characterised, I recorded the onset latency of the first and last laser-evoked action potential for each trial where a spike was evoked. The relative frequency of laser-evoked action potentials is plotted in Figure 4.8 for P2-P5 (A) and P6-P8 (B). Recorded cells had different distributions at the two developmental timepoints. At P2-P5, most initial spikes were evoked during the period of laser stimulation (100-200 ms after trial onset) and within the 20 ms after stimulus offset. A high proportion of spikes were still evoked, however, between 240-460 ms after trial onset. The distribution at P2-P5 of the last laser-evoked spike was broader, with spikes occurring 240 to 600ms after trial start (Figure 4.8A). Action potentials at P6-P8 were more time-locked. Most of the first spikes occurred during the period of laser stimulation, but the first spike generation window continued up to 360ms after trial onset. The window for generation of the last action potential was also narrower, with spikes occurring between 220 and 400ms after trial onset (Figure 4.8B). I then mapped afferent excitatory input onto Lpar1-GFP SPns at P2-P5 (n = 4 cells, 697 EPSCs) and P6-P8 (n = 5 cells, 614 EPSCs), pooling together all EPSCs detected at each age group (Figure 4.8C-H). Plotting their temporal distribution revealed that EPSC frequency peaked at P2-P5 between halfway through the laser pulse and about 100ms

after its offset (at 300ms after trial onset), with a further continuous tail of events detected up to around 600ms after trial onset, before decreasing to background spontaneous activity level. At P6-P8, EPSC distribution was more focused, with a large proportion of events detected between the half-point and offset of laser stimulation, before peaking at 220ms and decaying to background level around 400ms after the beginning of the trial (Figure 4.8D). The developmental narrowing of EPSC detection is apparent in Figure 4.8E, where the temporal distribution of events at P2-P5 (blue) is plotted against that at P6-P8 (red). Based on analysis of L5/6 pyramidal cell spike generation and Lpar1-GFP SPn EPSC detection, I decided to use as my evoked event detection window the period between onset of the first spike and onset of the last spike detected at L5/6 neurons, for each age group. As can be seen from cumulative frequency distribution plots for EPSCs at each timepoint, this decision enabled me to capture over 75% of recorded EPSCs.

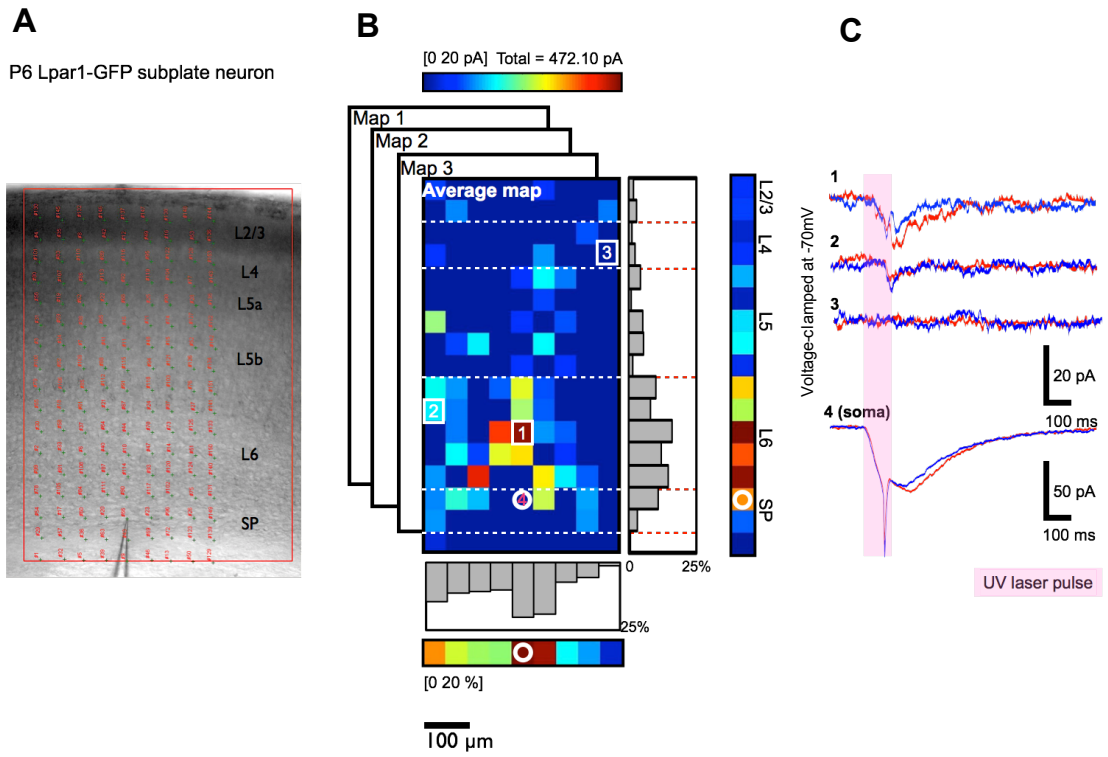


Figure 4.7. Mapping afferent cortical excitatory inputs onto Lpar1-GFP subplate neurons. A. Differential interference contrast image overlaid with virtual uncaging grid. This image was subsequently used during analysis to assign EPSCs to pre-synaptic layer of origin. **B.** Example average map for a P6 Lpar1-GFP SPn. For each mapped cell, 2-4 repeats of LSPS maps were performed and averaged. Each "pixel" corresponds to an uncaging spot defined by the grid in **A**. EPSC amplitude in pA is colour coded according to scale bar (top). Right, vertical (layer) profile of evoked synaptic responses. Bottom, horizontal (columnar) profile of evoked synaptic responses. Vertical and horizontal profiles are normalized to the recorded neuron's total evoked synaptic input (%). Values are colour-coded according to scale bar (bottom). **C.** Sample recording traces from two consecutive maps recorded in voltage clamp (-70mV). Example traces correspond to outlined pixels numbered 1-4 in average map (**B**).

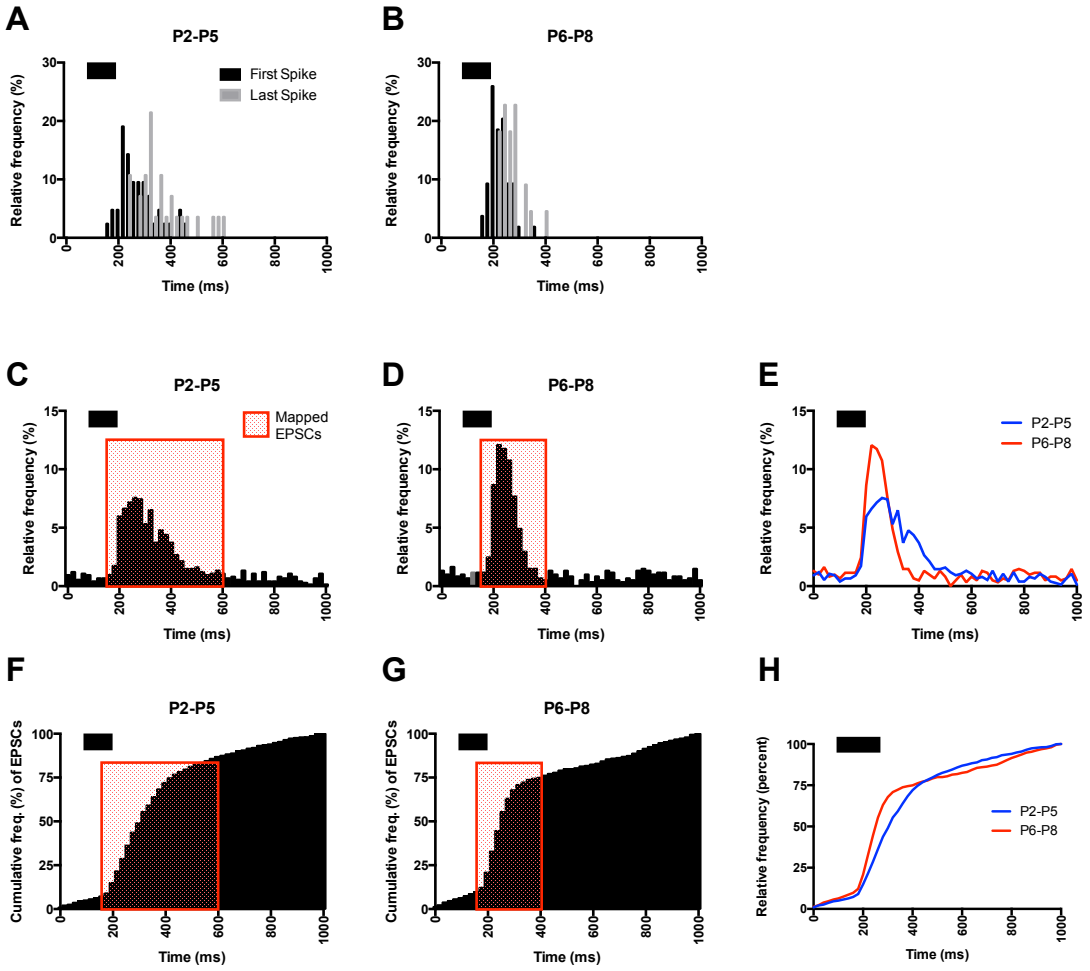


Figure 4.8. Pre-synaptic action potential and post-synaptic EPSC detection window. A. Temporal distribution (relative frequency) of the first (black) and last (grey) spike generated in a sample of 16 L5/6 pyramidal neurons at P2-P5. **B.** Temporal distribution (relative frequency) of the first (black) and last (grey) spike generated in a sample of 14 L5/6 pyramidal neurons at P6-P8. UV laser stimulation period indicated by black bar (top, 100-200ms after trial onset; indicated also in all subsequent figures in this panel). **C.** Temporal distribution (relative frequency) of detected EPSCs in a sample of 4 Lpar1-GFP SPns at P2-P5 (n = 697 EPSCs). Red boxed region indicates EPSC detection window determined from action potential and EPSC temporal distribution for P2-P5. **D.** Temporal distribution (relative frequency) of detected EPSCs in a sample of 5 Lpar1-GFP SPns at P6-P8 (n = 614 EPSCs). Red boxed region indicates EPSC detection window determined from action potential and EPSC temporal distribution for P6-P8. **E.** Temporal distribution (relative frequency) of detected EPSCs at P2-P5 (blue) plotted with P6-P8 (red). Numbers as in C and D. **F.** Cumulative relative frequency of detected EPSCs at P2-P5 with detection window (red box) superimposed. **G.** Cumulative relative frequency of detected EPSCs at P6-P8 with detection window (red box) superimposed. **H.** Cumulative relative frequency of detected EPSCs at P2-P5 (blue) plotted with P6-P8 (red). Numbers as in C and D.

4.5. Mapping excitatory cortical inputs onto Lpar1-GFP subplate neurons

Having determined temporal and spatial resolution, I used LSPS to map excitatory cortical input onto 93 Lpar1-GFP subplate neurons located in the barrel cortex between P0 and P8 (P0-P1 n = 9; P2-P5 n = 51; P6-P8 n = 33). GFP-expressing SPns were targeted for whole-cell patch-clamp recordings. Following assessment of their intrinsic electrophysiological properties (see 4.2) I washed in and recirculated a 0.2 mM caged glutamate in high-divalent cation Ringer's solution (HDC, see Materials and Methods chapter) for at least 5 minutes, before mapping afferent input.

To isolate AMPA-receptor mediated responses, cells were voltage-clamped at a holding potential of -70mV. Maps were repeated a minimum of 3 times. Extraction of evoked EPSCs using customised Matlab scripts and Minianalysis software enabled me to plot colour-coded maps showing the distribution of afferent input across the mapped area. I started by calculating for each cell the total excitatory synaptic input it received, by summing all detected EPSCs within the detection window. To assess the horizontal (columnar) and vertical (layer) profile of afferent input, total input per 50µm column and row (respectively) were calculated and plotted. Additionally, cortical layer boundaries were estimated from DIC images of the mapped area and evoked inputs were assigned to their layer of origin. Horizontal, vertical and layer profiles were normalised to each cell's total input. This provided an accurate portrayal of local afferent connectivity onto each recorded cell, as well as the relative influence of inputs originating from a particular row, column or layer (Figure 4.9).

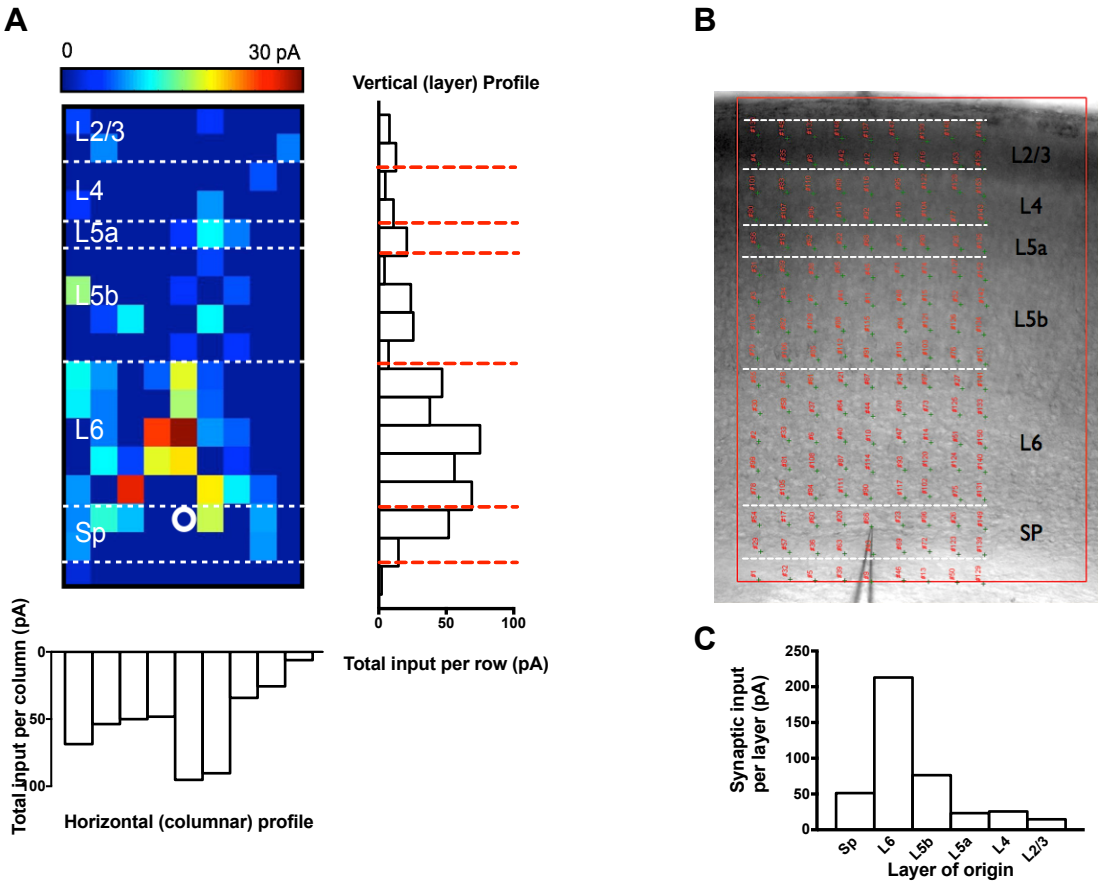


Figure 4.9. Mapping excitatory inputs onto Lpar1-GFP SPns – an example input map for a cell. A. LSPS input map, vertical profile and horizontal profile. Each spot in the input map corresponds to a spot where glutamate was uncaged. Responses are colour-coded according to the average EPSC evoked from uncaging glutamate over a particular spot. Vertical profile was determined for each cell by summing all inputs for each 50µm row. The converse approach was used for horizontal profiles, i.e., summing all inputs for each 50µm column. Vertical profiles allowed me to concentrate on layer information, whereas horizontal profiles enabled me to make inferences about the columnar organisation of inputs to a particular cell. Vertical and horizontal profiles were also normalised to a cell's total synaptic input for comparison across cells. **B.** Photomicrograph of the brain slice in which the cell in A was recorded, overlaid with LSPS grid. **C.** Layer of origin of excitatory synaptic inputs onto the SPn shown in A. A photomicrograph of the slice with uncaging grid overlaid was taken at the beginning of each experiment (**B**). This allowed me to correlate glutamate uncaging spots with putative evoked synaptic responses and thus assign layer of origin to each input evoked. For the cell in A, most inputs originated from L6.

4.5.1. Laminar organisation of excitatory inputs onto Lpar1-GFP subplate neurons over the first postnatal week

Subplate neurons occupy a key position in the developing cortex, as an early-born population that is the first in the cortex to receive thalamic and subcortical neuromodulatory inputs (Kanold & Luhmann, 2010). They have been implicated in the propagation of cholinergic-activated oscillatory network activity in the neonatal mouse cortex (Dupont et al., 2006) and their selective removal been shown to largely abolish endogenous and sensory-evoked spindle burst activity, as well as barrel formation (Tolner et al., 2012), and maturation of thalamocortical inputs to L4 (Kanold et al., 2003). SPns are clearly involved in the generation or propagation of early cortical network activity, which influences key cortical developmental processes (Khazipov & Luhmann, 2006; Kanold, 2009; Hanganu-Opatz, 2010; Kanold & Luhmann, 2010; Kilb et al., 2011). However, few studies have examined their functional integration in cortical circuits (Hanganu et al., 2002; Viswanathan et al., 2012). To understand the role SPns play in early network oscillations, it is important to determine how they fit into cortical circuitry, as this might provide part of the synaptic backbone underlying early cortical network events. Here I aimed to characterise the development of afferent cortical excitatory input onto the Lpar1-GFP SP population over the first postnatal week, using glutamate uncaging.

The total amount of cortical excitatory synaptic input onto Lpar1-GFP SPns remained constant throughout the first postnatal week, averaging 163± 23pA at P0-P1 (n = 9), 225± 23pA at P2-P5 (n = 51), and 195± 18pA at P6-P8 (n = 33) (Table 4.3). A Kruskal-Wallis test detected no significant difference in total synaptic input between the three age groups tested ($H(2) = 0.762$, $p = 0.683$). Therefore, Lpar1-GFP SPns are

integrated into the cortical excitatory network from birth, and the total amount of excitatory synaptic input is not developmentally regulated during the first postnatal week. Even if there is no change in the total amount of input received by these neurons, there might be developmental shifts in the identity of cortical layers providing input. My next goal was to identify where local cortical excitatory input arose from, and whether there were developmental shifts in afferent excitatory circuitry to Lpar1-GFP SPns. Figure 4.10 schematically illustrates the origin of local excitatory inputs for all 93 Lpar1-GFP SPns mapped. I calculated the vertical profile of each cell, normalised it to the cell's total synaptic input, and plotted this profile in a colour-coded map. Each one-pixel column therefore corresponds to a cell, ordered left to right by age, from P0 to P8. Each pixel within a column illustrates the proportion of total synaptic input that originated from that 50μm row, for a particular Lpar1-GFP SPn. Vertically, cells were aligned by the soma position. Approximate layer boundaries for each age group were estimated during cell alignment.

		Table 4.3. Proportion of synaptic input onto Lpar1-GFP SPns per layer (%)						
	N	**SP**	**L6**	**L5b**	**L5a**	**L4**	**L2/3/CP**	**Total (pA)**
P0-P1	9	44± 8	25± 8	13± 2	3± 2	15± 3	3± 1	163± 23
P2-P5	51	16± 2	39± 2	18± 2	9± 1	14± 2	3± 1	225± 23
P6-P8	33	12± 3	44± 3	19± 2	7± 1	12± 2	6± 2	195± 18

Table 4.3. Proportion of synaptic input onto Lpar1-GFP SPns per layer. Mean ± SEM.

At P0-P1 (n = 9 cells), most excitatory synaptic input seems to originate from the subplate, with L6 also providing a high proportion of input. At P2-P5 (n = 51 cells), subplate input is still present, but L6 input appears more prevalent. Finally, at P6-P8 (n = 33 cells) the proportion of input arising from the subplate seems to have been downregulated, with most input coming from L6 and L5b. Throughout all

developmental timepoints, upper layers seem to provide very little input to Lpar1-GFP SPns. To examine more closely the laminar origin of excitatory inputs onto Lpar1-GFP SPns, I calculated, for each age group, the proportion of excitatory synaptic input originating from each cortical layer (Table 4.3), aiming to answer two questions:

1) At each timepoint, which layers are providing the greatest proportion of excitatory input?
2) Does the contribution of each layer change throughout development?

To answer these questions, I performed 2-way ANOVA on the proportion of synaptic input, with Age and Layer of Origin as factors. This was followed up with planned multiple comparisons tests (corrected for multiple comparisons). To answer question 1, I compared, within each timepoint, the proportion of input arising from each layer. To answer question 2, I compared, within each layer, the proportion of input it provided at P0-P1 versus P2-P5, and at P2-P5 versus P6-P8. Figure 10 displays summary graphs for total excitatory input (4.11A) and proportion of total synaptic input from each cortical layer (4.11B-E), for Lpar1-GFP SPns. For clarity, the results and significance of post-hoc comparisons between layers are reported separately in Tables 4.4A-C. Developmental post-hoc tests are reported alongside the graph in Figure 4.11B.

Two-way ANOVA yielded significant effects for interaction ($F(10, 540) = 9.686$, $p < 0.001$) and Layer of Origin ($F(5, 540) = 48.85$, $p < 0.001$). At P0-P1, the subplate provided significantly more excitatory input than any other cortical layer (44± 8%).

L6 emerged also as a prominent input source, being responsible for 25± 8% of total synaptic input, and providing significantly more input than L5a (Figure 4.10C and Table 4.4A). There was a significant decrease in proportion of subplate input between P0-P1 (44± 8%) and P2-P5 (16± 2%), concurrent to a significant increase in input arising from L6 (25± 8% to 39± 2%) (Figure 4.11B). At P2-P5, the subplate was thus no longer the main source of cortical excitatory drive to Lpar1-GFP SPns. It provided significantly less input than L6, but still significantly more input than L2/3. L6 clearly emerged as the main excitatory input source, providing significantly more input than any other cortical layer. L5b provided significantly more input than L5a and L2/3, and L4 also provided significantly more input than L2/3 (Figure 4.11D and Table 4.4B). After P2-P5 there were no more developmental shifts, with no layer significantly increasing or decreasing the proportion of input provided (Figure 4.11B). L6 remained the main origin of cortical excitation to Lpar1-GFP SPns, providing a significantly higher proportion of input than all other layers. L5b provided significantly more input than layers 5a and 2/3 (Figure 4.11E and Table 4.4C).

One issue with comparing normalised input as opposed to analysing raw input is that with normalised input, a decrease in proportion of input originating from a particular layer will always imply an increase in proportion arising from some combination of other layers. Due to this reciprocity effect, it could be that the decrease/increase developmental dynamic seen in SP and L6 inputs does not correspond to a genuine increase of synaptic input arising from L6 (for example). In order to clarify this, two-way ANOVA analysis and post-hoc tests were repeated on raw pA input data. Since this data did not conform to the assumption of homogeneity of variance required for ANOVA, analysis was carried out instead on a square root transform. Two-way

ANOVA yielded significant effects of *interaction* ($F(10, 540) = 3.048$, $p < 0.01$) and *layer* ($F(5, 540) = 31.31$, $p < 0.001$) (Figure 4.11F-I, Table 4.4). Excitatory input from the subplate decreased significantly between P0-P1 and P6-P8, corroborating the normalised data finding. In contrast, L6 input increased significantly between P0-P1 and P2-P5. In terms of which layers provided most dominant input at each timepoint, at P0-P1 SP and L6 provided significantly more input than L5a and L2/3 (Table 4.6A). At P2-P5, L6 emerged as the clear excitatory driving force, providing significantly more input than any other layer. SP, L5b and L4 all provided significantly more input than L2/3 (Table 4.6B). L5b additionally provided more input than L5a. At P6-P8 the same pattern was observed for L6. L5b emerged as the second strongest source of input, providing significantly more input than SP, L5a and L2/3 (Table 4.6C). Therefore, the main findings obtained with normalised data – developmental decrease in SP input and increase in L6 input, and dominance of L6 and L5b at P6-P8 – were replicated when analysing raw total input data.

		Table 4.4. Total synaptic input (pA)						
	N	**SP**	**L6**	**L5b**	**L5a**	**L4**	**L2/3/CP**	**Total**
P0-P1	9	62± 13	42± 20	22± 6	7± 4	18± 7	3± 1	163± 23
P2-P5	51	30± 4	85± 12	38± 5	21± 4	30± 6	5± 1	225± 23
P6-P8	33	19± 4	97± 13	40± 7	18± 4	29± 13	15± 6	195± 18

Table 4.4. Total synaptic input onto Lpar1-GFP SPns per layer. Mean ± SEM.

To summarise, Lpar1-GFP SPns are synaptically integrated into excitatory cortical circuitry from birth, and the total amount of local excitatory input they receive does not change during the first postnatal week. They start out receiving the majority of their cortical excitatory input from the subplate itself. Between P0-P1 and P2-P5 there is a decrease in proportion of input from the subplate concurrent to an increase in input from L6, which emerges at that point and remains at P6-P8 as the main provider

of cortical excitation onto Lpar1-GFP SPns. These cells also receive weaker input from L5b and L4, and appear not to be engaged meaningfully by L5a and L2/3 excitatory neurons. Thus, in addition to receiving strong thalamic input during the first postnatal week, Lpar1-GFP SPns appear to integrate information from VB-recipient cortical populations (SP, L6, L5b and L4).

Analysing the development of cortical excitatory inputs onto Lpar1-GFP SPns, I found two significant developmental events: decrease in proportion of input provided by the subplate, and increase in proportion and total input from L6. How does this occur? In the next section I further analysed data from SP and L6 EPSCs in order to clarify this question.

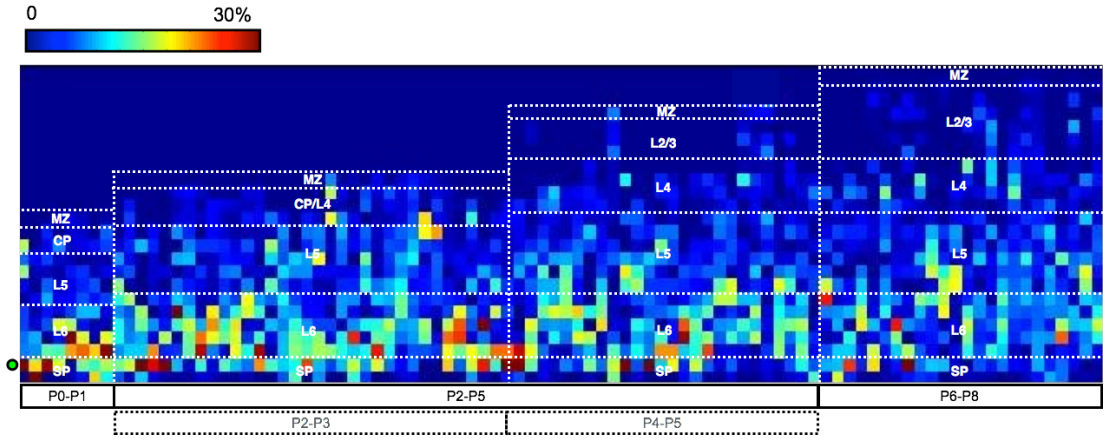


Figure 4.10. Normalised vertical profile for LSPS maps of excitatory input onto all Lpar1-GFP SPns recorded. A total of 93 cells were mapped. Total excitatory input per 50µm row was calculated for each cell and normalised to that cell's total excitatory synaptic input, determining the proportion of input originating from each 50µm row. Each cell's vertical profile was plotted as a one "pixel"-wide column and arranged side by side, in ascending age order from P0 to P8. Each column corresponds to a cell. Proportion of input arising from each 50µm row was colour-coded from 0 to 30% (see scale bar, top). Cells were aligned by their soma (green spot to the left of the diagram). Average layer boundaries for each age group were determined during alignment. Layers 2/3 to 5 show a continued increase during the first postnatal week, due to ongoing cell migration. Due to developmental growth of the cortex, for illustrative purposes only the P2-P5 group was split into P2-P3 and P4-P5. Note the decrease in input arising from within the SP after P3.

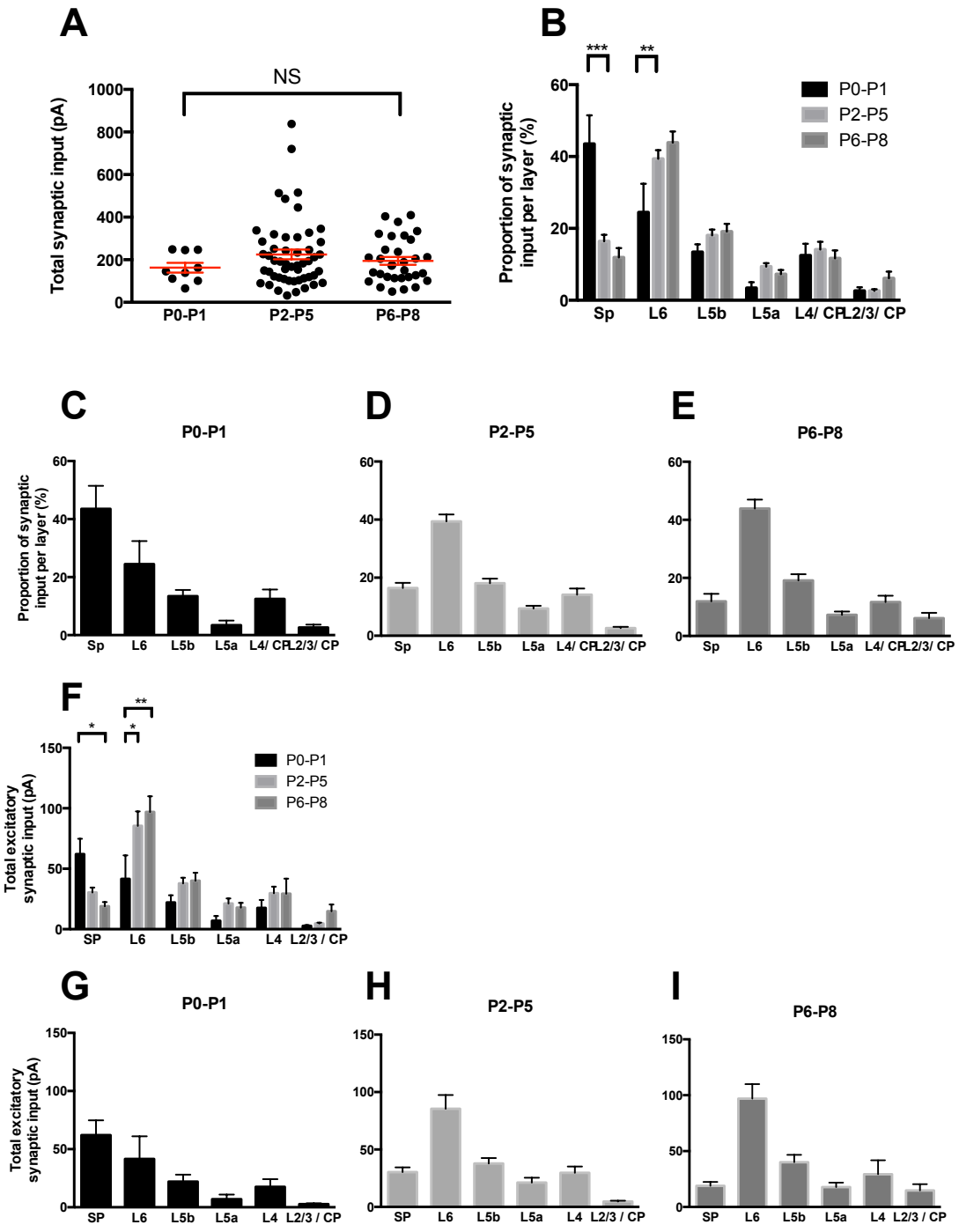


Figure 4.11. LSPS of afferent cortical excitatory input to Lpar1-GFP SPns. A. Total excitatory synaptic input onto Lpar1-GFP SPns at P0-P1 (n = 9), P2-P5 (n = 51) and P6-P8 (n = 33). Each circle corresponds to a cell. **B.** Developmental laminar distribution of synaptic input at each age group tested. Numbers reported on A apply to B and all subsequent graphs in this figure. **C-E.** Comparison, within each age group, of the proportion of input arising from each cortical layer. At P0-P1 (n = 9 cells), most excitatory synaptic input originates from the subplate, with L6 also contributing substantially. At P2-P5 (n = 51 cells), subplate input is still present, but L6 input appears more prevalent. Finally, at P6-P8 (n = 33 cells), subplate input has been downregulated, and most input arises from L6 and L5b.

Table 4.5A.

Normalised layer post-hoc comparisons – P0-P1						
	SP	L6	L5b	L5a	L4/CP	L2/3 / CP
SP						
L6	*					
L5b	***	NS				
L5a	***	**	NS			
L4/CP	***	NS	NS	NS		
L2/3 / CP	***	**	NS	NS	NS	

Table 4.5B.

Normalised layer post-hoc comparisons – P2-P5						
	SP	L6	L5b	L5a	L4/CP	L2/3 / CP
SP						
L6	***					
L5b	NS	***				
L5a	NS	***	**			
L4/CP	NS	***	NS	NS		
L2/3 / CP	***	***	***	NS	***	

Table 4.5C.

Normalised layer post-hoc comparisons – P6-P8						
	SP	L6	L5b	L5a	L4/CP	L2/3 / CP
SP						
L6	***					
L5b	NS	***				
L5a	NS	***	**			
L4/CP	NS	***	NS	NS		
L2/3 / CP	NS	***	***	NS	NS	

Table 4.5. Result of post-hoc comparisons between proportion of input provided by each cortical layer onto Lpar1-GFP SPns at P0-P1 (A), P2-P5 (B) and P6-P8 (C). Cell number per age as reported in Figure 4.11. * $p < 0.05$; ** $p < 0.01$; *** $p < 0.001$.

Table 4.6A.

Raw layer post-hoc comparisons – P0-P1						
	SP	L6	L5b	L5a	L4/CP	L2/3 / CP
SP						
L6	NS					
L5b	NS	NS				
L5a	**	*	NS			
L4/CP	NS	NS	NS	NS		
L2/3 / CP	***	**	NS	NS	NS	

Table 4.6B.

Raw layer post-hoc comparisons – P2-P5						
	SP	L6	L5b	L5a	L4/CP	L2/3 / CP
SP						
L6	***					
L5b	NS	***				
L5a	NS	***	*			
L4/CP	NS	***	NS	NS		
L2/3 / CP	***	***	***	NS	***	

Table 4.6C.

Raw layer post-hoc comparisons – P6-P8						
	SP	L6	L5b	L5a	L4/CP	L2/3 / CP
SP						
L6	***					
L5b	*	***				
L5a	NS	***	*			
L4/CP	NS	***	NS	NS		
L2/3 / CP	NS	***	***	NS	NS	

Table 4.6. Result of post-hoc comparisons between total raw input provided by each cortical layer onto Lpar1-GFP SPns at P0-P1 (A), P2-P5 (B) and P6-P8 (C). Cell number per age as reported in Figure 4.11. * $p < 0.05$; ** $p < 0.01$; *** $p < 0.001$.

4.5.2. Maturation of single EPSCs onto Lpar1-GFP subplate neurons during the first postnatal week

LSPS assessment of glutamatergic afferent input maps onto Lpar1-GFP SPns enabled us to establish the developmental sequence of engagement of Lpar1-GFP SPns by cortical excitatory neurons. The two main developmental events of the subplate's integration in the excitatory cortical network were a decrease in proportion of input arising from the SP and an increase in L6 input. The mechanism underlying this transition is not clear. Input from L6 could increase as a result of a selective strengthening of these synapses, i.e., an increase in amplitude of L6 EPSCs. Alternatively, new synapses could form over development between L6 and Lpar1-GFP SPns. This would presumably be seen as an increase in the number of EPSCs evoked from L6. Similarly, a developmental loss of subplate input could be due to weakening of SP-SP synapses or decrease in their number. To test these possibilities I examined single EPSCs used to generate input maps in a sample of 9 cells at P0-P1 (370 EPSCs), 10 cells at P2-P5 (769 EPSCs) and 10 cells at P6-P8 (471 EPSCs). Developmental effects were investigated using one-way ANOVA and post-hoc comparisons (P0-P1 vs P2-P5 and P2-P5 vs P6-P8) for average EPSC amplitude and number of EPSCs evoked from either the SP or L6.

Subplate

For SP-evoked inputs, there was a significant developmental effect for EPSC amplitude ($F(2, 26) = 6.23$, $p = 0.006$) (Figure 4.12A, left). SP EPSC amplitude significantly decreased from P0-P1 (7± 1pA) to P2-P5 (5± 1pA), and significantly increased from P2-P5 to P6-P8 (7± 1pA). There was no statistically significant developmental effect on number of SP-evoked EPSCs ($F(2, 26) = 2.8$, $p = 0.079$),

although the data suggested a trend for a decrease from P0-P1 (9± 2 EPSCs) to P2-P5 (5± 1 EPSCs) and P6-P8 (5± 1 EPSCs) (Figure 4.12B, left).

L6

No significant developmental effect was found for amplitude of L6 EPSCs ($F(2, 26) = 2.911$, $p = 0.072$), although a modest trend was observed for an increase from P0-P1 (6± 1pA) and P2-P5 (7± 1pA) to P6-P8 (9± 1pA). There was a significant effect in number of L6-evoked EPSCs ($F(2, 26) = 5.968$, $p = 0.007$), driven by a statistically significant increase in inputs from P0-P1 (12± 3 EPSCs) to P2-P5 (32± 5 EPSCs). No further changes were observed at P6-P8 (21± 4 EPSCs).

In conclusion, statistical analysis suggests that the developmental increase in L6 input is mainly driven by an increase in the number of EPSCs evoked from L6. For the subplate, no conclusive changes could be found in amplitude or number of inputs to account for a decrease in input, suggesting that the observed decrease in proportion of input arose as a consequence of increased input from L6.

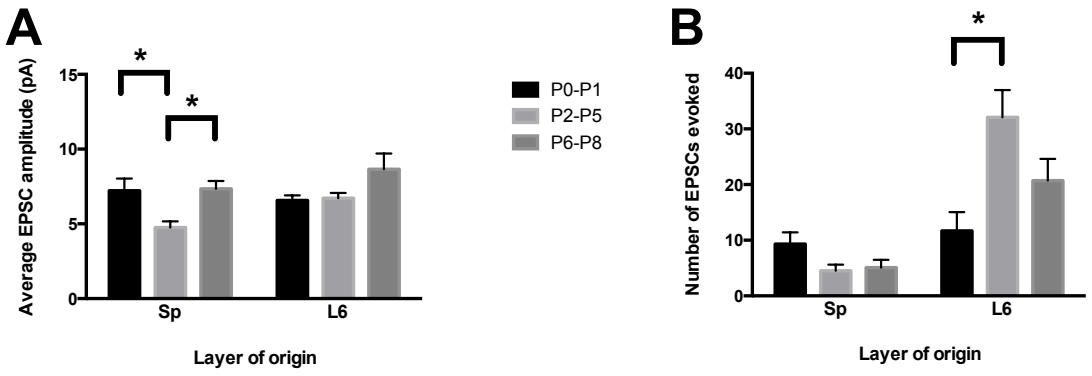


Figure 4.12. Analysis of single SP and L6-evoked EPSCs onto Lpar1-GFP SPns (total n = 1610 EPSCs). A. Average EPSC amplitude for SP and L6-evoked inputs at each developmental stage. **B.** Average number of EPSCs evoked from the SP and L6 at each

developmental stage. 9 cells were analysed at P0-P1 (370 EPSCs), 10 cells at P2-P5 (769 EPSCs) and 10 cells at P6-P8 (471 EPSCs).

4.5.3. Horizontal organisation of excitatory inputs onto Lpar1-GFP subplate neurons during the first postnatal week

It was evident from the recorded LSPS-evoked afferent input maps that SPns exhibited not only a layer, but also columnar organisation. In the present section I sought to determine the characteristics of this columnar organisation. Are cortical excitatory inputs onto Lpar1-GFP SPns confined to a barrel-defined column? Or do these cells integrate information across columnar domains? Defining the columnar organisation of cortical inputs onto Lpar1-GFP SPns could provide important insights into their circuit function in the neonatal cortex.

At all ages tested, inputs onto Lpar1-GFP SPns decreased with distance from the soma (Figure 4.13A-D, Table 4.7). Inputs followed a very similar horizontal distribution across the three age groups (Table 4.7). To test the null hypothesis that Lpar1-GFP SPns received equal amounts of input across horizontal domains, I ran a two-way ANOVA with *developmental period* and *distance from soma* as factors. I performed post-hoc comparisons to examine whether each 50µm column changed its relative contribution over development (P0-P1 vs P2-P5; P2-P5 vs P6-P8). Comparisons between 50µm columns within each age group allowed me to determine which distance from soma bins were providing the most input.

		Table 4.7. Distance from soma (µm)				
	N	0	50	100	150	200
P0-P1	9	18± 3	18± 2	12± 1	7± 1	4± 1
P2-P5	51	18± 1	16± 1	11± 1	8± 1	6± 1
P6-P8	33	17± 1	14± 1	12± 1	9± 1	7± 1

Table 4.7. Horizontal organisation of excitatory input onto Lpar1-GFP SPns. The proportion of input originating from each 50µm column was calculated for each SPn. Columns corresponding to the same distance from the cell soma (e.g. 50 and -50µm) were averaged together.

Two-way ANOVA revealed a significant *distance from soma* effect ($F(4, 450) = 51.49$, $p < 0.001$), indicating that excitatory inputs are not homogeneously distributed throughout the 50µm bins tested. Post-hoc comparisons revealed that at P0-P1, the 0µm and 50µm bins provided significantly more input than the 150 and 200µm bins, with the 100µm bin also providing significantly more excitation than the 200µm one. At P2-P5 the 0 and 50µm bins provided significantly more input than any other bin tested, and the 100µm bin provided more input than the 150 and 200µm bins. At P6-P8, the 0µm bin provided more input than any other except the 50µm bin. This bin provided significantly more input than the two farthest bins, and the 100µm bin provided more input than the 200µm one. There was no significant effect of *developmental period* ($F(2, 450) = 0.03$, $p = 0.972$), indicating that the proportion of input provided by each bin did not change significantly over development. Since no developmental effect was found, I performed linear regression on proportion of synaptic input, as a function of distance from the soma. Proportion of synaptic input cold be very accurately predicted from distance from the soma by the following equation: synaptic input = -0.06 x distance from soma + 17.76 ($R^2 = 0.99$; $F(1, 3) = 262.3$, $p < 0.001$) (Figure 4.13D).

In conclusion, Lpar1-GFP SPns receive fewer inputs the farther away we travel from the soma (within a 400µm window). The pattern of horizontal distribution of synaptic

inputs remained constant throughout development, with most inputs originating from a bilateral 0-100µm region, defining a 200µm column of cortical input. Therefore, at least at the local circuit level, Lpar1-GFP SPns are concerned with processing input from their home column.

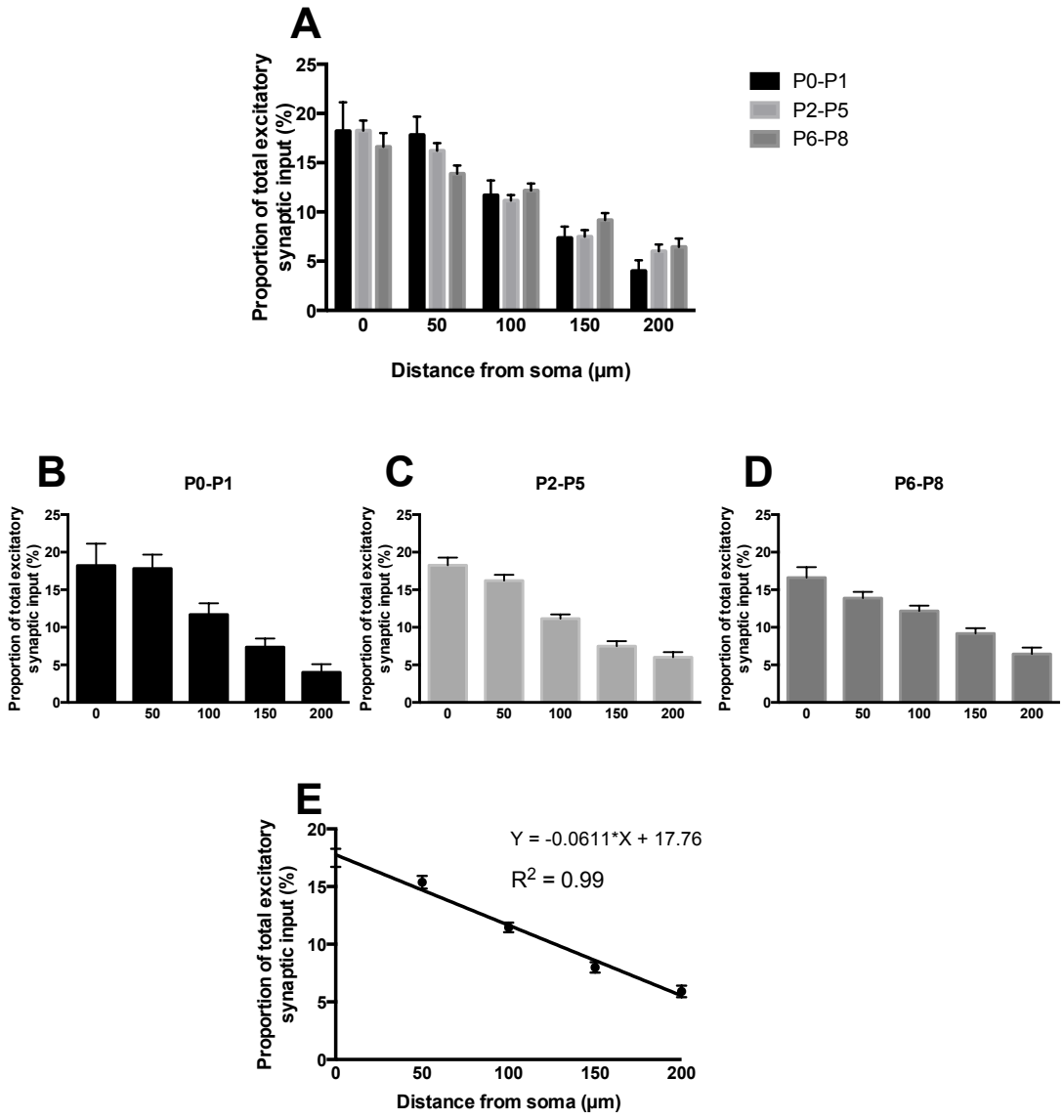


Figure 4.13. Horizontal organisation of excitatory input onto Lpar1-GFP SPns. The proportion of input originating from each 50µm column was calculated for each SPn. Columns corresponding to the same distance from the cell soma (e.g. 50 and -50µm) were averaged together. 9 cells recorded at P0-P1, 51 cells at P2-P5 and 33 at P6-P8. Numbers apply to all subsequent panels. **A.** Developmental comparison of proportion of excitatory input arising from each 50µm column. **B-D.** Proportion of excitatory input from each 50µm column at each developmental stage. **E.** Linear regression plot of proportion of excitatory input as a function of distance from soma. Data for all ages was pooled for this analysis, since no developmental effect in columnar organisation was found.

4.6. Chapter summary and discussion

Summary of results

In this chapter I have shown that the first postnatal week is a highly dynamic period for Lpar1-GFP SPns, both in terms of intrinsic property maturation and network integration for thalamic and local cortical excitatory afferent input (Figure 4.14). My key findings were that the intrinsic properties of Lpar1-GFP SPns showed a high degree of maturity by the end of the first postnatal week, and the P2-P5 to P6-P8 transition appeared to be the key period of maturation for most electrophysiological parameters. In terms of network integration, I found that most Lpar1-GFP SPns received direct thalamic input over the first postnatal week, but this input was transient, such that after P9 only a minority of cells were directly engaged by the thalamus, and the average amplitude of this input was weaker than at P0-P5. Regarding cortical inputs, the total amount of excitatory input received by Lpar1-GFP SPns did not change during the first postnatal week, but there was a shift in the laminar balance of these inputs. Lpar1-GFP SPns started out receiving most of their inputs from the SP, but after P1 there was a decrease in input evoked from the SP and an increase from L6, with this layer becoming the major source of cortical excitatory input to Lpar1-GFP SPns. Afferent cortical input was organised on the horizontal domain, with most inputs deriving from a 200µm column.

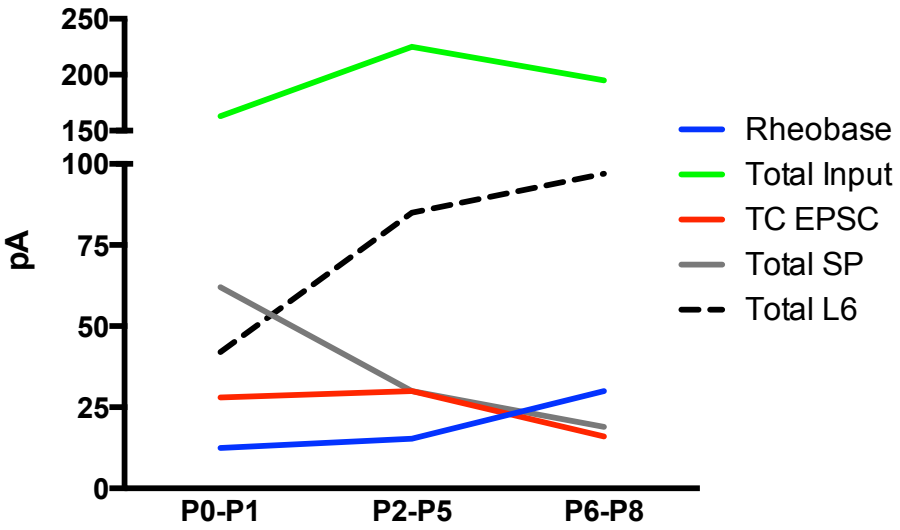


Figure 4.14. An overview of Lpar1-GFP SPn maturation during the critical period for thalamocortical plasticity. Rheobase (blue), average minimal thalamic EPSC amplitude (red) and total cortical (green), SP-derived (grey) and L6-derived (black, dashed) synaptic input measure using glutamate uncaging are plotted against the same pA scale. Total number of cells equals 107 (P0-P1: 10 cells; P2-P5: 57 cells; P6-P8: 40 cells).

Intrinsic maturation and changes in thalamic input

Amongst the developmental changes found in intrinsic properties of Lpar1-GFP SPns were an increase in rheobase and decrease in input resistance and membrane time constant. These changes imply that cells develop shorter integration windows, tuned for fast synaptic signalling, and that tighter temporal summation will be required for spike threshold to be reached. This could underlie a change in mode of operation of Lpar1-GFP SPns from relay cells to more sophisticated coincidence detectors. Interestingly, at P0-P5, before the main maturation step in rheobase, tau and input resistance occurs, Lpar1-GFP SPns show a bi-modal distribution of thalamic input amplitude, displaying a prominent cohort of 50-100pA inputs that are not present subsequently. Such strong inputs would lead SPns to fire bursts of action potentials, relaying thalamic inputs downstream immediately, with little need for summation of inputs from other sources. Short-term plasticity data supports a thalamic relay role for Lpar1-GFP SPns, as paired-pulse thalamic inputs were found to be depressing. This is

suggestive of a synapse with high release probability (Regehr, 2012), which would be a requirement for SPns to play a role relaying thalamic information in an accurate and timely fashion. At P6-P8 and P9-P15, fewer Lpar1-GFP SPns receive thalamic inputs, and these inputs are significantly weaker than at earlier periods. Intrinsic properties have also matured significantly at this point, meaning that single thalamic inputs, when they do engage SPns, will no longer be enough to drive them to spike, and summation with other inputs will be required. We did not see changes in PPR throughout development and thus pooled data for analysis. It would be interesting to investigate the development of thalamic-subplate PPR more closely. If PPR remains depressing after P6-P8, this would indicate that, in order to fire, Lpar1-GFP SPns likely need to summate thalamic inputs with inputs from a distinct source, rather than rely on high-frequency information from the thalamus. A developmental change from thalamic short-term depression to facilitation would also suggest a change of function, in the sense that it would become less important to accurately relay the first thalamic spike, and more to relay high-frequency or cooperative summating activity. It has previously been reported that, in rat barrel cortex, putatively thalamic (white-matter stimulation) inputs become facilitating after P8, with PPRs at earlier ages showing very variable short-term dynamics (Liao & Lee, 2011). Methodological aspects could underlie the difference in results; I tried to keep stimulating electrodes as close to the VB thalamus as possible, whereas Liao et al. stimulated the internal capsule. However, Liao et al. targeted unlabelled SP neurons, meaning they sampled a wider population than I did. It is an interesting possibility that different SP neuron types could show distinct thalamocortical dynamics and perform different developmental functions in the thalamocortical circuit. This hypothesis is supported by the fact that I observed a sharp drop in thalamic connectivity to Lpar1-GFP SPns, whereas no such

change was mentioned in other work examining thalamic input to SPns at later timepoints in somatosensory (Liao & Lee, 2011), auditory (Zhao et al., 2009) or visual (Torres-Reveron & Friedlander, 2007) cortices. In order to address this issue, it would be important to record non-GFP SPns and compare their properties to Lpar1-GFP SP cells. It is worth noting that circuit development in the barrel cortex is accelerated compared to the auditory cortex, and that Zhao et al. did not investigate thalamic connectivity after the auditory thalamocortical critical period (Zhao et al., 2009), which occurs at P12-P15 (Barkat et al., 2011), compared to P3-P8 for the barrel cortex (Crair & Malenka, 1995). It is therefore possible that loss of thalamic input onto SPns occurs after the critical period of plasticity in other primary sensory cortical areas and types of SPn as well.

Plasticity of thalamic inputs to Lpar1-GFP SPns?

What could be the mechanism for the drop in thalamic connectivity to Lpar1-GFP SPns? It has been previously reported that LTD can be induced at the thalamus-L4 synapse by low-frequency (0.1-0.33 Hz) stimulation of thalamic afferents whilst holding the postsynaptic cell at a depolarized -50mV potential, and that this process is NMDAR-dependent (Feldman et al., 1998). Curiously, the only difference between this LTD protocol and a previously published LTP protocol (Crair & Malenka, 1995) was the postsynaptic holding potential (-50mV vs 0mV). It is believed that both LTP and LTD at this synapse are dependent on NMDAR activation and postsynaptic calcium signalling, but that what sets these two phenomena apart are the characteristics of calcium influx. LTP would be induced by a large calcium signal, whereas LTD would result from a modest rise in postsynaptic calcium (Lisman, 1989; Isaac et al., 1997; Feldman et al., 1998). Depolarisation to -50mV would be predicted

to elicit <15% of the calcium influx evoked at 0mV, explaining the different results elicited by two apparently very similar protocols (Feldman et al., 1998).

In my experiments, at P0-P1 and P2-P5 there is a clear bi-modal distribution in minimal TC-EPSC amplitude, with the largest cluster of events showing amplitudes of 10-20pA, and a second cluster of events with amplitudes in the 50-90pA range (Figure 2E, G, H). At P6-P8 and P9-P15 the cluster of large amplitude events is no longer present (Figure 2I, J). At P6-P8 there is a large increase in the proportion of 20-30pA events, and a small increase in the proportion of 0-10pA inputs. By P9-P15, the frequency of 20-30pA events has dropped, but a sharp increase in 0-10pA events is observed. These data suggest a shift of the TC-EPSC amplitude distribution towards weak amplitudes. There are two possibilities: one is that large amplitude events observed at P0-P5 are simply pruned back and disappear. The second, more plausible alternative, is that they undergo a progressive developmental weakening via a form of synaptic plasticity, presumably an LTD-like mechanism. I would like to propose that through this mechanism, 50-90pA events get progressively shifted towards weaker amplitudes in the 20-50pA range, explaining their absence and the increase in 20-30pA amplitude events seen at P6-P8. This process would continue at P9-P15, only by this point the shift would have made these inputs even weaker. Accordingly, by P9-P15 the proportion of 20-30pA events is low, but there is a surge in weak 0-10pA events from around 10% at P6-P8 to 30% at P9-P15. A previous study examined white-matter evoked, putatively thalamic, inputs onto post-critical period subplate neurons in the barrel field (P10-P20) and found that both protocols pairing afferent input with postsynaptic spiking and protocols relying solely on low-frequency afferent stimulation at resting membrane potential preferentially resulted in

LTD, for subplate neurons (Torres-Reveron & Friedlander, 2007). Moreover, a study from the Luhmann lab examining *in vivo* LTP of the thalamocortical synapse induced by repetitive whisker stimulation reported layer-specific induction of LTP at P0-P8, but interestingly found it impossible to induce LTP at the thalamus-subplate synapse during this period *in vivo* or *in vitro* (An et al., 2012). It could be that SPns have a very high threshold for LTP induction; anything but the exact condition for LTP would result in LTD induction. Alternatively, thalamus-subplate inputs could be hard-wired and impervious to experience. The pharmacological basis for this disparity could be the expression in SP of NMDAR subunits with sharper temporal kinetics (Cull-Candy et al., 2001; Cull-Candy & Leszkiewicz, 2004). Early in development, GluN1/2B di-heteromers are the dominant form of NMDARs expressed at synapses. During the second postnatal week, there is a switch from GluN2B to GluN2A, which requires sensory activity to occur (Bellone & Nicoll, 2007; Sanz-Clemente et al., 2012). GluN2A subunit-containing NMDARs have shorter decay times (Vicini et al., 1998; Cull-Candy et al., 2001; Cull-Candy & Leszkiewicz, 2004; Sanz-Clemente et al., 2012) and therefore it is likely that a primarily GluN2A synapse will exhibit a shorter window for spike-timing dependent plasticity, effectively elevating the threshold for LTP induction. Thalamic inputs onto SPns have been shown to engage both GluN2B and GluN2A synapses at P0-P3 (Hanganu et al., 2002; Hirsch & Luhmann, 2008). Given the accelerated rate of intrinsic property and synaptic development evidenced by SPns, it is plausible that in this layer the GluN2B to GluN2A switch occurs earlier in development. This way, compared to other thalamorecipient layers, the SP would have an elevated threshold for induction of thalamocortical LTP. Interestingly, it has previously been shown that the time window for t-LTP at L4-L2/3 synapses in the barrel cortex is very narrow compared

to the t-LTD window at the same synapse. This disparity results in LTD of EPSPs that are uncorrelated with postsynaptic action potentials (Feldman, 2000). A similar temporal bias towards LTD could explain developmental weakening of thalamus-Lpar1-GFP synapses.

An LTD-like mechanism could therefore answer the question of how Lpar1-GFP SPns lose thalamic input. The question that follows from this is evidently why thalamic input onto Lpar1-GFP SPns is developmentally weakened. One of the proposed functions of the SP is to act as an amplifier and relay of thalamic information onto L4, acting as a teacher circuit to facilitate maturation of thalamic inputs via heterosynaptic LTP (Kanold, 2004; Kanold & Luhmann, 2010). Early in development, when thalamic inputs onto L4 are very weak, the SP would provide a parallel di-synaptic route for thalamic information to reach the cortex. Once the thalamus-L4 synapse is mature, such a parallel pathway would only degrade the temporal accuracy of sensory signalling, introducing noise or redundant and temporally delayed information about thalamic spiking. From the signal processing point of view, it would make sense to eliminate this redundant input, or at least greatly attenuate it. It fits with this view that thalamic inputs to Lpar1-GFP SPns start to get weakened towards the end of the thalamocortical critical period (P6-P8) and that the drop in thalamic connectivity is only observed after the end of this period (between P9-P15), after SPns have potentially fulfilled their relay function.

An alternative hypothesis to long-term depression of thalamic inputs to Lpar1-GFP SPns would be the programmed cell death of Lpar1-GFP neurons receiving the strongest thalamic inputs. However, this appears unlikely, as the Lpar1-GFP

population has been shown to be amongst the preferentially-surviving subplate neurons (Hoerder-Suabedissen & Molnár, 2012). Regardless of a plasticity, pruning or cell death effect, from the circuit viewpoint the conclusion is the same: there is a developmental disengagement of the subplate by thalamic inputs.

Cortical inputs to Lpar1-GFP SPns

Regarding my LSPS results, only one study has previously used glutamate uncaging to map the development of afferent cortical inputs onto SPns (Viswanathan et al., 2012). This study was performed in the mouse auditory cortex and focused on the finding that, after P10, SPns can be broadly divided into two subpopulations, according to the laminar origin of inputs: a large population that receives all of its input from infragranular layers, and a smaller population that receives a small proportion of input from L4. In our experiments we chose to focus on defining, over the first postnatal week, the layer identity of afferent cortical excitatory inputs onto Lpar1-GFP SPns and to examine any developmental shifts occurring over that period. Our first finding was that the total amount of cortical excitatory input onto Lpar1-GFP SPns did not change over the course of the first postnatal week, even though it was evident that intrinsic property maturation made these cells less excitable. Second, although total synaptic input did not change, the cortical sources providing this input did. We found between P0-P1 and P2-P5 a significant decrease in SP input and a significant increase in L6 input. Moreover, the laminar pattern of afferent excitatory input onto Lpar1-GFP SPns seemed to be fixed at P2-P5, with the vast majority of input originating from L6 and remaining cortical afferent excitation provided by the SP, L5b and L4. Although laminar input origin and development was not the focus of Viswanathan et al., our results seem in broad agreement, with Lpar1-GFP SPns

forming part of a network involving primary sensory thalamorecipient layers (L4, L5b, L6 and SP), that is at P0-P1 dominated by the SP and subsequently by L6, with this layer clearly providing the vast majority of excitatory input. We did come across cells receiving L4 input, but this was never the dominating input source for Lpar1-GFP SPns, and we found no evidence for a developmental increase in synaptic input from this layer, at least until P8.

Beyond circuit mapping, and more interestingly, my LSPS results suggest fundamental differences between SP and cortical pyramidal neurons. Using the same LSPS approach, our laboratory previously published on the development of afferent excitatory input onto L2/3 and L5 pyramidal cells (Anastasiades & Butt, 2012). Prior to P5, LSPS excitatory maps onto pyramidal neurons show very little organisation and very few LSPS-evoked inputs can be detected at -70mV holding potential ((Anastasiades & Butt, 2012), Marques-Smith & Butt, unpublished observations). Anastasiades and Butt found in the somatosensory cortex a continuous developmental increase in total excitatory synaptic input (recorded at -70mV, putatively AMPAR-mediated) onto L2/3 and L5 pyramidal neurons between P5-P8 and P13-P16. The first two postnatal weeks are a period when excitatory neurons in the barrel cortex undergo synaptic maturation that is highly sensitive to sensory experience (Feldman, 2009; Feldman & Brecht, 2005). By mapping afferent input onto L2/3 and L5 pyramidal neurons at -70 and +40mV, Anastasiades and Butt uncovered NMDAR-mediated inputs that predicted the formation of the mature canonical circuit. Through correlated bouts of activity it is believed that such NMDAR-expressing, "AMPA-silent" synapses can get converted, via AMPAR insertion, into functional AMPA-active synapses (Isaac et al., 1995; 1997; Rumpel et al., 2004). Work on the development of

the recurrent excitatory L4 network found evidence for similar circuit development mechanisms (Ashby & Isaac, 2011). Between P9 and P12, Ashby and Isaacs found a 3-fold increase in probability of connectivity between L4 spiny stellate cells that was prevented by whisker deprivation. In whisker-deprived animals, AMPA-based currents were significantly reduced, and the proportion of AMPA-silent synapses greatly increased. However, NMDAR-mediated communication was unaltered by deprivation. Ashby and Isaac's data suggests that NMDAR-mediated synaptic connections act as experience-independent templates, and that correlated activity induced by sensory experience recruits AMPARs onto silent synapses to construct the mature, functional network. Both sets of results (Anastasiades & Butt, 2012; Ashby & Isaac, 2011) suggest little AMPA-based synaptic connectivity in early postnatal development, at least *in vitro*. This contrasts starkly with my results for Lpar1-GFP SPns. Putatively AMPA-mediated connectivity was apparent from birth, with reliable, organised inputs readily detected, originating mostly from the SP and L6. Unlike for L2/3 and L5 pyramidal cells, I found no evidence, at least during the first postnatal week, for a period of massive excitatory synapse formation onto Lpar1-GFP SPns, as the total amount of cortical excitatory input onto this population remained stable throughout. These two findings suggest there may be fundamental differences in pyramidal-pyramidal and pyramidal-subplate excitatory connectivity. It is thus apparent that the development of SPns is not just accelerated in terms of intrinsic properties, but also excitatory network connectivity. It has previously been proposed that at nascent glutamatergic synapses transition between silent and labile states depending on afferent activity, and correlated pre and post-synaptic activity (through NMDAR activation) can stabilise a synapse from this switching behaviour into a mature stable state, modifiable only through conventional plasticity processes (Groc

et al., 2006; Hanse et al., 2009; 2013). Based on my results with SPns and results from experiments on L2/3, L4 and L5 excitatory neurons (Ashby & Isaac, 2011; Anastasiades & Butt, 2012) it is tempting to propose that cortical synapses onto Lpar1-GFP SPns exist in a stable state from birth, whereas those onto cortical pyramidal neurons start out unstable, transitioning between labile and silent states, before correlated activity, likely driven through early network activity patterns (Khazipov & Luhmann, 2006; Allène & Cossart, 2010; Kilb et al., 2011) stabilises them. This may be true not only for cortical but also thalamic inputs. Thalamic input onto SPns must be set up in a different way from the classical NMDAR, experience-dependent thalamocortical pathway. Thalamic axons arrive at and make functional synapses with the subplate even before birth (Friauf et al., 1990; Friauf & Shatz, 1991; Higashi et al., 2002; Molnár et al., 2003). My results are clearly in agreement with this, as very strong thalamic inputs can be detected at P0-P1 Lpar1-GFP SPns recorded at -70mV. This means that the thalamus-SP synapse has to be set up through sensory experience-independent mechanisms that are fundamentally different from, for instance, the development of the thalamus-L4 synapse. Based on these assertions, I would like to propose that Lpar1-GFP SPns form part of a synaptic network that is stable and functional from birth. The early, pre-sensory experience period generation of this network and stability in total excitatory cortical input received over the first postnatal week suggest that it could be hard-wired, or at least initially constructed in an experience-independent manner. SPns have been shown to play a role in the generation and propagation of carbachol-induced oscillations in the neonatal cortex (Sun & Luhmann, 2007; Hanganu et al., 2009;) and their removal largely abolishes these early activity patterns (Dupont et al., 2006; Tolner et al., 2012). Whether due to lack of patterned activity or another collateral effect, SP lesioning has been shown to

profoundly affect cortical development, namely barrel formation, maturation of thalamocortical synapses, formation of ocular dominance columns and maturation of cortical GABAergic inhibition (Ghosh & Shatz, 1992; Kanold, 2003; Kanold & Shatz, 2006; Tolner et al., 2012). SPns form an integral part of the circuitry underlying early cortical network activity patterns, and it may be that they fulfil a role as an early-born, intrinsically-mature cortical population that provides a stable synaptic backbone linking the sensory periphery and the cortical plate. The function of this backbone would be the propagation of early patterned activity prior to the onset of sensory experience, justifying the requirement for a hard-wired pyramidal/thalamic-subplate network.

To fulfil this vision of the subplate as a pool of early-born neurons receiving privileged synaptic connections and driving early activity patterns it is fundamental to clarify the outputs of this population. SPns have been shown by anatomical means to project across all layers of the cortex in the overlying cortical plate (Friauf et al., 1990; Friauf & Shatz, 1991; Hanganu, 2001; Hanganu et al., 2002; Luhmann et al., 2000) and even to make long-range connections between cortical areas as far as a few millimetres apart (Clancy & Cauller, 1999; Hoerder-Suabedissen & Molnár, 2011). Additionally, they project to primary thalamic sensory nuclei (McConnell et al., 1989; De Carlos & O'Leary, 1992; Molnar & Cordery, 1999) and across the corpus callosum (Hoerder-Suabedissen & Molnár, 2011). It is not known whether different types of SPn subserve different projections. Only one study has physiologically examined one output of SPns, documenting a projection from the SP to L4 in auditory cortex by photo-uncaging glutamate in the SP (Zhao et al., 2009). My own experiments have also shown that SPns project to the SP itself, especially at P0-P1.

Additionally, during thalamic stimulation experiments, no antidromic action potentials were evoked. Electrical stimulation of thalamic afferents to other subplate populations (CTGF-GFP) have been reported to often result in antidromic activation of SPns (P. Kanold, personal communication). These observations lend support to the hypothesis that Lpar1-GFP SPns are not amongst corticothalamic-projecting subplate neurons. L6a neurons have been reported to subserve 3 different types of communication: corticothalamic, cortico-cortical and cortico-claustral (Thomson, 2010). The strongest source of input to Lpar1-GFP SPns in my recordings was L6a. It would be interesting to use paired-recordings to examine exactly which L6a subpopulation is providing this input. One hypothesis, taking into account that Lpar1-GFP SPns are likely a non-corticothalamic population, is that L6a corticothalamic neurons provide a collateral that innervates Lpar1-GFP SPns.

The genetic intractability of SPns means that good Cre-driver lines have not yet been found, and makes it difficult to study the output of this population using optogenetic technology, especially to distant cortical areas or the thalamus. Nonetheless, it is interesting that SPns show axonal arbours capable not only of innervating all cortical layers in the column directly above them, but also promoting cortico-cortical (potentially cross-modal or sensorimotor) and corticothalamic communication. Due to their widespread axonal arbours, early maturing thalamic, cortical and neuromodulatory inputs, and accelerated intrinsic development, SPns are in a key position to amplify and relay peripherally-evoked patterned activity to overlying and related cortical areas. In this way, they could promote waves of correlated activity that would act to influence key activity-dependent processes in the cortex. One idea is that these early activity patterns could serve to stabilise AMPA-based pyramidal-

pyramidal communication and set up the cortex for the subsequent critical period of experience-dependent maturation and circuit construction. However, in order to test such a hypothesis, one would need a method for selectively stimulating subplate neurons and studying their outputs. There is currently a paucity of genetic tools for studying the subplate, namely Cre-driver mouse lines. Once such lines become available, it will be interesting to study the outputs of subplate neurons *in vitro* and *in vivo*, and how these neurons might contribute to the generation and propagation of early network activity.

Chapter 5 – Thalamocortical integration via a transient early developmental L5b-L4 circuit

5.1. Introduction

In the Lpar1-GFP mouse, GFP-labelled neurons in the cortex can be seen in the subplate. However, a significant cohort of GFP^+ cells appears to be located in the cortical layers above the subplate. These cells have non-pyramidal morphologies, and 49% of them can be labelled immunohistochemically for GABA (Hoerder-Suabedissen & Molnár, 2012). In the previous chapter, I showed that Lpar1-GFP SPns perform a function as early integrators and relays of thalamic input. Based on this data and previous work on immunohistochemical characterisation and birthdating of Lpar1-GFP non-subplate neurons (Hoerder-Suabedissen & Molnár, 2012), we hypothesised that these cells could be interneurons that also integrate early into the thalamocortical circuit. Taking into account their early birth-date and deep-layer location, putative Lpar1-GFP interneurons could be in a key position to synchronise cortical networks to early incoming thalamic input. To test this hypothesis, I characterised their intrinsic properties and morphology, aiming to determine whether they truly are interneurons. I then studied afferent thalamic and cortical excitatory input onto these cells.

5.2. The intrinsic properties and electrophysiological maturation of Lpar1-GFP non-subplate neurons

The Lpar1-GFP transgenic line labels neurons in cortical layers 2/3 to 6, in addition to those previously reported in the subplate. During experiments, most non-subplate GFP-labelled neurons appeared to be located in layers 5 and 6, so I focused on cells in

these layers for subsequent experiments. I performed whole-cell patch-clamp recordings from a total of 55 Lpar1-GFP positive cortical non-subplate neurons in the somatosensory barrel cortex, between the ages of P4 and P15. Cells were divided into three groups (P4-P6, n = 12; P7-P9, n = 14; and P10-P15, n = 29). To reveal the identity of the GFP^+ subpopulation, for each cell I administered current injection protocols similar to those used in Chapter 3 (see also Chapter 2). This analysis of intrinsic electrophysiological properties confirmed that all Lpar1-GFP non-subplate neurons are interneurons (Fig. 5.1 , Table 5.1), and that their intrinsic properties are consistent with those of previously described MGE-derived non-fast spiking (NFS), low-threshold spiking interneurons (Kawaguchi & Kubota, 1997; Markram et al., 2004; Wang et al., 2004; Miyoshi et al., 2007). Values for each measured parameter are presented in table 5.1 and representative recordings in figure 5.1. A summary of post-hoc comparisons is presented in table 5.2.

Some of the properties that can be used to distinguish low-threshold, non-fast spiking interneurons from pyramidal cells and other types of interneuron are their resting membrane potential, spike threshold, rheobase, maximum firing frequency and spike frequency adaptation. Lpar1-GFP interneurons displayed a depolarised resting membrane potential. As these neurons matured, spike threshold became significantly more negative ($F(2, 52) = 4.092$, $p < 0.05$) and closer to the resting membrane potential, suggesting Lpar1-GFP interneurons can easily be made to spike from rest. Accordingly, these cells had a low rheobase. Despite increasing significantly over development ($F(2, 50) = 10.81$, $p < 0.001$), by P10-P15 average rheobase was still only 30± 4pA. These properties are consistent with those of low-threshold spiking interneurons (Kawaguchi & Kubota, 1997; Markram et al., 2004; Wang et al., 2004;

Miyoshi et al., 2007). Input resistance showed a developmental decrease ($F(2, 52) = 51.10$, $p < 0.001$), as did the membrane time constant ($F(2, 52) = 38.91$, $p < 0.001$). Changes in these features suggest Lpar1-GFP interneurons could mature from swiftly relaying afferent input to integrating a higher number of synaptic inputs before firing. In terms of action potential properties, there was a significant developmental increase in maximum firing frequency ($F(2, 52) = 13.63$, $p < 0.001$), which plateaued at P10-P15 around 70Hz. Spike frequency adaptation was observed at all stages, and increased throughout development ($F(2, 52) = 4.451$, $p < 0.05$) to values around 30%. These properties set Lpar1-GFP interneurons apart from fast-spiking interneurons, for which much higher firing frequencies and lower spike frequency adaptation have been previously reported. Accordingly, slow after-hyperpolarisation amplitude was below values expected for fast-spiking interneurons (Miyoshi et al., 2007).

In conclusion, all recorded cortical Lpar1-GFP non-subplate cells were interneurons. Their physiological properties appeared relatively homogeneous, and were consistent with previously reported MGE-derived non-fast spiking (NFS), low-threshold spiking interneurons (Kawaguchi & Kubota, 1997; Markram et al., 2004; Wang et al., 2004; Miyoshi et al., 2007). Lpar1-GFP interneurons did on occasion exhibit rebound firing (Fig. 5.2), but such properties are consistent with NFS, somatostatin (SST)-positive interneurons (Wang et al., 2004).

Table 5.1.
Electrophysiological maturation of Lpar1-GFP interneurons

Age		P4-P6 (n = 12)	P7-P9 (n = 14)	P10-P15 (n = 29)
Membrane Properties	RMP (mV)	-58.0 ±2.1	-56.3 ±1.0	-56.6 ±0.8
	***R_{in} (MΩ)	1349 ±109	529 ±56	372 ±51
	***Tau (ms)	78.5 ±5.4	36.4 ±3.4	31.5 ±3.0
	***Rheobase (pA)	8± 1.0	17 ±2	30± 4
Action potential properties	*Spike threshold (mV)	-39.5 ±1.0	-43.0 ±0.9	-42.7 ±3.1
	**Spike height (mV)	58.5 ±2.8	68.7 ±2.9	69.6 ±1.7
	***Spike half-width (ms)	3.0±0.2	1.8±0.1	1.3±0.1
	*Adaptation (%)	19± 5	22± 3	30± 2
	*sAHP time (ms)	37.1± 3.7	24.2± 2.7	25.9± 3.1
	sAHP amp. (mV)	14.1± 0.5	13.7± 0.8	13.5± 1.1
	fAHP time (ms)	-	-	5.9± 0.4
	fAHP amp. (mV)	-	-	11.1± 1.2
	Voltage sag (mV)	1.8± 1.6	5.5± 0.7	6.4± 0.50
	***Max. Freq. (Hz)	38± 3	53± 3	70± 4

Table 5.1. Electrophysiological maturation of somatosensory cortex Lpar1-GFP Martinotti neurons. Values reported in each cell are average± SEM. Asterisks indicate one-way ANOVA or Kruskal-Wallis test significance *p* values: * $p< 0.05$; ** $p< 0.01$; *** $p< 0.001$.

Table 5.2A	Post-hoc comparisons for Membrane Properties		
	R(in)	Tau	Rheobase
P4-P6 vs P7-P9	***	***	NS
P7-P9 vs P10-P15	NS	NS	*

Table 5.2B	Post-hoc comparisons for Action Potential Properties					
	Spike threshold	Spike height	Spike half-width	Adaptation	sAHP time	Max. Freq.
P4-P6 vs P7-P9	*	*	***	NS	*	NS
P7-P9 vs P10-P15	NS	NS	*	NS	NS	*

Table 5.2. A. Post-hoc comparisons (Tukey) for Membrane Properties. Cell numbers as in Table 5.1. Only parameters in which a significant ANOVA effect was found were investigated. **B.** Post-hoc comparisons (Tukey) for Action Potential Properties. Only parameters in which a significant ANOVA effect was found were investigated. * $p < 0.05$; ** $p < 0.01$; *** $p < 0.001$; NS – non-significant.

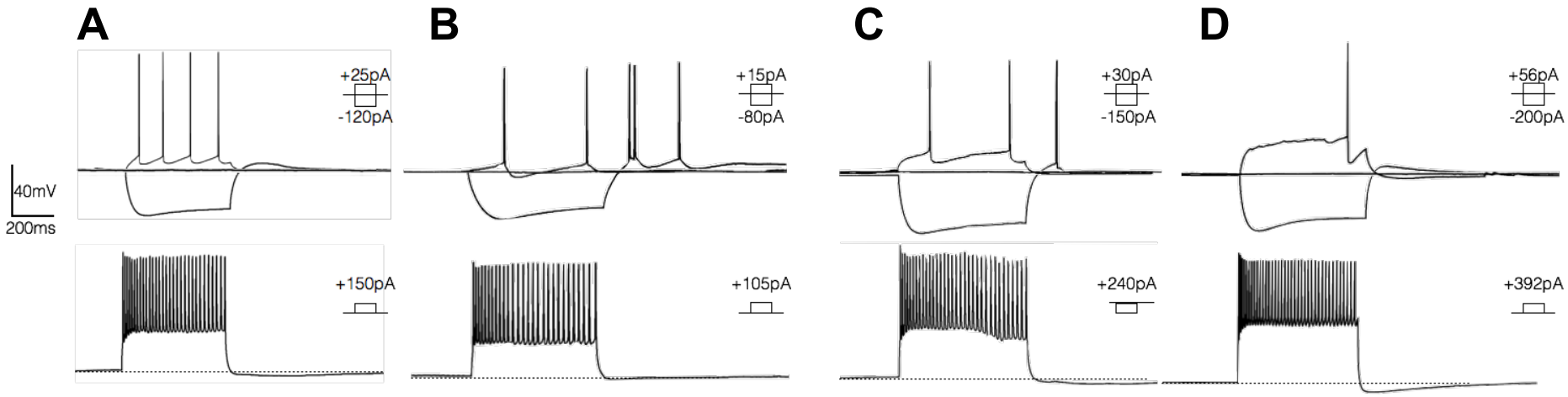
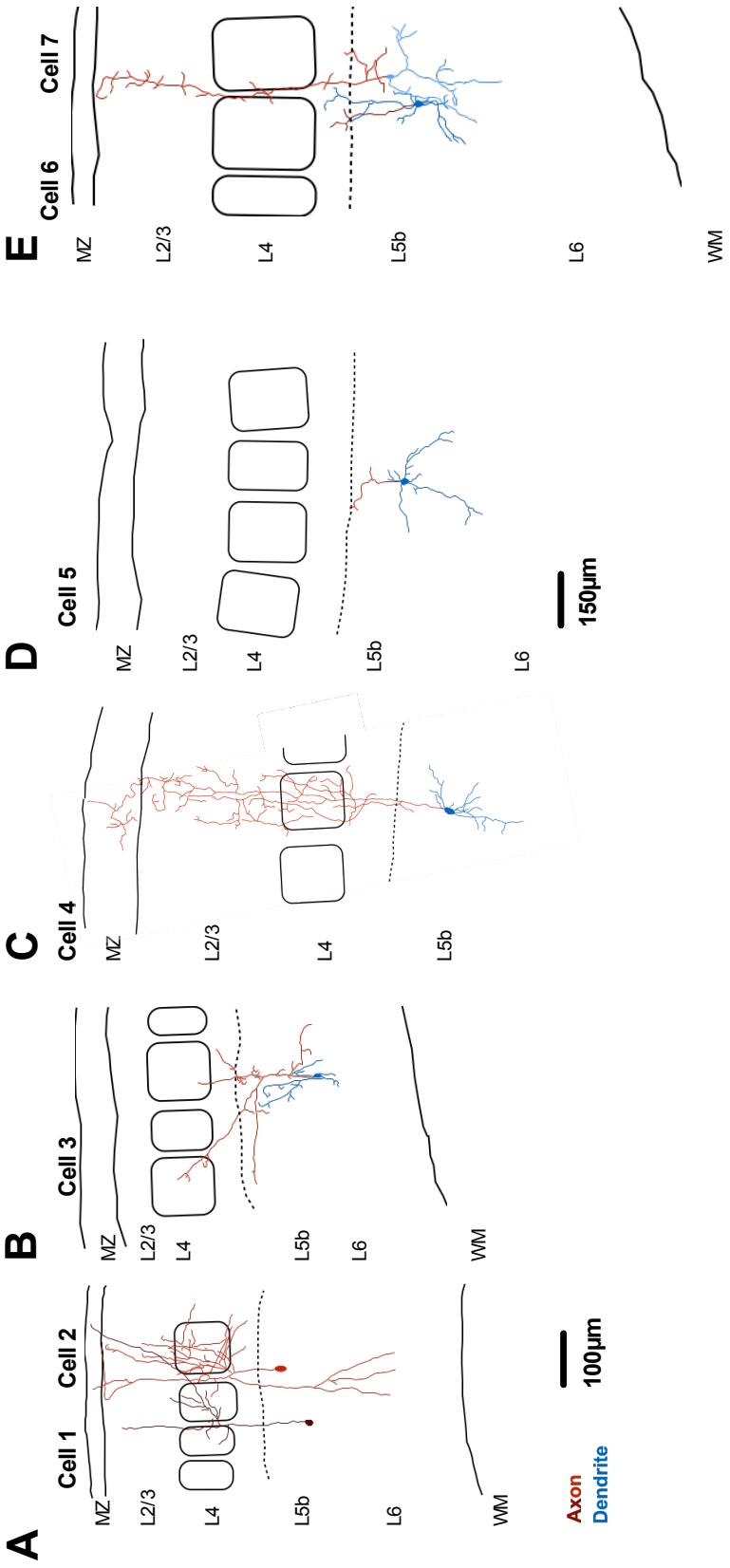


Fig 5.1. Electrophysiological properties of Lpar1-GFP interneurons at P10-P15. A. Low-threshold spiking Lpar1-GFP interneuron. **B.** Low-threshold spiking, rebound bursting Lpar1-GFP interneuron. **C.** Low-threshold spiking rebound single spiking Lpar1-GFP interneuron. **D.** P10 immature fast-spiking Lpar1-GFP interneuron. Top row positive trace shows approximate spike threshold recordings (pA current value below rectangle on right side of each recording). Negative trace represents current injection to -100mV. Bottom row shows recordings for approximate maximum firing frequency.

5.3. Morphological and immunohistochemical characterisation of Lpar1-GFP interneurons

In order to confirm the morphological identity of Lpar1-GFP interneurons, I included biocytin in the intracellular recording solution for select recordings. A total of 7 cells were recovered: 3 cells at P5, 1 cell at P9 and 3 cells at P12. Subsequent imaging and reconstruction of all recovered cells (Fig. 5.2) revealed all Lpar1-GFP interneurons had ascending axons. In two cases, the axonal reconstruction was incomplete due to severing (Cell 5 and Cell 6; Fig. 5.2 D, E). Four out of six cells (2 at P5, 1 at P9 and 1 at P12) had axons that reached L1 (Cells 1, 2, 4 and 7). In the two remaining cases, limited axonal filling was obtained. It is possible that the axons of these cells also projected to L1. This axonal morphology is characteristic of Martinotti cells, deep-layer interneurons whose axons project to L1 (Wahle, 1993; Wang et al., 2004). In addition, the majority of cells showed axonal branching in L4 (Fig. 5.2), a feature previously described in L5b Martinotti cells (Wang et al., 2004). Lpar1-GFP interneurons therefore appear to be Martinotti cells, and I will refer to them as Lpar1-GFP Martinotti cells (Lpar1-GFP MCs) henceforth.

Figure 5.2. Biocytin morphological reconstructions of Lpar1-GFP interneurons. A, B. Morphological reconstruction of 3 Lpar1-GFP interneurons cells at P5. **A.** In these two cells, only the soma and axon could be recovered. Axon for Cell 1 (left) drawn in brown to distinguish from Cell 2 (in red). **B.** Axon in red and dendrite in blue. Same scale as **A**. **C.** Morphological reconstruction of an Lpar1-GFP interneuron at P9. Axon drawn in red and dendrite in blue. Same scale bar used as **A** and **B**. **D, E.** Reconstruction of 3 Lpar1-GFP interneurons at P12. **D.** Axon in red and dendrite in blue. Note different scale bar, **E.** Axon of Cell 6 (left) drawn in brown to distinguish from Cell 7. Dendrite from Cell 7 drawn in light blue to distinguish from Cell 6. Same scale bar used as in **D**.



To further characterise Lpar1-GFP MCs, I performed immunohistochemistry on 20μm-thick frozen sections of the barrel cortex of Lpar1-GFP mice at P8 (Figure 5.3, 16 sections, 4 from each of 4 animals from different litters), using antibodies for GFP, Lhx6 and SST. GFP staining allowed me to quantify the layer distribution of Lpar1-GFP+ neurons in the barrel cortex. Lhx6 is a transcription factor that acts downstream of Nkx2-1 on MGE-derived interneurons (Xu et al., 2004; Butt et al., 2005; Wonders et al., 2008; Anastasiades & Butt, 2011; Inan et al., 2012), and testing for its expression allowed me to check whether Lpar1-GFP$^+$ cells are MGE-derived. Martinotti cells are the most numerous SST-positive interneuron type in the cortex (Rudy et al., 2011; Kelsom & Lu, 2013; Sultan et al., 2013). Under my conditions, the SST primary antibody failed to produce any staining in the brain (data not shown), and as such I shall focus on results from GFP and Lhx6 immunohistochemistry.

After immunostaining (see Chapter 2), I took confocal images of GFP (green) and Lhx6 (red) expression across a 425μm-wide region of the barrel cortex, spanning all cortical layers (Figure 5.3). For each image, I divided the cortex into 10 equally-sized bins from pial surface to just below the subplate, and then counted the number of red or green fluorescent cells in each bin, noting the relative position of layer boundaries and bins using DAPI staining as a reference. I quantified GFP and Lhx6 expression in a total of 16 slices, 4 from each of 4 animals at P8, originating from different litters. A total of 855 GFP$^+$ cells were found, mostly located in the subplate (45± 5%) and L5/6 (41± 2%), with fewer neurons found in L4 (9± 3%) and supragranular layers (L2/3: 4± 2; L1: 0%) (Figure 5.3A, 5.3B). Although I pooled numbers from L5a and L5b, it was apparent during counting that GFP expression within L5 appeared confined to its deeper aspect, L5b (Figure 5.3A). At P8, under the protocol used, a total of 1151 cells

were labelled by the Lhx6 antibody. Most of these cells were found in L5/6 (84± 2%). Few Lhx6^{+} cells were found in the subplate (4± 1%) L4 (7± 1%), L2/3 (5± 1%) or L1 (0%) (Figure 5.3A, 5.3C).

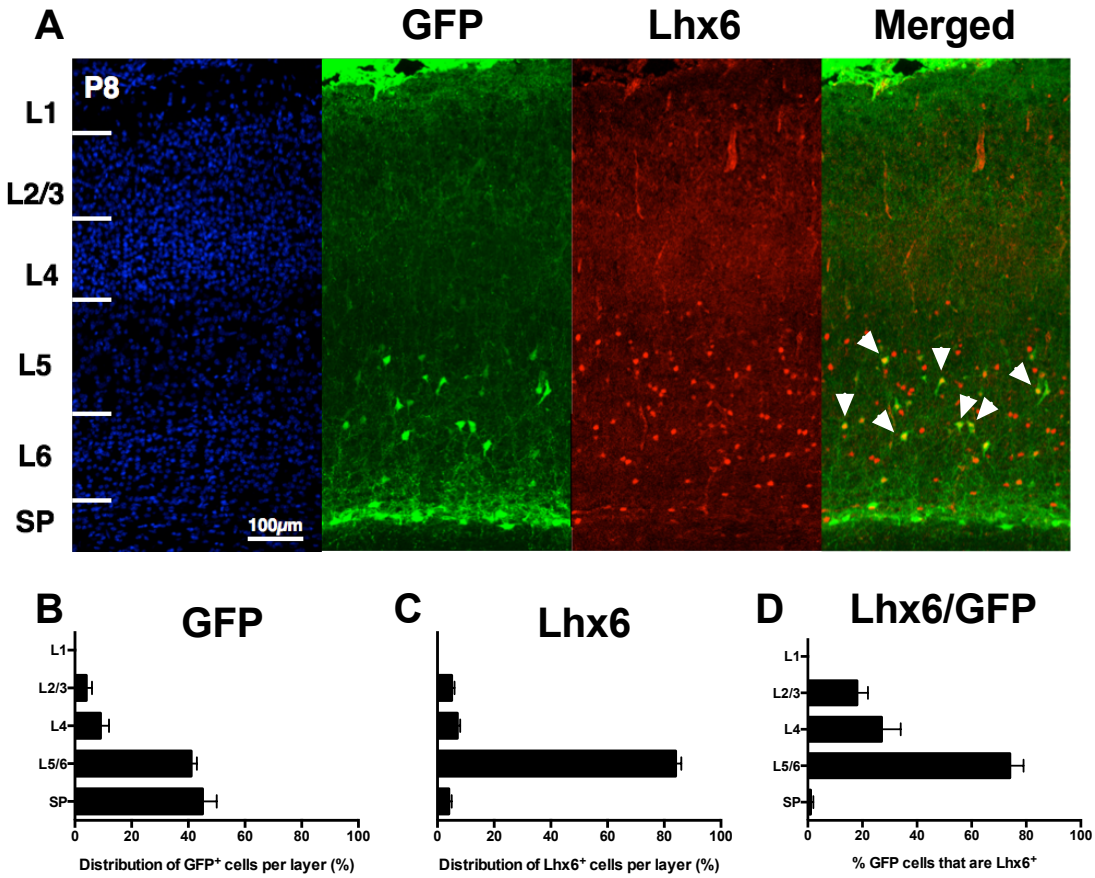


Figure 5.3. Immunohistochemical characterisation of Lpar1-GFP neurons in the barrel cortex. A. Confocal microscopy images of a sample 20μm-thick coronal section of the barrel cortex in an Lpar1-GFP mouse, at P8. Left (blue), DAPI nuclear stain. Centre-left, GFP stain (green). Centre-right, Lhx6 stain (red). Right, composite image of GFP and Lhx6 expression. Co-localisation highlighted by white arrows. To maintain clarity, only select examples of co-localisation have been highlighted. **B.** Percentage distribution of GFP^{+} cells per layer (n = 4 sections from each of 4 animals, total 16 sections). **C.** Percentage distribution of Lhx6^{+} cells per layer (n = 4 sections from each of 4 animals, total 16 sections). **D.** Percentage of GFP cells that co-express Lhx6 per cortical layer (n = 4 sections from each of 4 animals, total 16 sections).

I then examined co-localisation of GFP and Lhx6 by calculating what proportion of GFP-positive neurons also expressed Lhx6 (Figure 5.3A, D). A total of 284 GFP^{+} neurons were found to co-express Lhx6. Interestingly, Lpar1-GFP+ cells in the

subplate rarely ever expressed Lhx6 (1± 1%), consistent with a previous report that they are glutamatergic (Hoerder-Suabedissen & Molnár, 2012). In L5/6, 74± 5% of Lpar1-GFP MCs expressed Lhx6, confirming their MGE origin. In L4, 27± 7% of GFP cells expressed Lhx6, and in L2/3 this value was 18± 4%. No $Lhx6^{+}/GFP^{+}$ cells were found in L1. These results show that in the cortex, Lpar1-GFP cells are found almost exclusively in the subplate and L5(b)/6. Although Lpar1-GFP subplate neurons very rarely co-expressed Lhx6, the percentage of GFP cells in L5(b)/6 that expressed Lhx6 was very high, indicating that despite a common fluorescent tag, these populations likely have different embryonic origin, with Lpar1-GFP Martinotti cells originating from the MGE. Although it was impossible under my conditions to verify SST expression in Lpar1-GFP MCs, Lhx6 expression and MGE origin suggest either a PV or SST identity, and Martinotti cells have previously been shown to be SST-positive and PV-negative (Wang et al., 2004; Ma et al., 2006; Xu et al., 2006). It is therefore most likely that Lpar1-GFP MCs are somatostatin-positive interneurons.

5.4. Characterisation of thalamic inputs onto Lpar1-GFP interneurons

It has previously been reported that both fast-spiking and non-fast spiking interneurons receive thalamic input, in the barrel field (Porter et al., 2001). In particular, layer 5 SST-positive non-fast spiking interneurons in the X94 line were shown to receive thalamic input that could result in spiking (Tan et al., 2008). One other study documented a relatively weak thalamocortical projection to L5/6 low-threshold spiking interneurons, although only two cells were reported (Cruikshank et al., 2010). Since Lpar1-GFP SPns play a role as early relays of thalamic input, we hypothesised that Lpar1-GFP Martinotti cells could also receive and propagate early

thalamic inputs. This would put them in a key position to influence early cortical synchronisation to incoming patterns of thalamic activity.

I tested a total of 47 Lpar1-GFP positive interneurons for thalamic connectivity. A bipolar stimulating electrode was placed either directly in the ventrobasal thalamus or over the adjacent internal capsule and 10 spaced stimuli were delivered. Recorded cells were split into two age groups corresponding to the critical period for thalamocortical plasticity (P4-P9, n = 24) and a post-critical period group (P10-P15, n = 23). At P4-P9, the majority of Lpar1-GFP interneurons received monosynaptic thalamic input (15/24, 63%) (figure 5.4A). After P10, in contrast to Lpar1-GFP SPns (Chapter 3), this number increased even further, with 22/23 cells in slices with well-preserved thalamic connectivity showing direct thalamic inputs (96%). Using a minimal stimulation protocol (Raastad et al., 1992; Isaac et al., 1997), I found that Lpar1-GFP interneurons received modest thalamic inputs at P4-P9 (12± 4pA) and P10-P15 (11± 1pA). No significant differences in amplitude were observed between the two time-points ($t(29) = 0.246$, $p = 0.807$). However, the latency of TC-EPSCs onto Lpar1-GFP interneurons decreased significantly from P4-P9 (9.5± 0.3ms) to P10-P15 (7.9± 0.3ms) ($t(29) = 3.268$, $p < 0.01$). The observed changes in thalamic connectivity and latency could not be explained by stimulation amplitude, as there was no difference in stimulation parameters used between the two developmental stages examined ($t(29) = 0.274$, $p = 0.786$).

Having established the prevalence and characteristics of thalamic input onto Lpar1-GFP Martinotti neurons, I then examined the short-term dynamics of this synapse. Thalamic inputs to L4 and L5/6 fast-spiking interneurons have previously been shown

to be depressing (Cruikshank et al., 2010). In contrast to these cells, a study focusing on thalamic input onto L5 SST-positive X94 cells found that fast-spiking parvalbumin-positive cells show opposite behaviours to somatostatin-positive non-fast spiking cells during thalamic stimulation trains of 10-40Hz frequency. Thalamic inputs to SST-positive cells are facilitating and those to parvalbumin-positive cells are depressing. SST-positive neurons rarely fired to the first two to three thalamic stimuli but fired reliably afterward, whereas PV-positive neurons fired reliably to the first two to three stimuli, but not after (Tan et al., 2008). Different types of interneuron could thus perform different computational functions during thalamocortical processing. I used a paired-pulse stimulation protocol consisting of two pulses at an inter-stimulus interval of 50ms to study short-term plasticity of thalamic input onto Lpar1-GFP Martinotti neurons. The 50ms interval was chosen as it approximates the frequency of the spindle burst, the dominant pattern of network activity in the neonatal mouse cortex (Khazipov & Luhmann, 2006). Given that Lpar1-GFP Martinotti neurons have axons arborizing in L4 and the supragranular layers and that SST^+ neurons in L5 have been shown to receive facilitating input from the thalamus (Tan et al., 2008) and nearby pyramidal neurons (Silberberg & Markram, 2007), we hypothesised that these neurons received facilitating thalamic input. This would mean that during patterns of thalamic activity, Lpar1-GFP Martinotti cells would get increasingly recruited, placing them in a key position to synchronise networks of cortical neurons to incoming thalamic stimulation.

I recorded 21 Lpar1-GFP Martinotti cells across different ages for short-term plasticity experiments (P4-P9: n = 8, P10-P15: n = 13). Recordings from the two age groups were pooled together, as no developmental change was found in the direction

of short-term plasticity. 18/21 cells showed short-term facilitating responses to thalamic afferent stimulation, with an average amplitude of 11± 2pA for the first stimulus and 19± 3pA for the second (Figure 5.4F). Short-term facilitation was statistically significant, as determined by a Wilcoxon matched-pairs signed rank test ($W = 197$, $p < 0.001$, $r = 0.72$). Average PPR was 1.9± 0.2. Lpar1-GFP Martinotti cells, SPns and L4 spiny stellate cells differed in their short-term plasticity profiles. A one-way ANOVA determined that the PPR of Lpar1-GFP Martinotti neurons was significantly higher than that of Lpar1-GFP SPns (0.7± 0.1, n = 11) and L4 spiny stellate cells (0.9± 0.1, n = 11) (Figure 5.4G).

In conclusion, Lpar1-GFP Martinotti neurons receive thalamic input early in development and, contrary to Lpar1-GFP SPns, the proportion of cells receiving thalamic input increases throughout the first two postnatal weeks. There were no developmental changes in TC-EPSC amplitude, but there was a significant decrease in latency. Short-term plasticity experiments determined that thalamic inputs onto Lpar1-GFP Martinotti neurons are facilitating. Put together, this data lends support to our hypothesis that Lpar1-GFP Martinotti neurons could function as early integrators of thalamic input. In the next section, we aimed to determine the sources of excitatory cortical input onto Lpar1-GFP Martinotti cells, using glutamate uncaging.

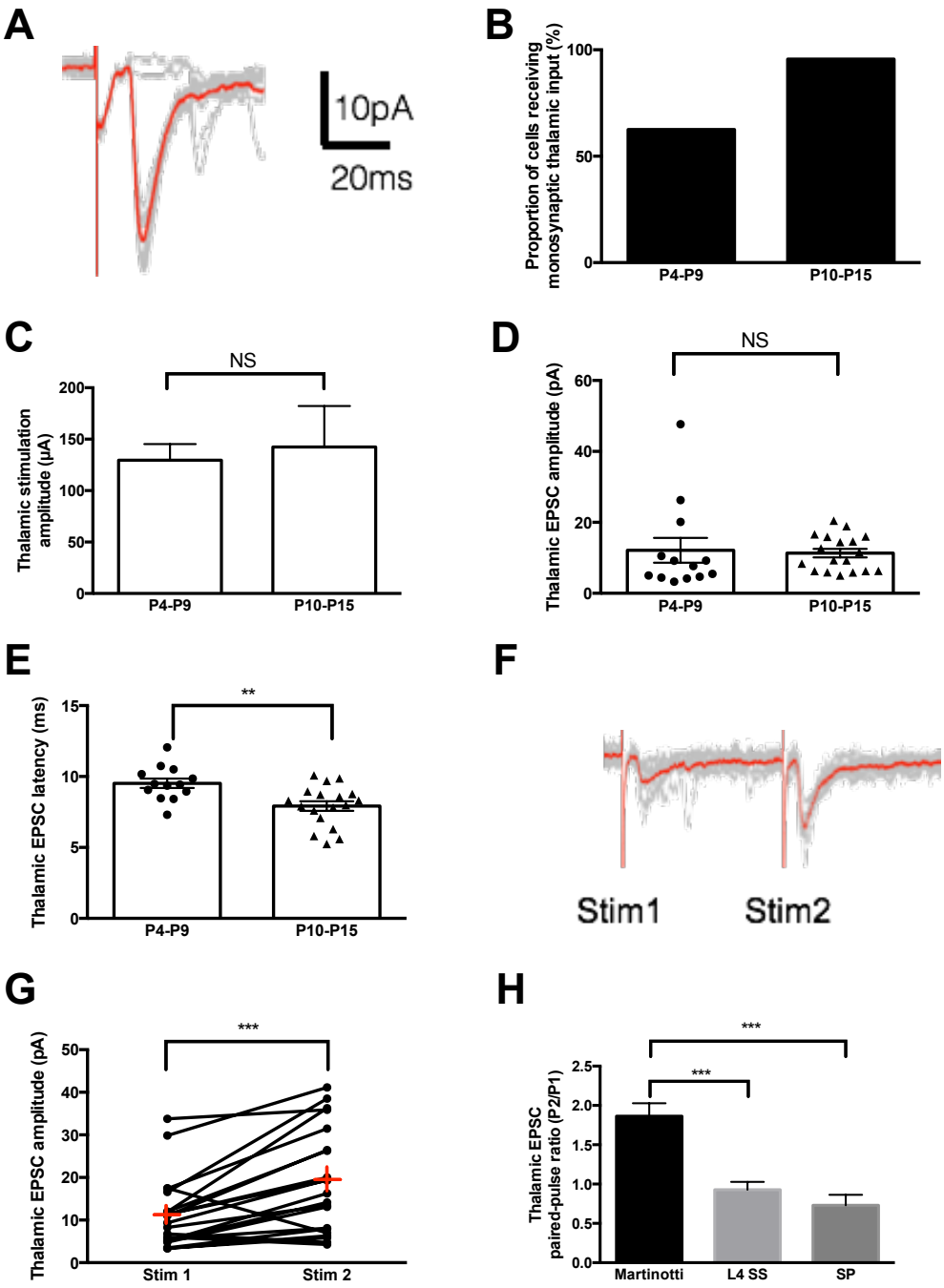


Figure 5.4. Thalamic input onto Lpar1-GFP MCs. A. Representative trace for a threshold TC-EPSC. **B.** Proportion of Lpar1-GFP interneurons receiving direct thalamic input at P4-P9 (n = 24; 15 cells received input) and P10-P15 (n = 23; 22 cells received input). **C.** Average thalamic stimulation amplitude (n = 47 cells; P4-P9: n = 24; P10-P15: n = 23). **D.** Average amplitude of thalamocortical EPSCs for Lpar1-GFP Martinotti cells at P4-P9 (n = 14) and P10-P15 (n = 18). Each symbol corresponds to the average of 10 recordings for a single cell. **E.** Average latency of thalamocortical EPSCs for Lpar1-GFP Martinotti cells at P4-P9 (n = 14) and P10-P15 (n = 18). Each symbol corresponds to the average of 10 recordings for a single cell. **F.** Representative trace for a paired-pulse recording of a TC-EPSC. **G**. Average TC-EPSC amplitude for the first and second pulse in short-term plasticity experiments, for each Lpar1-GFP Martinotti cell recorded (n = 21). Red lines indicate mean and SEM of TC-EPSC amplitude of all cells to the first and second pulses. Each symbol corresponds to

the average of 10 trials for a single cell **H.** Comparison of paired-pulse ratios between Lpar1-GFP interneurons (n = 21), L4 spiny stellate cells (n = 11), and Lpar1-GFP subplate neurons (n = 11). Error bars are ± SEM.

5.5. Mapping excitatory cortical inputs onto Lpar1-GFP interneurons

I used LSPS in conjunction with whole-cell patch-clamp electrophysiology to map cortical afferent excitatory input onto 29 Lpar1-GFP Martinotti neurons, voltage-clamped at -70mV. Cells were divided into the developmental groups previously used for analysis of intrinsic properties: P4-P6 (n=10), P7-P9 (n=10) and P10-P15 (n=9). I began by analysing the development of total amount of excitatory synaptic input onto Lpar1-GFP Martinotti cells (Figure 5.5A, table 5.3). The transition between P4-P6 and P7-P9 appeared to be critical in the synaptic development of Lpar1-GFP Martinotti neurons, as total excitatory synaptic input practically doubled between these timepoints. At P10-P15 there was a slight decrease in input. Statistically, a Kruskal-Wallis test found a marginally significant developmental effect on total excitatory input ($H(2) = 5.775$, $p = 0.056$). Since the p value was very close to significance, I performed post-hoc comparisons. A significant increase in total input was indeed observed between P4-P6 and P7-P9. This was different to the result obtained with Lpar1-GFP SPns, where no change in total synaptic input was observed. I then plotted input resistance, an important measure of the intrinsic electrophysiological maturity of a cell, against total synaptic input, which could be considered an indicator of a cell's network maturity (Fig 5.5B). Five cells at P10-P15 (in red) were found to have mature intrinsic properties (as indicated by low input resistance) but lower total synaptic input than their counterparts. These cells were interpreted as dropping out of the network, and excluded from regression analysis. I then fitted a one-phase decay curve to the data, resulting in an R squared value of

0.77. This data indicates that, contrary to Lpar1-GFP SPns, intrinsic maturity closely tracked network maturity, for Lpar1-GFP Martinotti cells.

Having examined total synaptic development in Lpar1-GFP Martinotti cells, I set out to characterise the laminar organisation of their cortical excitatory input. I plotted the normalised vertical profile of each mapped cell by calculating the proportion of input arising from each 50μm row. Vertical profiles were plotted for all cells as colour-coded one-dimensional maps in Figure 5.5C. Each one-pixel column corresponds to a cell, aligned left to right by age, and each colour-coded pixel denotes for a particular cell the proportion of input originating from that row. Profiles were aligned by L4. It can be seen by the vertical profiles that Lpar1-GFP Martinotti neurons start out by receiving most excitatory input from L4, with L5 and 6 also contributing. A subset of cells seemed also to receive considerable input from the developing L2/3. At P7-P9, infragranular layers dominated synaptic excitation onto Lpar1-GFP Martinotti neurons, but L4 was still providing input. By P10-P15, L4 and supragranular input was virtually gone and practically all input onto Martinotti neurons arose from deep L5 and L6. In Figure 5.5D, I plotted the average normalised vertical profile for each age group, according to the same L4/L5a border alignment. This data corroborated the impression of a progressive developmental loss of L4 excitatory input onto Lpar1-GFP Martinotti cells, concurrent to an increase in deep layer input.

In order to examine this phenomenon more closely, I plotted the average excitatory input map for each age group, aligned by the L4/L5a border (Figure 5.5E), which confirmed the progressive developmental switch in excitation from L4 to L5b/6. Moreover, it is important to note that these maps are not normalised, but plotted in

absolute, raw pA values. The fact that the developmental decrease/increase dynamic in L4 and L5b/6 input was still observed supports the idea that this is a genuine shift, and not just a reciprocity effect of normalised data. To hone in further on the laminar organisation of excitation to Lpar1-GFP interneurons, I determined, for each cell, the layer of origin of synaptic inputs, based on the overlay of LSPS spots and cortical layer boundaries evident in the DIC image (Figure 5.5F, table 5.3). I used two-way ANOVA to answer two questions:

1) At each timepoint, which are the layers providing most input?
2) How does the input provided by each layer change throughout development?

Table 5.3.

Proportion of total excitatory input onto Lpar1-GFP interneurons (%)

	L6	L5b	L5a	L4	L2/3	Total (pA)
P4-P6	15± 3	29± 5	11± 3	35± 5	9± 3	1625± 192
P7-P9	26± 5	48± 6	6± 2	16± 3	3± 1	3520± 478
P10-P15	30 ±6	57± 6	4± 1	5 ±1	2± 1	2927± 808

Table 5.3 Proportion (%) and total (pA) excitatory synaptic input onto Lpar1-GFP interneurons arising from each cortical layer. P4-P6: n=10 cells; P7-P9: n=10 cells; P10-P15: n=9 cells.

Analysis was initially performed on normalised data (Figure 5.5F, top). Two-way ANOVA revealed a highly significant *layer* ($F(4, 130) = 50.60$, $p < 0.001$) and *interaction* effect ($F(8, 130) = 8.784$, $p<0.001$). In terms of the first question, at P4-P6, L4 provided significantly more input than all other cortical layers except L5b. L5b provided significantly more input than layers 2/3 and 5a, but not L6. At P7-P9, L5b provided significantly more input than any other cortical layer. L6 provided more input than L5a and L2/3. At P10-P15, L5b was still the main source of excitatory input onto Lpar1-GFP interneurons, providing significantly more input than any other layer. L6 provided significantly more input than any other layer apart from 5b. By this

point, L4 did not provide significantly more input than any other layer and no other significant effects were detected. Addressing the second question (developmental effects), I observed a significant increase in proportion of L6 excitatory input between P4-P6 and P10-P15. L5b inputs increased significantly from P4-P6 to P7-P9 and P4-P6 to P10-P15. The opposite effect was observed for L4 inputs, with a significant decrease in inputs observed between P4-P6 and P7-P9 and from P4-P6 to P10-P15.

I then analysed raw total input data (5.5F, bottom). Since this dataset violated the critical ANOVA assumption of homogeneity of variance, raw input data was transformed using the square root. Under this condition, two-way ANOVA yielded significant *interaction* ($F(8, 130) = 5.151$, $p < 0.001$) and *layer* effects ($F(4, 130) = 49.94$, $p < 0.001$). There was a significant increase in total L5b input between P4-P6 and P10-P15, and a significant decrease in total L4 input between P7-P9 and P10-P15. At P4-P6, the dominant sources of excitatory input were L6, L5b and L4. All 3 layers provided significantly more input than L2/3. L5b and L4 also provided more input than L5a. At P7-P9, L5b emerged as the undisputed primary source of excitation, providing significantly more input than any other layer. L6 also had influence, providing more input than L5a and L2/3. L4 only provided significantly more input than L2/3. By P10-P15, L5b and L6 were the clear dominant sources of input onto Lpar1-GFP Martinotti cells, providing significantly more input than any other layer. L5b additionally contributed significantly more input than L6.

In summary, Lpar1-GFP Martinotti cells receive ample excitation from the cortex, in addition to thalamic input. The transition from P4-P6 to P7-P9 appears to be a key point for glutamatergic synaptogenesis for this cell population, with excitatory input

from the cortex approximately doubling over this time period, closely tracking intrinsic property maturation. Regarding laminar organisation, Lpar1-GFP Martinotti cells receive excitation from cortical layers that get thalamic input from core thalamic nuclei: L4, L5b and L6. Early in development, cortical excitation originates mostly from L4 and L5b, but there is a dynamic rearrangement in the circuit, such that input from L4 progressively decreases and input from L5b and L6 increases.

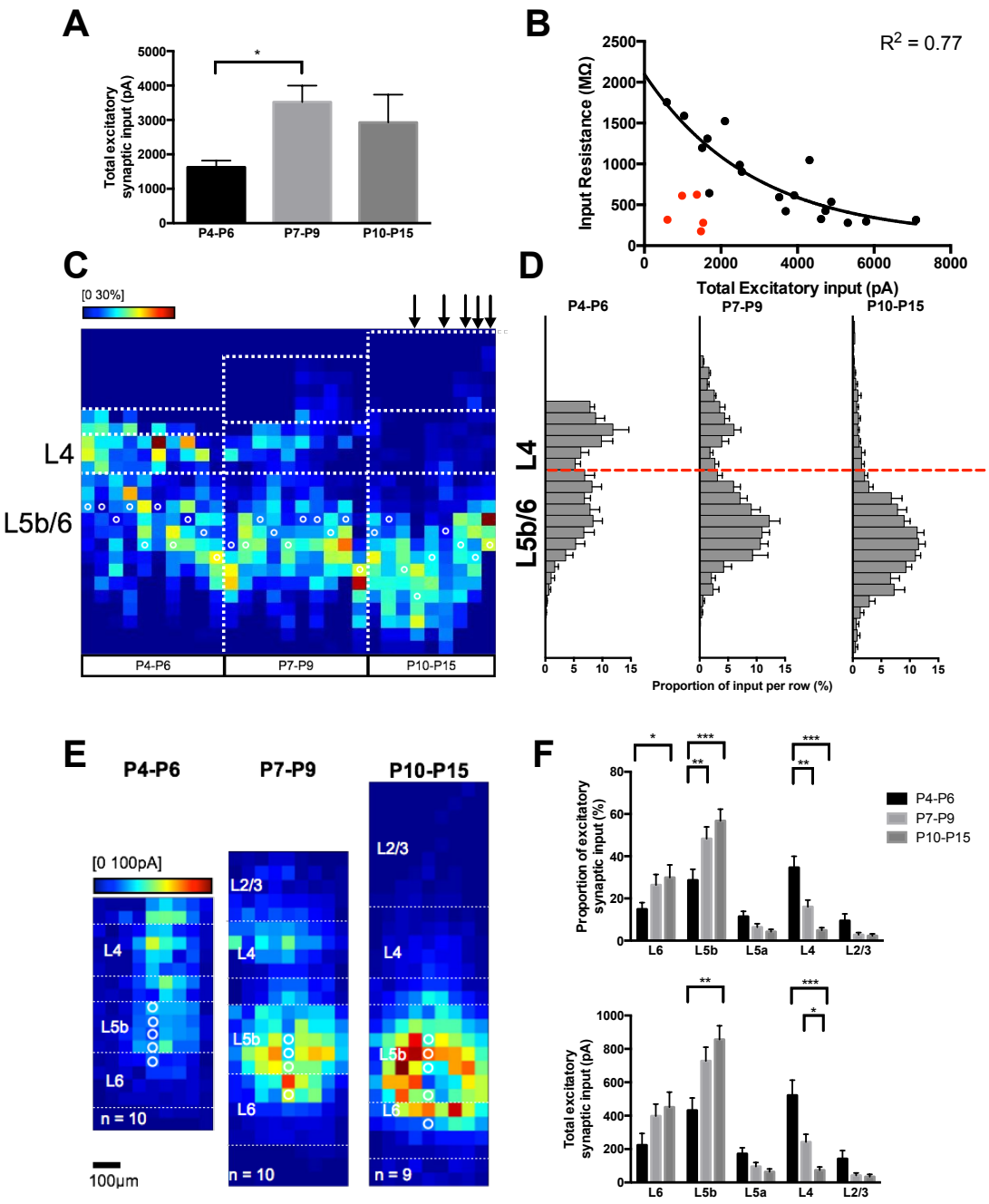


Figure 5.5. Cortical excitatory input onto Lpar1-GFP MCs. A. Total excitatory synaptic input onto Lpar1-GFP Martinotti neurons (n = 29 cells; P4-P6: n=10 cells; P7-P9: n=10 cells; P10-P15: n=9 cells). **B.** Input resistance plotted against total synaptic input for 23 Lpar1-GFP Martinotti cells (P4-P6: n=10 cells; P7-P9: n=10 cells; P10-P15: n=4 cells). Line indicates non-linear regression plot. Cells with mature intrinsic properties and low total synaptic input at P10-P15 were highlighted in red and excluded from regression analysis. **C.** Normalised vertical profiles for all Lpar1-GFP interneurons recorded. Numbers as in A. Inputs coming from each row were averaged into a single column, such that each column represents one cell. Cells are aligned by L4. Approximate L4-L2/3 layer boundaries and pial surface were determined during alignment. Numbers as in A. Open white circles indicate soma position. Black arrows indicate cells excluded from regression analysis in **B**, red. D**.** Average normalised vertical profiles. Red dashed line indicates L4-L5a border. Numbers as in A. **E.** Average excitatory input maps onto Lpar1-GFP Martinotti cells. Maps were aligned by L4. Open white circles represent soma positions for individual maps. Values are in pA and all plotted to the same scale (top

left, 0-100pA). Numbers as in A. **F.** Proportion of total excitatory synaptic input arising from each cortical layer, for all age groups analysed. Numbers as in A. Error bars are SEM. * $p < 0.05$; ** $p < 0.01$; *** $p < 0.001$.

5.5.1. Maturation of single EPSCs onto Lpar1-GFP interneurons

In the previous section, I showed a pronounced rewiring of excitatory inputs onto Lpar1-GFP Martinotti cells over the first two postnatal weeks. Though informative, this analysis does not explain how inputs from L4 decrease and their L5b/6 counterparts increase. Is the increase in L5b/6 input due to a greater number of synaptic contacts? Or does the amplitude of EPSCs evoked from these layers increase over development? In order to further investigate the mechanism behind circuit rewiring, I compared the amplitude and number of EPSCs mapped from L4 and L5b of 5 randomly selected cells from each developmental period. A total of 2412 EPSCs were analysed (P4-P6: 673; P7-P9: 1081; P10-P15: 658).

There was no change in average EPSC amplitude for L4-evoked inputs ($F(2, 12) = 1.048$, $p = 0.381$) (Figure 5.6A,). Looking at the frequency distribution of L4-evoked EPSC amplitudes, at all developmental stages there was a peak in events centred around 10pA that decreased sharply, showing very few events over 20pA (Figure 5.6C, red). One-way ANOVA detected a significant effect for L5b inputs, however ($F(2, 12) = 4.297$, $p < 0.05$), with average EPSC amplitude increasing significantly between P4-P6 (10± 1pA) and P10-P15 (24± 6pA). The frequency distribution of L5b-evoked EPSC amplitude started out virtually identical to L4, but over development there was a clear decrease in proportion of events under 20pA, concurrent to the emergence of a long tail of events over this amplitude (Figure 5.6C, blue).

In terms of number of events, a significant effect was found for L4-derived inputs ($F(2, 12) = 8.498$, $p < 0.01$) (Figure 4.6B). Specifically, there was a significant decrease between P7-P9 (95± 17 EPSCs) and P10-P15 (28± 8 EPSCs). No effect was found for L5b inputs ($F(2, 12) = 2.072$, $p = 0.169$). I further explored if there were any differences in the characteristics of L4 and L5b-derived inputs. To this end, I employed 2-way ANOVA, using *Layer* and *Developmental Stage* as factors, and carrying out post-hoc comparisons between L4 and L5b at each developmental stage. For average EPSC amplitude, this analysis yielded significant Interaction ($F(2, 24) = 4.59$, $p < 0.05$) and Layer effects ($F(1, 24) = 8.64$, $p < 0.01$). Multiple comparison tests revealed that average EPSC amplitude was higher for L5b than L4-evoked EPSCs at P10-P15, but not before. When number of events was tested, there was an effect of Developmental Stage ($F(2, 24) = 5.555$, $p < 0.05$) and Layer ($F(1, 24) = 10.34$, $p <0.01$). Multiple comparison tests revealed that a greater number of EPSCs was evoked from L5b than L4 at P10-P15, but not earlier than that timepoint.

In conclusion, the decrease in excitatory input from L4 onto Lpar1-GFP interneurons can be explained by a decrease in the number of EPSCs evoked from L4, likely corresponding to elimination of these synapses. The increase in excitatory input from L5b seems to occur via an increase in the average amplitude of L5b-evoked EPSCs. No change in number of events was evident for L5b inputs, suggesting that the increase in input from this layer results from synaptic plasticity of existing inputs and not synaptogenesis. By P10-P15, individual L5b inputs onto Lpar1-GFP Martinotti cells were significantly stronger and more numerous than inputs arising from L4. Prior to that age, no differences could be detected. One alternative explanation for changes in the number of events evoked relates to the excitability of pre-synaptic

neurons, i.e., the ability of LSPS to generate action potentials in cells providing afferent input. Laser settings for mapping excitatory input onto Lpar1-GFP Martinotti cells were obtained from calibration experiments performed for Chapter 3 on L5 and L6 pyramidal cells. As described in that chapter, optical stimulus amplitude was calibrated to maintain a constant action potential output throughout development, supporting the notion that changes in number of inputs reflect changes in synaptic contacts and not in number of pre-synaptic action potentials generated. However, to fully resolve this issue, I would have to compare the LSPS-induced excitability of L4 and L5/6 excitatory neurons.

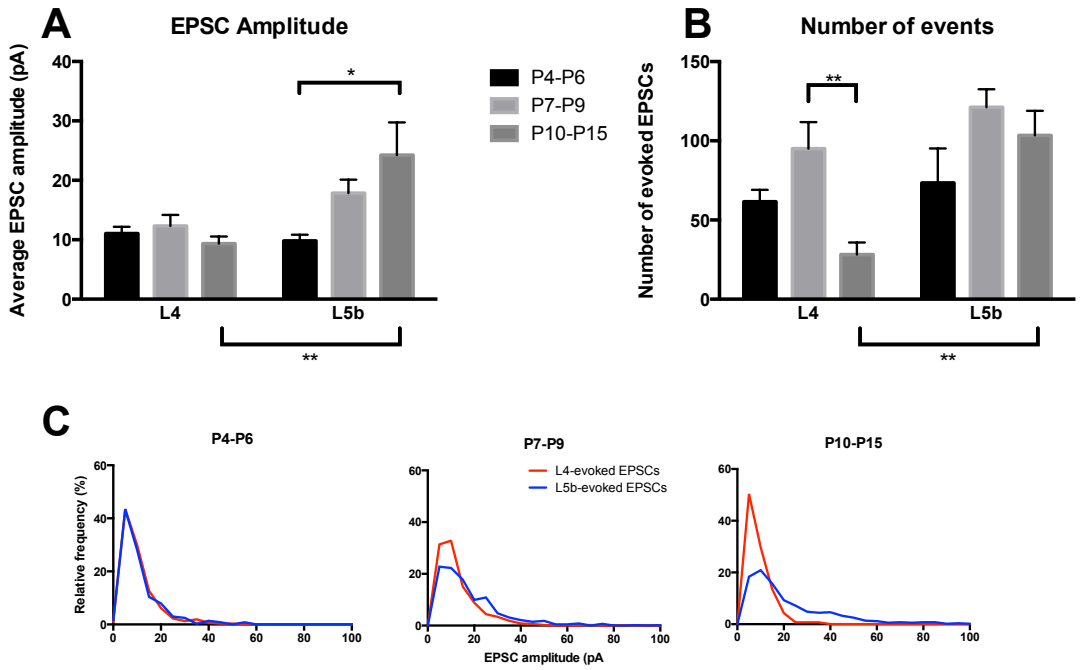


Figure 5.6. Developmental analysis of single EPSCs onto Lpar1-GFP MCs. A. Average amplitude of EPSCs onto 5 Lpar1-GFP Martinotti cells evoked from L4 (left) and L5b (right), at P4-P6 (673 EPSCs), P7-P9 (1081 EPSCs) and P10-P15 (658 EPSCs). Cell and total EPSC numbers apply to B and C as well. **B.** Average number of EPSCs evoked from L4 and L5b at the same developmental timepoints, for Lpar1-GFP Martinotti cells. * $p < 0.05$; ** $p < 0.01$. **C.** Relative frequency distribution of the amplitude of L4 (red) and L5b (blue)-evoked EPSCs, recorded at Lpar1-GFP Martinotti cells.

5.5.2. Horizontal organisation of excitatory inputs onto Lpar1-GFP Martinotti cells

Lpar1-GFP Martinotti cells receive input from the thalamus and are richly engaged by cortical excitatory neurons from an early age. So far, analysis of cortical inputs has focused on the emergent laminar organisation of afferent inputs onto this cell type. However, it was clear that maps of afferent input onto Martinotti cells showed a columnar organisation, which I next set out the characterise. This is an important attribute, as it can provide insight about the type of information integrated by the cell: does it only receive input from cells in the same column? Or does it integrate across columns, collecting information from cells with different receptive fields? For an interneuron, this information is especially important, due to the nature of computations performed by inhibitory cells in sensory cortex, and how they relate to circuit architecture (for example, feed-forward, feedback or lateral inhibition (Isaacson & Scanziani, 2011)). By resolving the columnar structure of glutamatergic input onto Lpar1-GFP Martinotti cells, we hoped to be able to glean more information about this cell type's functions in development and sensory processing.

To study the columnar organisation of excitatory input to Lpar1-GFP Martinotti cells, I calculated the proportion of input originating from each 50μm column in a map, obtaining normalised horizontal profiles for each cell. These profiles were colour-coded and are plotted in 5.7A. Each row corresponds to a cell, and each pixel in a row depicts the proportion of total cortical excitation derived for that cell, from that 50μm column. Table 5.4 displays the proportion of input originating from each 50μm bin of distance from the cell body. At P4-P6, Lpar1-GFP Martinotti neurons seem to receive most inputs from the column of their soma and the two columns either side of it, at

50µm distance from the soma (Fig. 5.7, B top). At P7-P9, the horizontal distribution of inputs appears flatter, with inputs in the distant 100-200µm columns increasing at the expense of inputs in the home column and the 50µm columns (Fig. 5.7, B middle, C middle). Between P7-P9 and P10-P15 there was little change in columnar organisation, with only a small further decrease in input from the soma column and increase in remaining columns occurring (Fig. 5.7, B bottom, C bottom, blue).

Statistically, I used 2-way ANOVA with *distance from soma* and *developmental stage* as factors, to address the following questions:

1) At each age group, which 50μm columns are providing most input?
2) Does the synaptic contribution of each 50μm column change throughout development?

2-way ANOVA revealed a significant effect of *distance from soma* ($F(4, 130) = 40.64$, $p < 0.001$) and an interaction effect ($F(8, 130) = 3.845$, $p < 0.001$). These effects were followed up with post-hoc comparisons. To answer Question 1, at P4-P6, the home and 50μm-distance columns provided significantly more input than any other. At P7-P9, these columns provided more input than the 150 and 200μm-distance columns. By P10-P15, the home, 50μm and 100μm-distance columns provided more input only than the 200μm column, with no other differences observed. The only developmental effect found (Question 2) was a significant decrease in proportion of input provided by the home column. These findings suggest that the majority of excitatory synaptic input onto Lpar1-GFP Martinotti cells arrives from the immediate proximity of the cell. However, over development there is a shifting of weights in the

horizontal distribution of input, with an increase in distal at the expense of proximal input. This was further confirmed by performing linear regression of proportion of synaptic input as a function of distance from the soma. A significant fit was achieved for each age group (P4-P6: $p < 0.01$; P7-P9 $p < 0.01$; P10-P15 $p < 0.05$; Figure 4.5D). Proportion of synaptic input (Y) could be very accurately predicted from distance from the soma (X) at each developmental stage by the following equations:

- P4-P6: $Y = -0.1005*X + 22.28$, $R^2 = 0.96$
- P7-P9: $Y = -0.0544*X + 17.05$, $R^2 = 0.96$
- P10-P15: $Y = -0.04398*X + 15.75$, $R^2 = 0.78$

Between P4-P6 and P10-P15, regression line slope becomes closer to zero, indicating less steep, and therefore the horizontal input distribution is becoming flatter. We decided to take the arbitrary threshold of 10% of total synaptic input to define the limits of a functional input column. By this definition, at P4-P6 columnar width was 200μm, increasing to approximately 300μm at P7-P9 and P10-P15 (Fig. 5.7B). Based on this data, we can conclude that Lpar1-GFP Martinotti cells are concerned with processing columnar input, and the horizontal breadth of input integrated expands over development.

Table 5.4.					
Proportion of total excitatory synaptic input (%) as a function of distance from soma (µm)					
	0	50	100	150	200
P4-P6	22± 3	19± 2	10± 2	6± 1	4± 1
P7-P9	16± 2	15± 1	13± 1	9± 1	5± 1
P10-P15	14± 1	15± 1	13± 1	9± 1	5± 1

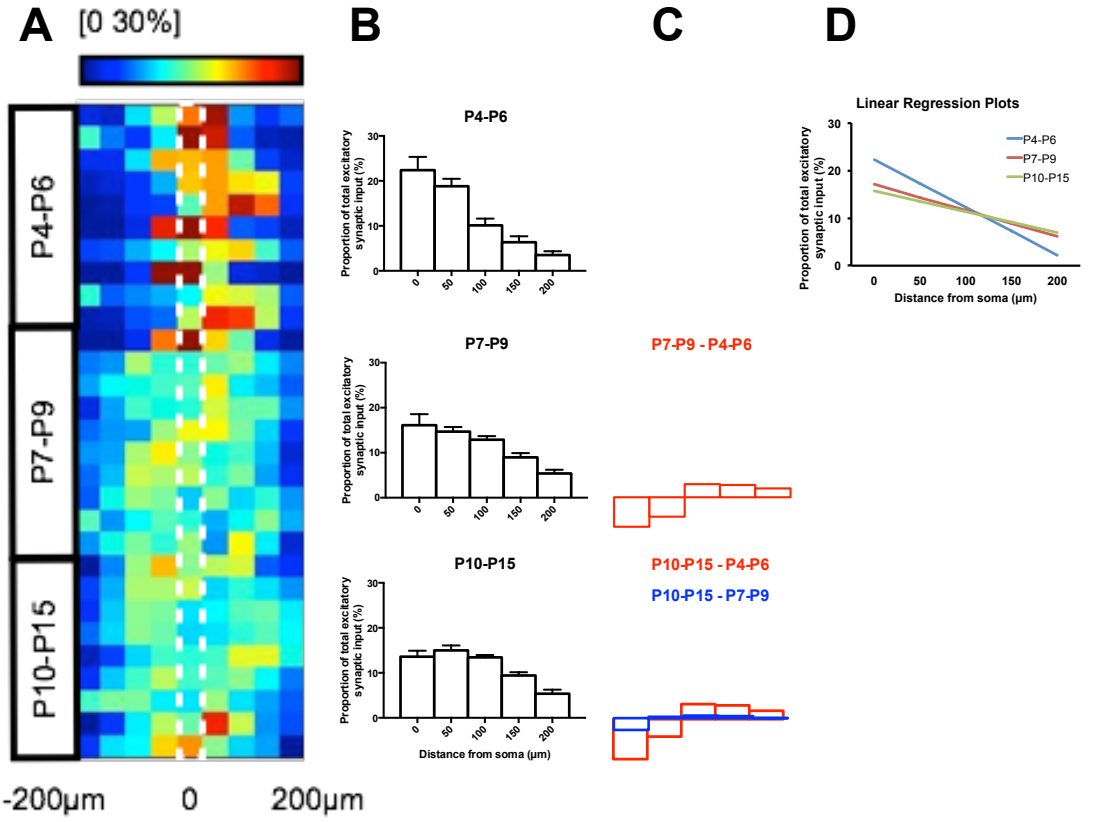


Fig 5.7. Columnar organisation of excitatory cortical inputs onto Lpar1-GFP MCs. A-C display the average horizontal profile of excitatory inputs onto Lpar1-GFP interneurons at P4-P6 through to P10-P15. Red bar chart to the right side of P7-P9 and P10-P15 graphs depict the difference between proportion of input arising from each 50μm bin at this age and at P4-P6. Blue bar chart to the right side of P10-P15 graph depicts difference between proportion of input arising from each 50μm bin at this age and P7-P9. Blue and red bar charts are plotted in the same scale as P4-P6, P7-P9 and P10-P15 horizontal profile plots. A total of 29 cells were analysed (P4-P6, n = 10; P7-P9, n = 10; P10-P15, n = 9; numbers apply to B-D as well). **A** displays horizontal profiles of excitatory input for all Lpar1-GFP interneurons recorded. For each map, inputs from each 50μm column were averaged, resulting in a single row. Each row corresponds to a cell. **D**, linear regression plots for the horizontal profile of excitatory inputs at each developmental period. Error bars are ±SEM.

5.6. The output of Lpar1-GFP Martinotti cells

Experiments in the previous sections revealed that Lpar1-GFP non-subplate neurons are non-fast spiking, LTS interneurons positive for Lhx6 (therefore originating from the MGE), and that morphologically they are Martinotti cells, characterised by an axon that ascends towards L1 and arborises in L4. They receive direct, facilitating thalamic input, and, in the cortex, most of their excitatory inputs originate from L4 and L5b, within a 200-300μm wide column. L4 input is transient and disappears by P10, whereas input from L5b/6 is upregulated during development. Given the intimate association that Lpar1-GFP Martinotti cells appear to have with L4, it occurred to us that there might be a reciprocal connection between the two. More specifically, taking into account that Lpar1-GFP Martinotti cells receive transient excitation from L4, we set out to test the hypothesis that they provide feedback GABAergic input to L4 spiny stellate neurons, via the characteristic Martinotti ascending axon. With no Lpar1 Cre-driver line available to selectively label our cohort of Martinotti cells it was impossible to use channelrhodopsin to selectively activate them and map their outputs. We opted instead to use LSPS to map the development of global inhibition onto L4 spiny stellate neurons, by using a Cesium-based electrode solution and recording at the reversal potential for glutamate (Xu & Callaway, 2009).

5.6.1. Mapping the development of GABAergic input onto L4 spiny stellate cells

I mapped GABAergic input from within a cortical column onto a total of 52 L4 spiny stellate neurons. To ensure I was recording from this population, I targeted small cells in L4 with circular somas, and, upon breakthrough, injected suprathreshold current to evoke an action potential, before the Cesium electrode solution dialyzed into the cell and I switched to voltage-clamp. To ensure I didn't record from interneurons, I

examined action potential shape (short spike half-width and deep after-hyperpolarisation amplitude). Cells were split according to developmental stage into three groups: P4-P6 (n = 16), P7-P9 (n = 15) and P10-P15 (n = 21). I aligned each map by the L4/L5a border and calculated normalised vertical profiles for each cell (Fig. 4.8A). According to the normalised vertical profiles, there is a transient L5b-L4 GABAergic projection, whose disappearance around P9 coincides with the end of the thalamocortical critical period for plasticity, in the barrel cortex. I next plotted the average vertical profiles for each age group, according to the same alignment (Fig. 5.8B). Group vertical profiles corroborated the presence of a transient L5b to L4 GABAergic projection. I then averaged together the maps for each age group, plotting them on the same raw pA scale (Fig. 5.8C). In accordance with data plotted in the two previous figures, I observed that at P4-P9 spiny stellate cells receive GABAergic inputs from both L5b and L4. At P4-P6, it seems even that most GABAergic input originates from L5. By P10-P15, L5 input is gone, and GABAergic input originates mostly from L4, although L2/3 also seems to provide feedback GABAergic input to spiny stellate cells. In order to examine laminar origin of GABAergic inputs in more detail, for each cell I established layer boundaries based on the pre-map DIC picture (see Methods) and determined where each input came from. For each cell, I normalised data to the cell's total GABAergic input. This allowed me to determine the relative influence of each layer providing input at each timepoint. The proportion of GABAergic input arising from each layer onto L4 spiny stellate cells is plotted in Fig. 5.8D and table 5.5. At P4-P6, L4 spiny stellate neurons received most of their GABAergic input from L5b (46± 4%), with the second strongest source of input arising locally from L4 (26± 4%). At P7-P9 there was an increase in the proportion of GABAergic input coming from L4 (48± 5%), along with a decrease of input coming

from L5b (25± 4%). Finally, at P10-P15, the vast majority of input onto L4 was mediated locally (67± 3%), with significant feedback GABAergic input coming from L2/3 (18± 2%), and very little input originating from the infragranular layers.

	Table 5.5. Proportion of total GABAergic synaptic input onto L4 spiny stellate neurons (%)						
	L6	L5b	L5a	L4/CP	L2/3/CP	Total (pA)	N
P4-P6	9± 3	46± 4	15± 2	26± 4	5± 2	1138± 151	16
P7-P9	2± 1	25± 5	15± 3	48± 5	10± 2	1671± 344	15
P10-P15	2± 1	5± 1	8± 1	67± 2	18± 2	2886± 453	21

Statistically, two-way ANOVA of GABAergic synaptic input revealed highly significant layer ($F(4, 245) = 118.4$, $p < 0.001$), and interaction effects ($F(8, 245) = 31.80$, $p < 0.001$) (Fig. 4.8D). L5b input significantly decreased throughout all three developmental timepoints. Input from L4 showed the converse effect, increasing continually throughout all developmental stages tested. There was also a significant increase in GABAergic input from L2/3 between P4-P6 and P10-P15. I next contrasted GABAergic input from each layer within a given timepoint. At P4-P6, L4 and L5b provided a significantly higher proportion of input than any other layer, with L5b also providing significantly more input than L4. At P7-P9, the same pattern was observed, except that now L4 provided a significantly higher proportion of GABAergic input than L5b. Additionally, L5a provided significantly more input than L6. At P10-P15, L4 clearly provided significantly more input than any other layer. L2/3 provided most of the remaining GABAergic input, and significantly more than L6, L5b and L5a.

Comparing normalised input data is an excellent way of determining the relative influence of each layer at a particular point in time, in a way that can be compared

across age groups without the confounding influence of increased overall synaptic input. However, normalised input data can be misleading due to reciprocity effects (discussed in Chapter 3). Having analysed normalised data, I then looked at raw input. Total GABAergic synaptic input matured significantly over development ($H(2) = 8.251$, $p < 0.05$) (Fig. 4.8D). According to post-hoc tests, there was a significant increase in total input between P4-P6 and P10-P15. I then re-analysed the contribution of each layer (in pA) to GABAergic input into L4 throughout development (Fig. 5.8E). Since raw total input data did not conform to normality and homogeneity of variance assumptions, analysis was carried out on a square root transform. Two-way ANOVA detected significant *interaction* ($F(8, 245) = 13.20$, $p < 0.001$), *layer* ($F(4, 245) = 43.65$, $p < 0.001$) and *developmental stage* effects ($F(2, 245) = 9.421$, $p < 0.001$). L5b input significantly decreased between P7-P9 and P10-P15. L4 and L2/3 GABAergic input showed the opposite effect, increasing significantly between P7-P9 and P10-P15. I then examined which layers provided most input, at each developmental stage. At P4-P6, L5b provided significantly more GABAergic input than any other layer except L4. L4 provided significantly more input than L6 and L2/3. At P7-P9, L4 began gaining preponderance, providing significantly more input than all layers except L5b. L5b provided significantly more input than L6 and L2/3 and L5a provided significantly more input than L6. Finally at P10-P15, L4 was the undisputed primary source of GABAergic input to L4, providing significantly more input than any other layer. L2/3 gained influence, providing significantly more input than L6 and L5b. L5a provided significantly more input than L6.

	Table 5.6. Total GABAergic synaptic input onto L4 spiny stellate neurons (pA)						
	L6	L5b	L5a	L4/CP	L2/3/CP	Total (pA)	N
P4-P6	89± 30	532± 93	162± 34	308± 56	46± 21	1138± 151	16
P7-P9	24± 8	474± 145	271± 78	1154± 300	242± 71	1671± 344	15
P10-P15	44± 12	126± 35	230± 57	1750± 327	489± 111	2886± 453	21

In conclusion, at P4-P6 the main source of GABAergic input onto L4 spiny stellate neurons was L5b, followed closely by L4. The L5b-L4 GABAergic projection was transient, and downregulated throughout development, in contrast to local L4 inhibition, which increased. At P7-P9 there was a reversal of roles, with L4 dominating GABAergic signalling onto itself, and L5b providing the second highest source of input. By P10-P15, the L5b-L4 projection had been virtually eliminated, with L4 spiny stellate cells receiving the vast majority of inhibition from their home layer, along with feedback inhibition from L2/3. Therefore, the data supports our initial hypothesis of a transient feedback GABAergic projection from L5b to L4, closing a loop with the transient excitatory projection from L4 to L5b Lpar1-GFP Martinotti cells.

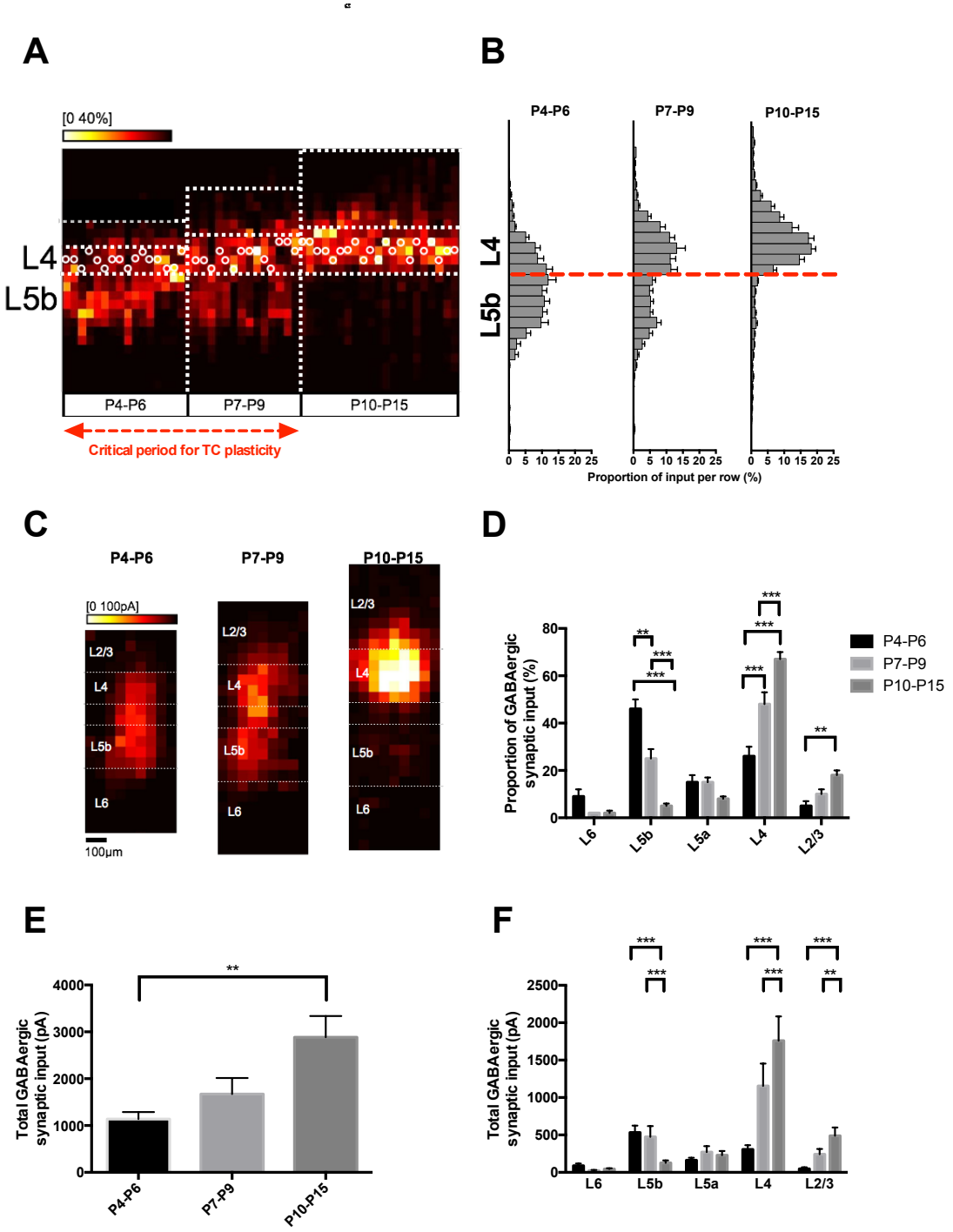


Figure 5.8. Development of GABAergic input onto L4 spiny stellate cells. A. Normalised vertical profile of GABAergic input for each L4 spiny stellate cell recorded (n = 52; P4-P6 n = 16; P7-P9 n = 15; P10-P15 n = 21; numbers apply to B-F as well). Each column corresponds to a cell, and each pixel in the column to the proportion of total GABAergic input derived from that 50μm row. **B.** Average normalised vertical profile of GABAergic inputs onto L4 spiny stellate cells by age group. **C.** Average LSPS maps of GABAergic input onto L4 spiny stellate cells by age group. **D.** Proportion of total synaptic GABAergic synaptic onto L4 spiny stellate cells arising from each cortical layer at different developmental stages. **E.** Total GABAergic synaptic input onto L4 cells. **F.** Total GABAergic synaptic input arising from each cortical layer. Red denotes analysis of data excluding L4. Y axis plotted on two scales to detail changes in L5b and L2/3 input. Error bars are ± SEM. * $p < 0.05$; ** $p < 0.01$; *** $p < 0.001$.

5.7. Experience-dependence of the development of GABAergic input onto L4 spiny stellate neurons

My previous results revealed a reconfiguration of an excitatory-inhibitory loop between L5b and L4 during the critical period for thalamocortical plasticity (Crair & Malenka, 1995; Isaac et al., 1997). These observations led us to question whether this remodelling of synaptic connections onto L4 is experience-dependent. To test this, infraorbital nerve (ION) transections were performed on P0-P1 Lpar1-GFP mouse pups. ION transection is an effective method of sensory experience manipulation, which, if performed on the day of birth, results not only in altered sensory experience, but also disturbed barrel organisation (Erzurumlu & Gaspar, 2012).

To test whether or not early GABAergic input requires normal sensory experience for correct development, I mapped afferent GABAergic input onto a total of 23 L4 spiny stellate cells in ION-sectioned pups at P4-P6 (n = 11) and P10-P15 (n = 12) and compared this to our previous results in control pups. Figure 5.9A (left) depicts average maps for Control and ION-sectioned animals, at P4-P6 and P10-P15. At P4-P6, both Control and ION-sectioned animals receive GABAergic input from L5b and L4, with a higher proportion of input seeming to arrive from L5b. However, it can be seen from the average maps that the total amount of input differs markedly between the two conditions. At P10-P15, the reverse effect can be observed. Whereas differences in total input are not immediately obvious, it is clear that the feedback GABAergic projection from L5b to L4 is not eliminated in ION-sectioned animals (Fig. 5.9A, right). In figure 5.9B I plotted the average vertical profiles at P4-P6 (left) and P10-P15 (right) for ION-sectioned (black) and Control (grey) animals. Whereas at P4-P6 the profiles appear largely overlapping and similar, at P10-P15 it is readily

apparent that a bi-modal distribution of input is still present in the ION-sectioned animals. For this group, L4 spiny stellate cells seem to, at P10-P15, still receive input from L5b, whereas in the control group little to no input from this layer is present.

In the previous section of this chapter, I reported that L4 spiny stellate neurons received a transient feedback GABAergic projection from L5b, which was eliminated by P10-P15. L4 and L5b are responsible for the majority of GABAergic inputs onto spiny stellate cells until P7-P9. After this period, L4 and L2/3 provide virtually all GABAergic input. Perturbing sensory experience seems to affect the developmentally-regulated elimination of the GABAergic feedback projection from L5b to L4. I investigated this effect further by looking at the development of laminar organisation of GABAergic input onto L4 spiny stellate cells in ION-sectioned and control animals (Fig. 5.9C, D). In essence, I aimed to answer the following questions:

1) Does the reorganisation of afferent GABAergic input onto L4 spiny stellate cells in ION-sectioned animals recapitulate that observed in Controls?
2) Does the laminar profile of GABAergic input onto L4 spiny stellate cells differ between Control and ION-sectioned animals at P4-P6 or at P10-P15?

To answer question 1, I performed two-way ANOVA of normalised laminar input onto L4 spiny stellate cells, using *developmental stage* and *layer* as factors. There were significant effects of *layer* ($F(4, 105) = 27.96$, $p < 0.001$) and *interaction* ($F(4, 105) = 12.17$, $p < 0.001$). Post-hoc tests found a significant decrease in proportion of input originating from L5b, and a significant increase in proportion of input from L4,

replicating the effect observed in Control animals. Contrary to these animals, there was no significant increase in proportion of L2/3 input.

Table 5.7. Proportion of total GABAergic synaptic input onto L4 spiny stellate neurons in ION-section vs Control groups (%)

	L6	L5b	L5a	L4/CP	L2/3/CP	Total (pA)
P4-P6$_{ION}$	6± 2	51 ±86	16± 5	22± 6	6± 2	395± 47
P4-P6$_{Ctrl}$	9± 3	46± 4	15± 2	26± 4	5± 2	1138± 151
P10-P15$_{ION}$	6± 2	24± 3	8± 2	47 ±4	15± 3	2707 ±324
P10-P15$_{Ctrl}$	2± 1	5± 1	8± 1	67± 2	18± 2	2886± 453

P4-P6$_{ION}$: n = 11 cells; P10-P15$_{ION}$: n = 12 cells. P4-P6$_{Ctrl}$: n = 16 cells; P10-P15$_{Ctrl}$: n = 21 cells

For question 2, I compared the laminar profiles of normalised GABAergic input onto Control and ION-sectioned animals at P4-P6 and P10-P15. To this end, I conducted two-way ANOVA of normalised laminar input onto L4 spiny stellate cells with *layer* and *condition* (ION vs Control) as factors. Separate ANOVAS were conducted for the P4-P6 and P10-P15 groups. At P4-P6, only a significant *layer* effect was achieved ($F(4, 120) = 39.27$, $p < 0.001$). No significant *condition* effect was observed, and post-hoc tests comparing proportion of input from each layer in Control and ION-sectioned animals found no differences in laminar profile. At P10-P15, both a significant *layer* ($F(4, 155) = 211$, $p < 0.001$) and *interaction* effect ($F(4, 155) = 23.41$, $p < 0.001$) were observed. Comparing ION-sectioned and Control groups, I found that at P10-P15 L5b provided significantly more normalised GABAergic input in ION-sectioned than Control animals. L4, on the other hand, provided significantly less input in ION-sectioned than Control animals. In conclusion, the data analysed suggests that sensory deprivation prevents elimination of the previously described transient L5b-L4 GABAergic projection, halting this transient circuit in the state displayed at P7-P9, during the critical period for thalamocortical plasticity in the barrel field.

I next focused on analysing raw GABAergic input in pA. The average maps plotted in figure 5.9A suggest that ION-sectioning could also have affected total afferent GABAergic input onto L4 spiny stellate cells. To test this hypothesis, I used two-way ANOVA with *age* and *condition* as factors. Since dada did not conform to the homogeneity of variance assumption required for ANOVA, analysis was performed on the square root transformation of total GABAergic input data. Two-way ANOVA yielded a significant *age* effect ($F(1, 51) = 36.86$, $p < 0.001$). (Fig. 5.9D, table 5.8). Total GABAergic input increased significantly between P4-P6 and P10-P15 for both Control and ION-sectioned animals. However, at P4-P6, total GABAergic input onto L4 spiny stellate cells was significantly higher for the Control group than for ION-sectioned animals. By P10-P15, no statistically significant difference could be observed.

Table 5.8. Total GABAergic synaptic input onto L4 spiny stellate neurons in ION-sectioned vs Control groups (pA)

	L6	L5b	L5a	L4/CP	L2/3/CP	Total
$P4\text{-}P6_{ION}$	21± 8	184 ±30	65± 19	96± 32	26± 10	395± 47
$P4\text{-}P6_{Ctrl}$	89± 30	532± 93	162± 34	308± 56	46± 21	1138± 151
$P10\text{-}P15_{ION}$	165± 47	593± 67	242± 57	1233± 177	471± 128	2707 ±324
$P10\text{-}P15_{Ctrl}$	44± 12	126± 35	230± 57	1750± 327	489± 111	2886± 453

$P4\text{-}P6_{ION}$: n = 11 cells; $P10\text{-}P15_{ION}$: n = 12 cells. $P4\text{-}P6_{Ctrl}$: n = 16 cells; $P10\text{-}P15_{Ctrl}$: n = 21 cells

To confirm that a reciprocity effect could not explain the statistically significant differences found in normalised data, I repeated analysis of questions 1 and 2 on raw pA data, transformed using a square root function. Using two-way ANOVA to contrast laminar profiles of ION-sectioned animals at P4-P6 and P10-P15 I found significant effects of *layer* ($F(4, 105) = 20.22$, $p < 0.001$), *developmental stage* ($F(1, 105) = 140.08$, $p < 0.001$) and *interaction* ($F(4, 105) = 9.55$, $p < 0.001$). Post-hoc tests

revealed a significant developmental increase in GABAergic input from all layers, congruent with the previously reported increase in total GABAergic input.

When comparing the laminar profile of total GABAergic input between ION-sectioned and Control animals, two-way ANOVA revealed *layer* ($F(4, 125) = 23.77$, $p < 0.001$) and *condition* ($F(1, 125) = 27.19$, $p < 0.001$) effects. At P4-P6, L5b and L4 provided significantly more GABAergic input in Control animals than their ION-sectioned counterparts. At P10-P15, an *interaction* ($F(4, 155) = 5.95$, $p < 0.001$) and *layer* effect ($F(4, 155) = 46.16$, $p < 0.001$) were observed. Post-hoc comparisons revealed that L5b provided significantly more GABAergic input in ION-sectioned animals than controls, at P10-P15.

In summary, altering the sensory experience of mouse pups by ION transection resulted in developmental upregulation of the L5b feedback GABAergic projection to L4 and affects early development of global afferent GABAergic input.

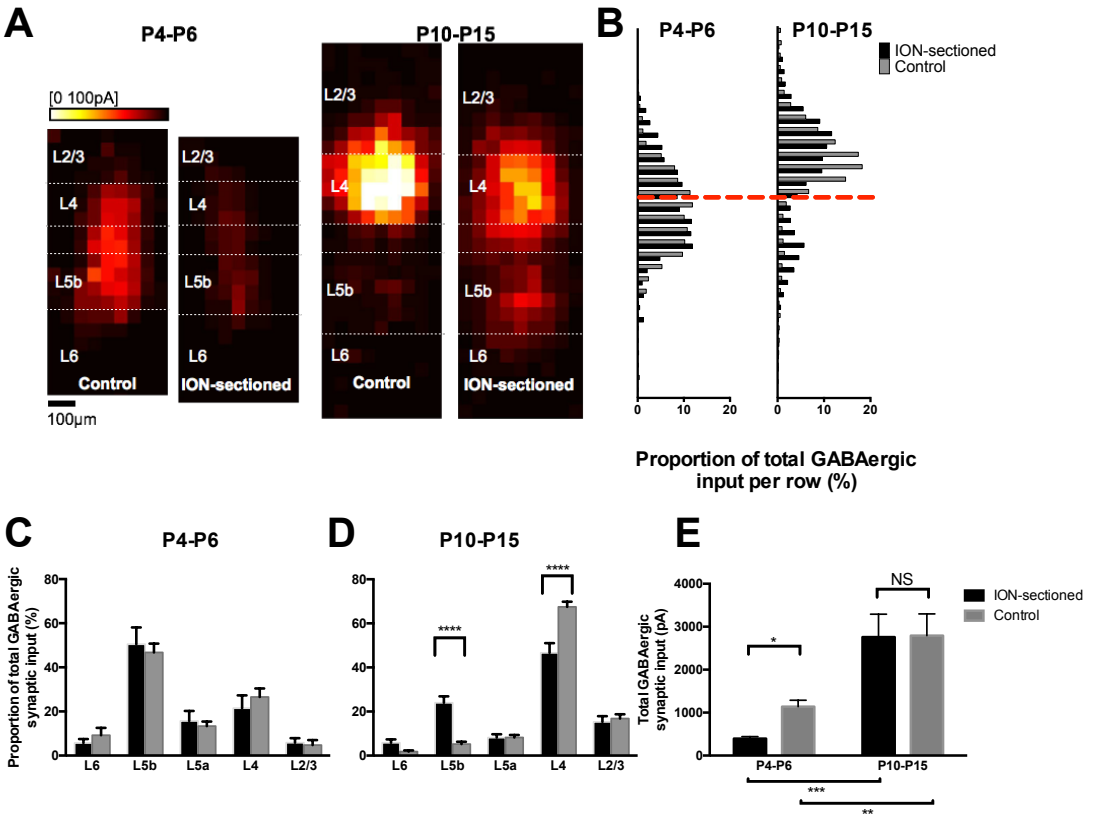


Figure 5.9. Development of GABAergic input onto L4 spiny stellate cells of ION-sectioned and control animals. A shows average LSPS maps for inhibitory inputs onto L4 spiny stellate cells for control and ION-sectioned groups at P4-P6 and P10-P15. Cell numbers were: P4-P6$_{ION}$: n = 11 cells; P10-P15$_{ION}$: n = 12 cells; P4-P6$_{Ctrl}$: n = 16 cells; P10-P15$_{Ctrl}$: n = 21 cells. Numbers applt to B-E as well. In **B** I plotted the average vertical profiles of inhibitory inputs onto cells from each group at the same ages. **C** and **D** show the proportion of total inhibitory synaptic input onto L4 spiny stellate cells arising from each cortical layer at different developmental stages for ION-sectioned versus Control L4 cells. **E** shows total inhibitory synaptic input onto L4 cells of ION-sectioned versus Control pups. Error bars are ± SEM, Control group in dark grey, ION-sectioned in black.

5.8. Discussion

Summary of results

In the experiments reported in this chapter, I described a population of cortical interneuron labelled fluorescently in the Lpar1-GFP transgenic mouse. These cells were mostly found in cortical layers 5b and 6, and expressed Lhx6, indicative of *Nkx2-1*-specification and MGE origin (Xu et al., 2004; Butt et al., 2005; Liodis et al., 2007; Xu et al., 2008; Du et al., 2008). The morphology of recovered cells was consistent with previously reported Martinotti cells, infragranular SST^+ interneurons characterised by axons projecting to L1 (Wang et al., 2004; Ma et al., 2006). L5b Martinotti cells have been reported to project not only to L1 but also L4 (Wang et al., 2004), which was also the case for Lpar1-GFP MCs. In terms of network integration, Lpar1-GFP MCs received facilitating input from the thalamus from the earliest age recorded, and the proportion of cells receiving thalamic input increased throughout development. Regarding cortical excitatory input, Lpar1-GFP MCs were strongly and dynamically integrated in the developing cortical network. Prior to P7, most of their early excitatory input originated from L4, with L5b also providing a high amount of excitation. At P7-P9, L4 input was still present but secondary to L5b. Total excitatory input onto these neurons peaked at this period. By P10-P15, L4 input had disappeared, and most excitation arose from L5b/6. To test whether connectivity with L4 was reciprocal, I mapped the development of GABAergic input onto L4 spiny stellate cells (Xu & Callaway, 2009). This revealed that prior to P7, the dominant source of GABAergic input onto L4 spiny stellate cells was L5b, with L4 coming second. L4 inhibitory inputs emerged at P7, dethroning L5b as the dominant source of GABAergic input. By P10-P15, L4 became the dominant source of GABAergic input onto L4 excitatory neurons as previously reported for mature cells (Kätzel et al.,

2010), and by this timepoint L5b input had been eliminated. Using ION transection, I found that early sensory activity plays an important role in GABAergic innervation of L4. At P4-P6, ION transectioned animals showed a drastic reduction in total GABAergic input compared to control animals. Whilst I observed for ION-sectioned animals a decrease in the amount of GABAergic input from each layer compared to controls, examining the normalised laminar distribution of input revealed that the organisation of GABAergic input (the proportion of input arising from each layer) was preserved. At P10-P15, the reverse situation was observed. Total GABAergic input onto L4 spiny stellate cells was undistinguishable between ION-sectioned and control animals, but laminar organisation of inputs was altered. Whereas in control animals throughout development L5b input disappeared and L4 input increased, in ION animals L5b input actually increased, as did L4 input. Moreover, ION-sectioned animals received less input from L4 than their control counterparts. This suggests that compensatory upregulation of infragranular inhibition made up for loss of local L4-derived GABAergic input.

5.8.1. Discussion of methodology

One caveat of the input mapping approach used is that since glutamate uncaging is blind to the identity of pre-synaptic cells stimulated, I cannot conclude with 100% certainty that, within L5b, early GABAergic input onto L4 spiny stellate neurons derived from Martinotti cells and not another cell class. However, given their axonal arborisations and reception of L4 excitation, as well as the fact that very few other interneuron types project across layers (Markram, et al., 2004; Wang et al., 2004), L5b Martinotti cells present the most likely candidate to subserve this projection,

making it a plausible assumption that they are the L5 interneurons projecting early in development to L4.

To investigate the role of early sensory experience in the development of GABAergic circuits, I performed sections of the infraorbital nerve in P0-P1 mice. One caveat of this approach is that it is known to induce neurodegenerative changes along the peripheral to central pathway until the thalamus, meaning it is not a pure approach for analysing the effects of sensory experience in circuit development (Erzurumlu & Gaspar, 2012). However, the alternatives of whisker plucking or trimming, whilst purer in their sensory but not degenerative effect, fall very short of blocking afferent sensory activity, as passive stimulation of the snout will still evoke activity (Erzurumlu & Gaspar, 2012). Moreover, whisker trimming is challenging at the earliest neonatal days, and since I was interested in examining the effects of sensory deprivation on the organisation of very early circuits (P4 onwards), we judged it best to perform ION sectioning than trimming or plucking whiskers.

5.8.2. Intrinsic and network development of Lpar1-GFP MCs

Both intrinsic physiological parameters (for instance input resistance and membrane time constant) and total amount of excitatory input onto Lpar1-GFP MCs appeared largely mature by P7-P9. Given our focus was on early circuit formation, my window of investigation did not extend beyond P15, and as such it is unclear whether the parameters analysed truly attained maturity by this stage or would subsequently show changes. It would be of interest to compare the maturation profile of deep-layer Martinotti cells with other interneurons, in order to test the idea that interneuron subtypes show different maturation profiles. However, at this point in time little data

is available, and the existing studies were conducted on FS interneurons in different cortical areas and layers (Doischer et al., 2008; Lazarus & Huang, 2011; Pangratz-Fuehrer & Hestrin, 2011; Yang et al., 2013a), hampering direct comparison. There is currently a lot of focus on the idea that in the mature cortex, different cortical interneuron types are involved in distinct functions during sensory and cognitive processing (Lee et al., 2012; Wilson et al., 2012; Fu et al., 2014). It is likely that there is a similar differential engagement of interneuron types by distinct steps and processes in cortical circuit development. Indeed, reports suggest that in the hippocampus, the first targets of GABAergic synapses are dendrites (Tyzio et al., 1999; Hennou et al., 2002), and early-generated, dendrite-targeting SST^+ hub neurons play an important role in synchronising network activity across vast numbers of neurons (Bonifazi et al., 2009; Picardo et al., 2011). In the visual cortex, soma-targeting PV^+ interneurons have been proposed to be involved in regulating the critical period for plasticity (Hensch, 2005; Levelt & Hübener, 2012), and in the barrel cortex, the emergence of potent thalamic-driven feed-forward inhibition in L4 is thought to shorten the temporal coincidence detection window for thalamic afferent and L4 excitatory activity, contributing to the closure of the critical period for plasticity (Daw et al., 2007a; 2007b; Chittajallu & Isaac, 2010). It could therefore be that the developmental role of PV/FS interneurons is to regulate critical periods of plasticity, whereas SST/NFS interneurons are pioneers that coordinate early networks.

It was interesting to observe cross-laminar excitatory and inhibitory connectivity at ages as early as P4-P6. This has only been reported previously for SPns (Viswanathan et al., 2012). Most studies examining early pyramidal-interneuron communication have employed paired recordings, which preclude testing of cross-laminar

connections (Pangratz-Fuehrer & Hestrin, 2011; but see Viswanathan et al., 2012; Yang et al., 2013a). The interest of such results lies not only on the fact that robust connections were observed between two non-adjacent layers, but perhaps even more so on the fact that connectivity patterns were dynamic and circuits were rearranged throughout development. For instance, judging from the P10-P15 home-layer dominated pattern of excitation onto Lpar1-GFP MCs, it would be entirely reasonable to suppose that throughout development, these cells simply accrue more and more glutamatergic inputs from neurons in their own layer. This piece-by-piece assembly view does not fit with my results, strengthening the notion of transient and dynamic motifs in the neonatal cortex. It would be interesting to further explore this issue. While such transient circuits do not seem present in feed-forward excitatory pathways connecting L4 and L2/3 (Bureau et al., 2004) or those connecting L2/3 and L5 pyramidal neurons (Anastasiades & Butt, 2012), it may be that this is a property of at least certain types of GABAergic interneurons. In line with the previously-mentioned suggestion that PV^+ and SST^+ interneurons may carry out different developmental functions, it would be of interest to track not only their intrinsic but also their network development, and test whether their integration in the pyramidal network progresses via static, accruement-based strategies, or through dynamic, rearranging circuit motif programs.

5.8.3. The functional role of early, transient connectivity between L5b Martinotti and L4 excitatory neurons

Having identified a thalamic-driven transient reciprocal connection between L4 excitatory and L5b inhibitory neurons, I would now like to discuss possible functions for this circuit. The first view that should perhaps be considered is that there is no

processing function. It could be that transient innervation of L4 by Martinotti cells merely represents early exuberance of Martinotti cell axons on their long journey from L5b to L1 (Innocenti & Price, 2005). This interpretation appears unlikely on the basis of several points: 1) it is not a unidirectional pathway that is transiently expressed, but rather a reciprocal loop connecting the two layers. It should be conceded that L4 axons innervating L5b Martinotti cells could be equally exuberant and on their way to form synapses with L5 or L6 pyramidal cells (Lübke et al., 2000; Feldmeyer, 2012), but it also seems improbable that energy and metabolic resources would be invested in establishing not one, but two transient pathways within the same circuit; 2) reciprocal L4-L5b connectivity at P4-P9 is robust, with evoked IPSC and EPSC amplitudes occurring on the order of 50-100pA which are large amplitudes in the context of such an early developmental stage; 3) Martinotti cells have been shown in mature circuits to have axons that arborise not only in L1 but also L4, which argues against a purely trophic or guidance function, since that would no longer be required at this stage (Wang et al., 2004). The mature presence of such axons when L4 spiny stellate cells clearly no longer receive L5b inhibition further raises the question of what cells they could innervate in L4, with possible targets including L4 PV^+ FS interneurons, an idea that will be considered in the general discussion (Chapter 6). Moreover, the presence of a cross-laminar projecting interneuron at the heart of an early circuit connecting thalamus, L5b and L4 raises interesting circuit computational possibilities that fit well with empirical observations on thalamocortical plasticity and early network oscillations. The P4-P9 window over which I observed a reciprocal L4-L5b circuit is a period that overlaps with key developmental events in the barrel cortex, namely the critical period for thalamocortical plasticity (Crair & Malenka, 1995; An et al., 2012), the emergence of PV-mediated feed-forward inhibition in L4

(Daw et al., 2007b; Chittajallu & Isaac, 2010) and early gamma oscillations (Minlebaev et al., 2011; Yang et al., 2013b) as well as spindle bursts (Colonnese et al., 2010; Hanganu-Opatz, 2010; Khazipov et al., 2013). This places Lpar1-GFP Martinotti cells at the forefront of two major developmental phenomena: thalamocortical plasticity and early network oscillations.

Involvement in thalamocortical plasticity

Recent *in vivo* work has revealed that early gamma oscillations synchronise topographically-corresponding thalamic and cortical domains and could serve to promote thalamocortical plasticity, by replaying afferent input multiple times at the thalamocortical synapse (Minlebaev et al., 2011; Yang et al., 2013b). At the synaptic level, maturation of thalamic inputs onto L4 spiny stellate cells has been shown to occur via NMDAR-dependent synapse unsilencing (Crair & Malenka, 1995; Isaac et al., 1997). GABA has been proposed as a possible source of depolarisation for relief of the voltage-dependent blockade of silent synapse NMDARs by Mg^{2+} (Ben-Ari et al., 1997; 2007), and there is evidence for this in the developing cortex (Wang & Kriegstein, 2008) and newborn hippocampal granule cells (Chancey et al., 2013). At first glance, PV^{+} FS interneurons in L4 would appear as attractive candidates to play this role, as they receive strong thalamic input and make potent GABAergic synapses with L4 spiny stellate neurons (Sun et al., 2006; Cruikshank et al., 2007). However, both afferent thalamic inputs and efferent connections from L4 FS interneurons are formed late in the first postnatal week (Daw, Ashby, & Isaac, 2007a; Chittajallu & Isaac, 2010), suggesting that they are not the principal mediators of depolarising GABA-mediated synapse unsilencing. In my experiments I was able to use glutamate uncaging to reveal that the earliest, strongest source of GABAergic input onto L4

spiny stellate neurons is actually L5b. Although my evidence is not causal, I would like to propose that this projection arises from Martinotti cells, possibly Lpar1-GFP positive, based on two observations. First, these cells have axons with prominent arborisation in L4 (Wang et al., 2004), and second, they receive excitatory input from L4 over the same time-course that L4 receives GABAergic input from L5b.

A combination of early, facilitating thalamic afferent input and robust GABAergic outputs to L4 means that Lpar1-GFP MCs are well suited to play a role as a facilitator of thalamocortical plasticity. Given that early thalamocortical synapses with L4 are largely silent (Isaac et al., 1997; Kidd & Isaac, 1999), spike trains in the thalamus would result in glutamate binding at NMDARs in L4, but likely not enough depolarisation of these cells for removal of the voltage-dependent Mg^{2+} block, correlated spiking activity, and ensuing NMDAR-driven plasticity processes. In contrast, thalamic input could trigger spiking in Martinotti cells, due to the facilitating nature of thalamic-Martinotti input and the hyperpolarised spike threshold of these cells. GABAergic projections from these cells onto L4 spiny stellate cells could under a shifted GABA reversal potential depolarise these neurons enough to activate NMDARs, promote correlated spiking, and initiate NMDAR-dependent synaptic plasticity signalling cascades. In support of this view, the reversal potential for GABA at L4 spiny stellate neurons is consistent with a depolarising action over the time period at which L5b-L4 GABAergic projections are present (Daw et al., 2007a). Further to robust thalamic activation of Lpar1-GFP Martinotti cells, excitation of L4 cells would be fed back to Martinotti cells via early glutamatergic projections, further driving them to spike and enabling sustained activity in the thalamus-L4-L5b circuit, which could couple thalamic and cortical activity for prolonged periods, promoting

LTP. Due to facilitating thalamic and cortical inputs onto Martinotti cells (Kapfer et al., 2007; Silberberg & Markram, 2007; Tan et al., 2008), this effect would be particularly robust during higher frequency activity, which has indeed been reported early in development through gamma oscillations at the thalamocortical synapse (Minlebaev et al., 2011; Yang et al., 2013b). Based on *in vivo* pharmacological experiments, the involvement of GABA in early gamma oscillations appears to be limited, at least before P6 (Minlebaev et al., 2011). However, pharmacological control of activity can be challenging *in vivo*, and a more compelling demonstration of the lack of involvement of GABA in this early rhythm would involve genetic silencing of GABAergic elements in the cortical circuit. Even if Lpar1-GFP MCs are not involved in early gamma oscillations, they would be in a good position to relay thalamic input, sustain activity in the L4-L5b circuit, and aid L4 in fulfilling depolarisation requirements for NMDAR activation.

It would be technically challenging to test the involvement of Lpar1-GFP MCs in thalamocortical plasticity, as accurate measurements of LTP at the single cell level require whole-cell access to study the potentiation of sub-threshold inputs. This would have to be performed without disrupting native intracellular chloride concentrations that sustain the depolarising action of GABA. One possibility would be to study LTP non-invasively at the population level, using field potential recordings in a single barrel. To do this, I would pair thalamic afferent electrical stimulation with activation of L5b Martinotti cells. In the absence of a Cre driver line selective for these neurons, this could be performed on SST-Cre or Nkx2-1 Cre lines. By expressing the heterologous P_2X_2 channel (Zemelman et al., 2003) in Cre^+ cells, laser stimulation could be directed to a spot in L5b from which GABAergic input onto L4 cells had

been verified in the same slice. This experiment would require also stimulation of a separate, control pathway without paired L5b stimulation. By comparing post-pairing thalamocortical transmission in the two pathways, I would gain insight on whether L5b GABAergic inputs to L4 facilitate thalamocortical LTP.

Spatiotemporal control of spindle burst activity

Early gamma oscillations and spindle bursts occur over a time at which thalamocortical and intra-cortical synapses are highly plastic and it is interesting to consider early network oscillations in the context of developmental synaptic plasticity, rather than isolating these phenomena from each other. The timing of pre- and post-synaptic activity is critical for plasticity (Bi & Poo, 2001; Dan & Poo, 2004; Caporale & Dan, 2008; Feldman, 2009), and network activity in the developing brain may assist induction of synaptic plasticity and maturation by promoting correlated, synchronised spiking in pre- and post-synaptic elements of a circuit within plasticity induction time windows (Khazipov et al., 2013).

Contrary to early network activity in the hippocampus (Ben-Ari et al., 1989; Dzhala et al., 2005; Sipilä et al., 2006; Tyzio et al., 2006), cortical spindle bursts have been shown *in vivo* not to rely on depolarising GABA for their generation or maintenance of their frequency characteristics. However, blockade of $GABA_A$ receptors resulted in increased incidence, spatial expansion of the cortical territory engaged and prolonged duration of spindle bursts (Minlebaev et al., 2007; 2009; Yang et al., 2009), implying that a GABAergic interneuron population is crucial for controlling the spatiotemporal spread of these oscillations. It is possible that Lpar1-GFP MCs provide such control. They are keenly suited to detect coincident high frequency activity in the thalamus

and cortex by virtue of facilitating excitatory connections from these sources. If Lpar1-GFP MC inputs to L4 are inhibitory or shunting (Borg-Graham et al., 1998; Gao et al., 1998; Lu & Trussell, 2001; Gulledge & Stuart, 2003), then during bouts of high frequency cortical activity induced by thalamic afferents, Lpar1-GFP MCs could provide feedback inhibition across the cortical column, preventing runaway excitation. To test this possibility, it would be of interest to record from Lpar1-GFP MCs *in vivo* during spindle burst oscillations, and examine how their spiking activity aligns with the oscillation phase. Another interesting experiment would be to express channelrhodopsin selectively in these neurons *in vivo* and examine how their coordinated activation affects spindle burst network dynamics. Given the current technical challenges to using optogenetics in the developing brain (see Chapter 3), one alternative would be to monitor network activity and effective connectivity in real time in slices using calcium imaging (Bonifazi et al., 2009; Picardo et al., 2011), and examine how stimulation of individual Lpar1-GFP MCs by current injection affects ongoing network oscillations.

It is unclear at the moment whether Lpar1-GFP Martinotti cells depolarise or hyperpolarise L4 spiny stellate neurons during the period in which they form reciprocal connections, and further experiments are required to clarify this issue in order to understand the function of this early circuit. What is readily apparent is that Lpar1-GFP MCs are pioneers that integrate early and richly in cortical excitatory circuitry and have characteristics that enable them to strongly influence activity in L4, meaning they merit further investigation.

5.8.5. Early sensory activity and the maturation of GABAergic circuits

The ION-sectioning experiment results suggest an experience-dependent developmental double-dissociation between laminar organisation and total amount of afferent GABAergic input onto L4 excitatory neurons. Total GABAergic input in P4-P6 ION-sectioned animals was sharply reduced in comparison to controls. This was driven by a reduction in GABAergic inputs originating from all cortical layers, that nonetheless preserved, compared to the control group, the laminar distribution of normalised input. GABAergic inputs from each layer were thus precisely scaled down by a factor that preserved their relative influence on L4. Conversely, at P10-P15, total GABAergic input was undistinguishable between control and ION-sectioned animals, largely due to a compensatory increase in GABAergic input from L5b and L6. Thus, infragranular input was not merely maintained in ION-sectioned animals at P10-P15: it was actively increased, whereas in control animals, input from these layers decreased developmentally. This increase worked to offset the decrease in total GABAergic input from L4 observed in ION-sectioned animals. Therefore, even though total GABAergic input was restored in P10-P15 ION-sectioned animals, the laminar organisation of this input was altered.

Reviewing the effect of sensory deprivation on developing GABAergic circuitry

The role of sensory experience in the development and plasticity of thalamocortical and intracortical excitatory circuitry in the barrel field has been extensively researched (Van der Loos & Woolsey, 1973; Fox, 1992; Glazewski & Fox, 1996; Glazewski et al., 1998; Kossut, 1998; Barth et al., 2000; Stern et al., 2001; Allen et al., 2003; Celikel et al., 2004; Clem et al., 2008; Erzurumlu & Gaspar, 2012). However, comparatively little attention has been devoted to understanding how

sensory activity shapes the maturation of inhibitory circuits in the barrel cortex. The classic model of study has been rat visual cortex, whose particular timings and loci for sensory-induced plasticity (Hensch, 2005; Maffei & Turrigiano, 2008; Levelt & Hübener, 2012) do not readily translate to the barrel field. An initial perspective was that that sensory deprivation during the critical period for ocular dominance plasticity arrests the development of cortical circuitry, preserving it in an immature state (Blasdel & Pettigrew, 1978; Fagiolini et al., 1994; Bartoletti et al., 2004). Subsequent work revealed a complex interplay between timing of visual deprivation, cortical layer and cell type in monocular V1, suggesting that interneuron types show different responses to sensory deprivation (Desai et al., 2002; Maffei et al., 2004; Maffei et al., 2006; Maffei & Turrigiano, 2008).

In the barrel cortex, initial studies following full whisker removal at birth reported a decrease in density and proportion of GABAergic neurons in L4 at P60 (Micheva & Beaulieu, 1995a; 1995b), with a corresponding loss of up to two thirds of GABAergic synaptic contacts (Micheva & Beaulieu, 1995a; 1995b; Sadaka et al., 2003) and a 44% reduction in density of thalamocortical synapses (Sadaka et al., 2003). Jiao and colleagues (Jiao et al., 2006) removed a whisker row at P7 and found a downregulation of perisomatic GABAergic boutons in spiny stellate cells, as well as a decrease in the number of PV-expressing cells at P30. The authors also reported a reduction in IPSC amplitude in L4 spiny stellate neurons of deprived barrels. In a subsequent study using the same deprivation protocol, mature FS cells in deprived cortex showed decreased intrinsic excitability, lower frequency of occurrence of spontaneous EPSCs and lower TC-EPSC amplitude in whisker-deprived barrels, whereas no differences were evident for regular-spiking non-pyramidal cells (Sun,

2009). These studies suggest that whisker deprivation during the first postnatal week results in weakened inhibition of L4, chiefly through alterations in PV^+, perisomatic-targeting interneurons. These data are consistent with findings that in culture, chronic blockade of activity leads to a decrease in output unitary IPSC amplitude mediated by PV^+ cells onto L4 excitatory neurons, but no change in SST^+ cell output (Bartley et al., 2008), and that perisomatic innervation is decreased by chronic activity blockade with TTX (Chattopadhyaya, 2004).

Activity-regulation of L4 and L5b GABAergic inputs onto spiny stellate neurons

ION sectioning eliminated the transmission of whisker-related information from the periphery to the barrel cortex. At P4-P6, this would result in decreased afferent excitation to thalamorecipient layers. Moreover, de-afferentiation has been shown to halve the rate of occurrence of early gamma oscillations and spindle bursts (Yang et al., 2009; Yang et al., 2013b). Gamma oscillations entrain strong excitatory activity in infragranular layers and L4 (Yang et al., 2009; Minlebaev et al., 2011; Yang et al., 2013b), and spindle bursts involve waves of excitatory activity that span the entire depth of the cortex (Yang et al., 2009; Khazipov et al., 2013). Therefore, ION transection would be predicted to reduce overall levels of excitation not only in thalamorecipient neurons, but across all layers of the somatosensory cortex. Activity is an important regulator of the formation and maturation of GABAergic synapses (Huang et al., 2007; Kuzirian & Paradis, 2011; Frias & Wierenga, 2013), and as such it is possible that in face of reduced thalamic and cortical excitation, GABAergic interneurons afferent to L4 formed weaker synapses with L4 spiny stellate neurons, matching reduced excitation levels in the cortex (Maffei & Turrigiano, 2008). This could occur via formation of a lower number of synaptic contacts or the same number,

but individually weaker synapses. Given the early disruption of sensory activity in my experiments, my results at P4-P6 likely reflect altered activity-dependent initial circuit formation, rather than homeostasis. Even though overall GABAergic drive was greatly reduced, laminar organisation of inputs was precisely maintained, suggesting that at least initial, pre-synaptic layer-specific targeting of GABAergic contacts to the correct post-synaptic neurons could be experience-independent, but that activity-dependent mechanisms regulate the strength of such contacts.

By P10-P15, total afferent GABAergic input had been rescued in ION-sectioned animals, with an increase in L5b/6 input compensating for a decrease in total amount of local L4-derived inhibition. Previous reports have suggested that local inhibition in L4 is chiefly mediated by PV^+/FS interneurons (Sun et al., 2006; Cruikshank et al., 2007; Daw et al., 2007a). SST^+/NFS interneurons are present in this layer, but show highly reduced connection probability with excitatory neurons compared to PV^+/FS cells (Maffei et al., 2004; Daw et al., 2007a;), and have been reported to mostly inhibit PV^+ interneurons in L4 (Xu et al., 2013). It is therefore plausible to assume that local inhibition of spiny stellate neurons in L4 is chiefly FS/PV-mediated. In contrast, given the fact that few interneurons apart from Martinotti cells project across non-adjacent cortical layers, and that L5b Martinotti cells have been shown to arborise in L4 (Wang et al., 2004), it seems plausible to assume that L5b GABAergic inputs to L4 spiny stellate cells are mainly mediated by SST^+ Martinotti cells, amongst them, Lpar1-GFP cells. These assumptions help explain my findings at P10-P15 in light of previous reports that FS/PV^+ and NFS/SST^+ interneurons react differently to reduced afferent drive and activity. FS/PV^+ interneurons scale down their outputs, making fewer and weaker synapses with pyramidal cells,

(Chattopadhyaya, 2004; Jiao et al., 2006; Bartley et al., 2008; Jiao et al., 2011; Takesian et al., 2013), whereas NFS/SST$^+$ interneurons do not alter their outputs (Chattopadhyaya, 2004; Jiao et al., 2006; Bartley et al., 2008; Jiao et al., 2011). ION sectioning results in a failure to developmentally upregulate inputs from the two main sources of synaptic excitation onto L4 FS/PV$^+$ cells: the thalamus and L4 excitatory neurons. Thalamic drive onto L4 FS/PV$^+$ interneurons is reduced following sensory loss (Chittajallu & Isaac, 2010; Takesian et al., 2013), and the recurrent excitatory network in L4 does not form under whisker trimming (Ashby & Isaac, 2011). The decreased afferent input onto L4 PV cells could result in a scaling down of their outputs, which I observe in ION-sectioned animals at the mesoscopic scale as a reduction in total GABAergic input arising from this layer onto spiny stellate neurons, compared to controls. NFS/SST$^+$ interneurons appear not to scale their outputs according to experience, and in accordance with this, I observed no reduction in L5b-derived inhibition. Actually, rather than a simple maintenance of this pathway at P10-P15, I observed an upregulation of deep-layer-derived inhibition which compensated for the drop in local L4 inhibition. One possible explanation for this increase could be that during development there is a competitive interaction for common targets by FS/PV$^+$ and NFS/SST$^+$ interneurons. Under normal developmental conditions, L4 FS/PV-derived input would be upregulated as a result of the activity-dependent increase in afferent excitatory drive to these cells. L5b NFS/SST-derived input would lose this competition, as shown by the coincidence of developmental decrease in GABAergic input from this layer and increase in GABAergic input from L4. It is possible that developmentally upregulated activity in the circuit remodels the circuit configuration of L5b MCs. Satb1 is an activity-dependent transcription factor that has been shown to be involved in the terminal specification and differentiation of Lhx6+

somatostatin interneurons (Close et al., 2012; Denaxa et al., 2012). Under sensory deprivation conditions we perturb this competitive interaction, such that L4 FS/PV$^+$ cell outputs do not scale up to the same extent, creating space for NFS/SST$^+$ L5b neurons to increase their inhibitory influence in L4. It has been reported that reducing basket cell spiking and excitability reduces the proportion of target principal cells innervated (Di Cristo et al., 2007; Baho & Di Cristo, 2012). It is unclear how such repressive interactions would occur at the molecular level, especially taking into account that FS/PV$^+$ and NFS/SST$^+$ interneurons target different subcellular domains (Somogyi et al., 1998). However, a number of molecular candidates, such as NL2, have been shown to specifically regulate the strength of PV$^+$ but not SST$^+$ interneuron outputs to pyramidal cells (Chubykin et al., 2007; Gibson et al., 2009). BDNF may also mediate interactions between activity and GABAergic synaptic strength regulation (Chattopadhyaya, 2011; Kuzirian & Paradis, 2011). It is secreted in activity-dependent fashion from excitatory neurons in the cortex and hippocampus (Kokaia et al., 1993; Miranda et al., 1993; Cohen & Greenberg, 2008; Hong et al., 2008) and its receptor, TrkB, is expressed both in pyramidal cells and interneurons (Cabelli et al., 1996; Cellerino et al., 1996). Furthermore, focal deletion of BDNF in the cortex led to a decrease of GABAergic synapses at the soma of excitatory neurons and a decrease in frequency of spontaneous IPSCs in these cells (Kohara et al., 2007). It is unclear whether such a reduction was specific to perisomatic synapses or whether it may also have affected dendritic-targeting ones, presumably from SST$^+$ interneurons. Additionally, it has been suggested that basket cells may compete for control of target neurons, and that GABA could serve as an indicator of pre-synaptic interneuron activity and stronger, more efficient synapses: a less capable cell may lose targets but would still form normal innervation in retained targets (Di Cristo et al.,

2007). In agreement with this hypothesis, suppressing transmitter release from single basket cells in culture resulted in a decrease in the number of innervated principal cells without changing the pattern of perisomatic innervation (Baho & Di Cristo, 2012). The idea of competitive interactions between PV+ and SST+ interneurons early in development is, to the extent of my knowledge, a novel concept, but one that could be very interesting to explore further.

Chapter 6 – Summary and final discussion

6.1. Introduction

The original objectives of my thesis were to 1) use optogenetics to study early thalamocortical interactions and plasticity; 2) study Lpar1-GFP subplate integration into thalamic and cortical circuitry; and 3) characterise a putative interneuron population also labelled fluorescently in the Lpar1-GFP line. I would summarise the key findings of my thesis under two themes: the dynamism of early cortical circuits and the importance of pioneer cell populations. Regarding the dynamism of the immature cortex, in the opening chapter of my thesis I likened the developmental assembly of cortical circuits to the construction of a house, emphasising the role of transient cell populations, connections, activity patterns and neurotransmitter modes of signalling that are absent from the mature brain. I reported in my thesis that Lpar1-GFP SPns form a recurrent excitatory network that is largely dismantled after P5. These neurons are initially strongly engaged by the thalamus, but after the critical period for thalamocortical plasticity lose thalamic input (Chapters 3 and 4). I identified also a novel, transient reciprocal circuit connecting Lpar1-GFP Martinotti cells in L5b with spiny stellate neurons in L4 that is present until P10 (Chapter 5). Moreover, my experiments with infraorbital nerve sectioning revealed that sensory activity is a critical regulator of the strength and laminar organisation of inhibitory circuits in the cortex (Chapter 5). These findings all reinforce a view of the developing cortex as a highly dynamic entity, with mature connectivity patterns developing under patterned activity and the support of cell populations that form early dynamic scaffolds. As far as concerns pioneer cell populations, I characterised Lpar1-GFP SPns and Lpar1-GFP Martinotti cells. Both these cell types integrate early into

thalamocortical and intracortical circuits, and are well positioned in these circuits to strongly influence early thalamocortical and cortical activity patterns and plasticity. In Section 6.2 I will provide a summary of the findings of my thesis. Within each individual chapter discussion, I related my findings to the corresponding literature. In Section 6.3 I will focus on bridging findings from the different chapters of my thesis, and showing how they integrate together. I shall close in Section 6.4 by providing suggestions for what I feel would be important future avenues of research.

6.2. Summary of findings

Chapter 3 - The use of optogenetics in developing circuits

The optogenetic approach, particularly CRACM, has become a mainstay of the circuit neuroscientist's experimental toolbox. In spite of its wide implementation in mapping local and long-range circuits in a variety of brain structures (Petreanu et al., 2007; 2009; Cruikshank et al., 2010; Kätzel et al., 2010), this approach has yet to be applied fruitfully to developing mammalian neural systems largely because of the strict timeframe available to ensure sufficient gene expression of optogenetic actuators or sensors at early stages of development. The experiments I reported in my thesis help clarify the reasons for this. During the first postnatal week, it was impossible to elicit ChR65-mediated spiking in thalamic relay neurons electroporated *in utero* at E11.5 (Chapter 3). Spiking probability increased throughout development, as did the temporal precision of laser-evoked action potentials, and after P12 I could reliably drive thalamic neurons using a 473nm laser beam of modest intensity. When I examined early photo-responses in L2/3 ChR65^{+} pyramidal neurons, I found that before P5, conductances were so low they could barely be detected above noise level.

A similar increase in spiking probability occurred throughout development such that after P7 reliable spiking could be evoked. Comparison and characterisation of photo-responses in pyramidal and thalamic relay neurons at different developmental stages led me to conclude that little if any functional ChR65 expression occurs prior to P3 and therefore this early period is out of reach with the methodology available to date. Focusing on the post-P10 period, I was able to study thalamic inputs onto L4 spiny stellate, L5b pyramidal and subplate neurons. After P10, I could not find any subplate neurons that received thalamic input, a finding I later largely corroborated using electrical stimulation. All L4 spiny stellate neurons and the vast majority of L5b pyramids received direct thalamic input. On average, the amplitude of evoked thalamic inputs at L4 was stronger than that at L5b, and, although non-significant, there was a suggestion that TC-EPSC latencies in L5b were delayed relative to L4, similar to results reported *in vivo* (Constantinople & Bruno, 2013). sCRACM was only successful in a minority of L4 cells, and these preparations differed from unsuccessful ones in that prior to drug administration, average optically-evoked TC-EPSC amplitude was higher, suggesting that robust responses are required for sCRACM implementation. sCRACM revealed markedly focused thalamic input maps onto L4, eliminating inputs detected by stimulating outside of the barrel both in the vertical and horizontal dimensions.

Chapter 4 - Early, dynamic integration of Lpar1-GFP SPns in thalamocortical and cortical circuitry

Subplate neurons have been proposed to amplify early thalamic inputs and provide an important conduit for rhythmic activity in the neonatal cortex (Kanold, 2004; Luhmann, 2009; Kanold & Luhmann, 2010). Here I sought to characterise the

intrinsic development and early excitatory inputs to a subpopulation, Lpar1-GFP SPns. As reported previously for unlabelled SPns (Hanganu, 2001; Luhmann et al., 2000; 2003), Lpar1-GFP SPns show remarkable intrinsic maturity already in the early neonatal period. In my experiments I found that the transition between P2-P5 and P6-P8 marks an important point in their development, with a high number of intrinsic properties attaining maturity. This key transition in intrinsic maturity was concomitant to changes in thalamic engagement, as Lpar1-GFP SPns lost high-amplitude thalamic inputs after P5. In fact, after the critical period for thalamocortical plasticity (P0-P8), there was a sharp decline in the proportion of Lpar1-GFP SPns that received direct thalamic input, and this appeared to be driven by an overall progressive shift of TC-EPSC amplitude towards weaker values. During the first postnatal week, Lpar1-GFP SPns receive input from essentially all cortical layers, with SP, L6, L5b and L4 providing the majority of excitation. The laminar pattern of excitatory input was developmentally regulated, such that up until P3, a recurrent excitatory network could be observed within the subplate which was subsequently dismantled. The pattern of cortical excitatory afferents to Lpar1-GFP SPns was mature by P2-P5, with L6 emerging as the major source of input, followed by L5b and L4.

Chapter 5 - Thalamocortical integration via an early, transient L4-L5b circuit

GFP-labelled cells in the Lpar1-GFP line are not restricted to the SP but can in fact also be found in L5b and L6. Morphological, immunohistochemical and intrinsic property characterisation of these cells determined them to be interneurons, more precisely, low-threshold spiking Martinotti cells. Lpar1-GFP MCs extended axons to the pial surface, which arborised in L4 and ramified collaterals in L5b. Early in development, a high proportion of these interneurons received thalamic input, which,

consistent with previous reports on Martinotti cells (Tan et al., 2008), was found to be facilitating at the tested frequency of 20Hz. Cortical glutamatergic inputs onto these neurons showed a dynamic developmental re-arrangement. At P4-P6, most input arose from L4, with a significant proportion originating from L5b. Throughout development there was a shift of influence, with L4 inputs weakening and eventually disappearing, and L5b/6 inputs increasing, such that at P10-P15 L5b/6 was the main provider of excitation onto Lpar1-GFP MCs. The development of afferent GABAergic inputs onto L4 showed a converse pattern. At P4-P6, the strongest source of input was L5b, although L4 GABAergic inputs could already be detected. Throughout development there was a sharp and continuous increase in L4 input, concomitant to a decrease, and eventual disappearance, of L5b GABAergic inputs. I tested the role of early sensory activity on the formation of inhibitory circuits with L4 by sectioning the ION of mouse pups at P0-P1. These experiments revealed a sharp decrease in total GABAergic input onto ION-sectioned L4 driven by decreases in inhibition arising from each cortical layer. In spite of an overall decrease in the strength of inhibition, the laminar organisation of input was preserved, with ION-sectioned and control groups undistinguishable on the proportion of GABAergic input arising from each layer. The converse result was found when mapping inhibitory inputs onto L4 at P10-P15. By this timepoint, the total amount of inhibition onto L4 excitatory neurons was undistinguishable between control and ION-sectioned animals. Compensation was driven by a developmental increase in ION-sectioned animals of inhibition arising from L5b. In control animals, the opposite was observed, with L5b inhibition decreasing from P4-P6 onwards, to the point where it had been virtually eliminated by P10-P15.

6.3. Integration of my findings

Three pathways for thalamic information into L4 during the critical period for thalamocortical plasticity

Early thalamic inputs onto L4 have been shown to be largely mediated via silent synapses (Isaac et al., 1997; Kidd & Isaac, 1999), which undergo developmental LTP over a critical period comprised between P0 and P8 (Crair & Malenka, 1995; Isaac et al., 1997; An et al., 2012). During this window, thalamic information can also reach L4 via a di-synaptic glutamatergic projection through the subplate, which receives thalamic input before L4 (Friauf et al., 1990; Hanganu et al., 2002; Higashi et al., 2002; Molnár et al., 2003), and projects to L4 before thalamic afferents do (Friauf et al., 1990; Friauf & Shatz, 1991; Higashi et al., 2002; Molnár et al., 2003; Zhao et al., 2009). This early, robust di-synaptic pathway has been proposed to be a key regulator of thalamocortical plasticity, contributing to the depolarisation of L4 required for NMDAR activation and thus contributing to plasticity of thalamocortical inputs via heterosynaptic LTP (Kanold, 2003; 2004; 2009; Kanold & Luhmann, 2010; Tolner et al., 2012). Despite evidence for the importance of GABA in several aspects of early circuit formation (Ben-Ari et al., 2007; Le Magueresse & Monyer, 2013), including generation of early network activity patterns via depolarising GABA in acute hippocampal and cortical *in vitro* slices (Ben-Ari et al., 1989; Allène et al., 2008; Allène & Cossart, 2010;) and the critical role of network-organising hub cells in promoting these patterns (Bonifazi et al., 2009; Picardo et al., 2011), previous reports suggested that GABA and interneurons played no role in establishing the key thalamocortical synapse (Daw et al., 2007a; Chittajallu & Isaac, 2010). This is because thalamorecipient FS/PV^{+} cells in L4 only receive thalamic afferent input and

form efferent connections to L4 at the end of the thalamocortical critical period for plasticity (Daw et al., 2007a; Chittajallu & Isaac, 2010), too late to have significant influence on this process. My discovery of an early thalamic-driven circuit reciprocally connecting L5b GABAergic interneurons and L4 spiny stellate cells as early as P4 challenges this view and suggests GABAergic circuits could have key influence in early thalamocortical plasticity. Therefore, during the thalamocortical critical period for plasticity, there are three pathways by which thalamic information can reach the cortex, each endowed with markedly different signalling properties: 1) a direct, immature, NMDAR-mediated projection from the thalamus to L4; 2) a di-synaptic, robust early pathway connecting the thalamus to SPns and SPns to L4 cells via AMPA receptors (Zhao et al., 2009); and 3) a di-synaptic, robust early pathway connecting the thalamus to L5b Martinotti cells and Martinotti cells to L4 spiny stellate neurons via GABA receptors.

It remains unclear why two indirect pathways (one glutamatergic, one GABAergic) with possibly similar functions would be necessary. It will be key to determine whether L5b GABAergic inputs onto L4 have, over the critical period, a depolarising or hyperpolarising influence, although current evidence suggests that until the end of the first postnatal week, GABA has a depolarising action on L4 spiny stellate cells (Daw et al., 2007a). If this is indeed the case, it could be that the SP and Martinotti circuits are sequentially engaged throughout development, with SPns providing at P0-P3 (Dupont et al., 2006; Yang et al., 2009; Yang et al., 2013b) a thalamic relay function designed to depolarise L4/CP and activate NMDARs that is then taken over by Martinotti cells. If Martinotti cell inputs onto L4 have a hyperpolarising effect,

they could serve to balance the excitatory thalamic relay function of SPns onto L4 at a time-point prior to the integration of L4 FS/PV^{+} cells into the circuit.

Pioneer neurons form early cortical circuits

In Chapter 4 and Chapter 5 of my thesis I studied two populations – Lpar1-GFP SPns and Lpar1-GFP MCs – which could be described (amongst other, as of yet not fully characterised populations) as pioneers in the cortical network. In order to develop this concept of "pioneer cell", I will compare SPns and MCs with each other, and with hippocampal hub neurons. I shall after offer a more precise definition of a pioneer neuron.

Lpar1-GFP SPns have been shown to belong to an early-born cohort of SPn, generated preferentially at E11.5 (Hoerder-Suabedissen & Molnár, 2012). Similarly, more detailed birthdating of Lpar1-GFP MCs is required (Hoerder-Suabedissen & Molnár, 2012), but their Lhx6 identity is consistent with an early-born GABAergic population (Miyoshi et al., 2007). Both cell types received thalamic input from the earliest timepoint tested. In fact, SPns have been shown to receive the first functional thalamic contacts in the cortex, which occur at late embryonic stages (Friauf et al., 1990; Friauf & Shatz, 1991; Higashi et al., 2002; Molnár et al., 2003). Lpar1-GFP MCs receive thalamic input at P4 (possibly even earlier), prior to L4 FS/PV+ interneurons (Daw et al., 2007a; Chittajallu & Isaac, 2010) . Moreover, L5b putative MCs form robust synapses with L4 spiny stellate neurons as early as P4, 2-3 days earlier than documented for L4 FS/PV^{+} interneurons (Daw et al., 2007a). I was able to record organised AMPA-mediated inputs onto Lpar1-GFP SPns as early as P0-P1, when most inputs originated from the SP. This contrasts with other deep-layer

pyramidal cells, which, prior to P5, receive little, if any, focused AMPA-mediated synaptic input (Anastasiades & Butt, 2012). One other feature common to the two pioneer cell types described is a rearrangement of the circuits they are involved in. Lpar1-GFP SPns start out by forming a recurrent excitatory network in the SP, which is dismantled at P2-P3 with the emergence of L6 as the principal local excitatory input source onto these cells. Lpar1-GFP MCs initially derive most of their input from L4, but throughout development lose this input and accrue input from L5b/6, such that by P10-P15, the totality of their local excitatory input derives from these layers. Last but not least, both SPns (Friauf et al., 1990; Friauf & Shatz, 1991; Hoerder-Suabedissen & Molnár, 2011; D. Liao et al., 2001) and Martinotti cells (Chapter 5, (Wang et al., 2004)) possess axons crossing the cortex from their home layer to its surface, often arborizing in L4, suggesting a close association to this layer. However, it should not be discounted that SP and MC axons could synapse with neurons occupying virtually all layers, given the extent of potential overlap between these axons and dendrites of pyramidal cells. Just as there are similarities, there are also interesting differences between Lpar1-GFP SPns and MCs. Whereas Lpar1-GFP MCs are GABAergic and mostly $Lhx6^{+}$, Lpar1-GFP SPns never co-label with GABA (Hoerder-Suabedissen & Molnár, 2011; 2012), and extremely rarely with Lhx6 (Chapter 5). Moreover, although GABAergic cells exist in the SP/L6b (Hanganu et al., 2009; Marx & Feldmeyer, 2012; Perrenoud et al., 2012), this layer presents the lowest interneuron/pyramidal cell ratio in the adult somatosensory cortex (Meyer et al., 2010c). Lpar1-GFP SPns and MCs show opposite patterns of short-term plasticity, with thalamic input onto SPns characterised by depression and that onto MCs being strongly facilitating. This suggests that the two cell types will be preferentially recruited by thalamic spike trains of different frequency ranges, with SPns engaged by

low-frequency inputs whereas MCs will preferentially spike during high-frequency trains of activity. Finally, thalamic inputs onto Lpar1-GFP MCs seem static, as thalamic connectivity onto these cells and input amplitude remains stable from early development through well past the critical period. Conversely, the pattern of thalamic recruitment of Lpar1-GFP SPns is dynamic. Early in development, most of these cells receive thalamic input, a significant proportion of which is high amplitude (over 40pA, Chapter 4). After P6, high amplitude events disappear, and after P10, very few SPns receive direct thalamic input (Chapters 3 and 4).

The early and intimate association of pioneer subplate neurons and Martinotti cells with thalamic input, their early integration into cortical circuits, and potential to influence several cortical layers (at least through L4) place these populations in a key position to impact the formation of thalamocortical and intracortical synapses, via heterosynaptic modulation of plasticity, relay of sensory-driven activity and synchronisation of cortical columnar activity. In agreement with this key role, ablation of SPns has a number of consequences on cortical organisation, namely lack of formation of barrels or ocular dominance columns (Kanold, 2003; Tolner et al., 2012), disruption of early network activity patterns (Dupont et al., 2006; Tolner et al., 2012), weakened thalamocortical synapses (Tolner et al., 2012) and immature inhibition in supragranular layers (Kanold & Shatz, 2006). It would be interesting to examine whether early ablation of Martinotti cells results in similar deficits.

Following comparison of SPns and MCs, I would like to contrast these cells that I term "pioneer neurons" to the "hub neuron", a similar concept previously described in the hippocampus (Bonifazi et al., 2009; Marissal et al., 2012; Picardo et al., 2011).

The term “hub neuron” is a more loaded one than I wish to ascribe to Lpar1-GFP SPns and MCs at the moment. Hub neurons are chiefly defined by their extremely vast axonal arborisations and ability to initiate, terminate, or modulate characteristics of network activity, and I do not wish to equate this concept with that of a pioneer neuron. First, I have not studied how Lpar1-GFP SPns and MCs participate in cortical network activity. SPns have been repeatedly implicated in early cortical oscillations (Dupont et al., 2006; Yang et al., 2009; Yang et al., 2013b), but it is not known whether, similar to hub neurons (Bonifazi et al., 2009), stimulation of a single SPn is able to significantly modulate network activity. Second, hub neurons have extremely vast axons that travel and arborise across hippocampal subfields. Though the axons of SPns and MCs travel the depth of the cortex up to the pial surface, their dimensions and area of arborisation are more modest than that of hub neurons. Moreover, the axons of hub cells arborise so densely that they almost appear to do so promiscuous and non-discriminately, connecting to any neuron within their range. Interestingly, L2/3 somatostatin-positive interneurons in cortex have recently been proposed to lack innervation selectivity, connecting promiscuously with pyramidal cells regardless of whether those cells form sub-networks or not (Fino & Yuste, 2011). This certainly does not appear to be the case either for SPns or Lpar1-GFP MCs, which appear to show a more focused, directed pattern of axonal innervation. Axons of Lpar1-GFP MCs in L5b bypass L5a and arborise profusely in L4, as well as L1/2 (Chapter 5). Although SPns project to several layers and cortical regions and show considerable (but reliably defined, see (Hanganu et al., 2002; Hoerder-Suabedissen & Molnár, 2011; Marx & Feldmeyer, 2012)) morphological diversity, their axons also appear more focused and less densely arborizing than those of hub cells. Moreover, the hippocampus and neocortex show very different topographical organisation, so it is

not readily apparent that the concept of a hippocampal hub cell should translate directly into the neocortex.

After highlighting the similarities between SPns and MCs (and some differences) and showing how these cells differ from hub neurons, I would like now to explain my usage of the term "pioneer neuron". I use this term to refer to neurons that show advanced states of intrinsic maturity and network integration early in development. SPns and MCs both receive early thalamic input, as well as organised, focused cortical inputs that are detectable from the very earliest days of postnatal development. Moreover, their outputs (MCs to L4 and SPns to the SP and L4) also mature early in development, and as such they are well-positioned to synchronise layers and cell types that will form part of the same processing stream. It is likely that the significant influence of single hub cells on network activity hinges largely on their impressive array of outputs. Via their extensive axonal arbors, hub neurons can drive early, global network activity in the hippocampus. Comparing them to SPns and MCs, I would predict that the effect of these cortical cells on network activity could be less drastic, less global and more spatially confined. This is not to downplay their potential effect on network activity; indeed, SPns have been shown to be important modulators of early gamma oscillations (Yang et al., 2009; Yang et al., 2013b;), spindle bursts (Sun & Luhmann, 2007; Yang et al., 2009; Yang et al., 2013b) and cholinergic oscillations (Dupont et al., 2006; Hanganu et al., 2007; 2009; Sun & Luhmann, 2007), and although the effects of Martinotti cells on network activity are as of yet unknown, their early network integration characteristics suggest they could have a powerful influence in coupling thalamic, L5b and L4 activity and influencing plasticity in this layer (Chapter 5). Moreover, they have been proposed to have the ability of

synchronising sub-networks of connected pyramidal cells in the mature organism (Silberberg & Markram, 2007; Cottam, 2011; Lee & Huguenard, 2011). Instead of synchronising activity across vast expanses of tissue as hub cells do, MCs and SPns (and other, unidentified pioneer neurons) may be more specialised and couple together layers and cell types that will define networks in the mature organism, for instance L6, L5b and L4 for processing of information from primary sensory thalamic nuclei, and L5a, L2/3 and L1 for information streams deriving from higher-order sensory thalamic nuclei. Further exploration of this issue will require monitoring of network activity during specific stimulation of SPns or MCs. It would also be interesting to explore by what mechanisms functionally-related cortical areas (for instance primary motor and sensory cortices, primary and higher-order sensory cortices) become coupled during development. SPns often project across cortical areas (Hoerder-Suabedissen & Molnár, 2011), and, in the mature organism, L6b cells have been found to project over long distances between different cortical regions (Tomioka et al., 2005; Higo et al., 2007; Hooks et al., 2013; Zingg et al., 2014), so these neurons may be good candidates for such communication early in development.

Thalamic-driven interactions between L4 and L5b and the dual strata view of thalamocortical processing

In Chapter 3 of my thesis, I showed that most L5b pyramidal neurons receive direct thalamic input, using optogenetics. In Chapter 5 it became apparent that Martinotti cells in L5b are also key elements of the thalamocortical circuit, with these neurons receiving early direct thalamic input that is maintained post-critical period (contrary to SPns, see Chapters 3 and 4). The traditional canonical circuit view of thalamocortical processing is that thalamic information is fed to L4 and redistributed

to the cortical column via projections from this layer and L2/3 to infragranular layers (Douglas & Martin, 2004; Feldmeyer et al., 2012). Deep layer principal neurons receive thalamic projections, but these inputs were thought to be modulatory (Guillery & Sherman, 2002; 2011; Viaene et al., 2011b). Recent developments in the field have shown that in the somatosensory cortex practically all principal neurons of the cortex could, by anatomical axodendritic overlap, receive thalamic input (from the VPM or POm), and that L5 pyramidal neurons particularly could be in a key position to integrate separate information streams (Meyer et al., 2010a; Wimmer et al., 2010; Oberlaender et al., 2012; Rah et al., 2013; Hill & Greenfield, 2014). A key finding *in vivo* was that L5 pyramidal cells receive a copy of VPM inputs independent from descending sensory information, and that these inputs act as drivers (Constantinople & Bruno, 2013). This body of work reinforced the view that thalamic information could be processed not serially, but in two parallel strata in the cortex, one concerned with cortico-cortical (L4), and the other with cortico-subcortical and action-oriented processing (L5b/6) (Constantinople & Bruno, 2013).

Evidence for parallel thalamocortical processing in L4 and L5b/6 raises the possibility of interactions between the two strata, which could endow the circuit with computational abilities such as temporal binding of sensory and action-oriented processing, or, opposite to this, a form of "contrast" enhancement by separation of processing in the two streams. L5b Martinotti cells mediate such a cross-strata interaction early in development, during the thalamocortical critical period for plasticity (Chapter 5). It is clear that after P10 these cells no long project to L4 spiny stellate neurons. However, there is evidence that the axons of L5b MCs persist in L4 into maturity, at least at P13-P16 (Wang et al., 2004). One interesting possibility is

that after P10, L5b MCs innervate other cellular elements in L4, for instance L4 FS/PV$^+$ interneurons. SST$^+$ interneurons have indeed been shown to inhibit PV$^+$ cells, promoting disinhibition of principal neurons (Pfeffer et al., 2013; Xu et al., 2013). Under this hypothetical circuit, high-frequency thalamic spike trains would preferentially recruit L5b MCs compared to FS/PV$^+$ cells (Tan et al., 2008), which would lead to disinhibition of L4 principal neurons via L5b MC inhibition of L4 FS/PV$^+$ cells. This circuit would generate synchronised spiking in the L4 and L5b/6 thalamocortical processing streams, providing a mechanism for feature binding in the "cortico-cortical" L4 strata and the "action-oriented" L5b/6 strata.

6.4. Future directions

Developmental activity-dependent remodelling of inhibitory circuitry and competition between FS/PV$^+$ and NFS/SST$^+$

The results of my ION sectioning experiments suggested that, in response to sensory deprivation, downregulation of local FS/PV$^+$-mediated inhibition could be compensated by upregulation of NFS/SST$^+$ inhibition. Moreover, I proposed that activity-driven competition between these cell types could be a process present in normative development. Though speculative, these suggestions fit well with existing data (Jiao et al., 2006; Bartley et al., 2008; Jiao et al., 2011; Lazarus & Huang, 2011; Takesian et al., 2013). I would like to explore this idea further through several lines of enquiry.

First, though it is plausible to assume that in L4 local inhibition is chiefly FS/PV-mediated and L5b inhibition is coordinated by NFS/SST$^+$ Martinotti cells, it would be

important to directly test this interpretation. This could be done by ablating an input source common to L4 FS/PV and L5b Martinotti cells (for instance sensory thalamic or L4 input) and examining how FS/PV$^+$ and NFS/SST$^+$ outputs adapt, over the course of development. This could be done with cell-type specificity using Cre-mediated expression of optogenetic constructs in FS/PV$^+$ and NFS/SST$^+$ cells using PV- or SST-specific Cre lines (Taniguchi et al., 2011; Taniguchi, 2014). Second, the differential impact of activity on output regulation of FS/PV$^+$ and NFS/SST$^+$ interneurons suggests that these cells could rely on distinct modes of integration into the cortical network. Consistent with their activity-dependent regulation of output, it could be that FS/PV$^+$ interneurons accrue excitatory inputs and match this engagement by upregulating their outputs onto pyramidal cells. NFS/SST$^+$ interneurons could integrate differently, given that they do not scale their outputs as a function of afferent activity. Indeed, the specific Lpar1-GFP MC population I examined showed a dynamic mode of integration into the network, receiving distinct laminar afferent connections and projecting to different layers throughout development (Chapter 5). To investigate this, it would be important to record from identified interneurons and determine their intrinsic maturation profiles, as well as laminar input sources (using LSPS) throughout development.

If activity differentially modulates integration and output scaling for distinct interneuron types, it would be of interest to search for the activity-dependent genes and transcription factors that could regulate this phenomenon. Finding such genes would open the possibility of examining whether this activity-dependent regulation is a phenomenon observed only during development or perturbation of activity, or whether it can also be observed during different behavioural and information

processing states, to confer fluidity to a network. On a related note, it has recently been shown that PV^+ interneurons modulate PV expression during different stages of learning (Donato et al., 2014), consistent with the possibility that interneurons fluidly shift their properties during distinct behavioural or brain states.

Finally, distinct modulation of interneuron types by activity-dependent mechanisms could also have an important clinical angle. For instance, PV^+ cell function has been shown to be compromised in several mouse models of schizophrenia, often through pathological mechanisms that result in reduced excitation of PV^+ interneurons (Marín, 2012). A key consequence of this deficit at the network level are impaired neural oscillations and synchrony, particularly gamma oscillations (Uhlhaas et al., 2008; Uhlhaas et al., 2010). It would be important to examine in these models whether deficient PV-mediated inhibition has been compensated in any way by changes in SST^+ or VIP^+ function, and whether the observed altered organisation of oscillations and synchrony could correspond not only to deficient PV^+ function, but also a distinct mode of network function brought about by compensatory changes in interneurons with markedly different properties from PV^+ cells.

Subplate neurons: still an enigma?

It has been 40 years since the first description of the subplate by Kostovic and Molliver (Kostovic & Molliver, 1974). Our understanding of the function of this intriguing layer has beyond doubt progressed significantly, but many questions still remain. It is clear that SPns have intrinsic and network properties that poise them as key players in generating and relaying rhythmic activity in the developing neocortex (Hanganu, 2001; Higashi et al., 2002; Hanganu et al., 2002; 2009; Molnár et al., 2003;

Dupont et al., 2006; Sun & Luhmann, 2007; Hirsch & Luhmann, 2008; Luhmann, 2009; Yang et al., 2009; Zhao et al., 2009; Tolner et al., 2012; Yang et al., 2013b;). Contrasting the results of the Luhmann (Dupont et al., 2006; Yang et al., 2009; Yang et al., 2013b;) and Khazipov laboratories (Khazipov et al., 2004; Minlebaev et al., 2007; 2009; 2011), it appears that SPns may be especially recruited and involved in network activity during the earliest stages of postnatal cortical development, between P0 and P3. Their criticality for thalamocortical synapse development at the functional and structural level in L4 has also been firmly established (Kanold, 2003; Kanold & Shatz, 2006; Tolner et al., 2012). However, at the circuit level, it remains unclear how SPns interact with L4, and it would still be of great interest to study directly the possibility of a hetero-synaptic plasticity interaction with incipient thalamocortical synapses at this layer (Kanold, 2004; Kanold & Luhmann, 2010). This would require input-specific activation, which could be achieved by expression of spectrally-separated channelrhodopsins at the thalamus and SP. Though it is challenging at present to use optogenetics in the neonatal brain, the encouraging speed of technical development in the field (Boyden et al., 2005; Fenno et al., 2011; Yizhar et al., 2011) may soon lead to important breakthroughs in developmental circuit neuroscience.

The involvement of the subplate in early network activity is clear (Dupont et al., 2006; Yang et al., 2009; Yang et al., 2013b), and morphological reconstructions suggest an early potential to influence activity across the entire cortical depth (Friauf & Shatz, 1991; Liao & Lee, 2011), but the functional and circuit basis of this influence remains elusive, and only a projection onto L4 has been functionally described so far (Zhao et al., 2009). It is unclear whether the SP has a privileged

relationship with L4, or whether SPns project to neurons in all cortical layers, providing stable conduits for propagation of early network activity.

The subplate as an amplifier of thalamic activity into L4 – testing the model

The foremost theory of subplate function postulates that this cell population serves as an amplifier designed to potentiate thalamic inputs into L4 (Luhmann, 2009; Kanold & Luhmann, 2011). An amplifier can be understood as a device that receives a small input signal and, after signal processing, delivers an output that is larger than the original input. The necessity for amplification in developing thalamocortical systems comes from the observation that immature thalamic inputs to L4 are weak, often silent, and unable to reliably drive action potentials in L4 spiny stellate cells (Isaac et al., 1997; Daw et al., 2007). This precludes not only signal propagation to other cortical layers and regions required for sensory processing, but also a fundamental requirement for LTP-mediated maturation and strengthening of thalamocortical inputs: correlated spiking activity between thalamic relay neurons and spiny stellate cells leading to synapse unsilencing (Crair & Malenka, 1995; Isaac et al., 1997; An et al., 2012). If the subplate amplifier is required to enable correlation of thalamic and L4 spiking activity, then destroying the amplifier early in development should prevent activity-dependent strengthening of the thalamus to L4 projection, which has been verified to be the case (Kanold et al., 2003; Tolner et al., 2012).

The subplate seems well positioned to perform a role as amplifier of thalamic activity into L4 because first, it receives very early and powerful thalamic input which can drive it to fire action potentials (Chapter 4; Friauf et al., 1990; Friauf & Shatz, 1991; Hanganu et al., 2002; Hirsch & Luhmann, 2008). Second, it projects to L4.

Reconstructions of early subplate morphologies showed axons spanning the entire depth of the cortex, often arborizing in L4 (Friauf et al., 1990; Friauf & Shatz, 1991; Luhmann et al., 2000; Hanganu et al., 2001; 2002; Hoerder-Suabedissen & Molnár, 2011), and in the auditory cortex, a subplate to L4 excitatory connection was physiologically recorded using glutamate uncaging (Zhao et al., 2009). Third, due to advanced intrinsic maturity and high excitability (Chapter 4; Luhmann et al., 2000; Hanganu et al., 2001; 2002), extensive recurrent connectivity (Chapter 4; Hanganu et al., 2002; Dupont et al., 2006; Hirsch & Luhmann, 2008; Hanganu et al., 2009; Viswanathan et al., 2012) and depolarising neuromodulatory inputs (Hanganu et al., 2009) the subplate may not only effectively relay thalamic input to L4, but potentially multiply it. Putting these three points together, the robustness of thalamic-subplate inputs means that even fairly sparse thalamic activity could recruit subplate neurons to spike. Due to extensive recurrent connectivity (glutamatergic, depolarizing GABAergic and gap-junctional), thalamic-driven spiking in the subplate could initiate persistent activity and thus generate even more spiking in this layer that would be relayed downstream to L4. Thus, a small number of thalamic spikes could potentially be multiplied in the subplate, leading to a more powerful indirect thalamic output via this layer into L4, than via the direct thalamic-L4 projection (Kanold, 2004; Luhmann et al., 2009; Kanold & Luhmann, 2011). Summation of direct and indirect thalamic inputs in L4 would result in correlated L4 and thalamic spiking and long-term potentiation of the thalamocortical synapse (Kanold, 2004; Luhmann et al., 2009; Kanold & Luhmann, 2011).

The amplifier model is useful additionally in the sense that it provides a link between two key sets of empirical findings on subplate function: its importance for maturation

of thalamic inputs into L4 (Friauf et al., 1990, 1991; Molnar et al., 2003; Kanold et al., 2003; Tolner et al., 2012; An et al., 2012) and its heavy involvement in early cortical rhythmic activity (Dupont et al., 2006; Sun & Luhmann, 2007; Yang et al., 2009; Tolner et al., 2012; Yang et al., 2013). Despite ample experimental evidence consistent with the model, it has never been put to direct experimental test. We do not know whether direct thalamic inputs into L4 are actually more or less potent than putative indirect inputs relayed via the subplate, and whether the two converge and summate. This is largely dependent on the intricacies of the synaptic and somatotopical alignment of elements in the thalamus-subplate-L4 circuit, which remain mostly unknown. I will lay down a proposal to address these gaps in our knowledge of subplate circuitry and test the amplifier model.

The circuit arrangement compatible with an LTP-inducing amplification and relay of thalamic input by the subplate into L4 requires 1) that SP and L4 neurons receive somatotopically-matching thalamic input; and 2) that SPns project to L4 neurons in a manner that preserves and maintains this somatotopy. This circuit layout means that stimulation of a particular whisker will engage neurons in thalamic barreloids, which will activate somatotopically-aligned SPns. These cells will then amplify and relay activity to L4 cells in the somatotopically-aligned barrel, which will summate with incoming activity from the corresponding thalamic barreloid. The key experiment to perform involves dual recordings of a subplate and L4 spiny stellate cell during minimal electrical stimulation of the VPM. If stimulation of the same fibre at minimal intensity reliably resulted in coincident EPSPs in both the SP and L4 neuron, this would mean that the same activated fibre is branching and contacting both cells. Upon finding pairs of cells receiving common thalamic input, the next step would be to

slowly increase the stimulation intensity and test whether and with what latency thalamic inputs generate spikes in SP and L4 neurons. The first requirement for amplifier circuitry, matching thalamic input in SP and L4, would thus be tested, and this experiment would also conclusively answer whether thalamic inputs onto the SP are more potent than those onto L4. In order to test whether somatotopy is preserved at the SP to L4 pathway, it would be necessary to find connected SP to L4 pairs. Given the large distance between SP and L4 (400-500 μm), connection probabilities *in vitro* would likely be very low. However, retrograde tracer injections into L4 *in vivo* prior to brain slicing (Wickersham et al., 2012) could help target subplate patching and enhance the probability of finding connected pairs. Though challenging, the successful configuration of thalamic stimulation with paired SP and L4 patching would allow the experimenter unparalleled access to the circuit, enabling recording of unitary connection amplitudes, paired-pulse ratio, probability and relative timing of thalamic/subplate-induced action potential firing, and even direct test of summation of convergent thalamic and subplate inputs onto L4. Filling SPns with biocytin and recovering morphologies would allow characterisation of the subplate's axonal output, enabling quantification of the proportion of boutons per cortical layer, as well as within and without the home barrel column. This would complement data from connected SP-L4 pairs and determine to what extent the SP to L4 projection preserves somatotopy, amplifying and relaying aligned thalamic barreloid activity.

These experiments are of critical importance, as the exact computation performed by SPns on thalamic input will depend on the relative somatotopical arrangement of thalamic afferents and subplate outputs into the overlying cortex and L4. I will next consider the impact that different configurations on the arrangement of thalamic,

subplate and L4 circuitry would have on hypothesised SP function (see also Figure 6.1).

1) Matching at the cellular level: in this configuration, the axon of a single thalamic relay neuron branches and contacts both subplate cells and L4 spiny stellate cells in the same barrel column. Subplate neurons receiving thalamic input project to L4 cells with which they share common thalamic afferents. Though precise in the extreme, it is not difficult to envisage how this configuration could come about during development. SPns are known to send axons to L4 prior to the arrival of thalamic afferents to this layer (Friauf et al., 1990; Kanold & Luhmann, 2011) and there is evidence that thalamocortical axons interact closely with corticothalamic axons of SPns, which provide a scaffold for thalamocortical axons to navigate along on their way to the cortical plate (Molnar & Blakemore, 1995; Molnar et al., 1998; Molnar & Cordery, 1999; López-Bendito & Molnár, 2003; Grant et al., 2012). It is possible that this intimate association continues in the cortical plate, and that incoming thalamocortical axons grow along the axons of columnar-oriented, L4-projecting SPns.
2) Matching at the somatotopical level: in this configuration, subplate and L4 cells do not necessarily receive input from branching collaterals originating from the same thalamic relay neuron, but from thalamic neurons located in the same barreloid. SP projections would preserve somatotopy, targetting preferentially L4 cells in the same barrel column innervated by thalamic afferents from the same barreloid. Though less precise than the first arrangement, SP and L4 cells would under this configuration still receive thalamic input driven by peripheral stimuli to the same whisker. However, coincidence of thalamic inputs in the SP and L4

would be far from perfect, as afferent information would be carried by different axons. Whether subplate inputs could coincide with and boost thalamic inputs onto L4 under this configuration depends on how coherent the activity of different thalamic neurons within a barreloid is *in vivo*.

3) Lack of matching: in the final configuration, there is no somatotopical alignment between the SP and L4. Three possible basic scenarios could be envisaged: 1) SPns receive input from different barreloids than L4 cells do but project to L4 within their home barrel; 2) SPns receive input from the same barreloids as overlying L4 barrel cells, but output to a different barrel; or 3) SPns receive input from different barreloids than L4 and project to L4 cells outside their home barrel. All three cases portray divergence in thalamocortical processing. It is unclear what the function of this divergence could be, except to promote functional interaction and connectivity between separate barrel columns, which is indeed present in the mature barrel system (Petersen, 2007).

Configuration 1 (Figure 6.1, left) would provide the strongest backbone for subplate-mediated amplification of thalamic inputs leading to plasticity at the thalamus-L4 synapse, by maximizing the coincidence and convergence of thalamic and subplate inputs in L4. The second configuration (Figure 6.1, right), where barreloid/barrel-level somatotopy is preserved, could still potentially allow summation of thalamic and subplate activity in L4 and induction of plasticity, but critically depends on how coherent activity is between different thalamic neurons within a barreloid. *In vivo* unit and field potential recordings suggest that this can be very precise and consistent during early gamma oscillations (Yang et al., 2013b). Configuration 3 could be

interpreted as cross-columnar relay, with L4 integrating information from different whiskers via principal whisker thalamic and non-principal whisker SP input.

Besides clearing up the anatomical arrangement of the thalamus-SP-L4 circuit, dual recording from connected SP and L4 pairs during electrical stimulation of the thalamus could produce a wealth of highly valuable functional data whose full complexity may best be understood by computational modelling. One should not discount the difficulty involved in obtaining it; this is a highly challenging experiment that would likely be very low-throughput and take a long time to perform. However, for the sake of its sheer power, let us consider as a thought experiment modelling such a rich dataset. For simplicity, let us assume that configuration 1 (cellular level matching) was observed. Successful paired recordings of SP to L4 inputs during thalamic stimulation could produce the following data:

1) Connection probability, unitary amplitude and latency, spike probability and latency and paired-pulse ratio for the following connections:
    a. Thalamus-L4
    b. Thalamus-SP
    c. SP-L4
2) Excitability indexes, in the form of input resistance and rheobase, for SP and L4 excitatory neurons
3) A time window for summation of thalamic and subplate inputs converging in L4

It would be possible using this data set to model, at the population rather than single cell level, how a given pattern of thalamic action potentials impacts activity in the subplate and L4. We could determine how much thalamic activity is necessary to cause SPns to spike, and how many SPns would be recruited to fire by such activity. Knowing the probability of SP to L4 connections and their unitary characteristics (amplitude, paired-pulse ratio, latency) we could estimate the impact of SP activity in L4. This would enable a comparison of the net activation of L4 by direct thalamic inputs with thalamic-evoked di-synaptic EPSPs relayed via the SP to L4, providing a test of the amplifier theory. By knowing the kinetics (rise time and decay) of each of these connections, we could further determine the time window within which they should coincide in order to summate optimally, and test whether the circuit structure and physiology actually allow for that to happen. One further modelling possibility would be to obtain similar connectivity parameters for intra-subplate circuits, and test how adding a module composed of recurrent subplate excitatory connections impacts thalamic-driven activity and amplification of this activity into L4.

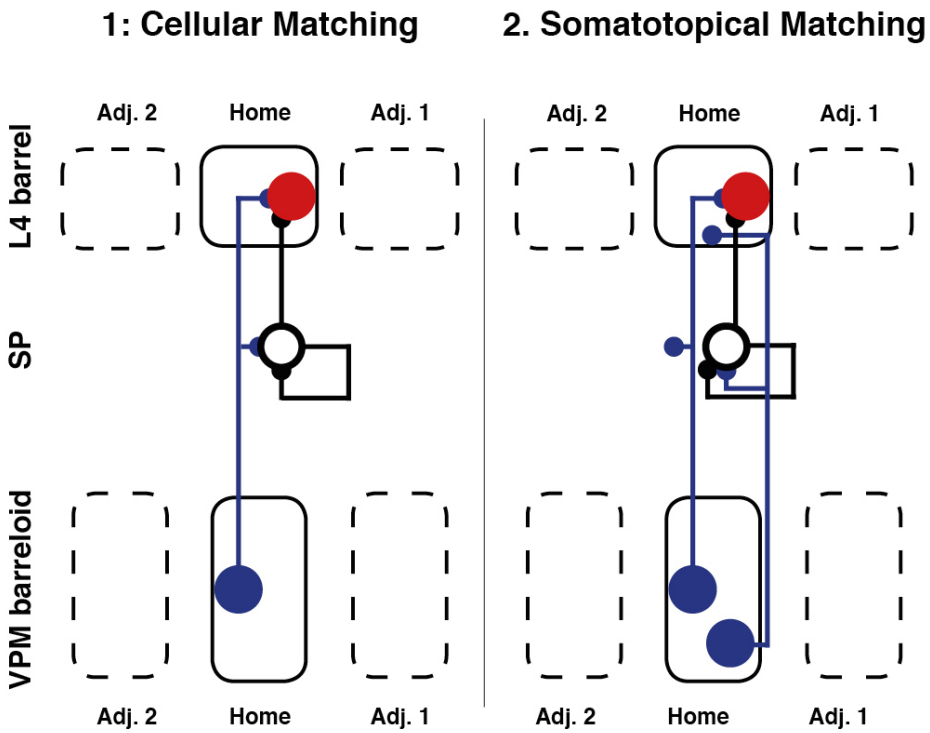


Figure 6.1. **Schematic diagrams for possible wiring of the thalamus-SP-L4 circuit that would permit amplification of thalamic inputs to L4 via activity relayed through the subplate.** For simplicity, only the circuitry of the home barrel is illustrated. Identical connections would be present in the two adjacent barrels (dashed). Adj. 2 - adjacent barrel column/barreloid 2; Home - home barrel column/barreloid; Adj. 1 - adjacent barrel column/barreloid 1.

I have so far refrained from delving into quantitative anatomy, i.e., number of neurons in each level of the circuit, number of synaptic contacts they make and probability of axodendritic overlap. A series of elegant and exciting studies published recently did exactly this for the thalamocortical system in the mature barrel cortex (Wimmer et al., 2010; Meyer et al., 2010a; Meyer et al., 2010b). Probably the most ambitious experiment would be to ally the aforementioned recordings to viral labelling of the VPM and do numerous biocytin reconstructions of thalamorecipient SPns projecting to L4. This would allow detailed computational anatomy of the number of SP and

thalamic synaptic boutons per layer. Allying connection probabilities obtained in physiology experiments to cell counts for the number of thalamic relay neurons, SPns and L4 cells per barrel column would allow estimates of how many SPns and L4 cells are innervated by a single thalamic axon and how many L4 cells are innervated by a single SPn. This would inform whether there is divergence or convergence at each level of the circuit.

The complexity level of such an integrated physiological and anatomical computational model is staggering. It must be acknowledged however, that even this highly ambitious model completely fails to take into account the presence of neuromodulatory inputs which likely play a fundamental role *in vivo* (Hanganu et al., 2007; 2009). Contemplating this could drive even the most rugged physiologist to tears (of wonder or despair?). There is ample on-going discussion, which escapes the scope of this thesis, about whether such large-scale integrated experimental/modelling projects are the future of neuroscience. I cannot add a well-formed opinion to this discussion, but I would conclude by pointing out that even modelling data on a mere tri-synaptic circuit can already lead to an amount of detail challenging to understand.

6.5. The importance of bridging developing circuit and network physiology

After combined effort from several groups, it is now clear that patterns of network activity in the developing and mature cortices are markedly different (Ben-Ari et al., 2004; Khazipov & Luhmann, 2006; Allène & Cossart, 2010; Khazipov et al., 2013). Network activity progresses throughout development from a discontinuous mode of bursting synchronous activation against a background of silence, to a mode of continuous baseline, asynchronous activity (Colonnese et al., 2010; Khazipov et al.,

2013). It is likely that this transition is brought about not only by maturation of intrinsic and synaptic properties of neurons, but largely by changes in cortical circuit organisation. In my thesis I found evidence for transient, non-exuberant connectivity in the developing brain, consistent with a view of cortical development as involving highly dynamic processes, rather than piece-by-piece hierarchical assembly of circuits. Though circuit-mapping at the mesoscopic and single cell level has become an ambitious (and likely attainable) goal of circuit neuroscience (Alivisatos et al., 2013; 2012; Oh et al., 2014; Zingg et al., 2014), comparatively little attention has been devoted to studying developing circuit organisation. Understanding the assembly of neural circuits and developmental progression of network activity patterns is crucial not only for building a roadmap of normative development, but also to understand at the circuit and cell type level which failures in reorganisation could lead to disease and how this can be prevented. A number of groups have been combining to great effect *in vivo* physiology (Minlebaev et al., 2009; 2011; Yang et al., 2009; Yang et al., 2013b;) and circuit mapping strategies (Hanganu et al., 2002; Higashi et al., 2002; Molnár et al., 2003; Daw et al., 2007a; Hirsch & Luhmann, 2008; Bonifazi et al., 2009; Zhao et al., 2009; Anastasiades & Butt, 2012; Viswanathan et al., 2012) to chart the emergence of network activity and cortical connectivity, and my own efforts in this thesis have provided a small, but I hope valuable, contribution to the field. Analysis at the cell type-specific level has been hampered by difficulties in migrating optogenetic tools from mature (Fenno et al., 2011; Yizhar et al., 2011) onto developing systems (Chapter 3). Nonetheless, the fast pace of development of optogenetic technologies (Boyden et al., 2005; Fenno et al., 2011; Yizhar et al., 2011), a rising interest in how single cell-level adult connectivity may be predicted from early developmental events (Li et al., 2012; Ohtsuki et al., 2012; Gao et al.,

2013), and the long-standing contributions of key contributors in the circuit development field, should all combine to make the next decade a very interesting one in the study of cortical circuit development.

References

Aboitiz, F. (1999). Evolution of isocortical organization. A tentative scenario including roles of reelin, p35/cdk5 and the subplate zone. *Cerebral Cortex (New York, NY : 1991)*, *9*(7), 655–661.

Aboitiz, F., Montiel, J., & García, R. R. (2005). Ancestry of the mammalian preplate and its derivatives: evolutionary relicts or embryonic adaptations? *Reviews in the Neurosciences*, *16*(4), 359–376.

Abrahamsson, T., Gustafsson, B., & Hanse, E. (2005). Synaptic fatigue at the naive perforant path-dentate granule cell synapse in the rat. *The Journal of Physiology*, *569*(Pt 3), 737–750. doi:10.1113/jphysiol.2005.097725

Abrahamsson, T., Gustafsson, B., & Hanse, E. (2007). Reversible synaptic depression in developing rat CA3 CA1 synapses explained by a novel cycle of AMPA silencing-unsilencing. *Journal of Neurophysiology*, *98*(5), 2604–2611. doi:10.1152/jn.00602.2007

Abrahamsson, T., Gustafsson, B., & Hanse, E. (2008). AMPA silencing is a prerequisite for developmental long-term potentiation in the hippocampal CA1 region. *Journal of Neurophysiology*, *100*(5), 2605–2614. doi:10.1152/jn.90476.2008

Adelsberger, H., Garaschuk, O., & Konnerth, A. (2005). Cortical calcium waves in resting newborn mice. *Nature Neuroscience*, *8*(8), 988–990. doi:10.1038/nn1502

Agmon, A., & Connors, B. W. (1991). Thalamocortical responses of mouse somatosensory (barrel) cortex in vitro. *Neuroscience*, *41*(2-3), 365–379.

Agmon, A., & Connors, B. W. (1992). Correlation between intrinsic firing patterns and thalamocortical synaptic responses of neurons in mouse barrel cortex. *The Journal of Neuroscience*, *12*(1), 319–329.

Agmon, A., Hollrigel, G., & O'Dowd, D. K. (1996). Functional GABAergic synaptic connection in neonatal mouse barrel cortex. *The Journal of Neuroscience*, *16*(15), 4684–4695.

Agmon, A., Yang, L. T., O'Dowd, D. K., & Jones, E. G. (1993). Organized growth of thalamocortical axons from the deep tier of terminations into layer IV of developing mouse barrel cortex. *The Journal of Neuroscience*, *13*(12), 5365–5382.

Al-Ghoul, W. M., & Miller, M. W. (1989). Transient expression of Alz-50 immunoreactivity in developing rat neocortex: a marker for naturally occurring neuronal death? *Brain Research*, *481*(2), 361–367.

Alivisatos, A. P., Chun, M., Church, G. M., Deisseroth, K., Donoghue, J. P., Greenspan, R. J., et al. (2013). Neuroscience. The brain activity map. *Science (New York, NY)*, *339*(6125), 1284–1285. doi:10.1126/science.1236939

Alivisatos, A. P., Chun, M., Church, G. M., Greenspan, R. J., Roukes, M. L., & Yuste, R. (2012). The Brain Activity Map Project and the Challenge of Functional Connectomics. *Neuron*, *74*(6), 970–974. doi:10.1016/j.neuron.2012.06.006

Allen, C. B., Celikel, T., & Feldman, D. E. (2003). Long-term depression induced by sensory deprivation during cortical map plasticity in vivo. *Nature Neuroscience*, *6*(3), 291–299. doi:10.1038/nn1012

Allendoerfer, K. L., & Shatz, C. J. (1994). The subplate, a transient neocortical structure: its role in the development of connections between thalamus and cortex. *Annual Review of Neuroscience*, *17*, 185–218. doi:10.1146/annurev.ne.17.030194.001153

Allene, C., & Cossart, R. (2010). Early NMDA receptor-driven waves of activity in the developing neocortex: physiological or pathological network oscillations? *The Journal of Physiology*, *588*(Pt 1), 83–91. doi:10.1113/jphysiol.2009.178798

Allene, C., Cattani, A., Ackman, J. B., Bonifazi, P., Aniksztejn, L., Ben-Ari, Y., & Cossart, R. (2008). Sequential generation of two distinct synapse-driven network patterns in developing neocortex. *The Journal of Neuroscience : the Official Journal of the Society for Neuroscience*, *28*(48), 12851–12863. doi:10.1523/JNEUROSCI.3733-08.2008

An, S., Yang, J. W., Sun, H., Kilb, W., & Luhmann, H. J. (2012). Long-Term Potentiation in the Neonatal Rat Barrel Cortex In Vivo. *The Journal of Neuroscience : the Official Journal of the Society for Neuroscience*, *32*(28), 9511–9516. doi:10.1523/JNEUROSCI.1212-12.2012

Anastasiades, P. G., & Butt, S. J. B. (2011). Decoding the transcriptional basis for GABAergic interneuron diversity in the mouse neocortex. *European Journal of Neuroscience*, *34*(10), 1542–1552. doi:10.1111/j.1460-9568.2011.07904.x

Anastasiades, P. G., & Butt, S. J. B. (2012). A role for silent synapses in the development of the pathway from layer 2/3 to 5 pyramidal cells in the neocortex. *The Journal of Neuroscience : the Official Journal of the Society for Neuroscience*, *32*(38), 13085–13099. doi:10.1523/JNEUROSCI.1262-12.2012

Anderson, S. A., Eisenstat, D. D., Shi, L., & Rubenstein, J. L. (1997). Interneuron migration from basal forebrain to neocortex: dependence on Dlx genes. *Science (New York, NY)*, *278*(5337), 474–476.

Anderson, S. A., Kaznowski, C. E., Horn, C., Rubenstein, J. L. R., & McConnell, S. K. (2002). Distinct origins of neocortical projection neurons and interneurons in vivo. *Cerebral Cortex (New York, NY : 1991)*, *12*(7), 702–709.

Angevine, J. B., & Sidman, R. L. (1961). Autoradiographic study of cell migration during histogenesis of cerebral cortex in the mouse. *Nature*, *192*, 766–768.

Anthony, T. E., Klein, C., Fishell, G., & Heintz, N. (2004). Radial glia serve as neuronal progenitors in all regions of the central nervous system. *Neuron*, *41*(6), 881–890.

Armstrong-James, M., Fox, K., & Das-Gupta, A. (1992). Flow of excitation within rat barrel cortex on striking a single vibrissa.

Ashby, M. C., & Isaac, J. T. R. (2011). Maturation of a recurrent excitatory neocortical circuit by experience-dependent unsilencing of newly formed dendritic spines. *Neuron*, *70*(3), 510–521. doi:10.1016/j.neuron.2011.02.057

Bagnall, M. W., Hull, C., Bushong, E. A., Ellisman, M. H., & Scanziani, M. (2011). Multiple clusters of release sites formed by individual thalamic afferents onto cortical interneurons ensure reliable transmission. *Neuron*, *71*(1), 180–194. doi:10.1016/j.neuron.2011.05.032

Baho, E., & Di Cristo, G. (2012). Neural activity and neurotransmission regulate the maturation of the innervation field of cortical GABAergic interneurons in an age-dependent manner. *The Journal of Neuroscience : the Official Journal of the Society for Neuroscience*, *32*(3), 911–918. doi:10.1523/JNEUROSCI.4352-11.2012

Bamann, C., Kirsch, T., Nagel, G., & Bamberg, E. (2008). Spectral characteristics of the photocycle of channelrhodopsin-2 and its implication for channel function. *Journal of Molecular Biology*, *375*(3), 686–694. doi:10.1016/j.jmb.2007.10.072

Bannister, N. J. (2005). Developmental Changes in AMPA and Kainate Receptor-Mediated Quantal Transmission at Thalamocortical Synapses in the Barrel Cortex. *The Journal of Neuroscience : the Official Journal of the Society for*

Neuroscience, *25*(21), 5259–5271. doi:10.1523/JNEUROSCI.0827-05.2005
Barabasi, A., & Albert, R. (1999). Emergence of scaling in random networks. *Science (New York, NY)*, *286*(5439), 509–512.
Barkat, T. R., Polley, D. B., & Hensch, T. K. (2011). A critical period for auditory thalamocortical connectivity. *Nature Neuroscience*, *14*(9), 1189–1194. doi:10.1038/nn.2882
Barth, A. L., McKenna, M., Glazewski, S., Hill, P., Impey, S., Storm, D., & Fox, K. (2000). Upregulation of cAMP response element-mediated gene expression during experience-dependent plasticity in adult neocortex. *The Journal of Neuroscience : the Official Journal of the Society for Neuroscience*, *20*(11), 4206–4216.
Bartley, A. F., Huang, Z. J., Huber, K. M., & Gibson, J. R. (2008). Differential Activity-Dependent, Homeostatic Plasticity of Two Neocortical Inhibitory Circuits. *Journal of Neurophysiology*, *100*(4), 1983–1994. doi:10.1152/jn.90635.2008
Bartoletti, A., Medini, P., Berardi, N., & Maffei, L. (2004). Environmental enrichment prevents effects of dark-rearing in the rat visual cortex. *Nature Neuroscience*, *7*(3), 215–216. doi:10.1038/nn1201
Bartos, M., Vida, I., & Jonas, P. (2007). Synaptic mechanisms of synchronized gamma oscillations in inhibitory interneuron networks. *Nature Reviews Neuroscience*, *8*(1), 45–56. doi:10.1038/nrn2044
Bastos, A. M., Usrey, W. M., Adams, R. A., Mangun, G. R., Fries, P., & Friston, K. J. (2012). Canonical microcircuits for predictive coding. [Neuron. 2012] - PubMed - NCBI. *Neuron*, *76*(4), 695–711. doi:10.1016/j.neuron.2012.10.038
Bayer, L., Serafin, M., Eggermann, E., Saint-Mleux, B., Machard, D., Jones, B. E., & Mühlethaler, M. (2004). Exclusive Postsynaptic Action of Hypocretin-Orexin on Sublayer 6b Cortical Neurons. *Jneurosci.org*.
Beck, A. T., & Clark, D. A. (1988). Anxiety and depression: An information processing perspective. *Anxiety Research*, *1*(1), 23–36.
Beierlein, M., & Connors, B. W. (2002). Short-term dynamics of thalamocortical and intracortical synapses onto layer 6 neurons in neocortex. *Journal of Neurophysiology*, *88*(4), 1924–1932.
Bellone, C., & Nicoll, R. A. (2007). Rapid Bidirectional Switching of Synaptic NMDA Receptors. *Neuron*, *55*(5), 779–785. doi:10.1016/j.neuron.2007.07.035
Ben-Ari, Y., & Spitzer, N. C. (2010). Phenotypic checkpoints regulate neuronal development. *Trends in Neurosciences*, *33*(11), 485–492. doi:10.1016/j.tins.2010.08.005
Ben-Ari, Y., Cherubini, E., Corradetti, R., & Gaiarsa, J. L. (1989). Giant synaptic potentials in immature rat CA3 hippocampal neurones. *Jp.Physoc.org*.
Ben-Ari, Y., Gaiarsa, J.-L., Tyzio, R., & Khazipov, R. (2007). GABA: a pioneer transmitter that excites immature neurons and generates primitive oscillations. *Physiological Reviews*, *87*(4), 1215–1284.
Ben-Ari, Y., Khalilov, I., Represa, A., & Gozlan, H. (2004). Interneurons set the tune of developing networks. *Trends in Neurosciences*, *27*(7), 422–427. doi:10.1016/j.tins.2004.05.002
Ben-Ari, Y., Khazipov, R., Leinekugel, X., Caillard, O., & Gaiarsa, J. L. (1997). GABAA, NMDA and AMPA receptors: a developmentally regulated 'ménage à trois'. *Trends in Neurosciences*, *20*(11), 523–529.
Ben-Ari, Y., Woodin, M. A., Sernagor, E., Cancedda, L., Vinay, L., Rivera, C., et al. (2012). Refuting the challenges of the developmental shift of polarity of GABA

actions: GABA more exciting than ever! *Frontiers in Cellular Neuroscience*, *6*, 35. doi:10.3389/fncel.2012.00035
Bender, K. J., Rangel, J., & Feldman, D. E. (2004). Development of Columnar Topography in the Excitatory Layer 4 to Layer 2/3 Projection in Rat Barrel Cortex. *Jneurosci.org*.
Betley, J. N., & Sternson, S. M. (2011). Adeno-associated viral vectors for mapping, monitoring, and manipulating neural circuits. *Human Gene Therapy*, *22*(6), 669–677. doi:10.1089/hum.2010.204
Bi, G., & Poo, M. (2001). Synaptic modification by correlated activity: Hebb's postulate revisited. *Annual Review of Neuroscience*, *24*, 139–166. doi:10.1146/annurev.neuro.24.1.139
Blaesse, P., Airaksinen, M. S., Rivera, C., & Kaila, K. (2009). Cation-chloride cotransporters and neuronal function. *Neuron*, *61*(6), 820–838. doi:10.1016/j.neuron.2009.03.003
Blasdel, G. G., & Pettigrew, J. D. (1978). Effect of prior visual experience on cortical recovery from the effects of unilateral eyelid suture in kittens. *The Journal of Physiology*, *274*, 601–619.
Bonifazi, P., Goldin, M., Picardo, M. A., Jorquera, I., Cattani, A., Bianconi, G., et al. (2009). GABAergic hub neurons orchestrate synchrony in developing hippocampal networks. *Science (New York, NY)*, *326*(5958), 1419–1424. doi:10.1126/science.1175509
Borg-Graham, L. J., Monier, C., & Frégnac, Y. (1998). Visual input evokes transient and strong shunting inhibition in visual cortical neurons. *Nature*, *393*(6683), 369–373. doi:10.1038/30735
Boyden, E. S., Zhang, F., Bamberg, E., Nagel, G., & Deisseroth, K. (2005). Millisecond-timescale, genetically targeted optical control of neural activity. *Nature Neuroscience*, *8*(9), 1263–1268. doi:10.1038/nn1525
Brecht, M., & Sakmann, B. (2002). Dynamic representation of whisker deflection by synaptic potentials in spiny stellate and pyramidal cells in the barrels and septa of layer 4 rat somatosensory cortex. *The Journal of Physiology*, *543*(Pt 1), 49–70.
Bresler, T., Shapira, M., Boeckers, T., Dresbach, T., Futter, M., Garner, C. C., et al. (2004). Postsynaptic density assembly is fundamentally different from presynaptic active zone assembly. *The Journal of Neuroscience : the Official Journal of the Society for Neuroscience*, *24*(6), 1507–1520. doi:10.1523/JNEUROSCI.3819-03.2004
Breunig, J. J., Haydar, T. F., & Rakic, P. (2011). Neural stem cells: historical perspective and future prospects. *Neuron*, *70*(4), 614–625. doi:10.1016/j.neuron.2011.05.005
Brodmann, K. (1909). *Vergleichende Lokalisationslehre der Grosshirnrinde in ihren Prinzipien dargestellt auf Grund des Zellenbaues*.
Bruno, R. M. & Sakmann, B. (2006). Cortex Is Driven by Weak but Synchronously Active Thalamocortical Synapses. *Science (New York, NY)*, *312*(5780), 1622–1627. doi:10.1126/science.1124593
Bureau, I., Saint Paul, von, F., & Svoboda, K. (2006). Interdigitated Paralemniscal and Lemniscal Pathways in the Mouse Barrel Cortex. *PLOS Biology*, *4*(12), e382. doi:10.1371/journal.pbio.0040382
Bureau, I., Shepherd, G. M. G., & Svoboda, K. (2004). Precise development of functional and anatomical columns in the neocortex. *Neuron*, *42*(5), 789–801. doi:10.1016/j.neuron.2004.05.002
Butt, S. J. B., Fuccillo, M., Nery, S., Noctor, S., Kriegstein, A., Corbin, J. G., &

Fishell, G. (2005). The Temporal and Spatial Origins of Cortical Interneurons Predict Their Physiological Subtype. *Neuron*, *48*(4), 591–604. doi:10.1016/j.neuron.2005.09.034

Cabelli, R. J., Allendoerfer, K. L., Radeke, M. J., Welcher, A. A., Feinstein, S. C., & Shatz, C. J. (1996). Changing patterns of expression and subcellular localization of TrkB in the developing visual system. *The Journal of Neuroscience*, *16*(24), 7965–7980.

Calarco, C. A., & Robertson, R. T. (1995). Development of basal forebrain projections to visual cortex: Dil studies in rat. *The Journal of Comparative Neurology*, *354*(4), 608–626. doi:10.1002/cne.903540409

Callaway, E. M. (1998). Prenatal development of layer-specific local circuits in primary visual cortex of the macaque monkey. *The Journal of Neuroscience*, *18*(4), 1505–1527.

Caporale, N., & Dan, Y. (2008). Spike timing-dependent plasticity: a Hebbian learning rule. *Annual Review of Neuroscience*, *31*, 25–46. doi:10.1146/annurev.neuro.31.060407.125639

Cardin, J. A., Carlen, M., Meletis, K., Knoblich, U., Zhang, F., Deisseroth, K., et al. (2009). Driving fast-spiking cells induces gamma rhythm and controls sensory responses. *Nature*, *459*(7247), 663–667. doi:10.1038/nature08002

Cauli, B., Audinat, E., Lambolez, B., Angulo, M. C., Ropert, N., Tsuzuki, K., et al. (1997). Molecular and physiological diversity of cortical nonpyramidal cells. *The Journal of Neuroscience*, *17*(10), 3894–3906.

Celikel, T., Szostak, V. A., & Feldman, D. E. (2004). Modulation of spike timing by sensory deprivation during induction of cortical map plasticity. *Nature Neuroscience*, *7*(5), 534–541. doi:10.1038/nn1222

Cellerino, A., Maffei, L., & Domenici, L. (1996). The distribution of brain-derived neurotrophic factor and its receptor trkB in parvalbumin-containing neurons of the rat visual cortex. *The European Journal of Neuroscience*, *8*(6), 1190–1197.

Chancey, J. H., Adlaf, E. W., Sapp, M. C., Pugh, P. C., Wadiche, J. I., & Overstreet-Wadiche, L. S. (2013). GABA Depolarization Is Required for Experience-Dependent Synapse Unsilencing in Adult-Born Neurons. *The Journal of Neuroscience : the Official Journal of the Society for Neuroscience*, *33*(15), 6614–6622. doi:10.1523/JNEUROSCI.0781-13.2013

Chattopadhyaya, B. (2004). Experience and Activity-Dependent Maturation of Perisomatic GABAergic Innervation in Primary Visual Cortex during a Postnatal Critical Period. *The Journal of Neuroscience : the Official Journal of the Society for Neuroscience*, *24*(43), 9598–9611. doi:10.1523/JNEUROSCI.1851-04.2004

Chattopadhyaya, B. (2011). Molecular Mechanisms Underlying Activity-Dependent GABAergic Synapse Development and Plasticity and Its Implications for Neurodevelopmental Disorders. *Neural Plasticity*, *2011*(6), 1–8. doi:10.1126/science.1150516

Chittajallu, R., & Isaac, J. T. R. (2010). Emergence of cortical inhibition by coordinated sensory-driven plasticity at distinct synaptic loci. *Nature Neuroscience*, *13*(10), 1240. doi:doi:10.1038/nn.2639

Christophe, E. (2005). Two Populations of Layer V Pyramidal Cells of the Mouse Neocortex: Development and Sensitivity to Anesthetics. *Journal of Neurophysiology*, *94*(5), 3357–3367. doi:10.1152/jn.00076.2005

Chubykin, A. A., Atasoy, D., Etherton, M. R., Brose, N., Kavalali, E. T., Gibson, J. R., & Südhof, T. C. (2007). Activity-Dependent Validation of Excitatory versus Inhibitory Synapses by Neuroligin-1 versus Neuroligin-2. *Neuron*, *54*(6), 919–

931. doi:10.1016/j.neuron.2007.05.029
Clancy, B., & Cauller, L. J. (1999). Widespread projections from subgriseal neurons (layer VII) to layer I in adult rat cortex. *The Journal of Comparative Neurology*, *407*(2), 275–286.
Clem, R. L., Celikel, T., & Barth, A. L. (2008). Ongoing in vivo experience triggers synaptic metaplasticity in the neocortex. *Science (New York, NY)*, *319*(5859), 101–104. doi:10.1126/science.1143808
Close, J., Xu, H., De Marco García, N., Batista-Brito, R., Rossignol, E., Rudy, B., & Fishell, G. (2012). Satb1 is an activity-modulated transcription factor required for the terminal differentiation and connectivity of medial ganglionic eminence-derived cortical interneurons. *The Journal of Neuroscience : the Official Journal of the Society for Neuroscience*, *32*(49), 17690–17705. doi:10.1523/JNEUROSCI.3583-12.2012
Cohen, S., & Greenberg, M. E. (2008). Communication between the synapse and the nucleus in neuronal development, plasticity, and disease. *Annual Review of Cell and Developmental Biology*, *24*, 183–209. doi:10.1146/annurev.cellbio.24.110707.175235
Colonnese, M. T., Kaminska, A., Minlebaev, M., Milh, M., Bloem, B., Lescure, S., et al. (2010). A conserved switch in sensory processing prepares developing neocortex for vision. *Neuron*, *67*(3), 480–498.
Colonnese, M. T., Shi, J., & Constantine-Paton, M. (2003). Chronic NMDA receptor blockade from birth delays the maturation of NMDA currents, but does not affect AMPA/kainate currents. *Journal of Neurophysiology*, *89*(1), 57–68. doi:10.1152/jn.00049.2002
Constantinople, C. M., & Bruno, R. M. (2013). Deep Cortical Layers Are Activated Directly by Thalamus. *Science (New York, NY)*, *340*(6140), 1591–1594. doi:10.1126/science.1236425
Corlew, R., Bosma, M. M., & Moody, W. J. (2004). Spontaneous, synchronous electrical activity in neonatal mouse cortical neurones. *The Journal of Physiology*, *560*(Pt 2), 377–390. doi:10.1113/jphysiol.2004.071621
Cottam, J. C. H. (2011). Identifying the Functional Role of Martinotti Cells in Cortical Sensory Processing. *Jn.Physiology.org*.
Crair, M. C., & Malenka, R. C. (1995). A critical period for long-term potentiation at thalamocortical synapses. *Nature*, *375*(6529), 325–328. doi:10.1038/375325a0
Crépel, V., Aronov, D., Jorquera, I., Represa, A., Ben-Ari, Y., & Cossart, R. (2007). A Parturition-Associated Nonsynaptic Coherent Activity Pattern in the Developing Hippocampus. *Neuron*, *54*(1), 105–120. doi:10.1016/j.neuron.2007.03.007
Cruikshank, S. J., Ahmed, O. J., Stevens, T. R., Patrick, S. L., Gonzalez, A. N., Elmaleh, M., & Connors, B. W. (2012). Thalamic control of layer 1 circuits in prefrontal cortex. *The Journal of Neuroscience : the Official Journal of the Society for Neuroscience*, *32*(49), 17813–17823. doi:10.1523/JNEUROSCI.3231-12.2012
Cruikshank, S. J., Lewis, T. J., & Connors, B. W. (2007). Synaptic basis for intense thalamocortical activation of feedforward inhibitory cells in neocortex. *Nature Neuroscience*, *10*(4), 462. doi:doi:10.1038/nn1861
Cruikshank, S. J., Rose, H. J., & Metherate, R. (2002). Auditory thalamocortical synaptic transmission in vitro. *Journal of Neurophysiology*, *87*(1), 361–384.
Cruikshank, S. J., Urabe, H., Nurmikko, A. V., & Connors, B. W. (2010). Pathway-specific feedforward circuits between thalamus and neocortex revealed by

selective optical stimulation of axons. *Neuron*, *65*(2), 230–245. doi:10.1016/j.neuron.2009.12.025
Cull-Candy, S. G. (2007). NMDA receptors. *eLS*. doi:10.1002/9780470015902.a0000254.pub2
Cull-Candy, S. G., & Leszkiewicz, D. N. (2004). Role of distinct NMDA receptor subtypes at central synapses. *Science's STKE : Signal Transduction Knowledge Environment*, *2004*(255), re16. doi:10.1126/stke.2552004re16
Cull-Candy, S., Brickley, S., & Farrant, M. (2001). NMDA receptor subunits: diversity, development and disease. *Current Opinion in Neurobiology*, *11*(3), 327–335.
da Costa, N. M., & Martin, K. A. C. (2010). Whose Cortical Column Would that Be? *Frontiers in Neuroanatomy*, *4*, 16. doi:10.3389/fnana.2010.00016
da Costa, N. M., & Martin, K. A. C. (2011). How thalamus connects to spiny stellate cells in the cat's visual cortex. *The Journal of Neuroscience : the Official Journal of the Society for Neuroscience*, *31*(8), 2925–2937. doi:10.1523/JNEUROSCI.5961-10.2011
Dalva, M. B., & Katz, L. C. (1994). Rearrangements of synaptic connections in visual cortex revealed by laser photostimulation. *Science (New York, NY)*, *265*(5169), 255–258.
Dan, Y., & Poo, M.-M. (2004). Spike Timing-Dependent Plasticity of Neural Circuits. *Neuron*, *44*(1), 23–30. doi:10.1016/j.neuron.2004.09.007
Dantzker, J. L., & Callaway, E. M. (2000). Laminar sources of synaptic input to cortical inhibitory interneurons and pyramidal neurons. *Nature Neuroscience*, *3*(7), 701–707. doi:10.1038/76656
Datwani, A., Iwasato, T., Itohara, S., & Erzurumlu, R. S. (2002). NMDA receptor-dependent pattern transfer from afferents to postsynaptic cells and dendritic differentiation in the barrel cortex. *Molecular and Cellular Neurosciences*, *21*(3), 477–492.
Daw, M. I., Ashby, M. C., & Isaac, J. T. R. (2007a). Coordinated developmental recruitment of latent fast spiking interneurons in layer IV barrel cortex. *Nature Neuroscience*, *10*(4), 453. doi:doi:10.1038/nn1866
Daw, M. I., Scott, H. L., & Isaac, J. T. R. (2007b). Developmental synaptic plasticity at the thalamocortical input to barrel cortex: Mechanisms and roles. *Molecular and Cellular Neuroscience*, *34*(4), 493–502. doi:10.1016/j.mcn.2007.01.001
De Carlos, J. A., & O'Leary, D. D. (1992). Growth and targeting of subplate axons and establishment of major cortical pathways. *The Journal of Neuroscience*, *12*(4), 1194–1211.
De Kock, C. P. J., Bruno, R. M., Spors, H., & Sakmann, B. (2007). Layer- and cell-type-specific suprathreshold stimulus representation in rat primary somatosensory cortex. *The Journal of Physiology*, *581*(1), 139–154. doi:10.1113/jphysiol.2006.124321
Del Río, J. A., Martínez, A., Auladell, C., & Soriano, E. (2000). Developmental history of the subplate and developing white matter in the murine neocortex. Neuronal organization and relationship with the main afferent systems at embryonic and perinatal stages. *Cerebral Cortex (New York, NY : 1991)*, *10*(8), 784–801.
Denaxa, M., Kalaitzidou, M., Garefalaki, A., Achimastou, A., Lasrado, R., Maes, T., & Pachnis, V. (2012). Maturation-promoting activity of SATB1 in MGE-derived cortical interneurons. *Cell Reports*, *2*(5), 1351–1362. doi:10.1016/j.celrep.2012.10.003

Desai, N. S., Cudmore, R. H., Nelson, S. B., & Turrigiano, G. G. (2002). Critical periods for experience-dependent synaptic scaling in visual cortex. *Nature Neuroscience*, *5*(8), 783–789. doi:10.1038/nn878

Di Cristo, G., Chattopadhyaya, B., Kuhlman, S. J., Fu, Y., Bélanger, M.-C., Wu, C. Z., et al. (2007). Activity-dependent PSA expression regulates inhibitory maturation and onset of critical period plasticity. *Nature Neuroscience*, *10*(12), 1569–1577. doi:10.1038/nn2008

Ramón y Cajal, S. (1907). Die Struktur der sensiblen Ganglien des Menschen und der Tiere.

Doischer, D., Aurel Hosp, J., Yanagawa, Y., Obata, K., Jonas, P., Vida, I., & Bartos, M. (2008). Postnatal Differentiation of Basket Cells from Slow to Fast Signaling Devices. *The Journal of Neuroscience : the Official Journal of the Society for Neuroscience*, *28*(48), 12956–12968. doi:10.1523/JNEUROSCI.2890-08.2008

Donato, F., Rompani, S. B., & Caroni, P. (2014). Parvalbumin-expressing basket-cell network plasticity induced by experience regulates adult learning. *Nature*, *504*(7479), 272–276. doi:10.1038/nature12866

Douglas, R. J., & Martin, K. A. (1991). A functional microcircuit for cat visual cortex. *The Journal of Physiology*, *440*, 735–769.

Douglas, R. J., & Martin, K. A. C. (2004). Neuronal circuits of the neocortex. *Annual Review of Neuroscience*, *27*, 419–451. doi:10.1146/annurev.neuro.27.070203.144152

Douglas, R. J., & Martin, K. A. C. (2007). Mapping the Matrix: The Ways of Neocortex. *Neuron*, *56*(2), 226–238. doi:10.1016/j.neuron.2007.10.017

Douglas, R. J., Martin, K., & Whitteridge, D. (1989). A canonical microcircuit for neocortex. *Neural Computation*.

Du, T., Xu, Q., Ocbina, P. J., & Anderson, S. A. (2008). NKX2.1 specifies cortical interneuron fate by activating Lhx6. *Dev.Biologists.org*.

Dupont, E., Hanganu, I. L., Kilb, W., Hirsch, S., & Luhmann, H. J. (2006). Rapid developmental switch in the mechanisms driving early cortical columnar networks. *Nature*, *439*(7072), 79–83. doi:10.1038/nature04264

Durand, G. M., & Konnerth, A. (1996). Long-term potentiation as a mechanism of functional synapse induction in the developing hippocampus. *Journal of Physiology, Paris*, *90*(5-6), 313–315.

Dzhala, V. I., Talos, D. M., Sdrulla, D. A., Brumback, A. C., Mathews, G. C., Benke, T. A., et al. (2005). NKCC1 transporter facilitates seizures in the developing brain. *Nature Medicine*, *11*(11), 1205–1213. doi:10.1038/nm1301

Economo, von, C. F., & Koskinas, G. N. (1929). *Atlas of Cytoarchitectonics of the Adult Human Cerebral Cortex*. S. Karger AG (Switzerland).

Erzurumlu, R. S., & Gaspar, P. (2012). Development and critical period plasticity of the barrel cortex. *European Journal of Neuroscience*, *35*(10), 1540–1553. doi:10.1111/j.1460-9568.2012.08075.x

Hoerder-Suabedissen, A., Oeschger, F. M., Krishnan, M. L., Belgard, T. G., Wang, W.-Z., Lee, S., et al. (2013). Expression profiling of mouse subplate reveals a dynamic gene network and disease association with autism and schizophrenia. Proceedings of the National Academy of Sciences of the United States of America, 110(9), 3555–3560. doi:10.1073/pnas.1218510110

Fagiolini, M., Pizzorusso, T., Berardi, N., Domenici, L., & Maffei, L. (1994). Functional postnatal development of the rat primary visual cortex and the role of visual experience: dark rearing and monocular deprivation. *Vision Research*, *34*(6), 709–720.

Fanselow, E. E., Richardson, K. A., & Connors, B. W. (2008). Selective, State-Dependent Activation of Somatostatin-Expressing Inhibitory Interneurons in Mouse Neocortex. *Jn.Physiology.org*, *100*(5), 2640–2652. doi:10.1152/jn.90691.2008

Feldman, D. E. (2000). Timing-based LTP and LTD at vertical inputs to layer II/III pyramidal cells in rat barrel cortex. *Neuron*, *27*(1), 45–56.

Feldman, D. E. (2011). Synaptic Mechanisms for Plasticity in Neocortex. *Dx.Doi.org*.

Feldman, D. E., & Brecht, M. (2005). Map plasticity in somatosensory cortex. *Science (New York, NY)*, *310*(5749), 810–815. doi:10.1126/science.1115807

Feldman, D. E., Nicoll, R. A., & Malenka, R. C. (1999). Synaptic plasticity at thalamocortical synapses in developing rat somatosensory cortex: LTP, LTD, and silent synapses. *Journal of Neurobiology*, *41*(1), 92–101. doi:10.1002/(SICI)1097-4695(199910)41:1<92::AID-NEU12>3.0.CO;2-U

Feldman, D. E., Nicoll, R. A., Malenka, R. C., & Isaac, J. T. (1998). Long-term depression at thalamocortical synapses in developing rat somatosensory cortex. *Neuron*, *21*(2), 347–357.

Feldmeyer, D. (2012). Excitatory neuronal connectivity in the barrel cortex. *Frontiers in Neuroanatomy*, *6*, 24. doi:10.3389/fnana.2012.00024

Feldmeyer, D., Brecht, M., Helmchen, F., Petersen, C. C. H., Poulet, J. F. A., Staiger, J. F., et al. (2012). Barrel cortex function. *Progress in Neurobiology*, *103*, 3–27. doi:10.1016/j.pneurobio.2012.11.002

Feldmeyer, D., Egger, V., Lubke, J., & Sakmann, B. (1999). Reliable synaptic connections between pairs of excitatory layer 4 neurones within a single "barrel" of developing rat somatosensory cortex. *The Journal of Physiology*, *521 Pt 1*, 169–190.

Fenno, L., Yizhar, O., & Deisseroth, K. (2011). The development and application of optogenetics. *Annual Review of Neuroscience*, *34*, 389–412. doi:10.1146/annurev-neuro-061010-113817

Fenno, L., Yizhar, O., & Deisseroth, K. (2011). The Development and Application of Optogenetics. *Http://Dx.Doi.org/10.1146/Annurev-Neuro-061010-113817*.

Ferrer, I., Fabregues, I., & Condom, E. (1986). A Golgi study of the sixth layer of the cerebral cortex. I. The lissencephalic brain of Rodentia, Lagomorpha, Insectivora and Chiroptera. *Journal of Anatomy*, *145*, 217–234.

Ferster, D., Chung, S., & Wheat, H. (1996). Orientation selectivity of thalamic input to simple cells of cat visual cortex. *Nature*, *380*(6571), 249–252. doi:10.1038/380249a0

Finney, E. M., Stone, J. R., & Shatz, C. J. (1998). Major glutamatergic projection from subplate into visual cortex during development. *The Journal of Comparative Neurology*, *398*(1), 105–118.

Fino, E., & Yuste, R. (2011). Dense Inhibitory Connectivity in Neocortex. *Neuron*, *69*(6), 1188–1203. doi:10.1016/j.neuron.2011.02.025

Fishell, Gord, & Kriegstein, A. R. (2003). Neurons from radial glia: the consequences of asymmetric inheritance. *Current Opinion in Neurobiology*, *13*(1), 34–41.

Fishell, Gord, & Rudy, B. (2011). Mechanisms of Inhibition within the Telencephalon: "Where the Wild Things Are." *Http://Dx.Doi.org/10.1146/Annurev-Neuro-061010-113717*.

Flames, N., Pla, R., Gelman, D. M., Rubenstein, J. L. R., Puelles, L., & Marín, O. (2007). Delineation of multiple subpallial progenitor domains by the combinatorial expression of transcriptional codes. *The Journal of Neuroscience : the Official Journal of the Society for Neuroscience*, *27*(36), 9682–9695.

doi:10.1523/JNEUROSCI.2750-07.2007
Fogarty, M., Grist, M., Gelman, D., Marín, O., Pachnis, V., & Kessaris, N. (2007). Spatial genetic patterning of the embryonic neuroepithelium generates GABAergic interneuron diversity in the adult cortex. *The Journal of Neuroscience : the Official Journal of the Society for Neuroscience*, *27*(41), 10935–10946. doi:10.1523/JNEUROSCI.1629-07.2007
Fox, K. (1992). A critical period for experience-dependent synaptic plasticity in rat barrel cortex. *Jneurosci.org*.
Frias, C. P., & Wierenga, C. J. (2013). Activity-dependent adaptations in inhibitory axons. *Frontiers in Cellular Neuroscience*, *7*. doi:10.3389/fncel.2013.00219
Friauf, E., & Shatz, C. J. (1991). Changing patterns of synaptic input to subplate and cortical plate during development of visual cortex. *Journal of Neurophysiology*, *66*(6), 2059–2071.
Friauf, E., McConnell, S. K., & Shatz, C. J. (1990). Functional synaptic circuits in the subplate during fetal and early postnatal development of cat visual cortex. *The Journal of Neuroscience*, *10*(8), 2601–2613.
Friedman, H. V., Bresler, T., Garner, C. C., & Ziv, N. E. (2000). Assembly of new individual excitatory synapses: time course and temporal order of synaptic molecule recruitment. *Neuron*, *27*(1), 57–69.
Fries, P. (2009). Neuronal gamma-band synchronization as a fundamental process in cortical computation. *Annual Review of Neuroscience*, *32*, 209–224. doi:10.1146/annurev.neuro.051508.135603
Fu, Y., Tucciarone, J. M., Espinosa, J. S., Sheng, N., Darcy, D. P., Nicoll, R. A., et al. (2014). A Cortical Circuit for Gain Control by Behavioral State. *Cell*, *156*(6), 1139–1152. doi:10.1016/j.cell.2014.01.050
Fukuchi-Shimogori, T., & Grove, E. A. (2001). Neocortex patterning by the secreted signaling molecule FGF8. *Science (New York, NY)*, *294*(5544), 1071–1074. doi:10.1126/science.1064252
Gabernet, L., Jadhav, S. P., Feldman, D. E., Carandini, M., & Scanziani, M. (2005). Somatosensory integration controlled by dynamic thalamocortical feed-forward inhibition. *Neuron*, *48*(2), 315–327. doi:10.1016/j.neuron.2005.09.022
Gao, B. X., Cheng, G., & Ziskind-Conhaim, L. (1998). Development of spontaneous synaptic transmission in the rat spinal cord. *Journal of Neurophysiology*, *79*(5), 2277–2287.
Gao, P., Sultan, K. T., Zhang, X.-J., & Shi, S.-H. (2013). Lineage-dependent circuit assembly in the neocortex. *Development (Cambridge, England)*, *140*(13), 2645–2655. doi:10.1242/dev.087668
Garaschuk, O., Hanse, E., & Konnerth, A. (1998). Developmental profile and synaptic origin of early network oscillations in the CA1 region of rat neonatal hippocampus. *The Journal of Physiology*, *507 (Pt 1)*, 219–236.
Garaschuk, O., Linn, J., Eilers, J., & Konnerth, A. (2000). Large-scale oscillatory calcium waves in the immature cortex. *Nature Neuroscience*, *3*(5), 452–459. doi:10.1038/74823
Gaspard, N., & Vanderhaeghen, P. (2010). From stem cells to neural networks: recent advances and perspectives for neurodevelopmental disorders. *Developmental Medicine & Child Neurology*, *53*(1), 13–17. doi:10.1111/j.1469-8749.2010.03827.x
Gelman, D. M., & Marín, O. (2010). Generation of interneuron diversity in the mouse cerebral cortex. *European Journal of Neuroscience*, *31*(12), 2136–2141. doi:10.1111/j.1460-9568.2010.07267.x

Gelman, D. M., Martini, F. J., Nóbrega-Pereira, S., Pierani, A., Kessaris, N., & Marín, O. (2009). The embryonic preoptic area is a novel source of cortical GABAergic interneurons. *The Journal of Neuroscience : the Official Journal of the Society for Neuroscience*, *29*(29), 9380–9389. doi:10.1523/JNEUROSCI.0604-09.2009

Ghanem, N., Yu, M., Long, J., Hatch, G., Rubenstein, J. L. R., & Ekker, M. (2007). Distinct cis-regulatory elements from the Dlx1/Dlx2 locus mark different progenitor cell populations in the ganglionic eminences and different subtypes of adult cortical interneurons. *The Journal of Neuroscience : the Official Journal of the Society for Neuroscience*, *27*(19), 5012–5022. doi:10.1523/JNEUROSCI.4725-06.2007

Ghosh, A., & Shatz, C. (1992). Involvement of subplate neurons in the formation of ocular dominance columns. *Science (New York, NY)*, *255*(5050), 1441–1443. doi:10.1126/science.1542795

Gibson, J. R., Beierlein, M., & Connors, B. W. (1999). Two networks of electrically coupled inhibitory neurons in neocortex. *Nature*, *402*(6757), 75–79. doi:10.1038/47035

Gibson, J. R., Huber, K. M., & Sudhof, T. C. (2009). Neuroligin-2 Deletion Selectively Decreases Inhibitory Synaptic Transmission Originating from Fast-Spiking but Not from Somatostatin-Positive Interneurons. *The Journal of Neuroscience : the Official Journal of the Society for Neuroscience*, *29*(44), 13883–13897. doi:10.1523/JNEUROSCI.2457-09.2009

GIL, Z., & AMITAI, Y. (1996). Properties of convergent thalamocortical and intracortical synaptic potentials in single neurons of neocortex. *The Journal of Neuroscience*, *16*(20), 6567–6578.

GIL, Z., Connors, B. W., & AMITAI, Y. (1997). Differential regulation of neocortical synapses by neuromodulators and activity. *Neuron*, *19*(3), 679–686.

GIL, Z., Connors, B. W., & AMITAI, Y. (1999). Efficacy of thalamocortical and intracortical synaptic connections: quanta, innervation, and reliability. *Neuron*, *23*(2), 385–397.

Glazewski, S., & Fox, K. (1996). Time course of experience-dependent synaptic potentiation and depression in barrel cortex of adolescent rats. *Journal of Neurophysiology*, *75*(4), 1714–1729.

Glazewski, S., Herman, C., McKenna, M., Chapman, P. F., & Fox, K. (1998). Long-term potentiation in vivo in layers II/III of rat barrel cortex. *Neuropharmacology*, *37*(4-5), 581–592.

Goldberg, E. M., Jeong, H.-Y., Kruglikov, I., Tremblay, R., Lazarenko, R. M., & Rudy, B. (2011). Rapid developmental maturation of neocortical FS cell intrinsic excitability. *Cerebral Cortex*, *21*(3), 666–682. doi:10.1093/cercor/bhq138

Golshani, P., Gonçalves, J. T., Khoshkhoo, S., Mostany, R., Smirnakis, S., & Portera-Cailliau, C. (2009). Internally mediated developmental desynchronization of neocortical network activity. *The Journal of Neuroscience*, *29*(35), 10890–10899.

Gomperts, S. N., Rao, A., Craig, A. M., Malenka, R. C., & Nicoll, R. A. (1998). Postsynaptically silent synapses in single neuron cultures. *Neuron*, *21*(6), 1443–1451.

Grant, E., Hoerder-Suabedissen, A., & Molnár, Z. (2012). Development of the corticothalamic projections. *Frontiers in Neuroscience*, *6*, 53. doi:10.3389/fnins.2012.00053

Groc, L., Gustafsson, B., & Hanse, E. (2002). Spontaneous unitary synaptic activity in CA1 pyramidal neurons during early postnatal development: constant contribution of AMPA and NMDA receptors. *The Journal of Neuroscience : the*

Official Journal of the Society for Neuroscience, *22*(13), 5552–5562.
Groc, L., Gustafsson, B., & Hanse, E. (2003). In vivo evidence for an activity-independent maturation of AMPA/NMDA signaling in the developing hippocampus. *Neuroscience*, *121*(1), 65–72.2007
Groc, L., Gustafsson, B., & Hanse, E. (2006). AMPA signalling in nascent glutamatergic synapses: there and not there! *Trends in Neurosciences*, *29*(3), 132–139. doi:10.1016/j.tins.2006.01.005
Grossberg, S., & Seitz, A. (2003). Laminar development of receptive fields, maps and columns in visual cortex: the coordinating role of the subplate. *Cerebral Cortex (New York, NY : 1991)*, *13*(8), 852–863.
Guillery, R. W., & Sherman, S. M. (2002). Thalamic relay functions and their role in corticocortical communication: generalizations from the visual system. *Neuron*, *33*(2), 163–175.
Guillery, R. W., & Sherman, S. M. (2011). Branched thalamic afferents: What are the messages that they relay to the cortex? *Brain Research Reviews*, *66*(1-2), 205–219. doi:10.1016/j.brainresrev.2010.08.001
Gulledge, A. T., & Stuart, G. J. (2003). Excitatory actions of GABA in the cortex. *Neuron*, *37*(2), 299–309.
Hanganu, I. L. (2001). Spontaneous Synaptic Activity of Subplate Neurons in Neonatal Rat Somatosensory Cortex. *Cerebral Cortex*, *11*(5), 400–410. doi:10.1093/cercor/11.5.400
Hanganu, I. L., & Luhmann, H. J. (2004). Functional nicotinic acetylcholine receptors on subplate neurons in neonatal rat somatosensory cortex. *Journal of Neurophysiology*, *92*(1), 189–198. doi:10.1152/jn.00010.2004
Hanganu, I. L., Kilb, W., & Luhmann, H. J. (2002). Functional synaptic projections onto subplate neurons in neonatal rat somatosensory cortex. *The Journal of Neuroscience : the Official Journal of the Society for Neuroscience*, *22*(16), 7165–7176. doi:20026716
Hanganu, I. L., Okabe, A., Lessmann, V., & Luhmann, H. J. (2009). Cellular mechanisms of subplate-driven and cholinergic input-dependent network activity in the neonatal rat somatosensory cortex. *Cerebral Cortex*, *19*(1), 89–105. doi:10.1093/cercor/bhn061
Hanganu, I. L., Staiger, J. F., Ben-Ari, Y., & Khazipov, R. (2007). Cholinergic Modulation of Spindle Bursts in the Neonatal Rat Visual Cortex In Vivo. *The Journal of Neuroscience : the Official Journal of the Society for Neuroscience*, *27*(21), 5694–5705. doi:10.1523/JNEUROSCI.5233-06.2007
Hanganu-Opatz, I. L. (2010). Between molecules and experience: role of early patterns of coordinated activity for the development of cortical maps and sensory abilities. *Brain Research Reviews*, *64*(1), 160–176. doi:10.1016/j.brainresrev.2010.03.005
Hangya, B., Pi, H.-J., Kvitsiani, D., Ranade, S. P., & Kepecs, A. (2014). From circuit motifs to computations: mapping the behavioral repertoire of cortical interneurons. *Current Opinion in Neurobiology*, *26*, 117–124. doi:10.1016/j.conb.2014.01.007
Hanse, E., Durand, G. M., Garaschuk, O., & Konnerth, A. (1997). Activity-dependent wiring of the developing hippocampal neuronal circuit. *Seminars in Cell & Developmental Biology*, *8*(1), 35–42. doi:10.1006/scdb.1996.0119
Hanse, E., Seth, H., & Riebe, I. (2013). AMPA-silent synapses in brain development and pathology. *Nature Reviews Neuroscience*, *14*(12), 839–850. doi:10.1038/nrn3642

Hanse, E., Taira, T., Lauri, S., & Groc, L. (2009). Glutamate synapse in developing brain: an integrative perspective beyond the silent state. *Trends in Neurosciences*, *32*(10), 532–537. doi:10.1016/j.tins.2009.07.003

Hansen, D. V., Lui, J. H., Flandin, P., Yoshikawa, K., Rubenstein, J. L., Alvarez-Buylla, A., & Kriegstein, A. R. (2013). Non-epithelial stem cells and cortical interneuron production in the human ganglionic eminences. *Nature Neuroscience*, *16*(11), 1576–1587. doi:10.1038/nn.3541

Harris, K. D., & Mrsic-Flogel, T. D. (2013). Cortical connectivity and sensory coding. *Nature*, *503*(7474), 51–58. doi:10.1038/nature12654

Hägglund, M., Dougherty, K. J., Borgius, L., Itohara, S., Iwasato, T., & Kiehn, O. (2013). Optogenetic dissection reveals multiple rhythmogenic modules underlying locomotion. *Pnas.org*.

Hennou, S., Khalilov, I., Diabira, D., Ben-Ari, Y., & Gozlan, H. (2002). Early sequential formation of functional GABA(A) and glutamatergic synapses on CA1 interneurons of the rat foetal hippocampus. *The European Journal of Neuroscience*, *16*(2), 197–208.

Hensch, T. K. (2005). Critical period plasticity in local cortical circuits. *Nature Reviews Neuroscience*, *6*(11), 877–888. doi:10.1038/nrn1787

Hestrin, S. (2009). Cell-type identity: a key to unlocking the function of neocortical circuits. *Current Opinion in Neurobiology*, *19*(4), 415–421. doi:10.1016/j.conb.2009.07.011

Higashi, S., Molnar, Z., Kurotani, T., & Toyama, K. (2002). Prenatal development of neural excitation in rat thalamocortical projections studied by optical recording. *Neuroscience*, *115*(4), 1231–1246. doi:10.1016/S0306-4522(02)00418-9

Higo, S., Udaka, N., & Tamamaki, N. (2007). Long-range GABAergic projection neurons in the cat neocortex. *The Journal of Comparative Neurology*, *503*(3), 421–431. doi:10.1002/cne.21395

Hill, M. R. H., & Greenfield, S. A. (2014). Characterization of early cortical population response to thalamocortical input in vitro. *Frontiers in Neuroscience*, *7*. doi:10.3389/fnins.2013.00273

Hirsch, S., & Luhmann, H. J. (2008). Pathway-specificity in N-methyl-d-aspartate receptor-mediated synaptic inputs onto subplate neurons. *Current Opinion in Neurobiology*, *153*(4), 1092–1102. doi:10.1016/j.neuroscience.2008.01.068

Hoerder-Suabedissen, A., & Molnár, Z. (2011). Morphology of mouse subplate cells with identified projection targets changes with age. *The Journal of Comparative Neurology*, *520*(1), 174–185. doi:10.1002/cne.22725

Hoerder-Suabedissen, A., & Molnár, Z. (2012). Molecular Diversity of Early-Born Subplate Neurons. *Cerebral Cortex*. doi:10.1093/cercor/bhs137

Hoerder-Suabedissen, A., Wang, W.-Z., Lee, S., Davies, K. E., Goffinet, A. M., Rakic, S., et al. (2009). Novel markers reveal subpopulations of subplate neurons in the murine cerebral cortex. *Cerebral Cortex*, *19*(8), 1738–1750. doi:10.1093/cercor/bhn195

Hohnke, C. D., Oray, S., & Sur, M. (2000). Activity-dependent patterning of retinogeniculate axons proceeds with a constant contribution from AMPA and NMDA receptors. *The Journal of Neuroscience : the Official Journal of the Society for Neuroscience*, *20*(21), 8051–8060.

Hong, E. J., McCord, A. E., & Greenberg, M. E. (2008). A biological function for the neuronal activity-dependent component of Bdnf transcription in the development of cortical inhibition. *Neuron*, *60*(4), 610–624. doi:10.1016/j.neuron.2008.09.024

Hooks, B. M., Hires, S. A., Zhang, Y.-X., Huber, D., Petreanu, L., Svoboda, K., &

Shepherd, G. M. G. (2011). Laminar analysis of excitatory local circuits in vibrissal motor and sensory cortical areas. *PLOS Biology*, *9*(1), e1000572. doi:10.1371/journal.pbio.1000572

Hooks, B. M., Mao, T., Gutnisky, D. A., Yamawaki, N., Svoboda, K., & Shepherd, G. M. G. (2013). Organization of cortical and thalamic input to pyramidal neurons in mouse motor cortex. *The Journal of Neuroscience : the Official Journal of the Society for Neuroscience*, *33*(2), 748–760. doi:10.1523/JNEUROSCI.4338-12.2013

Horton, J. C., & Adams, D. L. (2005). The cortical column: a structure without a function. *Philosophical Transactions of the Royal Society B: Biological Sciences*, *360*(1456), 837–862. doi:10.1098/rstb.2005.1623

Hsia, A. Y., Malenka, R. C., & Nicoll, R. A. (1998). Development of excitatory circuitry in the hippocampus. *Journal of Neurophysiology*, *79*(4), 2013–2024.

Huang, Z. J., Di Cristo, G., & Ango, F. (2007). Development of GABA innervation in the cerebral and cerebellar cortices. *Nature Reviews Neuroscience*, *8*(9), 673–686. doi:10.1038/nrn2188

Hubel, D. H., & Wiesel, T. N. (1962). Receptive fields, binocular interaction and functional architecture in the cat's visual cortex. *The Journal of Physiology*, *160*, 106–154.

HUBEL, D. H., & WIESEL, T. N. (1963). Shape and arrangement of columns in cat's striate cortex. *The Journal of Physiology*, *165*, 559–568.

HUBEL, D. H., & WIESEL, T. N. (1964). Effects of monocular deprivation in kittens. *Naunyn-Schmiedebergs Archiv Für Experimentelle Pathologie Und Pharmakologie*, *248*, 492–497.

Hull, C., Isaacson, J. S., & Scanziani, M. (2009). Postsynaptic Mechanisms Govern the Differential Excitation of Cortical Neurons by Thalamic Inputs. *Jneurosci.org*, *29*(28), 9127–9136. doi:10.1523/JNEUROSCI.5971-08.2009

Inan, M., & Crair, M. C. (2007). Development of cortical maps: perspectives from the barrel cortex. *The Neuroscientist : a Review Journal Bringing Neurobiology, Neurology and Psychiatry*, *13*(1), 49–61. doi:10.1177/1073858406296257

Inan, M., Welagen, J., & Anderson, S. A. (2012). Spatial and temporal bias in the mitotic origins of somatostatin- and parvalbumin-expressing interneuron subgroups and the chandelier subtype in the medial ganglionic eminence. *Cerebral Cortex*, *22*(4), 820–827. doi:10.1093/cercor/bhr148

Innocenti, G. M., & Price, D. J. (2005). Exuberance in the development of cortical networks. *Nature Reviews Neuroscience*, *6*(12), 955–965. doi:10.1038/nrn1790

Inta, D., Alfonso, J., Engelhardt, von, J., Kreuzberg, M. M., Meyer, A. H., van Hooft, J. A., & Monyer, H. (2008). Neurogenesis and widespread forebrain migration of distinct GABAergic neurons from the postnatal subventricular zone. *Proceedings of the National Academy of Sciences of the United States of America*, *105*(52), 20994–20999. doi:10.1073/pnas.0807059105

Isaac, J. (2003). Postsynaptic silent synapses: evidence and mechanisms. *Neuropharmacology*, *45*(4), 450–460. doi:10.1016/S0028-3908(03)00229-6

Isaac, J. T., Crair, M. C., Nicoll, R. A., & Malenka, R. C. (1997). Silent synapses during development of thalamocortical inputs. *Neuron*, *18*(2), 269–280.

Isaac, J. T., Nicoll, R. A., & Malenka, R. C. (1995). Evidence for silent synapses: implications for the expression of LTP. *Neuron*, *15*(2), 427–434.

Isaacson, J. S., & Scanziani, M. (2011). How inhibition shapes cortical activity. *Neuron*, *72*(2), 231–243. doi:10.1016/j.neuron.2011.09.027

Iwasato, T., Datwani, A., Wolf, A. M., Nishiyama, H., Taguchi, Y., Tonegawa, S., et

al. (2000). Cortex-restricted disruption of NMDAR1 impairs neuronal patterns in the barrel cortex. *Nature*, *406*(6797), 726–731. doi:10.1038/35021059
Jacob, V., Petreanu, L., Wright, N., Svoboda, K., & Fox, K. (2012). Regular Spiking and Intrinsic Bursting Pyramidal Cells Show Orthogonal Forms of Experience-Dependent Plasticity in Layer V of Barrel Cortex. *Neuron*, *73*(2), 391–404. doi:10.1016/j.neuron.2011.11.034
Jacobs, E. C., Campagnoni, C., Kampf, K., Reyes, S. D., Kalra, V., Handley, V., et al. (2007). Visualization of corticofugal projections during early cortical development in a tau-GFP-transgenic mouse. *The European Journal of Neuroscience*, *25*(1), 17–30. doi:10.1111/j.1460-9568.2006.05258.x
Jakovcevski, I., Mayer, N., & Zecevic, N. (2011). Multiple origins of human neocortical interneurons are supported by distinct expression of transcription factors. *Cerebral Cortex*, *21*(8), 1771–1782. doi:10.1093/cercor/bhq245
Jiao, Y. (2006). Major Effects of Sensory Experiences on the Neocortical Inhibitory Circuits. *The Journal of Neuroscience : the Official Journal of the Society for Neuroscience*, *26*(34), 8691–8701. doi:10.1523/JNEUROSCI.2478-06.2006
Jiao, Y., Zhang, Z., Zhang, C., Wang, X., Sakata, K., Lu, B., & Sun, Q.-Q. (2011). A key mechanism underlying sensory experience-dependent maturation of neocortical GABAergic circuits in vivo. *Proceedings of the National Academy of Sciences of the United States of America*, *108*(29), 12131–12136. doi:10.1073/pnas.1105296108
Kandler, K., & Katz, L. C. (1998). Coordination of neuronal activity in developing visual cortex by gap junction-mediated biochemical communication. *The Journal of Neuroscience*, *18*(4), 1419–1427.
Kanold, P. O. (2003). Role of Subplate Neurons in Functional Maturation of Visual Cortical Columns. *Science (New York, NY)*, *301*(5632), 521–525. doi:10.1126/science.1084152
Kanold, P. O. (2004). Transient microcircuits formed by subplate neurons and their role in functional development of thalamocortical connections. *Neuroreport*, *15*(14), 2149.
Kanold, P. O. (2009). Subplate neurons: crucial regulators of cortical development and plasticity. *Frontiers in Neuroanatomy*, *3*, 16. doi:10.3389/neuro.05.016.2009
Kanold, P. O., & Luhmann, H. J. (2010). The subplate and early cortical circuits. *Annual Review of Neuroscience*, *33*, 23–48. doi:10.1146/annurev-neuro-060909-153244
Kanold, P. O., & Shatz, C. J. (2006). Subplate Neurons Regulate Maturation of Cortical Inhibition and Outcome of Ocular Dominance Plasticity. *Neuron*, *51*(5), 627–638. doi:10.1016/j.neuron.2006.07.008
Kapfer, C., Glickfeld, L. L., Atallah, B. V., & Scanziani, M. (2007). Supralinear increase of recurrent inhibition during sparse activity in the somatosensory cortex. *Nature Neuroscience*, *10*(6), 743–753. doi:10.1038/nn1909
Katz, L. C., & Shatz, C. J. (1996). Synaptic activity and the construction of cortical circuits. *Science (New York, NY)*, *274*(5290), 1133–1138.
Kawaguchi, Y. (1995). Physiological subgroups of nonpyramidal cells with specific morphological characteristics in layer II/III of rat frontal cortex. *Jneurosci.org*.
Kawaguchi, Y., & Kubota, Y. (1997). GABAergic cell subtypes and their synaptic connections in rat frontal cortex. *Cerebral Cortex (New York, NY : 1991)*, *7*(6), 476–486.
Kawaguchi, Y., Katsumaru, H., Kosaka, T., Heizmann, C. W., & Hama, K. (1987). Fast spiking cells in rat hippocampus (CA1 region) contain the calcium-binding

protein parvalbumin. *Brain Research*, *416*(2), 369–374.
Kätzel, D., & Miesenböck, G. (2014). Experience-Dependent Rewiring of Specific Inhibitory Connections in Adult Neocortex. *PLOS Biology*, *12*(2), e1001798. doi:10.1371/journal.pbio.1001798
Kätzel, D., Zemelman, B. V., Buetfering, C., Wölfel, M., & Miesenböck, G. (2010). The columnar and laminar organization of inhibitory connections to neocortical excitatory cells. *Nature Neuroscience*, *14*(1), 100–107. doi:10.1038/nn.2687
Kelsom, C., & Lu, W. (2013). Development and specification of GABAergic cortical interneurons. *Cell & Bioscience*, *3*(1), 19. doi:10.1016/j.biopsych.2011.03.027
Kepecs, A., & Fishell, G. (2014). Interneuron cell types are fit to function. *Nature*, *505*(7483), 318–326. doi:doi:10.1038/nature12983
Kerchner, G. A., & Nicoll, R. A. (2008). Silent synapses and the emergence of a postsynaptic mechanism for LTP. *Nature Reviews Neuroscience*, *9*(11), 813–825. doi:10.1038/nrn2501
Khazipov, R., & Luhmann, H. J. (2006). Early patterns of electrical activity in the developing cerebral cortex of humans and rodents. *Trends in Neurosciences*, *29*(7), 414–418. doi:10.1016/j.tins.2006.05.007
Khazipov, R., Colonnese, M., & Minlebaev, M. (2013). *Neonatal Cortical Rhythms*. *Neural Circuit Development and Function in the Heathy and Diseased Brain* (Vol. #volume#, pp. 131–153). Elsevier Inc. doi:10.1016/B978-0-12-397267-5.00141-2
Khazipov, R., Sirota, A., Leinekugel, X., Holmes, G. L., Ben-Ari, Y., & Buzsáki, G. (2004). Early motor activity drives spindle bursts in the developing somatosensory cortex. *Nature*, *432*(7018), 758–761. doi:10.1038/nature03132
Kidd, F. L., & Isaac, J. T. R. (1999). Developmental and activity- dependent regulation of kainate receptors at thalamocortical synapses. *Nature*, *400*(6744), 569. doi:doi:10.1038/23040
Kilb, W. (2012). Development of the GABAergic System from Birth to Adolescence. *The Neuroscientist*, *18*(6), 613–630. doi:10.1177/1073858411422114
Kilb, W., Hanganu, I. L., Okabe, A., Sava, B. A., Shimizu-Okabe, C., Fukuda, A., & Luhmann, H. J. (2008). Glycine receptors mediate excitation of subplate neurons in neonatal rat cerebral cortex. *Journal of Neurophysiology*, *100*(2), 698–707. doi:10.1152/jn.00657.2007
Kilb, W., Kirischuk, S., & Luhmann, H. J. (2011). Electrical activity patterns and the functional maturation of the neocortex. *European Journal of Neuroscience*, *34*(10), 1677–1686. doi:10.1111/j.1460-9568.2011.07878.x
Kinnischtzke, A. K., Sewall, A. M., Berkepile, J. M., & Fanselow, E. E. (2012). Postnatal maturation of somatostatin-expressing inhibitory cells in the somatosensory cortex of GIN mice. *Frontiers in Neural Circuits*, *6*. doi:10.3389/fncir.2012.00033
Kiritani, T., Wickersham, I. R., Seung, H. S., & Shepherd, G. M. G. (2012). Hierarchical Connectivity and Connection-Specific Dynamics in the Corticospinal-Corticostriatal Microcircuit in Mouse Motor Cortex. *The Journal of Neuroscience : the Official Journal of the Society for Neuroscience*, *32*(14), 4992–5001. doi:10.1523/JNEUROSCI.4759-11.2012
Klausberger, T., & Somogyi, P. (2008). Neuronal diversity and temporal dynamics: the unity of hippocampal circuit operations. *Science (New York, NY)*, *321*(5885), 53–57. doi:10.1126/science.1149381
Kohara, K., Yasuda, H., Huang, Y., Adachi, N., Sohya, K., & Tsumoto, T. (2007). A local reduction in cortical GABAergic synapses after a loss of endogenous brain-

derived neurotrophic factor, as revealed by single-cell gene knock-out method. *The Journal of Neuroscience : the Official Journal of the Society for Neuroscience*, *27*(27), 7234–7244. doi:10.1523/JNEUROSCI.1943-07.2007

Kokaia, Z., Bengzon, J., Metsis, M., Kokaia, M., Persson, H., & Lindvall, O. (1993). Coexpression of neurotrophins and their receptors in neurons of the central nervous system. *Pnas*, *90*(14), 6711–6715.

Kossut, M. (1998). Experience-dependent changes in function and anatomy of adult barrel cortex. *Experimental Brain Research. Experimentelle Hirnforschung. Expérimentation Cérébrale*, *123*(1-2), 110–116.

Molliver, M. E., KOSTOVIC, I., & Van der Loos, H. (1974). The development of synapses in cerebral cortex of the human fetus. Brain Research, 50(2), 403–407.

Kostovic, I., & Rakic, P. (1980). Cytology and time of origin of interstitial neurons in the white matter in infant and adult human and monkey telencephalon. *Journal of Neurocytology*, *9*(2), 219–242. doi:10.1007/BF01205159

Kovacs, M., & Beck, A. T. (1978). Maladaptive cognitive structures in depression. *American Journal of Psychiatry*, *135*(5), 525–533.

König, N., Roch, G., & Marty, R. (1975). The onset of synaptogenesis in rat temporal cortex. *Anatomy and Embryology*, *148*(1), 73–87.

Kullmann, D. M. (1994). Amplitude fluctuations of dual-component EPSCs in hippocampal pyramidal cells: implications for long-term potentiation. *Neuron*, *12*(5), 1111–1120.

Kuzirian, M. S., & Paradis, S. (2011). Emerging themes in GABAergic synapse development. *Progress in Neurobiology*, *95*(1), 68–87. doi:10.1016/j.pneurobio.2011.07.002

Lavdas, A. A., Grigoriou, M., Pachnis, V., & Parnavelas, J. G. (1999). The medial ganglionic eminence gives rise to a population of early neurons in the developing cerebral cortex. *The Journal of Neuroscience : the Official Journal of the Society for Neuroscience*, *19*(18), 7881–7888.

Lazarus, M. S., & Huang, Z. J. (2011). Distinct maturation profiles of perisomatic and dendritic targeting GABAergic interneurons in the mouse primary visual cortex during the critical period of ocular dominance plasticity. *Journal of Neurophysiology*, *106*(2), 775–787. doi:10.1152/jn.00729.2010

Le Magueresse, C., & Monyer, H. (2013). GABAergic interneurons shape the functional maturation of the cortex. *Neuron*, *77*(3), 388–405. doi:10.1016/j.neuron.2013.01.011

Le Magueresse, C., Alfonso, J., Khodosevich, K., Arroyo Martín, A. A., Bark, C., & Monyer, H. (2011). "Small axonless neurons": postnatally generated neocortical interneurons with delayed functional maturation. *The Journal of Neuroscience : the Official Journal of the Society for Neuroscience*, *31*(46), 16731–16747. doi:10.1523/JNEUROSCI.4273-11.2011

Lee, C. K., & Huguenard, J. R. (2011). Martinotti Cells: Community Organizers. *Neuron*, *69*(6), 1042–1045. doi:10.1016/j.neuron.2011.03.003

Lee, L.-J., Iwasato, T., Itohara, S., & Erzurumlu, R. S. (2005). Exuberant thalamocortical axon arborization in cortex-specific NMDAR1 knockout mice. *The Journal of Comparative Neurology*, *485*(4), 280–292. doi:10.1002/cne.20481

Lee, S., Hjerling-Leffler, J., Zagha, E., Fishell, G., & Rudy, B. (2010). The Largest Group of Superficial Neocortical GABAergic Interneurons Expresses Ionotropic Serotonin Receptors. *Jneurosci.org*.

Lee, S.-H., Kwan, A. C., Zhang, S., Phoumthipphavong, V., Flannery, J. G., Masmanidis, S. C., et al. (2012). Activation of specific interneurons improves V1

feature selectivity and visual perception. *Nature*. doi:doi:10.1038/nature11312
Lefort, S., Tomm, C., Floyd Sarria, J.-C., & Petersen, C. C. H. (2009). The Excitatory Neuronal Network of the C2 Barrel Column in Mouse Primary Somatosensory Cortex. *Neuron*, *61*(2), 301–316. doi:10.1016/j.neuron.2008.12.020
Leinekugel, X., Medina, I., Khalilov, I., Ben-Ari, Y., & Khazipov, R. (1997). Ca2+ Oscillations Mediated by the Synergistic Excitatory Actions of GABAA and NMDA Receptors in the Neonatal Hippocampus. *Neuron*, *18*(2), 243–255. doi:10.1016/S0896-6273(00)80265-2
Letinic, K., Zoncu, R., & Rakic, P. (2002). Origin of GABAergic neurons in the human neocortex. *Nature*, *417*(6889), 645–649. doi:10.1038/nature00779
Levelt, C. N., & Hübener, M. (2012). Critical-Period Plasticity in the Visual Cortex. *Dx.Doi.org*.
Li, H., Tornberg, J., Kaila, K., Airaksinen, M. S., & Rivera, C. (2002). Patterns of cation-chloride cotransporter expression during embryonic rodent CNS development. *The European Journal of Neuroscience*, *16*(12), 2358–2370.
Li, Y., Lu, H., Cheng, P.-L., Ge, S., Xu, H., Shi, S.-H., & Dan, Y. (2012). Clonally related visual cortical neurons show similar stimulus feature selectivity. *Nature*, *486*(7401), 118–121. doi:10.1038/nature11110
Liao, C.-C., & Lee, L.-J. (2011). Evidence for structural and functional changes of subplate neurons in developing rat barrel cortex. *Brain Structure and Function*, *217*(2), 275–292. doi:10.1007/s00429-011-0354-5
Liao, D., & Malinow, R. (1996). Deficiency in induction but not expression of LTP in hippocampal slices from young rats. *Learning & Memory (Cold Spring Harbor, N.Y.)*, *3*(2-3), 138–149.
Liao, D., Hessler, N. A., & Malinow, R. (1995). Activation of postsynaptically silent synapses during pairing-induced LTP in CA1 region of hippocampal slice. *Nature*, *375*(6530), 400–404. doi:10.1038/375400a0
Liao, D., Scannevin, R. H., & Huganir, R. (2001). Activation of silent synapses by rapid activity-dependent synaptic recruitment of AMPA receptors. *The Journal of Neuroscience : the Official Journal of the Society for Neuroscience*, *21*(16), 6008–6017.
Liao, D., Zhang, X., O'Brien, R., Ehlers, M. D., & Huganir, R. L. (1999). Regulation of morphological postsynaptic silent synapses in developing hippocampal neurons. *Nature Neuroscience*, *2*(1), 37–43. doi:10.1038/4540
Liodis, P., Denaxa, M., Grigoriou, M., Akufo-Addo, C., Yanagawa, Y., & Pachnis, V. (2007). Lhx6 Activity Is Required for the Normal Migration and Specification of Cortical Interneuron Subtypes. *The Journal of Neuroscience : the Official Journal of the Society for Neuroscience*, *27*(12), 3078–3089. doi:10.1523/JNEUROSCI.3055-06.2007
Lisman, J. (1989). A mechanism for the Hebb and the anti-Hebb processes underlying learning and memory. *Proceedings of the National Academy of Sciences of the United States of America*, *86*(23), 9574–9578.
Lissin, D. V., Gomperts, S. N., Carroll, R. C., Christine, C. W., Kalman, D., Kitamura, M., et al. (1998). Activity differentially regulates the surface expression of synaptic AMPA and NMDA glutamate receptors. *Pnas*, *95*(12), 7097–7102.
Little, J. P., & Carter, A. G. (2012). Subcellular synaptic connectivity of layer 2 pyramidal neurons in the medial prefrontal cortex. *The Journal of Neuroscience : the Official Journal of the Society for Neuroscience*, *32*(37), 12808–12819. doi:10.1523/JNEUROSCI.1616-12.2012

Longair, M. H., Baker, D. A., & Armstrong, J. D. (2011). Simple Neurite Tracer: open source software for reconstruction, visualization and analysis of neuronal processes. *Bioinformatics (Oxford, England)*, *27*(17), 2453–2454. doi:10.1093/bioinformatics/btr390

López-Bendito, G., & Molnár, Z. (2003). Thalamocortical development: how are we going to get there? *Nature Reviews Neuroscience*, *4*(4), 276–289. doi:10.1038/nrn1075

Lu, T., & Trussell, L. O. (2001). Mixed excitatory and inhibitory GABA-mediated transmission in chick cochlear nucleus. *The Journal of Physiology*, *535*(Pt 1), 125–131.

Luhmann, H. (2009). Subplate cells: amplifiers of neuronal activity in the developing cerebral cortex. *Frontiers in Neuroanatomy*, *3*, 19. doi:10.3389/neuro.05.019.2009

Luhmann, H. J., Hanganu, I., & Kilb, W. (2003). Cellular physiology of the neonatal rat cerebral cortex. *Current Opinion in Neurobiology*, *60*(4), 345–353. doi:10.1016/S0361-9230(03)00059-5

Luhmann, H. J., Kirischuk, S., Sinning, A., & Kilb, W. (2014). Early GABAergic circuitry in the cerebral cortex. *Current Opinion in Neurobiology*, *26*, 72–78. doi:10.1016/j.conb.2013.12.014

Luhmann, H. J., Reiprich, R. A., Hanganu, I., & Kilb, W. (2000). Cellular physiology of the neonatal rat cerebral cortex: intrinsic membrane properties, sodium and calcium currents. *Journal of Neuroscience Research*, *62*(4), 574–584.

Luhmann, H. J., Schubert, D., K ouml tter, R., & Staiger, J. F. (1999). Cellular Morphology and Physiology of the Perinatal Rat Cerebral Cortex. *Developmental Neuroscience*, *21*(3-5), 298–309. doi:10.1159/000017379

Luskin, M. B., & Shatz, C. J. (1985). Studies of the earliest generated cells of the cat's visual cortex: cogeneration of subplate and marginal zones. *The Journal of Neuroscience*, *5*(4), 1062–1075.

Lübke, J., & Feldmeyer, D. (2007). Excitatory signal flow and connectivity in a cortical column: focus on barrel cortex. *Brain Structure and Function*, *212*(1), 3–17. doi:10.1007/s00429-007-0144-2

Lübke, J., Egger, V., Sakmann, B., & Feldmeyer, D. (2000). Columnar organization of dendrites and axons of single and synaptically coupled excitatory spiny neurons in layer 4 of the rat barrel cortex. *The Journal of Neuroscience : the Official Journal of the Society for Neuroscience*, *20*(14), 5300–5311.

Ma, T., Wang, C., Wang, L., Zhou, X., Tian, M., Zhang, Q., et al. (2013). Subcortical origins of human and monkey neocortical interneurons. *Nature Neuroscience*, *16*(11), 1588–1597. doi:10.1038/nn.3536

Ma, Y., Hu, H., Berrebi, A. S., Mathers, P. H., & Agmon, A. (2006). Distinct Subtypes of Somatostatin-Containing Neocortical Interneurons Revealed in Transgenic Mice. *The Journal of Neuroscience : the Official Journal of the Society for Neuroscience*, *26*(29), 7545–7546. doi:10.1523/JNEUROSCI.2361-06.2006

MacLean, J. N., Fenstermaker, V., Watson, B. O., & Yuste, R. (2006). A visual thalamocortical slice. *Nature Methods*, *3*(2), 129–134. doi:10.1038/nmeth849

Maffei, A., & Turrigiano, G. (2008). The age of plasticity: developmental regulation of synaptic plasticity in neocortical microcircuits. *Optogenetics: Tools for Controlling and Monitoring Neuronal Activity*, *169*, 211–223. doi:10.1016/S0079-6123(07)00012-X

Maffei, A., Nataraj, K., Nelson, S. B., & Turrigiano, G. G. (2006). Potentiation of

cortical inhibition by visual deprivation. *Nature*, *443*(7107), 81–84. doi:10.1038/nature05079
Maffei, A., Nelson, S. B., & Turrigiano, G. G. (2004). Selective reconfiguration of layer 4 visual cortical circuitry by visual deprivation. *Nature Neuroscience*, *7*(12), 1353–1359. doi:10.1038/nn1351
Malatesta, P., Hack, M. A., Hartfuss, E., Kettenmann, H., Klinkert, W., Kirchhoff, F., & Götz, M. (2003). Neuronal or glial progeny: regional differences in radial glia fate. *Neuron*, *37*(5), 751–764.
Malatesta, P., Hartfuss, E., & Götz, M. (2000). Isolation of radial glial cells by fluorescent-activated cell sorting reveals a neuronal lineage. *Development (Cambridge, England)*, *127*(24), 5253–5263.
Manns, I. D., Sakmann, B., & Brecht, M. (2004). Sub- and suprathreshold receptive field properties of pyramidal neurones in layers 5A and 5B of rat somatosensory barrel cortex. *The Journal of Physiology*, *556*(2), 601–622. doi:10.1113/jphysiol.2003.053132
Maravall, M., Stern, E. A., & Svoboda, K. (2004). Development of Intrinsic Properties and Excitability of Layer 2/3 Pyramidal Neurons During a Critical Period for Sensory Maps in Rat Barrel Cortex. *Journal of Neurophysiology*, *92*(1), 144–156. doi:10.1152/jn.00598.2003
Marin-Padilla, M. (1970). Prenatal and early postnatal ontogenesis of the human motor cortex: a golgi study. I. The sequential development of the cortical layers. *Brain Research*, *23*(2), 167–183.
Marin-Padilla, M. (1971). Early prenatal ontogenesis of the cerebral cortex (neocortex) of the cat (Felis domestica). A Golgi study. I. The primordial neocortical organization. *Zeitschrift Für Anatomie Und Entwicklungsgeschichte*, *134*(2), 117–145.
Marin-Padilla, M. (1978). Dual origin of the mammalian neocortex and evolution of the cortical plate. *Anatomy and Embryology*, *152*(2), 109–126.
Marissal, T., Bonifazi, P., Picardo, M. A., Nardou, R., Petit, L. F., Baude, A., et al. (2012). Pioneer glutamatergic cells develop into a morpho-functionally distinct population in the juvenile CA3 hippocampus. *Nature Communications*, *3*, 1316. doi:10.1038/ncomms2318
Marín, O. (2012). Interneuron dysfunction in psychiatric disorders. *Nature Reviews Neuroscience*, *13*(2), 107–120. doi:doi:10.1038/nrn3155
Markram, H., Toledo-Rodriguez, M., Wang, Y., Gupta, A., Silberberg, G., & Wu, C. (2004). Interneurons of the neocortical inhibitory system. *Nature Reviews Neuroscience*, *5*(10), 793–807. doi:doi:10.1038/nrn1519
Marx, M., & Feldmeyer, D. (2012). Morphology and Physiology of Excitatory Neurons in Layer 6b of the Somatosensory Rat Barrel Cortex. *Cerebral Cortex*. doi:10.1093/cercor/bhs254
Matsui, A., Yoshida, A. C., Kubota, M., Ogawa, M., & Shimogori, T. (2011). Mouse in utero electroporation: controlled spatiotemporal gene transfection. *JoVE (Journal of Visualized Experiments)*, (54). doi:10.3791/3024
McCabe, A. K., Chisholm, S. L., Picken-Bahrey, H. L., & Moody, W. J. (2006). The self-regulating nature of spontaneous synchronized activity in developing mouse cortical neurones. *The Journal of Physiology*, *577*(Pt 1), 155–167. doi:10.1113/jphysiol.2006.117523
McConnell, S. K., Ghosh, A., & Shatz, C. J. (1994). Subplate pioneers and the formation of descending connections from cerebral cortex. *The Journal of Neuroscience*, *14*(4), 1892–1907.

McConnell, S., Ghosh, A., & Shatz, C. (1989). Subplate neurons pioneer the first axon pathway from the cerebral cortex. *Science (New York, NY)*, *245*(4921), 978–982. doi:10.1126/science.2475909

McGarry. (2010). Quantitative classification of somatostatin-positive neocortical interneurons identifies three interneuron subtypes. *Frontiers in Neural Circuits*, *4*. doi:10.3389/fncir.2010.00012

Mechawar, N., & Descarries, L. (2001). The cholinergic innervation develops early and rapidly in the rat cerebral cortex: a quantitative immunocytochemical study. *Neuroscience*, *108*(4), 555–567. doi:10.1016/S0306-4522(01)00389-X

Meinecke, D. L., & Peters, A. (1987). GABA immunoreactive neurons in rat visual cortex. *The Journal of Comparative Neurology*, *261*(3), 388–404. doi:10.1002/cne.902610305

Meyer, H. S., Wimmer, V. C., Hemberger, M., Bruno, R. M., de Kock, C. P. J., Frick, A., et al. (2010a). Cell type-specific thalamic innervation in a column of rat vibrissal cortex. *Cerebral Cortex (New York, NY : 1991)*, *20*(10), 2287–2303. doi:10.1093/cercor/bhq069

Meyer, H. S., Wimmer, V. C., Oberlaender, M., de Kock, C. P. J., Sakmann, B., & Helmstaedter, M. (2010b). Number and laminar distribution of neurons in a thalamocortical projection column of rat vibrissal cortex. *Cerebral Cortex (New York, NY : 1991)*, *20*(10), 2277–2286. doi:10.1093/cercor/bhq067

Meyer, H. S., Schwarz, D., Wimmer, V. C., Schmitt, A. C., Kerr, J. N. D., Sakmann, B., & Helmstaedter, M. (2010c). Inhibitory interneurons in a cortical column form hot zones of inhibition in layers 2 and 5A. *Pnas.org*.

Micheva, K. D., & Beaulieu, C. (1995a). An anatomical substrate for experience-dependent plasticity of the rat barrel field cortex. *Pnas*, *92*(25), 11834–11838.

Micheva, K. D., & Beaulieu, C. (1995b). Neonatal sensory deprivation induces selective changes in the quantitative distribution of GABA-immunoreactive neurons in the rat barrel field cortex. *The Journal of Comparative Neurology*, *361*(4), 574–584. doi:10.1002/cne.903610403

Minlebaev, M., Ben-Ari, Y., & Khazipov, R. (2007). Network mechanisms of spindle-burst oscillations in the neonatal rat barrel cortex in vivo. *Journal of Neurophysiology*, *97*(1), 692–700.

Minlebaev, M., Ben-Ari, Y., & Khazipov, R. (2009). NMDA receptors pattern early activity in the developing barrel cortex in vivo. *Cerebral Cortex*, *19*(3), 688–696. doi:10.1093/cercor/bhn115

Minlebaev, M., Colonnese, M., Tsintsadze, T., Sirota, A., & Khazipov, R. (2011). Early Gamma Oscillations Synchronize Developing Thalamus and Cortex. *Science (New York, NY)*, *334*(6053), 226–229. doi:10.1126/science.1210574

Miranda, R. C., Sohrabji, F., & Toran-Allerand, C. D. (1993). Neuronal colocalization of mRNAs for neurotrophins and their receptors in the developing central nervous system suggests a potential for autocrine interactions. *Pnas*, *90*(14), 6439–6443.

Miyata, T., Kawaguchi, A., Okano, H., & Ogawa, M. (2001). Asymmetric inheritance of radial glial fibers by cortical neurons. *Neuron*, *31*(5), 727–741.

Miyoshi, G., Butt, S. J. B., Takebayashi, H., & Fishell, G. (2007). Physiologically distinct temporal cohorts of cortical interneurons arise from telencephalic Olig2-expressing precursors. *The Journal of Neuroscience : the Official Journal of the Society for Neuroscience*, *27*(29), 7786–7798. doi:10.1523/JNEUROSCI.1807-07.2007

Miyoshi, G., Hjerling-Leffler, J., Karayannis, T., Sousa, V. H., Butt, S. J. B., Battiste, J., et al. (2010). Genetic Fate Mapping Reveals That the Caudal Ganglionic

Eminence Produces a Large and Diverse Population of Superficial Cortical Interneurons. *Jneurosci.org*.
Molnar, Z., & Blakemore, C. (1995). How do thalamic axons find their way to the cortex? *Trends in Neurosciences*, *18*(9), 389–397.
Molnar, Z., & Cordery, P. (1999). Connections between cells of the internal capsule, thalamus, and cerebral cortex in embryonic rat. *The Journal of Comparative Neurology*, *413*(1), 1–25.
Molnar, Z., Adams, R., & Blakemore, C. (1998). Mechanisms underlying the early establishment of thalamocortical connections in the rat. *The Journal of Neuroscience*, *18*(15), 5723–5745.
Molnár, Z., & Butt, S. J. B. (2013). Best-laid schemes for interneuron origin of mice and men. *Nature Neuroscience*, *16*(11), 1512–1514. doi:10.1038/nn.3557
Molnár, Z., Kurotani, T., Higashi, S., Yamamoto, N., & Toyama, K. (2003). Development of functional thalamocortical synapses studied with current source-density analysis in whole forebrain slices in the rat. *Brain Research Bulletin*, *60*(4), 355–371. doi:10.1016/S0361-9230(03)00061-3
Molnár, Z., Métin, C., Stoykova, A., Tarabykin, V., Price, D. J., Francis, F., et al. (2006). Comparative aspects of cerebral cortical development. *The European Journal of Neuroscience*, *23*(4), 921–934. doi:10.1111/j.1460-9568.2006.04611.x
Montiel, J. F., Wang, W.-Z., Oeschger, F. M., Hoerder-Suabedissen, A., Tung, W. L., García-Moreno, F., et al. (2011). Hypothesis on the Dual Origin of the Mammalian Subplate. *Frontiers in Neuroanatomy*, *5*. doi:10.3389/fnana.2011.00025
Morris, R. G. M. (2006). Elements of a neurobiological theory of hippocampal function: the role of synaptic plasticity, synaptic tagging and schemas. *European Journal of Neuroscience*, *23*(11), 2829–2846. doi:10.1111/j.1460-9568.2006.04888.x
Mountcastle, V. B. (1957). Modality and topographic properties of single neurons of cat's somatic sensory cortex. *Journal of Neurophysiology*, *20*(4), 408–434.
Mountcastle, V. B. (1997). The columnar organization of the neocortex. *Brain : a Journal of Neurology*, *120 (Pt 4)*, 701–722.
Mueller, A. L., Taube, J. S., & Schwartzkroin, P. A. (1984). Development of hyperpolarizing inhibitory postsynaptic potentials and hyperpolarizing response to gamma-aminobutyric acid in rabbit hippocampus studied in vitro. *The Journal of Neuroscience*, *4*(3), 860–867.
Murayama, M., Pérez-Garci, E., Nevian, T., Bock, T., Senn, W., & Larkum, M. E. (2009). Dendritic encoding of sensory stimuli controlled by deep cortical interneurons. *Nature*, *457*(7233), 1137–1141. doi:10.1038/nature07663
Myme, C. I. O., Sugino, K., Turrigiano, G. G., & Nelson, S. B. (2003). The NMDA-to-AMPA ratio at synapses onto layer 2/3 pyramidal neurons is conserved across prefrontal and visual cortices. *Journal of Neurophysiology*, *90*(2), 771–779. doi:10.1152/jn.00070.2003
Nery, S., Fishell, G., & Corbin, J. G. (2002). The caudal ganglionic eminence is a source of distinct cortical and subcortical cell populations. *Nature Neuroscience*, *5*(12), 1279–1287. doi:10.1038/nn971
Noctor, S. C., Flint, A. C., Weissman, T. A., Dammerman, R. S., & Kriegstein, A. R. (2001). Neurons derived from radial glial cells establish radial units in neocortex. *Nature*, *409*(6821), 714–720. doi:10.1038/35055553
Noctor, S. C., Martínez-Cerdeño, V., Ivic, L., & Kriegstein, A. R. (2004). Cortical neurons arise in symmetric and asymmetric division zones and migrate through

specific phases. *Nature Neuroscience*, *7*(2), 136–144. doi:10.1038/nn1172
Obata, K., Oide, M., & Tanaka, H. (1978). Excitatory and inhibitory actions of GABA and glycine on embryonic chick spinal neurons in culture. *Brain Research*, *144*(1), 179–184.
Oberlaender, M., De Kock, C. P. J., Bruno, R. M., Ramirez, A., Meyer, H. S., Dercksen, V. J., et al. (2012). Cell Type-Specific Three-Dimensional Structure of Thalamocortical Circuits in a Column of Rat Vibrissal Cortex. *Cerebral Cortex*, *22*(10), 2375–2391. doi:10.1093/cercor/bhr317
Oh, S. W., Harris, J. A., Ng, L., Winslow, B., Cain, N., Mihalas, S., et al. (2014). A mesoscale connectome of the mouse brain. *Nature*. doi:10.1038/nature13186
Ohtsuki, G., Nishiyama, M., Yoshida, T., Murakami, T., Histed, M., Lois, C., & Ohki, K. (2012). Similarity of Visual Selectivity among Clonally Related Neurons in Visual Cortex. *Neuron*, *75*(1), 65–72. doi:10.1016/j.neuron.2012.05.023
Okabe, S., Miwa, A., & Okado, H. (2001). Spine formation and correlated assembly of presynaptic and postsynaptic molecules. *The Journal of Neuroscience : the Official Journal of the Society for Neuroscience*, *21*(16), 6105–6114.
Okaty, B. W., Miller, M. N., Sugino, K., Hempel, C. M., & Nelson, S. B. (2009). Transcriptional and electrophysiological maturation of neocortical fast-spiking GABAergic interneurons. *The Journal of Neuroscience : the Official Journal of the Society for Neuroscience*, *29*(21), 7040–7052. doi:10.1523/JNEUROSCI.0105-09.2009
Oláh, S., Füle, M., Komlósi, G., Varga, C., Báldi, R., Barzó, P., & Tamás, G. (2009). Regulation of cortical microcircuits by unitary GABA-mediated volume transmission. *Nature*, *461*(7268), 1278–1281. doi:10.1038/nature08503
Oláh, S., Komlósi, G., Szabadics, J., Varga, C., Tóth, E., Barzó, P., & Tamás, G. (2007). Output of neurogliaform cells to various neuron types in the human and rat cerebral cortex. *Frontiers in Neural Circuits*, *1*, 4. doi:10.3389/neuro.04.004.2007
Osheroff, H., & Hatten, M. E. (2009). Gene expression profiling of preplate neurons destined for the subplate: genes involved in transcription, axon extension, neurotransmitter regulation, steroid hormone signaling, and neuronal survival. *Cerebral Cortex*, *19 Suppl 1*, i126–34. doi:10.1093/cercor/bhp034
Oswald, A.-M. M., & Reyes, A. D. (2008). Maturation of intrinsic and synaptic properties of layer 2/3 pyramidal neurons in mouse auditory cortex. *Journal of Neurophysiology*, *99*(6), 2998–3008. doi:10.1152/jn.01160.2007
Owens, D. F., & Kriegstein, A. R. (2002). Is there more to GABA than synaptic inhibition? *Nature Reviews Neuroscience*, *3*(9), 715–727. doi:10.1038/nrn919
Owens, D. F., Liu, X., & Kriegstein, A. R. (1999). Changing properties of GABA(A) receptor-mediated signaling during early neocortical development. *Journal of Neurophysiology*, *82*(2), 570–583.
Packer, A. M., Roska, B., & Häusser, M. (2013). Targeting neurons and photons for optogenetics. *Nature Neuroscience*, *16*(7), 805–815. doi:doi:10.1038/nn.3427
Pangratz-Fuehrer, S., & Hestrin, S. (2011). Synaptogenesis of electrical and GABAergic synapses of fast-spiking inhibitory neurons in the neocortex. *The Journal of Neuroscience : the Official Journal of the Society for Neuroscience*, *31*(30), 10767–10775. doi:10.1523/JNEUROSCI.6655-10.2011
Parnavelas, J. G. (2000). The origin and migration of cortical neurones: new vistas. *Trends in Neurosciences*, *23*(3), 126–131.
Perrenoud, Q., Rossier, J., Geoffroy, H., Vitalis, T., & Gallopin, T. (2012). Diversity of GABAergic Interneurons in Layer VIa and VIb of Mouse Barrel Cortex.

Cercor.Oxfordjournals.org.
Petersen, C. C. H. (2007). The functional organization of the barrel cortex. *Neuron*, *56*(2), 339–355. doi:10.1016/j.neuron.2007.09.017
Petersen, C. C., & Sakmann, B. (2000). The excitatory neuronal network of rat layer 4 barrel cortex. *The Journal of Neuroscience : the Official Journal of the Society for Neuroscience*, *20*(20), 7579–7586.
Petilla Interneuron Nomenclature Group, Ascoli, G. A., Alonso-Nanclares, L., Anderson, S. A., Barrionuevo, G., Benavides-Piccione, R., et al. (2008). Petilla terminology: nomenclature of features of GABAergic interneurons of the cerebral cortex. *Nature Reviews Neuroscience*, *9*(7), 557–568. doi:10.1038/nrn2402
Petreanu, L., Gutnisky, D. A., Huber, D., Xu, N.-L., O'connor, D. H., Tian, L., et al. (2012). Activity in motor-sensory projections reveals distributed coding in somatosensation. *Nature*, *489*(7415), 299. doi:doi:10.1038/nature11321
Petreanu, L., Huber, D., Sobczyk, A., & Svoboda, K. (2007). Channelrhodopsin-2-assisted circuit mapping of long-range callosal projections. *Nature Neuroscience*, *10*(5), 663–668. doi:10.1038/nn1891
Petreanu, L., Mao, T., Sternson, S. M., & Svoboda, K. (2009). The subcellular organization of neocortical excitatory connections. *Nature*, *457*(7233), 1142–1145. doi:10.1038/nature07709
Pfeffer, C. K. (2014). Inhibitory Neurons: Vip Cells Hit the Brake on Inhibition. *Current Biology*, *24*(1), R18–R20. doi:10.1016/j.cub.2013.11.001
Pfeffer, C. K., Xue, M., He, M., Huang, Z. J., & Scanziani, M. (2013). Inhibition of inhibition in visual cortex: the logic of connections between molecularly distinct interneurons. *Nature Neuroscience*, –. doi:10.1038/nn.3446
Pi, H.-J., Hangya, B., Kvitsiani, D., Sanders, J. I., Huang, Z. J., & Kepecs, A. (2013). Cortical interneurons that specialize in disinhibitory control. *Nature*, –. doi:10.1038/nature12676
Picardo, M. A., Guigue, P., Bonifazi, P., Batista-Brito, R., Allene, C., Ribas, A., et al. (2011). Pioneer GABA Cells Comprise a Subpopulation of Hub Neurons in the Developing Hippocampus. *Neuron*, *71*(4), 695–709. doi:10.1016/j.neuron.2011.06.018
Pickard, L., Noël, J., Henley, J. M., Collingridge, G. L., & Molnar, E. (2000). Developmental changes in synaptic AMPA and NMDA receptor distribution and AMPA receptor subunit composition in living hippocampal neurons. *The Journal of Neuroscience : the Official Journal of the Society for Neuroscience*, *20*(21), 7922–7931.
Piñon, M. C., Jethwa, A., Jacobs, E., Campagnoni, A., & Molnár, Z. (2009). Dynamic integration of subplate neurons into the cortical barrel field circuitry during postnatal development in the Golli-tau-eGFP (GTE) mouse. *The Journal of Physiology*, *587*(Pt 9), 1903–1915. doi:10.1113/jphysiol.2008.167767
Plotkin, M. D., Snyder, E. Y., Hebert, S. C., & Delpire, E. (1997). Expression of the Na-K-2Cl cotransporter is developmentally regulated in postnatal rat brains: a possible mechanism underlying GABA's excitatory role in immature brain. *Journal of Neurobiology*, *33*(6), 781–795.
Porter, J. T., Johnson, C. K., & Agmon, A. (2001). Diverse types of interneurons generate thalamus-evoked feedforward inhibition in the mouse barrel cortex. *The Journal of Neuroscience : the Official Journal of the Society for Neuroscience*, *21*(8), 2699–2710.
Powell, T. P., & Mountcastle, V. B. (1959). Some aspects of the functional organization of the cortex of the postcentral gyrus of the monkey: a correlation of

findings obtained in a single unit analysis with cytoarchitecture. *Bulletin of the Johns Hopkins Hospital*, *105*, 133–162.
Price, C. J., Cauli, B., Kovacs, E. R., Kulik, A., Lambolez, B., Shigemoto, R., & Capogna, M. (2005). Neurogliaform neurons form a novel inhibitory network in the hippocampal CA1 area. *The Journal of Neuroscience : the Official Journal of the Society for Neuroscience*, *25*(29), 6775–6786. doi:10.1523/JNEUROSCI.1135-05.2005
Price, D. J., Aslam, S., Tasker, L., & Gillies, K. (1997). Fates of the earliest generated cells in the developing murine neocortex. *The Journal of Comparative Neurology*, *377*(3), 414–422.
Raastad, M., Storm, J. F., & Andersen, P. (1992). Putative Single Quantum and Single Fibre Excitatory Postsynaptic Currents Show Similar Amplitude Range and Variability in Rat Hippocampal Slices. *European Journal of Neuroscience*, *4*(1), 113–117. doi:10.1111/j.1460-9568.1992.tb00114.x
Rah, J.-C., Bas, E., Colonell, J., Mishchenko, Y., Karsh, B., Fetter, R. D., et al. (2013). Thalamocortical input onto layer 5 pyramidal neurons measured using quantitative large-scale array tomography. *Frontiers in Neural Circuits*, *7*. doi:10.3389/fncir.2013.00177
Rakic, P. (1977). Prenatal development of the visual system in rhesus monkey. *Philosophical Transactions of the Royal Society of London. Series B, Biological Sciences*, *278*(961), 245–260.
Rakic, P. (2009). Evolution of the neocortex: a perspective from developmental biology. *Nature Reviews Neuroscience*, *10*(10), 724–735. doi:10.1038/nrn2719
Rao, A., Kim, E., Sheng, M., & Craig, A. M. (1998). Heterogeneity in the molecular composition of excitatory postsynaptic sites during development of hippocampal neurons in culture. *The Journal of Neuroscience*, *18*(4), 1217–1229.
Reep, R. L. (2000). Cortical layer VII and persistent subplate cells in mammalian brains. *Brain, Behavior and Evolution*, *56*(4), 212–234.
Regehr, W. G. (2012). Short-Term Presynaptic Plasticity. *Cold Spring Harbor Perspectives in Biology*, *4*(7), a005702–a005702. doi:10.1101/cshperspect.a005702
Rheims, S., Represa, A., Ben-Ari, Y., & Zilberter, Y. (2008). Layer-specific generation and propagation of seizures in slices of developing neocortex: role of excitatory GABAergic synapses. *Journal of Neurophysiology*, *100*(2), 620–628. doi:10.1152/jn.90403.2008
Rickmann, M., Chronwall, B. M., & Wolff, J. R. (1977). On the development of non-pyramidal neurons and axons outside the cortical plate: the early marginal zone as a pallial anlage. *Anatomy and Embryology*, *151*(3), 285–307.
Rico, B., & Marín, O. (2011). Neuregulin signaling, cortical circuitry development and schizophrenia. *Current Opinion in Genetics & Development*, *21*(3), 262–270. doi:10.1016/j.gde.2010.12.010
Rivera, C., Voipio, J., Payne, J. A., Ruusuvuori, E., Lahtinen, H., Lamsa, K., et al. (1999). The K+/Cl- co-transporter KCC2 renders GABA hyperpolarizing during neuronal maturation. *Nature*, *397*(6716), 251–255. doi:10.1038/16697
Rubenstein, J. L. R. (2010). Annual Research Review: Development of the cerebral cortex: implications for neurodevelopmental disorders. *Journal of Child Psychology and Psychiatry*, *52*(4), 339–355. doi:10.1111/j.1469-7610.2010.02307.x
Rudy, B., Fishell, G., Lee, S., & Hjerling-Leffler, J. (2011). Three groups of interneurons account for nearly 100% of neocortical GABAergic neurons -

Developmental Neurobiology - Wiley Online Library. *Developmental Neurobiology*, *71*(1), 45–61. doi:10.1002/dneu.20853
Rumpel, S., Hatt, H., & Gottmann, K. (1998). Silent synapses in the developing rat visual cortex: evidence for postsynaptic expression of synaptic plasticity. *The Journal of Neuroscience*, *18*(21), 8863–8874.
Rumpel, S., Kattenstroth, G., & Gottmann, K. (2004). Silent synapses in the immature visual cortex: layer-specific developmental regulation. *Journal of Neurophysiology*, *91*(2), 1097–1101. doi:10.1152/jn.00443.2003
Sadaka, Y., Weinfeld, E., Lev, D. L., & White, E. L. (2003). Changes in mouse barrel synapses consequent to sensory deprivation from birth. *The Journal of Comparative Neurology*, *457*(1), 75–86. doi:10.1002/cne.10518
Sanz-Clemente, A., Nicoll, R. A., & Roche, K. W. (2012). Diversity in NMDA Receptor Composition: Many Regulators, Many Consequences. *The Neuroscientist*, *19*(1), 62–75. doi:10.1177/1073858411435129
Schindelin, J., Arganda-Carreras, I., Frise, E., Kaynig, V., Longair, M., Pietzsch, T., et al. (2012). Fiji: an open-source platform for biological-image analysis. *Nature Methods*, *9*(7), 676–682. doi:10.1038/nmeth.2019
Schoenenberger, P., Schärer, Y.-P. Z., & Oertner, T. G. (2011). Channelrhodopsin as a tool to investigate synaptic transmission and plasticity. *Experimental Physiology*, *96*(1), 34–39. doi:10.1113/expphysiol.2009.051219
Shepherd, G. M. G. (2012). Circuit mapping by ultraviolet uncaging of glutamate. *Cold Spring Harbor Protocols*, *2012*(9), 998–1004. doi:10.1101/pdb.prot070664
Shepherd, G. M. G., Pologruto, T. A., & Svoboda, K. (2003). Circuit analysis of experience-dependent plasticity in the developing rat barrel cortex. *Neuron*, *38*(2), 277–289.
Shimogori, T. (2006). Micro in utero electroporation for efficient gene targeting in mouse embryos. *CSH Protocols*, *2006*(1). doi:10.1101/pdb.prot4447
Shimogori, T., & Ogawa, M. (2008). Gene application with in utero electroporation in mouse embryonic brain. *Development, Growth & Differentiation*, *50*(6), 499–506. doi:10.1111/j.1440-169X.2008.01045.x
Silberberg, G., & Markram, H. (2007). Disynaptic inhibition between neocortical pyramidal cells mediated by Martinotti cells. *Neuron*, *53*(5), 735–746. doi:10.1016/j.neuron.2007.02.012
Simon, A., Oláh, S., Molnár, G., Szabadics, J., & Tamás, G. (2005). Gap-junctional coupling between neurogliaform cells and various interneuron types in the neocortex. *The Journal of Neuroscience : the Official Journal of the Society for Neuroscience*, *25*(27), 6278–6285. doi:10.1523/JNEUROSCI.1431-05.2005
Sipilä, S. T., Huttu, K., Voipio, J., & Kaila, K. (2006). Intrinsic bursting of immature CA3 pyramidal neurons and consequent giant depolarizing potentials are driven by a persistent Na +current and terminated by a slow Ca 2+-activated K +current. *European Journal of Neuroscience*, *23*(9), 2330–2338. doi:10.1111/j.1460-9568.2006.04757.x
Sohal, V. S., Zhang, F., Yizhar, O., & Deisseroth, K. (2009). Parvalbumin neurons and gamma rhythms enhance cortical circuit performance. *Nature*, *459*(7247), 698–702. doi:10.1038/nature07991
Somogyi, P., Tamás, G., Lujan, R., & Buhl, E. H. (1998). Salient features of synaptic organisation in the cerebral cortex. *Brain Research. Brain Research Reviews*, *26*(2-3), 113–135.
Sousa, V. H., Miyoshi, G., Hjerling-Leffler, J., Karayannis, T., & Fishell, G. (2009). Characterization of Nkx6-2-derived neocortical interneuron lineages. *Cerebral*

Cortex, *19 Suppl 1*, i1–10. doi:10.1093/cercor/bhp038
Stern, E. A., Maravall, M., & Svoboda, K. (2001). Rapid development and plasticity of layer 2/3 maps in rat barrel cortex in vivo. *Neuron*, *31*(2), 305–315.
Sultan, K. T., Brown, K. N., & Shi, S.-H. (2013). Production and organization of neocortical interneurons. *Frontiers in Cellular Neuroscience*, *7*. doi:10.3389/fncel.2013.00221
Sun, J.-J., & Luhmann, H. J. (2007). Spatio-temporal dynamics of oscillatory network activity in the neonatal mouse cerebral cortex. *European Journal of Neuroscience*, *26*(7), 1995–2004. doi:10.1111/j.1460-9568.2007.05819.x
Sun, Q.-Q. (2009). Experience-dependent intrinsic plasticity in interneurons of barrel cortex layer IV. *Journal of Neurophysiology*, *102*(5), 2955–2973. doi:10.1152/jn.00562.2009
Sun, Q.-Q., Huguenard, J. R., & Prince, D. A. (2006). Barrel cortex microcircuits: thalamocortical feedforward inhibition in spiny stellate cells is mediated by a small number of fast-spiking interneurons. *The Journal of Neuroscience : the Official Journal of the Society for Neuroscience*, *26*(4), 1219–1230. doi:10.1523/JNEUROSCI.4727-04.2006
Swadlow, H. A., & Gusev, A. G. (2002). Receptive-field construction in cortical inhibitory interneurons. *Nature Neuroscience*, *5*(5), 403–404. doi:10.1038/nn847
Takesian, A. E., Kotak, V. C., Sharma, N., & Sanes, D. H. (2013). Hearing loss differentially affects thalamic drive to two cortical interneuron subtypes. *Jn.Physiology.org*. Retrieved from http://jn.physiology.org/content/110/4/999.abstract?etoc
Tan, Z., Tan, Z., Hu, H., Hu, H., Huang, Z. J., Huang, Z. J., et al. (2008). Robust but delayed thalamocortical activation of dendritic-targeting inhibitory interneurons. *Proceedings of the National Academy of Sciences of the United States of America*, *105*(6), 2187–2192. doi:10.1073/pnas.0710628105
Taniguchi, H. (2014). Genetic dissection of GABAergic neural circuits in mouse neocortex. *Frontiers in Cellular Neuroscience*, *8*. doi:10.3389/fncel.2014.00008
Taniguchi, H., He, M., Wu, P., Kim, S., Paik, R., Sugino, K., et al. (2011). A Resource of Cre Driver Lines for Genetic Targeting of GABAergic Neurons in Cerebral Cortex. *Neuron*, *71*(6), 995–1013. doi:10.1016/j.neuron.2011.07.026
Thomson, A. M. (2003). Interlaminar Connections in the Neocortex. *Cerebral Cortex*, *13*(1), 5–14. doi:10.1093/cercor/13.1.5
Thomson, A. M. (2010). Neocortical layer 6, a review. *Frontiers in Neuroanatomy*, *4*, 13. doi:10.3389/fnana.2010.00013
Thomson, A. M., & Lamy, C. (2007). Functional maps of neocortical local circuitry. *Frontiers in Neuroscience*, *1*(1), 19–42. doi:10.3389/neuro.01.1.1.002.2007
Tolner, E. A., Sheikh, A., Yukin, A. Y., Kaila, K., & Kanold, P. O. (2012). Subplate neurons promote spindle bursts and thalamocortical patterning in the neonatal rat somatosensory cortex. *The Journal of Neuroscience : the Official Journal of the Society for Neuroscience*, *32*(2), 692–702. doi:10.1523/JNEUROSCI.1538-11.2012
Tomioka, R., Okamoto, K., Furuta, T., Fujiyama, F., Iwasato, T., Yanagawa, Y., et al. (2005). Demonstration of long-range GABAergic connections distributed throughout the mouse neocortex. *The European Journal of Neuroscience*, *21*(6), 1587–1600. doi:10.1111/j.1460-9568.2005.03989.x
Torres-Reveron, J., & Friedlander, M. J. (2007). Properties of persistent postnatal cortical subplate neurons. *The Journal of Neuroscience : the Official Journal of the Society for Neuroscience*, *27*(37), 9962–9974.

doi:10.1523/JNEUROSCI.1536-07.2007
Tyzio, R., Cossart, R., Khalilov, I., Minlebaev, M., Hübner, C. A., Represa, A., et al. (2006). Maternal oxytocin triggers a transient inhibitory switch in GABA signaling in the fetal brain during delivery. *Science (New York, NY)*, *314*(5806), 1788–1792. doi:10.1126/science.1133212
Tyzio, R., Represa, A., Jorquera, I., Ben-Ari, Y., Gozlan, H., & Aniksztejn, L. (1999). The establishment of GABAergic and glutamatergic synapses on CA1 pyramidal neurons is sequential and correlates with the development of the apical dendrite. *The Journal of Neuroscience*, *19*(23), 10372–10382.
Uhlhaas, P. J., Haenschel, C., Nikolić, D., & Singer, W. (2008). The role of oscillations and synchrony in cortical networks and their putative relevance for the pathophysiology of schizophrenia. *Schizophrenia Bulletin*, *34*(5), 927–943. doi:10.1093/schbul/sbn062
Uhlhaas, P. J., Roux, F., Rodriguez, E., Rotarska-Jagiela, A., & Singer, W. (2010). Neural synchrony and the development of cortical networks. *Trends in Cognitive Sciences*, *14*(2), 72–80. doi:10.1016/j.tics.2009.12.002
Valcanis, H., & Tan, S.-S. (2003). Layer specification of transplanted interneurons in developing mouse neocortex. *The Journal of Neuroscience : the Official Journal of the Society for Neuroscience*, *23*(12), 5113–5122.
Van der Loos, H., & Woolsey, T. A. (1973). Somatosensory cortex: structural alterations following early injury to sense organs. *Science (New York, NY)*, *179*(4071), 395–398.
Verhage, M. (2000). Synaptic Assembly of the Brain in the Absence of Neurotransmitter Secretion. *Science (New York, NY)*, *287*(5454), 864–869. doi:10.1126/science.287.5454.864
Viaene, A. N., Petrof, I., & Sherman, S. M. (2011a). Properties of the thalamic projection from the posterior medial nucleus to primary and secondary somatosensory cortices in the mouse. *Proceedings of the National Academy of Sciences of the United States of America*, *108*(44), 18156–18161. doi:10.1073/pnas.1114828108
Viaene, A. N., Petrof, I., & Sherman, S. M. (2011b). Synaptic properties of thalamic input to the subgranular layers of primary somatosensory and auditory cortices in the mouse. *The Journal of Neuroscience : the Official Journal of the Society for Neuroscience*, *31*(36), 12738–12747. doi:10.1523/JNEUROSCI.1565-11.2011
Vicini, S., Wang, J. F., Li, J. H., Zhu, W. J., Wang, Y. H., Luo, J. H., et al. (1998). Functional and pharmacological differences between recombinant N-methyl-D-aspartate receptors. *Journal of Neurophysiology*, *79*(2), 555–566.
Viswanathan, S., Bandyopadhyay, S., Kao, J. P. Y., & Kanold, P. O. (2012). Changing microcircuits in the subplate of the developing cortex. *The Journal of Neuroscience : the Official Journal of the Society for Neuroscience*, *32*(5), 1589–1601. doi:10.1523/JNEUROSCI.4748-11.2012
Voigt, T. (2005). Activation of Early Silent Synapses by Spontaneous Synchronous Network Activity Limits the Range of Neocortical Connections. *The Journal of Neuroscience : the Official Journal of the Society for Neuroscience*, *25*(18), 4605–4615. doi:10.1523/JNEUROSCI.3803-04.2005
Voigt, T., Opitz, T., & de Lima, A. D. (2001). Synchronous oscillatory activity in immature cortical network is driven by GABAergic preplate neurons. *The Journal of Neuroscience : the Official Journal of the Society for Neuroscience*, *21*(22), 8895–8905.
Vucurovic, K., Gallopin, T., Ferezou, I., Rancillac, A., Chameau, P., van Hooft, J. A.,

et al. (2010). Serotonin 3A receptor subtype as an early and protracted marker of cortical interneuron subpopulations. *Cerebral Cortex*, *20*(10), 2333–2347. doi:10.1093/cercor/bhp310

Wahle, P. (1993). Differential regulation of substance P and somatostatin in Martinotti cells of the developing cat visual cortex. *The Journal of Comparative Neurology*, *329*(4), 519–538. doi:10.1002/cne.903290408

Wang, C., Shimizu-Okabe, C., Watanabe, K., Okabe, A., Matsuzaki, H., Ogawa, T., et al. (2002). Developmental changes in KCC1, KCC2, and NKCC1 mRNA expressions in the rat brain. *Brain Research. Developmental Brain Research*, *139*(1), 59–66.

Wang, D. D., & Kriegstein, A. R. (2008). GABA Regulates Excitatory Synapse Formation in the Neocortex via NMDA Receptor Activation. *The Journal of Neuroscience : the Official Journal of the Society for Neuroscience*, *28*(21), 5547–5558. doi:10.1523/JNEUROSCI.5599-07.2008

Wang, D. D., & Kriegstein, A. R. (2009). Defining the role of GABA in cortical development. *The Journal of Physiology*, *587*(9), 1873–1879. doi:10.1113/jphysiol.2008.167635

Wang, H.-P., Spencer, D., Fellous, J.-M., & Sejnowski, T. J. (2010). Synchrony of thalamocortical inputs maximizes cortical reliability. *Science (New York, NY)*, *328*(5974), 106–109. doi:10.1126/science.1183108

Wang, L., Kloc, M., Gu, Y., Ge, S., & Maffei, A. (2013). Layer-Specific Experience-Dependent Rewiring of Thalamocortical Circuits. *The Journal of Neuroscience : the Official Journal of the Society for Neuroscience*, *33*(9), 4181–4191. doi:10.1523/JNEUROSCI.4423-12.2013

Wang, Y., Toledo-Rodriguez, M., Gupta, A., Wu, C., Silberberg, G., Luo, J., & Markram, H. (2004). Anatomical, physiological and molecular properties of Martinotti cells in the somatosensory cortex of the juvenile rat. *The Journal of Physiology*, *561*(Pt 1), 65–90. doi:10.1113/jphysiol.2004.073353

Washbourne, P., Bennett, J. E., & McAllister, A. K. (2002). Rapid recruitment of NMDA receptor transport packets to nascent synapses. *Nature Neuroscience*, *5*(8), 751–759. doi:10.1038/nn883

Wehr, M., & Zador, A. M. (2003). Balanced inhibition underlies tuning and sharpens spike timing in auditory cortex. *Nature*, *426*(6965), 442–446. doi:10.1038/nature02116

Wen, J. A., & Barth, A. L. (2011). Input-specific critical periods for experience-dependent plasticity in layer 2/3 pyramidal neurons. *The Journal of Neuroscience : the Official Journal of the Society for Neuroscience*, *31*(12), 4456–4465. doi:10.1523/JNEUROSCI.6042-10.2011

Whittington, M. A., Cunningham, M. O., LeBeau, F. E. N., Racca, C., & Traub, R. D. (2011). Multiple origins of the cortical γ rhythm. *Developmental Neurobiology*, *71*(1), 92–106. doi:10.1002/dneu.20814

Wichterle, H., Garcia-Verdugo, J. M., Herrera, D. G., & Alvarez-Buylla, A. (1999). Young neurons from medial ganglionic eminence disperse in adult and embryonic brain. *Nature Neuroscience*, *2*(5), 461–466. doi:10.1038/8131

Wichterle, H., Turnbull, D. H., Nery, S., Fishell, G., & Alvarez-Buylla, A. (2001). In utero fate mapping reveals distinct migratory pathways and fates of neurons born in the mammalian basal forebrain. *Development (Cambridge, England)*, *128*(19), 3759–3771.

Wickersham, I. R., Sullivan, H. A., & Seung, H. S. (2010). Production of glycoprotein-deleted rabies viruses for monosynaptic tracing and high-level gene

expression in neurons. *Nature Protocols*, *5*(3), 595–606. doi:10.1038/nprot.2009.248

Wilson, N. R., Runyan, C. A., Wang, F. L., & Sur, M. (2012). Division and subtraction by distinct cortical inhibitory networks in vivo. *Nature*. doi:doi:10.1038/nature11347

Wimmer, V. C., Bruno, R. M., de Kock, C. P. J., Kuner, T., & Sakmann, B. (2010). Dimensions of a projection column and architecture of VPM and POm axons in rat vibrissal cortex. *Cerebral Cortex (New York, NY : 1991)*, *20*(10), 2265–2276. doi:10.1093/cercor/bhq068

Wonders, C. P., & Anderson, S. A. (2006). The origin and specification of cortical interneurons. *Nature Reviews Neuroscience*, *7*(9), 687–696. doi:10.1038/nrn1954

Wonders, C. P., Taylor, L., Welagen, J., Mbata, I. C., Xiang, J. Z., & Anderson, S. A. (2008). A spatial bias for the origins of interneuron subgroups within the medial ganglionic eminence. *Developmental Biology*, *314*(1), 127–136. doi:10.1016/j.ydbio.2007.11.018

Woolsey, T. A., & Van der Loos, H. (1970). The structural organization of layer IV in the somatosensory region (SI) of mouse cerebral cortex. The description of a cortical field composed of discrete cytoarchitectonic units. *Brain Research*, *17*(2), 205–242.

Xiao, M.-Y., Wasling, P., Hanse, E., & Gustafsson, B. (2004). Creation of AMPA-silent synapses in the neonatal hippocampus. *Nature Neuroscience*, *7*(3), 236–243. doi:10.1038/nn1196

Xu, G., Broadbelt, K. G., Haynes, R. L., Folkerth, R. D., Borenstein, N. S., Belliveau, R. A., et al. (2011). Late development of the GABAergic system in the human cerebral cortex and white matter. *Journal of Neuropathology and Experimental Neurology*, *70*(10), 841–858. doi:10.1097/NEN.0b013e31822f471c

Xu, H., Jeong, H.-Y., Tremblay, R., & Rudy, B. (2013). Neocortical somatostatin-expressing GABAergic interneurons disinhibit the thalamorecipient layer 4. *Neuron*, *77*(1), 155–167. doi:10.1016/j.neuron.2012.11.004

Xu, Q. (2004). Origins of Cortical Interneuron Subtypes. *The Journal of Neuroscience : the Official Journal of the Society for Neuroscience*, *24*(11), 2612–2622. doi:10.1523/JNEUROSCI.5667-03.2004

Xu, Q., Tam, M., & Anderson, S. A. (2008). Fate mapping Nkx2.1-lineage cells in the mouse telencephalon. *The Journal of Comparative Neurology*, *506*(1), 16–29. doi:10.1002/cne.21529

Xu, X., & Callaway, E. M. (2009). Laminar specificity of functional input to distinct types of inhibitory cortical neurons. *The Journal of Neuroscience : the Official Journal of the Society for Neuroscience*, *29*(1), 70–85. doi:10.1523/JNEUROSCI.4104-08.2009

Xu, X., Roby, K. D., & Callaway, E. M. (2006). Mouse cortical inhibitory neuron type that coexpresses somatostatin and calretinin. *The Journal of Comparative Neurology*, *499*(1), 144–160. doi:10.1002/cne.21101

Yang, J. M., Zhang, J., Yu, Y. Q., Duan, S., & Li, X. M. (2013a). Postnatal Development of 2 Microcircuits Involving Fast-Spiking Interneurons in the Mouse Prefrontal Cortex. *Cerebral Cortex*, *24*(1), 98–109. doi:10.1093/cercor/bhs291

Yang, J. W., An, S., Sun, J. J., Reyes-Puerta, V., Kindler, J., Berger, T., et al. (2013b). Thalamic Network Oscillations Synchronize Ontogenetic Columns in the Newborn Rat Barrel Cortex. *Cerebral Cortex*, *23*(6), 1299–1316. doi:10.1093/cercor/bhs103

Yang, J.-W., Hanganu-Opatz, I. L., Sun, J.-J., & Luhmann, H. J. (2009). Three Patterns of Oscillatory Activity Differentially Synchronize Developing Neocortical Networks In Vivo. *The Journal of Neuroscience : the Official Journal of the Society for Neuroscience*, *29*(48), 15029–15030. doi:10.1523/JNEUROSCI.4567-09.2009

Yashiro, K., & Philpot, B. D. (2008). Regulation of NMDA receptor subunit expression and its implications for LTD, LTP, and metaplasticity. *Neuropharmacology*, *55*(7), 1081–1094. doi:10.1016/j.neuropharm.2008.07.046

Yizhar, O., Fenno, L. E., Davidson, T. J., Mogri, M., & Deisseroth, K. (2011). Optogenetics in neural systems. *Neuron*, *71*(1), 9–34. doi:10.1016/j.neuron.2011.06.004

Yoshimura, Y., & Callaway, E. M. (2005). Fine-scale specificity of cortical networks depends on inhibitory cell type and connectivity. *Nature Neuroscience*, *8*(11), 1552–1559. doi:10.1038/nn1565

Yu, Y.-C., Bultje, R. S., Wang, X., & Shi, S.-H. (2009). Specific synapses develop preferentially among sister excitatory neurons in the neocortex. *Nature*, *458*(7237), 501–504. doi:10.1038/nature07722

Yu, Y.-C., He, S., Chen, S., Fu, Y., Brown, K. N., Yao, X.-H., et al. (2012). Preferential electrical coupling regulates neocortical lineage-dependent microcircuit assembly. *Nature*, *486*(7401), 113–117. doi:10.1038/nature10958

Yuste, R., Peinado, A., & Katz, L. C. (1992). Neuronal domains in developing neocortex. *Science (New York, NY)*, *257*(5070), 665–669.

Zecevic, N., Hu, F., & Jakovcevski, I. (2011). Interneurons in the developing human neocortex. *Developmental Neurobiology*, *71*(1), 18–33. doi:10.1002/dneu.20812

Zemelman, B. V., Zemelman, B. V., Nesnas, N., Lee, G. A., & Miesenböck, G. (2003). Photochemical gating of heterologous ion channels: Remote control over genetically designated populations of neurons. *Proceedings of the National Academy of Sciences*, *100*(3), 1352–1357. doi:10.1073/pnas.242738899

Zhang, F., Aravanis, A. M., Adamantidis, A., de Lecea, L., & Deisseroth, K. (2007). Circuit-breakers: optical technologies for probing neural signals and systems. *Nature Reviews Neuroscience*, *8*(8), 577–581. doi:10.1038/nrn2192

Zhang, J., Ackman, J. B., Xu, H.-P., & Crair, M. C. (2012). Visual map development depends on the temporal pattern of binocular activity in mice. *Nature Neuroscience*, *15*(2), 298–307. doi:doi:10.1038/nn.3007

Zhang, Y.-P., & Oertner, T. G. (2007). Optical induction of synaptic plasticity using a light-sensitive channel. *Nature Methods*, *4*(2), 139–141. doi:10.1038/nmeth988

Zhang, Z. W. (2003). Maturation of Layer V Pyramidal Neurons in the Rat Prefrontal Cortex: Intrinsic Properties and Synaptic Function. *Journal of Neurophysiology*, *91*(3), 1171–1182. doi:10.1152/jn.00855.2003

Zhao, C., Kao, J. P. Y., & Kanold, P. O. (2009). Functional excitatory microcircuits in neonatal cortex connect thalamus and layer 4. *The Journal of Neuroscience : the Official Journal of the Society for Neuroscience*, *29*(49), 15479–15488. doi:10.1523/JNEUROSCI.4471-09.2009

Zhu, J. J., & Malinow, R. (2002). Acute versus chronic NMDA receptor blockade and synaptic AMPA receptor delivery. *Nature Neuroscience*, *5*(6), 513–514. doi:10.1038/nn0602-850

Zingg, B., Hintiryan, H., Gou, L., Song, M. Y., Bay, M., Bienkowski, M. S., et al. (2014). Neural networks of the mouse neocortex. *Cell*, *156*(5), 1096–1111. doi:10.1016/j.cell.2014.02.023

Zito, K., Scheuss, V., Knott, G., Hill, T., & Svoboda, K. (2009). Rapid functional

maturation of nascent dendritic spines. *Neuron*, *61*(2), 247–258. doi:10.1016/j.neuron.2008.10.054

Zsiros, V., & Maccaferri, G. (2005). Electrical coupling between interneurons with different excitable properties in the stratum lacunosum-moleculare of the juvenile CA1 rat hippocampus. *The Journal of Neuroscience : the Official Journal of the Society for Neuroscience*, *25*(38), 8686–8695. doi:10.1523/JNEUROSCI.2810-05.2005